# ZIKV Protein Accumulation is a Major Regulator of Innate Immunity, Controlling Viral Replication and Spread

Amy Lu

A dissertation

submitted in partial fulfillment of the

requirements for the degree of

Doctor of Philosophy

University of Washington

2023

Reading Committee:

Michael Gale, Jr., Chair

Gael Kurath

Michael Lagunoff

Rhea Coler

Program Authorized to Offer Degree:

Pathobiology

University of Washington

# Abstract

ZIKV Protein Accumulation is a Major Regulator of Innate Immunity, Controlling Viral Replication and Spread

Amy Lu

Chair of the Supervisory Committee:

Michael Gale, Jr., PhD

Departments of Global Health and Immunology

Asian lineage Zika virus (ZIKV) strains emerged globally, causing outbreaks linked with critical clinical disease outcomes unless ZIKV is effectively restricted by host immunity. We have previously shown that retinoic acid-inducible gene-I (RIG-I) senses ZIKV to trigger innate immunity to direct interferon (IFN) production and antiviral responses that can control ZIKV infection. However, ZIKV proteins have been demonstrated to antagonize IFN. Here, we conducted *in vitro* analyses to assess how divergent prototypic ZIKV variants differ in virologic properties, innate immune regulation, and infection outcome. We comparatively assessed African lineage

ZIKV/Dakar/1984/ArD41519 (ZIKV/Dakar) and Asian lineage ZIKV/Malaysia/1966/P6740 (ZIKV/Malaysia) in a human epithelial cell infection model. *De novo* viral sequence determination identified amino acid changes within the ZIKV/Dakar genome compared to ZIKV/Malaysia. Viral growth analyses revealed that ZIKV/Malaysia accumulated viral proteins and genome earlier and to higher levels than ZIKV/Dakar. Both ZIKV strains activated RIG-I/interferon regulatory factor (IRF) 3 and nuclear factor kappa B (NFκB) pathways to induce inflammatory cytokine expression and types I and III IFNs. However, ZIKV/Malaysia, but not ZIKV/Dakar, potently blocked downstream IFN signaling. Remarkably, ZIKV/Dakar protein accumulation and genome replication were rescued in RIG-I knockout (KO) cells late in acute infection, resulting in ZIKV/Dakar-mediated antagonism of IFN signaling. We found that RIG-I signaling specifically restricts viral protein accumulation late in acute infection where early accumulation of viral proteins in infected cells confers enhanced ability to limit IFN signaling, promoting viral replication and spread. Our results reveal a novel function of RIG-I-mediated innate immune signaling in restricting ZIKV protein accumulation, which permits IFN signaling and antiviral actions that control ZIKV infection.

## Acknowledgements

This work would not have been possible without the countless individuals who helped me throughout the course of this study and graduate school in general. I would like to begin by thanking my mentor, Michael Gale, Jr., for taking a chance on me, for always being optimistic and enthusiastic about science, and for your unwavering support over the past several years. Thank you for giving me the opportunity to explore and grow into an independent scientist. I would also like to thank the individuals who contributed directly to this project: Andrew Gustin for your help in the Nanostring analysis and for patiently answering my endless questions regarding bioinformatics analysis; Daniel Newhouse for your help assembling viral genome sequences and for walking me through the assembly process; and the Gale lab sequencing group for your help with library prep and sequencing. I would like to extend my gratitude to my thesis committee members Rhea Coler, Jennifer Hyde, Michael Lagunoff, and Gael Kurath for their input and support throughout my PhD and for reminding me of all that I have accomplished over the past few years.

I would also like to thank my colleagues in the Gale lab both past and present for their endless support, their help with troubleshooting, and for all our valuable scientific and non-scientific discussions. A special thank you to Justin Roby for getting me settled into the lab during my rotation, for the countless hours and weekends you set aside to train me during my rotation, and for teaching me the basics of almost everything I know today. A big thank you to Elyse Verstelle for being a great lab manager and making sure that everything in the lab runs smoothly so that we can focus on doing fun, exciting science every day, and for introducing me to the beauty of Washington’s wilderness. I

would also like to thank the members of Flavi Club for the good discussions and feedback over the past year.

Graduate school is especially hard when you live halfway across the world (over 6000 miles!) from your family. Luckily, I have an amazing support system here in Seattle. I want to thank Alyssa Brokaw, Lizette Carrasco, Nika Hajari, Olivia Kern, Brittany Ulloa, Sean Windle, my partner Tony Barnett, and everyone else for their support in and out of lab. Thank you all for the dinners, game nights, conversations, camping trips, hikes, road trips, and countless wonderful memories. Thank you to the members of Grub Club for trying out new restaurants in Seattle and Vancouver with me. To all my friends in Seattle, thank you from the bottom of my heart for being my home away from home. And to my best friend, Lori Wang, thank you for your support from far away, for the late night phone calls/Facetime sessions, and for being by my side since 7th grade. Lastly, I want to thank my parents, sister, and brother for their continuous support from halfway across the world. Thank you for always encouraging me, for helping me see the brighter side when my experiments fail, and for allowing me to pursue my passion in the biological sciences.

# Table of Contents

# List of Figures

## Chapter 1



## Chapter 3

# List of Tables

## Chapter 2



## Appendix

# Abbreviations

aa: amino acid

AGC: anchored gene count

ATP: adenosine triphosphate

ATPase: adenosine triphosphatase

C: capsid

CARD: caspase activation and recruitment domain

cDMEM: complete Dulbecco's modified Eagle medium

C-terminal: carboxy-terminal

CV: coefficient of variation

CZS: congenital ZIKV syndrome

DAPI: 4', 6-diamidino-2-phenylindole dihydrochloride

DC-SIGN: dendritic cell-specific intracellular adhesion molecule-3-grabbing non-integrin

DENV: dengue virus

dsRNA: double-stranded RNA

E: envelope

ER: endoplasmic reticulum

FBS: fetal bovine serum

GBS: Guillain-Barré syndrome

GMP: guanosine monophosphate

GOI: gene of interest

GPI: glycosyl-phosphatidylinositol

GTP: guanosine triphosphate

GTPase: guanosine triphosphatase

HK: housekeeping

hpi: hours post-infection

HRP: horseradish peroxide

IFIT: IFN-induced protein with tetratricopeptide repeats

IFN: interferon

IFNAR: IFN α/β receptor

IFNLR: IFNλ receptor

IκB: inhibitor of NFκB

IKKε: IκB kinase ε

IL-10R2: interleukin-10 receptor 2

iPSC: induced pluripotent stem cell

IRF: interferon regulatory factor

ISG: IFN stimulated gene

ISGF3: interferon stimulated gene factor 3

ISRE: IFN-stimulated response element

JAK/STAT: Janus kinase/signal transducers and activators of transcription

KO: knockout

LGP2: laboratory of genetics and physiology 2

M: membrane

MAM: mitochondrial-associated membranes

MAVS: mitochondrial antiviral-signaling protein

MDA5: melanoma-associated gene 5

MFI: median fluorescence intensity

MerTK: Mer tyrosine kinase

miRNA: microRNA

MOI: multiplicity of infection

mRNA: messenger RNA

MTase: methyltransferase

N-terminal: amino-terminal

NFκB: nuclear factor kappa B

NGS: normal goat serum

NHP: non-human primate

NLS: nuclear localization sequence

nm: nanometer

NMD: nonsense-mediated mRNA decay

NPC: neural progenitor cell

NS: non-structural

NTC: non-targeting control

NTPase: nucleotide triphosphatase

PAMP: pathogen-associated molecular pattern

PBS: phosphate buffered saline

PBSA: bovine serum albumin in PBS

PBST: PBS plus Tween-20

PCA: principal component analysis

PIAS: protein inhibitor of activated STAT

polyA: polyadenylated

prM: precursor membrane

PRR: pattern recognition receptor

RdRp: RNA-dependent RNA polymerase

RIG-I: retinoic acid-inducible gene-I

RIPA: radioimmunoprecipitation assay

RLR: RIG-I-like receptor

RNAi: RNA interference

RTPase: RNA triphosphatase

SDS: sodium dodecyl sulfate

sfRNA: subgenomic flavivirus RNA

SLA: stem loop A

SOCS: suppressor of cytokine signaling proteins

TAM: Tyro3, AXL, and MerTK

TBK1: TANK-binding kinase 1

TBS: Tris-buffer saline

TBST: TBS containing Tween-20

TIM: T-cell immunoglobulin domain and mucin domain

TIR: toll/interleukin-1 receptor

TLR: toll-like receptor

TMB: 3,3’,5,5’-tetramethylbenzinide

TRIF: TIR-domain-containing adapter-inducing IFNβ

TRIM25: tripartite motif-containing protein 25

Tyk2: tyrosine kinase 2

Tyro3: tyrosine-protein kinase receptor 3

UAR: upstream AUG region

UFS: UAR-flanking stem

UTR: untranslated region

WT: wild-type

xrRNA: XRN1-resistant RNA

ZIKV: Zika virus

3’ SL: 3’ stem loop

# Chapter 1. Introduction

## 1.1 ZIKV epidemiology

Zika virus (ZIKV) is a mosquito-borne member of the *Flavivirus* genus within the Flaviviridae family. ZIKV was first isolated from a rhesus macaque in the Zika Forest of Uganda in 1947 (1). The first ZIKV infection in humans was reported in Nigeria in 1954, indicating a westward expansion of ZIKV into western Africa and establishing the African lineage (2, 3). In 1966, a strain of ZIKV, termed P6740, was isolated from mosquitoes in Malaysia, marking the spread of ZIKV from Africa into Asia (4). P6740 is the first ZIKV strain isolated in Asia, and after its initial isolation, other ZIKV strains were isolated in several countries in southeast Asia, establishing the Asian lineage (3, 5).

In the wild, ZIKV is maintained by transmission between mosquitoes and non-human primates (NHPs), whereas urban transmission cycles are maintained by *Aedes* species mosquitoes and humans (Fig. 1-1) (6, 7). Prior to 2007, ZIKV circulated largely undetected and maintained endemic transmission throughout Africa and Asia with only 14 human cases reported globally (8). The first largescale ZIKV outbreak was reported in 2007 in the Yap State of the Federated States of Micronesia in the Pacific where an estimated 73% of the population over the age of 3 was infected, underscoring the epidemic potential of ZIKV (9). Indeed, in 2013 and 2015, major ZIKV epidemics were reported in French Polynesia and the Americas, respectively (10, 11). Both epidemics were caused by Asian lineage-derived ZIKV strains (Fig. 1-2) (12). The introduction of ZIKV into French Polynesia likely originated from Yap State or Cambodia as the virus isolated in French Polynesia was closely related to the Asian lineage viruses isolated in 2007 in Yap State and in 2010 in Cambodia, while ZIKV was likely introduced into the

Americas from French Polynesia (10, 11, 13). The 2015 ZIKV epidemic in Central and South America was unprecedented given its breadth, such that it was declared a public health emergency of international concern in 2016, and the reports of mosquito-independent transmission routes (14–20). During the 2015 outbreak, human-to-human ZIKV transmission was shown to occur through blood and sexual contact, and vertically across the maternal-fetal interface (Fig. 1-1) (7, 14–19). However, two case studies argue against the emergence of these novel transmission routes during the 2015 ZIKV outbreak as they provide evidence for potential sexual transmission of ZIKV in cases reported in 2008 and 2013 (16, 21). Furthermore, case studies from southeast Asia reported evidence for vertical transmission of local ZIKV strains, indicating that endemic ZIKV strains are capable of crossing the maternal-fetal barrier as well (22, 23). It is likely that the large number of infected individuals and vigorous ZIKV testing employed during the 2015 ZIKV outbreak helped shed light on the mosquito-independent transmission routes. Nevertheless, these novel transmission routes could provide the opportunity for human-to-human transmission in the absence of competent mosquito vectors.

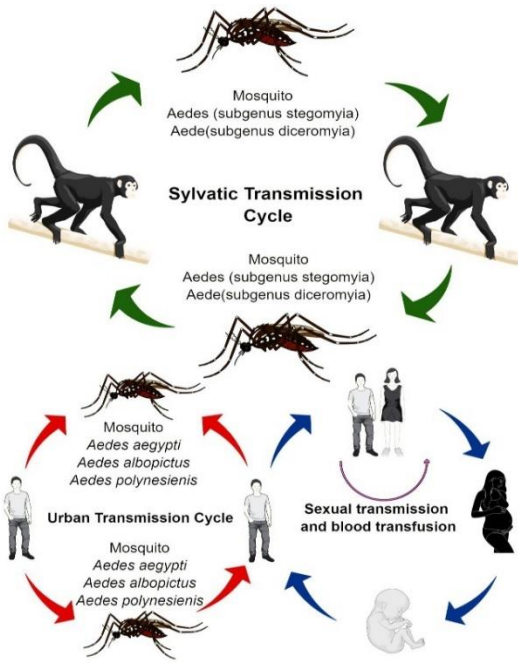


Fig. 1-1. Top: ZIKV transmission cycle in the wild. ZIKV is maintained through transmission between NHPs and forest-dwelling mosquitoes. Bottom: urban ZIKV transmission cycles. ZIKV is predominantly transmitted in urban areas between mosquitoes and humans through the bite of a ZIKV-infected mosquito. ZIKV transmission has also been reported to occur through blood products and sex, and vertically from a mother to her fetus. Image adopted from Rather et al., 2017 (7).

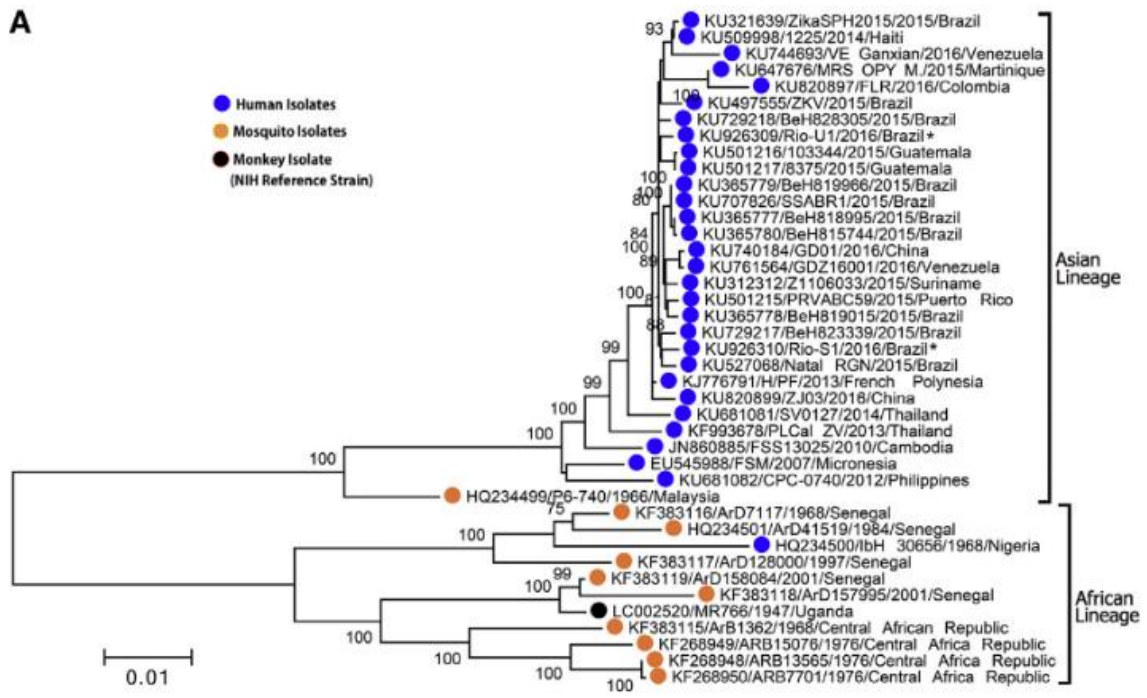


Fig. 1-2. ZIKV isolates can be clustered into two distinct lineages: African and Asian. The Asian lineage includes the emerging strains responsible for the recent outbreaks. Image adopted from Wang et al., 2016 (12).

With increasing ease of global travel, importation of ZIKV into areas with no current reports of ZIKV circulation presents a major risk for future epidemics particularly in areas with competent mosquito vectors (Fig. 1-3) (24). There have been several reported incidences of imported ZIKV cases from returning infected travelers that led to autochthonous transmission in France, the United States, and Angola where *Aedes* species mosquitoes are abundant (25–29). Additionally, with increasing global temperatures, the distribution of *Aedes* mosquitoes can expand to more temperate regions, bringing along arboviruses, including ZIKV, and increasing the potential for largescale ZIKV outbreaks and endemic transmission as observed with other arboviruses (30).

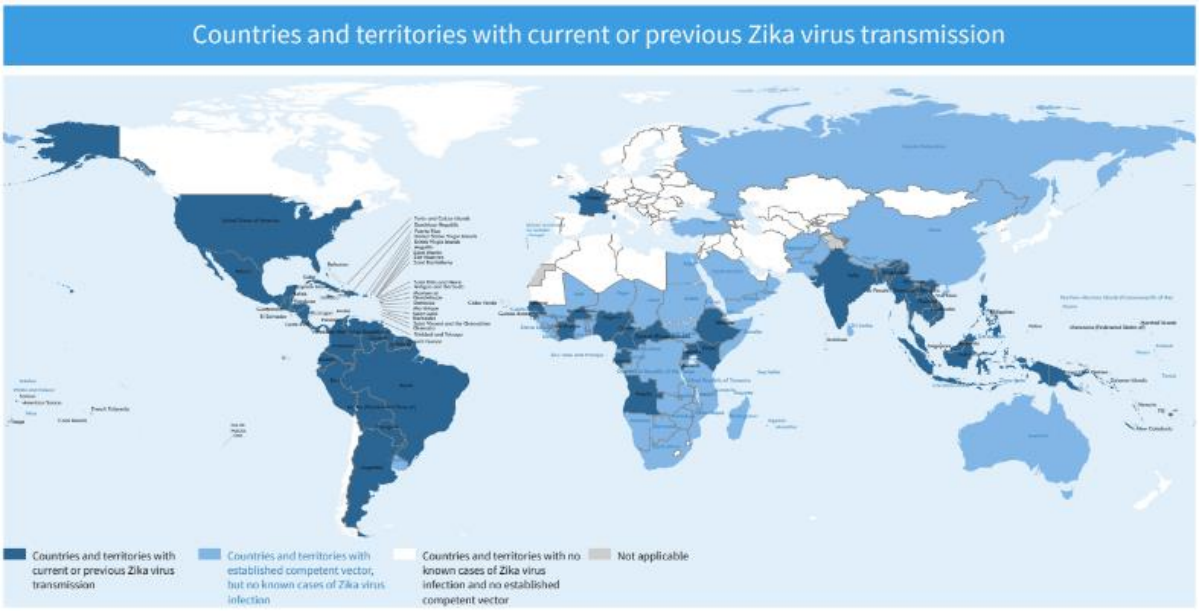


Fig. 1-3. Global distribution of regions with reported ZIKV transmission and regions with competent mosquito vectors but no known ZIKV cases as of February 2022. Adapted from the World Health Organization (WHO, 2022) (22).

## 1.2 ZIKV pathology

Infection with ZIKV typically results in asymptomatic disease or in mild flu-like illnesses in approximately 25% of cases (31, 32). However, during the 2013 ZIKV outbreak in French Polynesia, severe disease was reported with ZIKV infection. Specifically, adult ZIKV infection was linked to an increased incidence of Guillain-Barré syndrome (GBS), an autoimmune neurological disorder triggered by viral or bacterial infections (33–35). A case-control study in French Polynesia observed that GBS-affected individuals were significantly more likely to have anti-ZIKV IgM or IgG antibodies and that 100% of GBS-affected individuals had neutralizing anti-ZIKV antibodies compared to 56% of unaffected controls (34). Similar reports pointing to the association of ZIKV infection with the onset of GBS emerged in the Americas during the 2015 outbreak (Fig. 1-4) (36). It is thought that ZIKV-induced immune responses trigger

immunopathological effects on peripheral nerves, resulting in GBS (33). ZIKV-induced GBS, however, appears to be transient with the majority of affected individuals recovering though the mechanism of resolution remains unclear (35).

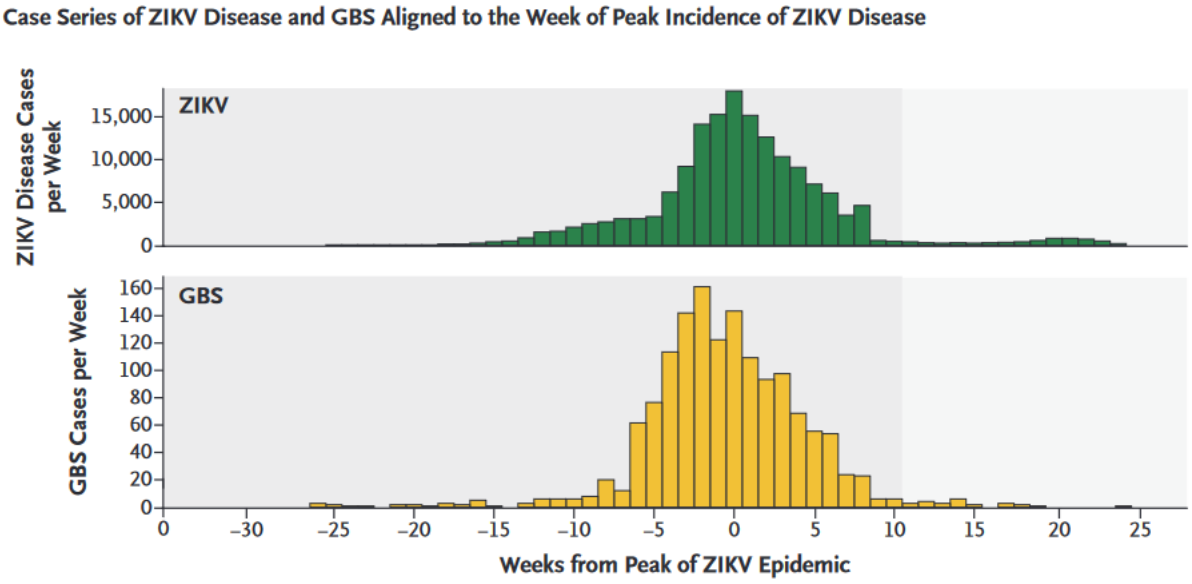


Fig. 1-4 Weekly incidence of reported ZIKV infection (top) and GBS cases (bottom) aligned to the week of peak ZIKV infection across 7 regions. Image adopted from dos Santos et al., 2016 (36).

The most striking disease manifestation associated with ZIKV infection was widely reported during the 2015 outbreak, which arises as a consequence of *in utero* infection particularly during the first trimester of pregnancy (Fig. 1-5) (22, 37). Vertical transmission of ZIKV during pregnancy can result in congenital ZIKV syndrome (CZS) (22, 38–41). CZS encompasses a wide array of clinical manifestations ranging from congenital abnormalities, including microcephaly, to fetal demise (42). In the majority of CZS cases, viral RNA and infectious virus can be isolated from the amniotic fluid, placenta, and fetal tissues, including the brain (18, 22, 23, 38, 43). The presence of replicating ZIKV in the fetal brain and the associated brain damage indicate that ZIKV is neurotropic. Indeed, *in vitro* studies have demonstrated that ZIKV preferentially infects

neural progenitor cells (NPCs) and can induce cell death of NPCs, impairing fetal neurodevelopment and contributing to microcephaly (44–46). The cellular preference for NPCs may explain why severe cases of CZS, like microcephaly, are less common when ZIKV infection occurs during the second or third trimesters of pregnancy when NPCs are sparse. Despite the absence of overt congenital abnormalities at the time of birth, infants and children who were exposed to ZIKV *in utero* can exhibit neurodevelopmental delays later in life, highlighting the long-lasting impact of ZIKV exposure during pregnancy (47–49).

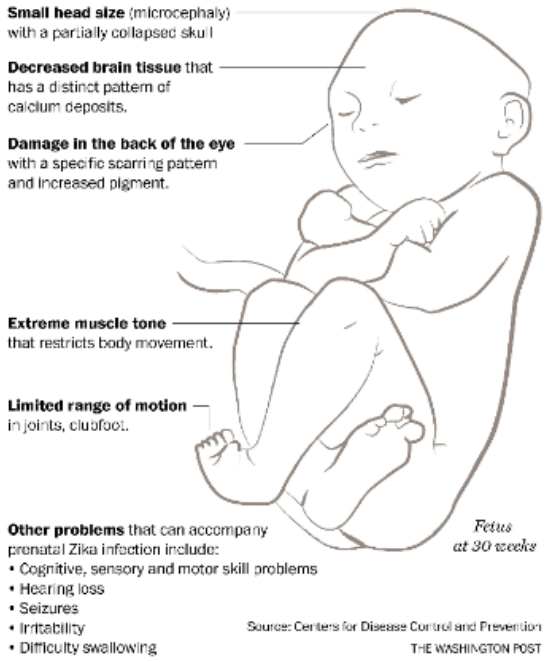


Fig. 1-5 Clinical features of CZS. Clinical manifestations range from microcephaly to cognitive disorders. Image adapted from The Washington Post, 2016 (37).

Given the devastating clinical outcome of *in utero* ZIKV infection, there is an urgent need for the development of effective therapeutics and/or vaccines to combat future ZIKV epidemics. Currently, there are no clinically approved vaccines or therapeutics for preventing or treating ZIKV infection (32). Vaccine design and development of anti-ZIKV drugs will have to consider both the healthy and pregnant populations, the fetus, and potential neurological side effects.

## 1.3 ZIKV biology

### 1.3.1 ZIKV life cycle

ZIKV infection begins upon binding to receptors on host cells (50, 51). Members of the T-cell immunoglobulin domain and mucin domain (TIM) and TAM (tyrosine-protein kinase receptor 3 (Tyro3), AXL, and Mer tyrosine kinase (MerTK)) receptor families, such as AXL, Tyro3, and TIM1, and the glycosaminoglycan dendritic cell-specific intracellular adhesion molecule-3-grabbing non-integrin (DC-SIGN) have been identified as putative ZIKV receptors (52–54). However, cells lacking these receptors remain susceptible to ZIKV infection, suggesting that ZIKV can utilize a wide array of host proteins or glycans as entry receptors (53, 55). Indeed, the dependency on AXL and TIM1 for ZIKV infection appears to be cell type-specific as antibody-mediated blockade of AXL abolished ZIKV infection in astrocytes and microglial cells but not in NPCs (53).

Binding of ZIKV to its cognate receptors leads to virion internalization via clathrin-mediated endocytosis (50, 51, 56). Acidification of endosomes induces conformational changes in the envelope protein to expose the fusion loop, mediating viral fusion with the endosomal membrane and release of the viral genome into the cytoplasm (50, 51). Since ZIKV is a positive-sense single-stranded RNA virus, its genome can be read as messenger RNA (mRNA) by the host translational machinery and be translated into a single polyprotein that is subsequently processed by host and viral proteases (50, 57). The translated viral proteins form replication complexes within vesicle packets located in the endoplasmic reticular (ER) membranes and initiate *de novo* genome replication (50, 57). During genome replication, negative-sense RNA is generated from the positive-

sense RNA genome and serves as a template for new positive-sense RNA that can then be translated or packaged into virions (50, 58). Synthesis of the negative-sense RNA generates a double-stranded RNA (dsRNA) replication intermediate (50, 58). Virion packaging or assembly takes place in the ER, budding into the ER lumen and producing immature virions (50). The immature virion traffics through the Golgi where changes in the pH induce conformational changes in the viral protein precursor membrane (prM) to expose its furin protease cleavage site (50, 59). Cleaved prM remains associated with the viral envelope protein to prevent premature fusion with endosomal membranes as the immature virion exits the cell (51, 59). Upon release of virions into the extracellular space, the neutral pH leads to the release of cleaved prM from immature viral particles, generating infectious virions that can initiate subsequent rounds of infection (50).

As ZIKV infection is predominantly transmitted via mosquito bites, cells in the skin are the first targets for ZIKV infection (54, 60). Studies have identified CD14+ CD16+ monocytes as the main ZIKV cellular targets in the blood and Hofbauer cells (placental macrophages) as a target of ZIKV infection in the female reproductive organs, which can serve as Trojan horses to disseminate ZIKV to other tissues and to facilitate vertical transmission of ZIKV (43, 61, 62). As such, ZIKV displays broad tissue tropism with cellular targets identified in the brain, eyes, blood, placenta, and reproductive organs (Fig. 1-6) (32, 42).

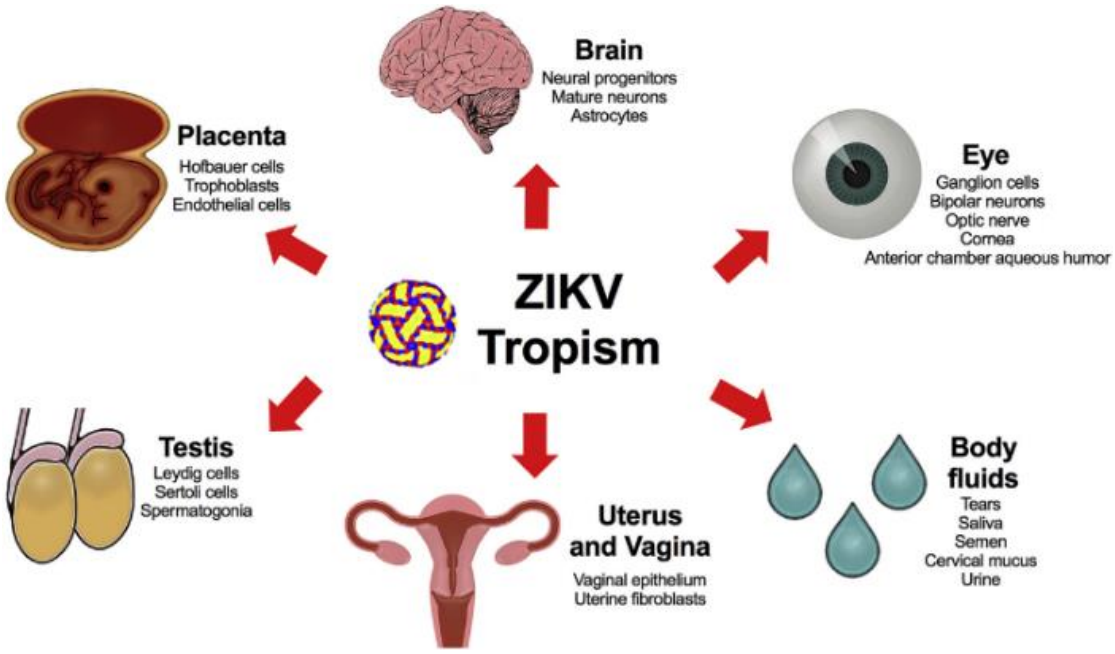


Fig. 1-6 Tissue and cellular tropism of ZIKV. ZIKV has been detected in various tissues and cell types in infected humans and mice, highlighting its broad tissue tropism. Image adopted from Miner and Diamond, 2017 (42).

### 1.3.2 ZIKV genome

The ZIKV genome is approximately 11 kilobases in length, comprising of a single open reading frame flanked by 5' and 3' untranslated regions (UTRs) (Fig. 1-7) (57, 63, 64). The viral genome contains a methylated cap upstream of the 5' UTR and lacks a polyadenylated (polyA) tail downstream of the 3' UTR (57, 65). Both the 5' and 3' UTRs contain secondary RNA structures that play important roles in 5' capping, initiation of viral translation and replication, and generation of subgenomic flavivirus RNAs (sfRNAs) (57, 65, 66).

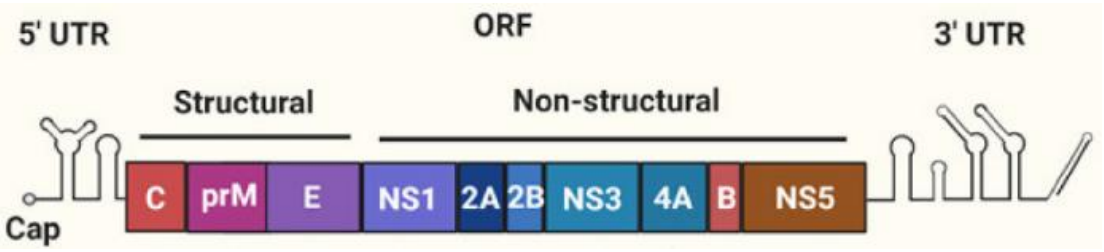


Fig. 1-7 Schematic of the ZIKV genome. The ZIKV genome is flanked by highly structured 5' and 3' UTRs. It has a methylated cap upstream of the 5' UTR and lacks a polyA tail at the 3' end. Image adapted from Coldbeck-Shackley et al., 2020 (63).

Generation of the 5' cap on the flavivirus genome requires the conserved adenosine and guanosine nucleosides at positions +1 and +2 of the genome and stem loop A (SLA) in the 5' UTR (67, 68). The flavivirus 5' cap is composed of the cap0 and cap1 structures; cap0 comprises of a guanosine nucleoside attached to the adenosine nucleoside at position +1 and methylation of the nitrogen at position 7 of the guanosine nucleoside, while the cap1 structure involves methylation of the ribose 2'-oxygen of the adenosine nucleoside at position +1 (Fig. 1-8) (65, 67). Biochemical studies have demonstrated that the cap0 N7-methylation reaction occurs prior to the cap1 2'-O methylation reaction (69). The 5' SLA is required for N7-methylation of the cap0 structure but not for 2'-O methylation (68). The 5' cap allows the viral genome to mimic host mRNAs, enabling translation of the viral genome in a cap-dependent method (57, 65). As such, flaviviruses deficient in the cap0 structure exhibit defective viral translation initiation (69). Additionally, the flavivirus 5' cap camouflages the viral genome from the host antiviral effectors interferon (IFN)-induced protein with tetratricopeptide repeats (IFITs) that recognize RNA lacking 2'-O methylation to block translation (70, 71). Studies with 5' cap-deficient flavivirus mutants have demonstrated that these mutants

exhibit impaired replication kinetics and are attenuated *in vitro* and *in vivo* compared to wild-type (WT) 5’ capped viruses (70, 72, 73).

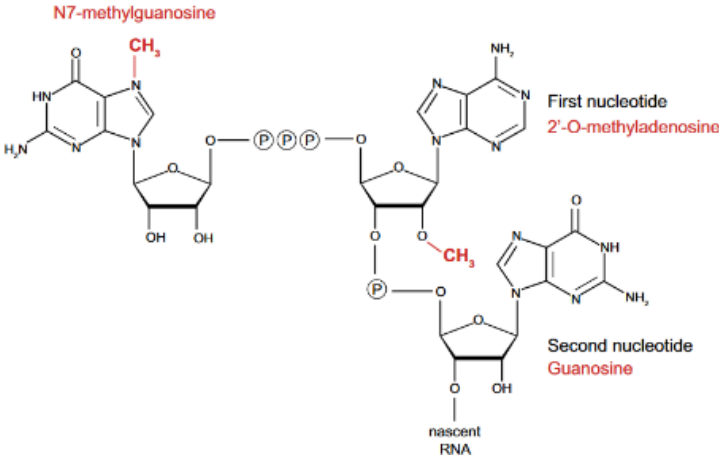


Fig. 1-8 Structure of the flavivirus 5’ cap. The flavivirus 5’ cap consists of cap0 (N7-methylguanosine) and cap1 (2’-O-methyladenosine) structures. Image adopted from Ruggieri et al., 2021 (67).

Initiation of flavivirus genome replication and synthesis of the negative-sense RNA template are also dependent on key secondary structures in the 5’ and 3’ UTRs. The viral polymerase binds to 5’ SLA to induce formation of a circularized panhandle structure that allows the transfer of the viral polymerase from SLA to the conserved 3’ stem loop (3’ SL) in the 3’ UTR (Fig. 1-9) (57, 65, 74). Binding of the polymerase to SLA disrupts the conformation of the 5’ upstream AUG region (UAR)-flanking stem (UFS), facilitating the transfer of the viral polymerase from SLA to the 3’ SL (75). The conformational change of the UFS serves as a switch between polymerase recruitment and circularization of the viral genome for negative-sense RNA synthesis (75). Additionally, recruitment of the viral polymerase to SLA and subsequent genome circularization inhibit viral translation, prompting a switch from translation to replication of the viral genome (76). Complementary cyclisation sequences present in the UTRs promote their hybridization to circularize the viral genome and facilitate long range RNA interactions (57, 65, 77, 78). The UARs located upstream of the polyprotein start codon and in the 3’ SL also contribute to genome circularization (57, 78). Circularization of the

viral genome allows the viral polymerase to utilize the AG dinucleotide at the 5’ end of the genome as a primer for negative-sense RNA synthesis as the 3’ terminus of the viral genome ends with a CU dinucleotide (57). The 3’ terminal CU dinucleotide is essential for flavivirus replication as mutations of the penultimate C and terminal U completely abrogate and significantly inhibit replication, respectively (79). During viral genome replication, levels of the positive-sense RNA are higher than those of the negative-sense template (80). The discrepancy in the abundance of positive- and negative-sense RNA is due to the increased affinity of the viral polymerase for the 3’ end of the negative-sense RNA compared to the 3’ UTR of the positive-sense genome (81). As such, the increased affinity for the 3’ end of the negative-sense RNA results in the accumulation of higher levels of positive-sense RNA.

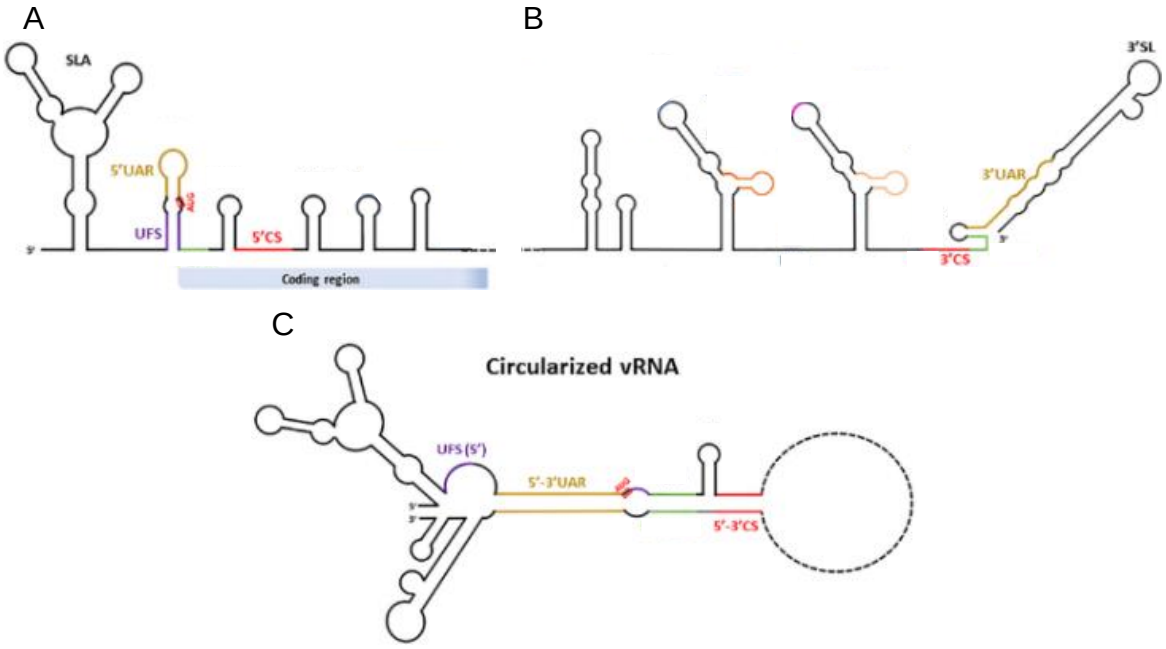


Fig. 1-9 Schematic of the secondary RNA structures in (A) the 5’ and (B) 3’ UTRs. Secondary structures and sequences involved in viral replication and genome circularization are annotated. (C) Schematic depicting the circularized flavivirus genome during genome replication. Image adapted from Mazeaud et al., 2018 (57).

In addition to their role in genome replication, the structural elements in the 3' UTR are also involved in the synthesis of sfRNAs during flavivirus infection (66, 82). sfRNAs are non-coding RNAs that are generated when the 5'-3' host exoribonuclease XRN1 stalls on the secondary RNA structures in the 3' UTR during degradation of uncapped viral genomes (Fig. 1-10A) (65, 66, 82, 83). The ZIKV 3' UTR contains two XRN1-resistant RNAs (xrRNAs) in stem loops 1 and 2 that result in the generation of two sfRNA species (Fig. 1-10B) (65, 83). Mutations disrupting these structures reduce the abundance of ZIKV sfRNAs, underscoring the importance of these secondary structures in sfRNA synthesis (83). ZIKV sfRNAs were detected during infection of human and NHP cell lines, mosquito cells, and mouse neurons, indicating that the generation of these non-coding RNA species occurs across many host species (83). ZIKV sfRNAs have been demonstrated to enhance viral replication *in vitro* and *in vivo* and have been implicated in mediating ZIKV disease; ZIKV sfRNA-deficient mutants are attenuated *in vitro* and *in vivo* and exhibit less efficient vertical transmission and infection of fetal brains in IFN α/β receptor (IFNAR) knockout (KO) mice (84).

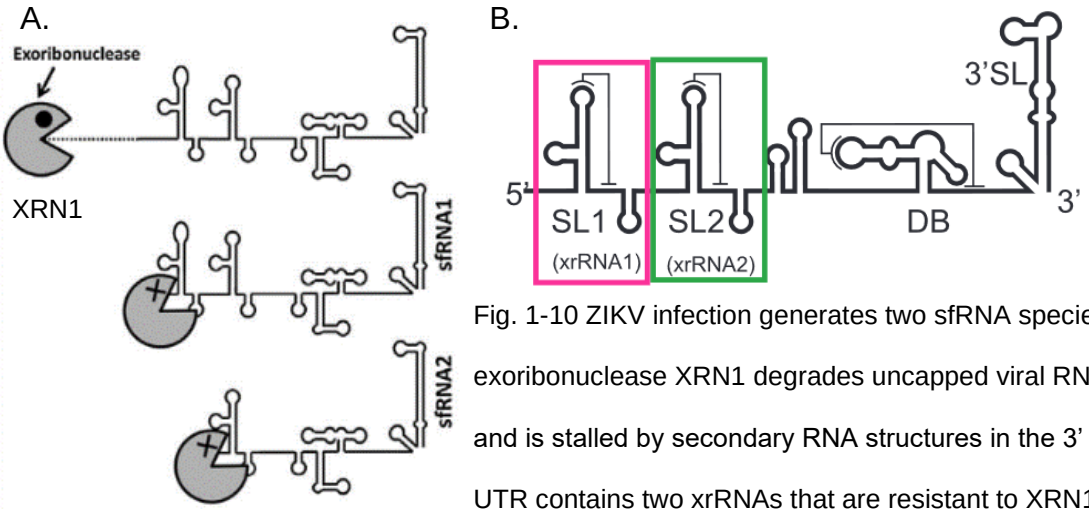


Fig. 1-10 ZIKV infection generates two sfRNA species. (A) Host exoribonuclease XRN1 degrades uncapped viral RNAs in a 5'-3' manner and is stalled by secondary RNA structures in the 3' UTR. (B) ZIKV 3' UTR contains two xrRNAs that are resistant to XRN1 degradation. Stalling of XRN1 at these xrRNAs generates sfRNAs. Image adapted from Göertz et al., 2018 and Akiyama et al., 2016 (65, 83).

Located between the highly structured 5’ and 3’ UTRs is the ZIKV single open reading frame (64, 85). The ZIKV genome is translated as a polyprotein that is cleaved co- and post-translationally by host and viral proteases into three structural proteins (capsid (C), prM, and envelope (E)) and seven non-structural (NS) proteins (NS1, NS2A, NS2B, NS3, NS4A, NS4B, and NS5), leaving behind a transmembrane anchored capsid and a 2K linker (Fig. 1-11) (64, 85).

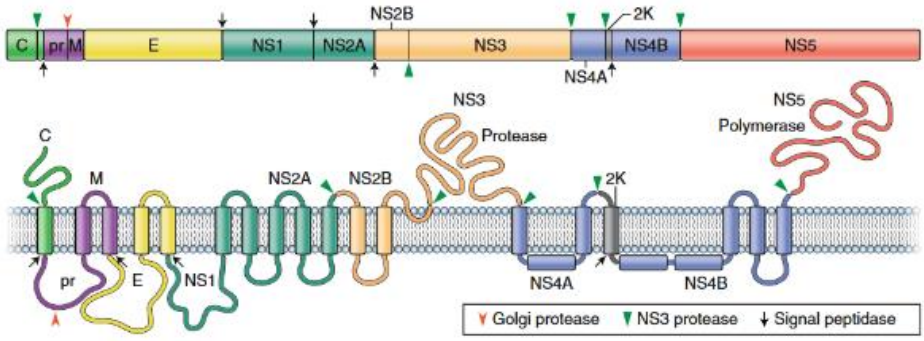


Fig. 1-11 Schematic of the flavivirus genome with the polyprotein cleavage sites indicated. Polyprotein processing takes place co- and post-translationally. Polyprotein cleavage is carried out by the viral protease in the cytoplasm, host signal peptidase in the ER lumen, and host furin protease in the Golgi. Image adopted from Pierson and Diamond, 2020 (85).

### 1.3.3 ZIKV structural proteins

The ZIKV genome encodes three structural proteins: C, prM, and E. prM consists of the pr peptide and the membrane (M) protein and is only present as prM on the surface of immature non-infectious virions (51, 59, 86). The surface of the immature virion consists of 60 trimeric prM:E heterodimer spikes, and the immature virion is approximately 60 nanometers (nm) in diameter (87). Mature flavivirus virions are smaller than their immature counterparts, measuring approximately 50 nm in diameter (51, 59). The host-derived viral membrane on mature particles is surrounded by 180 copies each of the M and E proteins with the M proteins under a layer of E proteins (50,

51, 59, 88). The E proteins are arranged in antiparallel dimers, forming a herringbone pattern on the virion surface, and lie flat against the viral membrane, creating a smooth exterior (85, 88, 89). Within the viral particle, 60 C homodimers coat the viral genome, forming the nucleocapsid core (51, 58, 59, 90).

*Capsid*

The C protein is composed of a charged N-terminal loop and five α-helices that make up the transmembrane domain (90). The fifth α-helix directly precedes prM and serves as a signal peptide to translocate prM through the ER membrane into the ER lumen (90). During polyprotein processing, the C protein is cleaved between the amino-terminal (N-terminal) loop and the transmembrane α-helices by the viral protease and between the fifth α-helix and prM by host signal peptidase (85). Cleavage of the C protein at these two sites leaves the α-helices behind in the ER membrane, generating the membrane-bound anchored capsid. Though largely thought to serve as the translocation sequence for prM, anchored capsid has additionally been demonstrated to stabilize ZIKV structural proteins to prevent their degradation (91). Structural studies of immature ZIKV particles showed that the C protein forms homodimers that serve as bridges between the negatively charged viral RNA and lipid membrane to facilitate viral assembly (90). These C homodimers are located beneath the transmembrane domains of the prM and E proteins and potentially interact with trimeric prM:E heterodimers to attract the nucleocapsid core to sites of budding virions (90).

In addition to its role in genome coating and virion assembly, *in vitro* studies have demonstrated that the C protein disrupts several host processes that contribute to neuropathogenesis. These pathogenic consequences are potentially attributed to the

nuclear localization of the C protein, allowing the viral structural protein to interact with host nuclear proteins (92). Indeed, a study in neurons showed that the nuclear localization of ZIKV C protein induces ribosomal stress and apoptosis of post-mitotic neurons, which may contribute to microcephaly following initial successful neurogenesis (93). Other *in vitro* and *in vivo* studies have provided further evidence of the role of ZIKV C protein in neuropathogenesis. In human induced pluripotent stem cell-derived NPCs, ZIKV C protein was shown to target a component of the nonsense-mediated mRNA decay (NMD) pathway for degradation to enhance ZIKV infectivity (94). Disruption of the NMD pathway has been associated with microcephaly and neurodevelopmental disorders, suggesting that C protein-mediated disruption of this pathway underlies ZIKV-induced microcephaly (94, 95). ZIKC C protein has also been shown to interact with host Dicer protein, which enhances ZIKV neuropathogenicity (96). As Dicer synthesizes critical miRNAs involved in neurogenesis and mediates the RNA interference (RNAi) antiviral pathway, C protein-mediated inhibition of Dicer impairs the RNAi pathway to promote efficient ZIKV replication, but ultimately impairs the production of miRNAs essential for neurogenesis and disrupts brain development (96–98). Together, these studies shed light on the contribution of ZIKV C protein to ZIKV neuropathogenesis.

*prM*

prM is localized in the ER lumen with the two transmembrane domains of the M protein embedded in the ER membrane (59, 85). prM is cleaved by host signal peptidase between anchored capsid and the pr peptide and between the M and E proteins (85). The three copies of prM in the trimeric prM:E heterodimers cap the fusion loop of the E protein to prevent premature fusion of the viral and endosomal

membranes during maturation (50, 51, 87). The pr peptide is cleaved from the M protein during virus maturation in the Golgi under low pH conditions but does not dissociate until the virion is secreted into the extracellular space where the pH is neutral (50, 51). In addition to preventing premature viral fusion, prM plays a critical role in virion assembly, the rearrangement of structural proteins during virion maturation, and virus secretion. Studies have demonstrated that mutations of a conserved region in prM reduce virion secretion as a result of improper prM:E dimerization or of defective viral budding and transport of the virion to the Golgi (99). Moreover, the stem region of prM exhibits a higher affinity for both the lipid membrane and the E protein at low pH, suggesting that the prM stem region can pull the E protein closer to the viral membrane during the maturation process (100). This could mediate the rearrangement of E protein "spikes" into antiparallel E homodimers that lay flat on the viral membrane of the mature virion. Ubiquitination and subsequent proteasomal degradation of prM have also been shown to enhance virion secretion, highlighting the critical role that prM plays in virus secretion (101).

prM has additionally been implicated in ZIKV neurovirulence. *In vivo* studies have identified a mutation in prM at position 17 present in epidemic Asian lineage-derived strains that contributes to severe microcephaly, providing evidence for the role of ZIKV structural proteins in viral pathogenesis (102). Other studies have also demonstrated that prM encoded by African lineage viruses enhances neuroinvasion compared to prM encoded by epidemic Asian lineage-derived strains, suggesting that amino acid (aa) differences in ZIKV prM contribute to ZIKV neurovirulence (103).

*Envelope protein*

The E protein is the major surface protein on flavivirus particles and the dominant antigen recognized by the host immune system (104). The E protein is localized in the ER lumen and contains two transmembrane domains (59, 85). The topology of the E protein is determined by the preceding signal sequence in prM (59). The E protein ectodomain (localized in the ER lumen prior to virion assembly) consists of three distinct domains. Domain I is connected to domains II and III and is involved in E protein conformational changes during membrane fusion; domain II contains the fusion loop involved in pH-dependent fusion of the viral and endosomal membranes; domain III adopts an immunoglobulin-like structure that is thought to mediate cell attachment (59, 86, 105). Structural studies of the E protein in immature and mature virions have revealed the dynamic nature of this viral protein. During flavivirus maturation, the E protein must rearrange from a trimeric form with the fusion loop directed outwards from the viral membrane to a dimeric form lying parallel to the viral membrane (59, 87–89). Upon exposure to the acidic environment of host endosomes, the E dimers must dissociate into monomers to reassociate into the fusogenic trimeric form with the fusion loop directed towards the host endosomal membrane (59, 87, 89). These studies highlight the dynamic nature of the E protein that accommodates the major conformational changes that it must undergo throughout the flavivirus life cycle.

Structural studies of mature ZIKV particles have also identified a glycosylation site at position 154 (88). E protein glycosylation is thought to mediate cell attachment or contribute to disease severity as previously demonstrated for other flaviviruses (106–108). Indeed, glycosylation of the E protein has been shown to enhance cell

attachment, viral pathogenesis, and infectivity (109–111). E protein glycosylation increases viral pathogenicity and facilitates infection in the periphery of IFNAR KO mice, and enhances viral infectivity in *Aedes aegypti* mosquitoes (109, 110, 112). The increase in ZIKV infectivity and pathogenicity may be due to enhanced viral fusion or viral assembly and secretion as E protein glycosylation has been shown to play an important role in the fusion of the viral and endosomal membranes and in the production of virus-like particles (113). However, studies have also demonstrated that non-glycosylated ZIKV strains exhibit enhanced cell attachment, infectivity, and viral pathogenesis compared to glycosylated variants (109–111, 114). Studies in mosquito cells have shown that mutation of the E protein glycosylation site increases viral infectivity and entry into mosquito cells (110, 111). Intracranial infection of newborn Balb/c mice with non-glycosylated ZIKV strains resulted in increased neurovirulence with a higher viral load in the brain (114). These studies suggest that the contribution of E protein glycosylation to viral infectivity and pathogenesis may be dependent on the infection model.

### 1.3.4 ZIKV non-structural proteins

The ZIKV genome encodes seven non-structural proteins: NS1, NS2A, NS2B, NS3, NS4A, NS4B, and NS5 where NS4A and NS4B are connected by a 2K peptide linker (50, 85). As flaviviruses replicate in the cytoplasm of host cells, they must encode all the necessary replication machinery in their genome to carry out their life cycle. The non-structural proteins play critical roles in viral replication directly or indirectly through the remodeling of ER membranes and formation of replication compartments where genome replication takes place (50, 57, 58, 115, 116). Formation of replication

compartments increases the concentration and accessibility of host and viral proteins involved in replication and shields the viral genome from cellular immune sensors to promote efficient genome replication (116, 117).

*NS1*

The signal peptide present in the carboxy-terminus (C-terminus) of the E protein ensures translocation of NS1 into the ER lumen (58, 85). Deletion of NS1 significantly impairs flavivirus replication, indicating that NS1 plays a critical role in genome replication (118–120). NS1 is thought to exist in three distinct pools during infection; a population of NS1 homodimers are involved in genome replication, another population of NS1 homodimers are associated with the plasma membrane, and a third population of NS1 hexamers composed of a trimer of dimers is secreted into the extracellular space (121). Dimerization of NS1 forms two unique surfaces where one surface is hydrophobic and contains a hydrophobic loop that extends outwards and the other is hydrophilic (122–124). The hydrophobic surface and loop of the NS1 homodimer mediate interaction with lipid bilayers, lipid rafts, and liposomes, implicating NS1 in ER membrane remodeling (124, 125). Indeed, expression of NS1 alone in cells was sufficient to induce the formation of ultrastructures resembling replication compartments observed during flavivirus infection (118, 126). NS1-mediated rearrangement of ER membranes is dependent on its localization to the ER lumen and its interaction with the membrane via the hydrophobic surface of NS1 homodimers (118). These studies identify NS1 as a key determinant in flavivirus genome replication through the remodeling of ER membranes to form replication compartments. As NS1 is localized in the ER lumen and genome replication takes place within cytoplasmic replication

compartments, it was unclear how NS1 is involved in genome replication. Studies have revealed that NS1 co-localizes and interacts with dsRNA and other non-structural proteins, suggesting that the interactions with other non-structural proteins allow NS1 to regulate viral replication in the cytoplasm from the ER lumen (120, 126–128). Lastly, NS1 was also shown to directly interact and co-localize with structural proteins to mediate virion production, indicating that NS1 is involved in this process as well (129).

A small fraction of NS1 localizes with lipid rafts on the surface of infected cells (125). NS1 lacks a transmembrane domain to mediate interaction with or insertion into lipid bilayers, but the coding sequence of NS1 is immediately upstream of a glycosyl-phosphatidylinositol (GPI) anchor addition signal present in the hydrophobic domain of the N-terminus of NS2A (130). GPI linkage targets proteins to the cell surface, and addition of GPI to NS1 has been demonstrated to enhance NS1 association with lipid rafts and NS1 expression on the cell surface (125, 130). GPI linkage to NS1 results in signal transduction upon binding of anti-NS1 antibodies, potentially enhancing viral replication and pathogenesis (130).

The hydrophilic surface of NS1 homodimers contains two glycosylation sites (122, 123). NS1 glycosylation enhances NS1 secretion into the extracellular space as treatment with glycosylation inhibitors reduces NS1 secretion (131). NS1 is secreted as a hexamer composed of a trimer of NS1 homodimers held together by weak hydrophobic interactions (131, 132). The hydrophobic surface of NS1 dimers faces inwards, creating a hydrophobic channel in the center of the hexamer, and the polar surface of NS1 dimers faces outwards (122, 124). The hydrophilic face of NS1 homodimers exhibits a greater degree of sequence divergence compared to the

hydrophobic face (123). The diversity of the sequences in the hydrophilic face of NS1 hexamers can elicit distinct immune responses and impart unique interactions with host proteins. The central channel of NS1 hexamers binds to lipids, which promotes NS1 secretion as inhibition of lipid biosynthesis reduces NS1 secretion but not the total intracellular levels of NS1 (132). During flavivirus infection, NS1 is secreted into the bloodstream at high levels and has been demonstrated to enhance mosquito infectivity though NS1 secretion has been shown to be dispensable for genome replication and virion production (129, 133–135). NS1 secretion has additionally been implicated in flavivirus disease by disrupting cell-surface glycosaminoglycans (135–138). Disruption of cell-surface glycosaminoglycans has been shown to increase the permeability of endothelial cells *in vitro* and of placental villous explants *ex vivo* and induce vascular leakage in the brain *in vivo* (136, 138). Mechanistically, ZIKV NS1 binds to cell surfaces to trigger endocytosis in a glycosylation-dependent manner, leading to endothelial dysfunction (137). The ability of ZIKV NS1 to increase endothelial permeability and cause vascular leakage in the brain and placenta may contribute to ZIKV vertical transmission and pathogenesis.

*NS2A*

ZIKV NS2A is a hydrophobic membrane-associated protein anchored in the ER by one transmembrane domain (139). The N-terminus of NS2A localized in the ER lumen is cleaved by host signal peptidase while the cytoplasmic C-terminus is cleaved by the viral protease (85, 140). Immunofluorescence and cryo-electron microscopy analyses of cells infected with Kunjin virus revealed that NS2A co-localizes with dsRNA and other non-structural proteins at sites of genome replication, suggesting that NS2A is

part of the flavivirus replication complex and is involved in flavivirus replication (141). Indeed, studies of NS2A have demonstrated that it plays a critical role in viral genome replication and virion production (139, 140, 142–148). Studies of Dengue virus (DENV) and ZIKV NS2A have revealed that there are two distinct pools of NS2A during infection where one set of NS2A is involved in genome replication and the other in virion assembly (139, 142). Direct interactions between NS2A and the viral polymerase provide further evidence for the role of NS2A in genome replication (141).

NS2A has also been demonstrated to facilitate virion assembly and production (145, 148, 149). A mutation at position 59 of NS2A abolished virion production and disrupted ER membrane rearrangements, suggesting that the inability of NS2A to rearrange ER membranes impairs virion assembly (145). However, as mutations at other sites of NS2A also abrogate virion production without affecting ER membrane rearrangement, disruption of ER membrane remodeling is unlikely the only mechanism underlying NS2A-mediated virion assembly (139, 142–144, 147–149). Several studies have shown that NS2A interacts with NS3, the 3’ SL, and the structural proteins and implicated these interactions as critical for virion production (141, 147–149). NS2A recruits both the C-prM-E polyprotein and NS3 to sites of virion assembly for polyprotein processing to produce the structural proteins necessary for virion formation (148, 149). NS2A additionally binds to the 3’ SL to recruit nascent vRNA from replication compartments to sites of virion assembly for nucleocapsid formation, which can then be packaged into immature virions (148, 149). These findings provide mechanistic insight into the role of NS2A in virion assembly and production.

In addition to its role in viral genome replication and virion assembly, NS2A has been identified as a viroporin (150, 151). Overexpression of NS2A in bacteria and mammalian cells revealed that NS2A alters membrane integrity (150, 151). Studies of a West Nile virus (WNV) NS2A mutant demonstrated that cells infected with the mutant exhibited less apoptosis compared to cells infected with WT virus though WT NS2A alone does not induce apoptosis (152). Together, these results suggest that NS2A may cooperate with other viral proteins to function as a viroporin to induce apoptosis.

*NS2B*

NS2B is an integral protein localized in the ER with cytoplasmic N- and C-termini (153, 154). Cleavage of NS2B from the viral polyprotein is mediated by the viral protease in *cis* in an autolytic fashion (155). NS2B serves as a cofactor for the viral protease NS3, forming the NS2B/3 complex, and is necessary for NS3 proteolytic activity (156–160). Structural studies of the NS2B/3 complex revealed that NS2B wraps around the viral protease domain and completes the viral protease substrate-binding site (161, 162). Mutations and large deletions within NS2B have been demonstrated to abolish the proteolytic activity of the viral protease (157, 158). A 40 aa stretch within the hydrophilic region of NS2B is critical for viral protease activity where expression of this region alone was sufficient to activate NS3 protease activity (157, 163, 164). The aa residues in this region are involved in NS2B/3 complex formation since mutations in this region impact the formation of the NS2B/3 complex, which impairs NS3 proteolytic activity (163). This hydrophilic region in NS2B is flanked by hydrophobic regions that function to anchor the NS2B/3 complex in membranes (153). Insertion of the NS2B/3 complex into the membrane occurs co-translationally and enhances the proteolytic

activity of the viral protease (153). As such, the hydrophilic region of NS2B interacts with NS3 to form the NS2B/3 complex while the hydrophobic regions retain this complex in the ER membrane, allowing NS2B to serve as the cofactor for the viral protease.

NS2B co-localizes with dsRNA and other non-structural proteins, including the viral protease, within membranous structures housing sites of viral genome replication, suggesting that NS2B may additionally be involved in replication (128). Indeed, mutations within either the hydrophilic or hydrophobic regions of NS2B significantly impair viral replication and virion assembly without affecting viral protease activity (163, 165). The hydrophobic regions of NS2B are critical for proper localization of NS3 to the ER as NS3 mislocalizes to the mitochondria in the absence of these hydrophobic regions in NS2B (159). These results indicate that NS2B facilitates genome replication by properly recruiting NS3 to sites of viral replication.

Like NS2A, NS2B is a hydrophobic protein containing a hydrophilic region that also functions as a viroporin. Expression of NS2B in bacteria has demonstrated that NS2B localizes to bacterial membranes and permeabilizes bacterial membranes and erythrocyte ghost membranes, suggesting that NS2B may mediate virus-induced cytopathic effects (CPE) (151, 166). Previous work has shown that NS2A alone is incapable of inducing apoptosis, suggesting that other viral proteins may contribute to virus-induced CPE (152). Since NS2B was identified as another viroporin, NS2A and NS2B may potentially work together to mediate virus-induced cell death.

*NS3*

NS3 is a cytoplasmic protein that undergoes self-cleavage at the NS2B-NS3 and NS3-NS4A junctions (155, 156, 158). It is recruited to the ER by NS2B where it co-

localizes with other non-structural proteins and dsRNA for genome replication (128, 159). The N-terminus of NS3 adopts a chymotrypsin-like fold and encodes protease activity, functioning as the viral serine protease for polyprotein processing (156, 162, 167–169). NS3 cleaves at a site downstream of two consecutive basic residues like other serine proteases, and its proteolytic activity is dependent on the NS2B cofactor and a catalytic triad (156–160, 168, 169). Studies using protease-dead mutants underscore the importance of NS3 protease activity in viral replication as cells infected with these mutants are unable to generate infectious viruses likely due to the absence of cleaved viral factors required for genome replication and virion assembly (169).

In addition to its protease activity, NS3 also exhibits RNA triphosphatase (RTPase), helicase, adenosine triphosphatase (ATPase), and nucleotide triphosphatase (NTPase) activities (167, 170–175). NS3 RTPase activity removes the terminal phosphate from tri-phosphorylated ends of RNA, implicating this viral protein in removal of the terminal phosphate from the 5’ end of the viral genome for capping (172). NS3 helicase activity unwinds the secondary structures in the UTRs and the double-stranded replication intermediate to release newly synthesized viral genome from the negative-sense template (58). Structural studies of the helicase domain revealed three distinct regions responsible for NTPase activity, RTPase activity, and RNA binding (171). The catalytic residues for NTPase and helicase activities are located within the N-terminus of NS3 near the protease catalytic triad (167). NS3 helicase activity has been shown to require adenosine triphosphate (ATP) hydrolysis and the presence of divalent cations (172, 173, 176). NS3-mediated ATP hydrolysis is carried out by its ATPase and NTPase functions, which are enhanced in the presence of single-stranded RNA (173, 174). NS3

ATPase and NTPase activities are dependent on a cluster of basic aa residues in the helicase domain (167, 177). Studies of DENV and ZIKV NS3 have also revealed that NS3-mediated NTPase, RTPase, and helicase activities are enhanced in the presence of the viral polymerase, NS5 (170, 175, 177). Studies in cells infected with Japanese encephalitis virus provided evidence of a direct interaction between NS3 and NS5 (178). Together, these studies establish NS3 as a multi-functional protein involved in different stages of the viral life cycle and provide evidence for synergistic interactions between viral non-structural proteins.

*NS4A*

NS4A is an integral membrane protein localized in the ER with cytoplasmic N- and C-terminal tails generated by NS3-mediated cleavage (179, 180). The C-terminal 2K peptide in NS4A serves as a signal sequence for correct insertion of downstream NS4B into the ER lumen and for cleavage by host signal peptidase (180). NS3-facilitated cleavage of NS4A at the NS4A-2K junction must occur prior to host signal peptidase-mediated cleavage at the 2K-NS4B junction to generate the mature NS4A protein (180). In DENV-infected cells, the predominant NS4A species lacks the 2K peptide (179). During infection, NS4A co-localizes with dsRNA and other structural and non-structural proteins within virus-induced membrane structures, indicating that NS4A may be involved in viral replication (141, 179). Studies of WNV and DENV NS4A have demonstrated that NS4A is responsible for inducing membrane rearrangements to house replication complexes though the contribution of the 2K peptide in this process is debatable (179, 181, 182). Roosendaal et al. showed that the 2K peptide is required for NS4A to localize to the ER to mediate ER membrane rearrangements, whereas two

other studies demonstrated that the 2K peptide inhibits NS4A-mediated membrane remodeling (179, 181, 182). These studies, however, clearly establish that NS4A contributes indirectly to viral replication by inducing ER membrane rearrangements. Furthermore, NS4A directly interacts with vimentin, a component of the host cytoskeleton, through its N-terminal cytoplasmic tail to establish viral replication compartments (183). These findings demonstrate that NS4A sets up viral replication compartments to facilitate genome replication.

Oligomerization of NS4A has also been shown to be critical for viral replication (184, 185). NS4A oligomerization is mediated by one of its transmembrane domains, and mutations within this region abolish NS4A oligomerization, destabilizing NS4A and attenuating viral replication (184, 185). Hence, NS4A oligomerization likely stabilizes NS4A to promote NS4A-driven ER membrane rearrangements that are critical for replication. Additionally, a patch of negatively charged residues located in the N-terminal cytoplasmic tail of NS4A allows NS4A to serve as a cofactor for the NS3 helicase by reducing ATP consumption during RNA unwinding (186). By decreasing the ATP requirements for the viral helicase, NS4A can help sustain RNA unwinding during conditions of low ATP. These findings demonstrate that interactions between NS4A and itself or other viral proteins play a critical role in viral replication.

Several studies have additionally implicated NS4A in viral pathogenesis. Studies in epithelial cells demonstrated that NS4A activates autophagy to promote cell survival to enhance viral replication (187). Similarly, studies of ZIKV infection in neural stem cells revealed that NS4A induces autophagy, which subsequently impairs neurogenesis (188). These findings suggest that flaviviruses activate autophagy to prevent apoptosis

of infected cells to sustain viral replication, but consequently, impairs neurogenesis in infected neural stem cells, which may contribute to microcephaly during *in utero* ZIKV infection. Studies of ZIKV infection in a *Drosophila* model identified a key interaction between NS4A and the host protein ANKLE2, which can harbor mutations that cause microcephaly in humans (189). This study revealed that the interaction between NS4A and ANKLE2 induces microcephaly, driving ZIKV disease (189). Together, these studies demonstrate that NS4A modulates cellular processes to create a host environment conducive to viral replication and mediates interactions with host proteins that contribute to ZIKV pathology.

*NS4B*

NS4B is an ER integral membrane protein with its N-terminal tail localized in the ER lumen and its C-terminal tail in the cytoplasm (190). Integration of NS4B into the ER membrane is independent of the 2K peptide and is instead mediated by its transmembrane domains near the C-terminal region (190). Mature NS4B is generated upon cleavage at the 2K-NS4B and NS4B-NS5 junctions by host signal peptidase and NS3, respectively (156, 180). NS4B co-localizes with dsRNA and other viral proteins, including NS3, at sites of genome replication, implicating NS4B in viral replication (182, 190–192). Indeed, studies of flavivirus NS4B have demonstrated that NS4B rearranges ER membranes and interacts with NS3 and NS4A to facilitate genome replication (182, 191–194). The cytosolic loop of NS4B directly interacts with the NS3 helicase domain to dissociate the viral helicase from single-stranded RNA, shifting NS3 from single-stranded RNA substrates to dsRNA substrates to promote dsRNA unwinding (191, 192, 194). Heterodimerization of NS4B with NS4A is important for viral replication though the

underlying mechanism remains undefined (193). These studies demonstrate that NS4B plays a crucial role in viral genome replication.

NS4B also modulates cellular processes to promote viral replication. ZIKV NS4B has been shown to induce autophagy to enhance viral replication; consequently, neurogenesis in fetal neural stem cells and neurosphere formation are disrupted, contributing to ZIKV pathogenesis (188). Studies of DENV and ZIKV have also identified mutations in NS4B that enhance viral replication and significantly increase viral pathogenesis in mice (195–197). The mutations identified in each of these studies were unique though, interestingly, two of these mutations enhanced viral replication specifically in mammalian cells but not in mosquito cells (195, 197). Although the underlying mechanisms remain unclear, these results suggest that NS4B may be important in maintaining and regulating efficient replication in both the mammalian host and the mosquito vector.

*NS5*

NS5 is the largest protein encoded by flaviviruses and is localized in the cytoplasm and nucleus in the case of ZIKV (58, 198, 199). Cleavage at the NS4B-NS5 junction is mediated by the NS2B/3 protease complex in the cytoplasm (156). Crystal structures of full-length NS5 revealed that this viral protein consists of an N-terminal methyltransferase (MTase) and a C-terminal RNA-dependent RNA polymerase (RdRp) domain connected by a linker (200). Functional studies of NS5 proteins revealed that NS5 exhibits RNA capping activity in the presence of NS3 and RdRp activity in the absence of cellular and viral factors (201–203). As genome replication takes place at the ER membrane, cytoplasmic NS5 must localize to the ER (50, 57). Through its

interaction with NS3, cytoplasmic NS5 localizes to the ER for viral genome replication (58). Interactions between NS5 and other non-structural proteins have also been identified, indicating that flavivirus non-structural proteins work closely with NS5 during genome replication (141). Indeed, previous studies have demonstrated that NS5 directly interacts with NS3 to enhance NS3 NTPase, RTPase, and helicase activities (170, 175, 177, 178). NS5 has also been shown to interact with NS2A and NS4A though the consequences of these interactions remain unclear (141). However, as NS2A and NS4A are implicated in membrane rearrangements, their interactions with NS5 may regulate ER membrane remodeling (145, 179, 181, 182). NS2A also plays a critical role in shuttling the nascent RNA to sites of virion assembly; as such, the interaction between NS2A and NS5 may couple genome replication to virion assembly (148, 149). Additionally, NS5 binds to the secondary structures in the UTRs to regulate the transition between genome translation and replication and to circularize the viral genome for negative-sense RNA synthesis (57, 76–78). Together, these findings highlight that NS5 plays multiple crucial roles during viral replication in enzymatic-dependent and -independent manners.

Structural studies of full-length ZIKV NS5 or the MTase domain alone indicated that ZIKV MTase structurally resembles that of other flaviviruses and other known MTases (204–207). The MTase domain adds a cap1 structure to the 5’ end of the viral genome through its guanosine triphosphatase (GTPase), guanylyltransferase, and N7- and 2’O-methylation activities (69, 203, 204, 208). The MTase domain contains a guanosine triphosphate (GTP) binding site that hydrolyzes GTP and binds to guanosine-capped RNAs (204, 206, 209). The GTPase activity of the MTase domain is

stimulated by NS3 RTPase activity and exhibits specificity for RNA substrates starting with an adenosine nucleoside as is the case for the viral genome (203). GTP hydrolysis releases a pyrophosphate moiety and produces a covalently linked guanosine monophosphate- (GMP) NS5 intermediate where the GMP is subsequently transferred onto the diphosphorylated adenosine residue that is generated by NS3 RTPase activity (203). NS5 GTPase activity is also enhanced by oxidative stress induced late in infection, suggesting that there is an underlying mechanism regulating genome capping and replication (210). Following addition of the GMP residue to the 5' end of the viral genome, NS5 carries out two sequential methylation steps. The MTase domain transfers a methyl moiety to the nitrogen at position 7 of the guanosine residue followed by methylation of the ribose 2'-oxygen of the adenosine residue at position +1 (69, 208). NS5 MTase activity is dependent on a KDKE catalytic motif; the aspartate (D) residue is necessary for its N7 MTase activity while the entire KDKE motif is required for its 2'O-MTase activity (69, 204, 208). NS5 exhibits 2'O-MTase activity for RNA substrates with a cap0 structure only and has a much higher binding affinity for capped RNA sequences that begin with an AG sequence, such as the flavivirus genome (204, 209). N7 methylation of the 5' end of the viral genome is essential for virus viability, whereas viruses deficient in 2'O-MTase activity are attenuated (70, 72, 73, 208).

Crystal structures of the ZIKV RdRp domain revealed that the RdRp domain adopts a right-hand structure similar to that observed for other flaviviruses (207, 211). The only significant difference in the RdRp structure between ZIKV and other flaviviruses lies within the priming loop, which regulates RNA binding and polymerization (211). Flavivirus RdRp synthesizes RNA in a primer-independent

manner (50, 57). The RdRp catalytic site comprises of a GDD motif, and mutations within this active site abolish RdRp activity (201). NS5 polymerase activity can be regulated by post-translational modifications; specifically, phosphorylation of ZIKV NS5 near the catalytic GDD motif by the host kinase Akt reduces polymerase initiation activity, suggesting that phosphorylation of ZIKV NS5 can have an antiviral effect (212). NS5 RdRp activity can additionally be modulated by interactions with the MTase domain. The two enzymatic domains of NS5 are connected by a linker, allowing the two distinct domains to interact with each other (200, 213). The interdomain linker and the interdomain interactions are critical for viral replication as viruses containing mutations within the linker and chimeric viruses with heterologous MTase and RdRp domains exhibit significantly impaired replication (200, 214). The MTase domain stimulates RdRp initiation and elongation activities by enhancing the affinity of RdRp for RNA substrates and the initiating ATP nucleotide, and by increasing the catalytic activity of RdRp (207, 215, 216). Moreover, NS5 dimerization can also regulate RdRp and MTase activities. Crystal structures of full-length NS5 revealed that NS5 exists stably as a dimer with residues in the MTase domain mediating NS5 dimerization (214, 217). NS5 dimerization impairs RdRp elongation activity, suggesting a potential mechanism in regulating the elongation activity of the polymerase (217). As one of the residues involved in facilitating NS5 dimerization is also involved in GTP binding for RNA capping, high levels of GTP impair NS5 dimerization, thereby possibly regulating NS5 RNA capping and polymerase activities (217). These studies reveal the importance of intramolecular and intermolecular interactions of NS5 in regulating the enzymatic activities of the

MTase and RdRp domains and suggest a functional role of these interactions in modulating NS5 enzymatic activities throughout different stages of the viral life cycle.

A proportion of NS5 of some flaviviruses, including ZIKV, localize to the nucleus (198, 199, 218). Sequence analysis revealed that DENV and ZIKV NS5 contain two nuclear localization sequence (NLS) motifs that drive NS5 nuclear localization (198, 218). These two NLS motifs are distinct where one NLS binds only to importin-β while the other binds to the importin-α/β complex (218). Intriguingly, in the case of DENV NS5, only one NLS motif is functional at a time where binding of importin to one site prevents binding of importin to the other site (218). Furthermore, the binding site for NS3 on NS5 overlaps with the importin-β binding site, leading to competition between these two proteins for NS5 binding (218, 219). Competition for NS5 binding may regulate NS5 localization in infected cells where interactions with NS3 retain NS5 in the cytoplasm to carry out capping and polymerase functions, and interactions with host importins sequester NS5 to the nucleus. Functionally, NS5 nuclear localization is critical for viral replication as it prevents NS5 degradation in the cytoplasm by host proteases and allows the virus to modulate host transcriptional responses (198, 220, 221). Studies of Kunjin virus and ZIKV have demonstrated that NS5 nuclear localization promotes NS5-mediated regulation of antiviral gene expression, dampening the ability of infected cells to mount an antiviral response (199, 220). Studies of DENV NS5 have shown that NS5 sequesters host spliceosome components and increases intron retention in transcripts, such that transcripts of antiviral genes are not properly spliced and expressed, creating a less restrictive cellular environment for viral replication (221). The ability of NS5 to modulate host gene expression is independent of its enzymatic

activities, demonstrating that NS5 additionally regulates the host transcriptional response during infection (221).

NS5 has also been implicated in contributing to ZIKV disease in models of persistence and neurodevelopment. In ZIKV-infected human brain microendothelial cells, NS5 is SUMOylated, which also targets it to the nucleus where it modulates the expression of cell cycle and antiviral genes to promote cell survival and to dampen cellular antiviral responses, respectively (199). Modulation of cell cycle and antiviral gene expression promotes ZIKV persistence in brain microendothelial cells, potentially contributing to ZIKV-mediated neurological disease (199). Further studies have demonstrated that NS5 oligomers interact with NPC cilial bases to induce premature neurogenesis, which impairs brain development as NPCs are not regenerated (222). Thus, ZIKV NS5-mediated premature neurogenesis contributes to ZIKV-induced microcephaly and neurodevelopmental defects. Moreover, expression of ZIKV NS5 in NPCs induces apoptosis, suggesting that NS5-driven apoptosis of NPCs may also impair neurodevelopment during *in utero* infection (223). Together, these studies provide evidence that NS5 modulates cellular processes to create an environment favourable for viral replication and may directly contribute to ZIKV disease.

## 1.4 Comparison of ZIKV lineages

Prior to the 2013 and 2015 ZIKV outbreaks, ZIKV infection predominantly presented as asymptomatic or mild flu-like illness (31, 32). However, during the recent ZIKV epidemics, adult infection with ZIKV was linked to an increased incidence of GBS while *in utero* infection was associated with congenital abnormalities (22, 33, 34, 38, 42). The emergence of severe clinical manifestations that were previously unreported

as a result of ZIKV infection spurred research to delineate how ZIKV has evolved to cause more severe disease. As the recent ZIKV epidemics were fueled by infection with Asian lineage-derived viruses, comparative analyses between African and Asian lineage strains and between pre-epidemic and epidemic Asian lineage viruses have been carried out to investigate how and why Asian lineage-derived epidemic strains are more pathogenic (10, 11, 13).

### 1.4.1 Viral transmission

As ZIKV is primarily transmitted to humans through mosquito bites, lineage-specific differences in the interactions between the mosquito vector and ZIKV may impact the spread of Asian lineage-derived epidemic strains. Comparative studies evaluating the infection, dissemination, and transmission rates of African and Asian lineage viruses in mosquitoes have revealed lineage-dependent differences in these properties. Compared to Asian lineage viruses, African lineage ZIKV strains exhibit higher rates of infectivity, dissemination, and transmission in *Aedes aegypti* and *Aedes albopictus* mosquitoes (224–229). One study, however, demonstrated that African lineage ZIKV strains were less efficient at establishing infection in *Aedes aegypti* mosquitoes than Asian lineage-derived epidemic strains (230). Differences in the experimental methods used may contribute to this discrepancy, but these findings identify differences in the infectivity, dissemination, and transmissivity of distinct ZIKV lineages in the mosquito vector. As African lineage strains generally exhibit greater infectivity, dissemination, and transmissivity in the mosquito vector than Asian lineage variants, these studies suggest that the extent of the outbreaks caused by Asian

lineage-derived epidemic strains is not primarily driven by differences in mosquito-ZIKV interactions.

### 1.4.2 Viral properties

The mechanisms by which Asian lineage-derived epidemic ZIKV strains contribute to severe disease remain unclear. To better understand these underlying mechanisms, studies have comparatively assessed ZIKV isolates from each lineage to characterize their replication properties in mosquito and mammalian cells. They have demonstrated that African lineage viruses replicate faster and to higher titers than Asian lineage viruses in these cell types (227, 230–238). These findings were recapitulated in an *in vivo* pig model where *in utero* infection with an African lineage virus resulted in higher viral titers in the placenta and fetal brains, demonstrating that African lineage viruses replicate to higher levels than Asian lineage strains (239). Moreover, competition assays in mammalian and mosquito cell lines have shown that African lineage strains outcompete epidemic ZIKV variants, indicating that African lineage strains exhibit higher viral fitness in these cell lines (228). These findings also support the observations that African lineage viruses infect and disseminate from mosquitoes better than Asian lineage strains (225–229). However, studies in NPCs and astrocytomas have demonstrated that epidemic strains exhibit enhanced infectivity and replicate faster and to higher levels than African lineage viruses and pre-epidemic Asian lineage variants, though studies in other neuronal cell lines did not support these findings, suggesting that the replicative fitness of ZIKV variants may additionally be cell type-dependent (232–235, 237, 240). Characterization of epidemic and pre-epidemic Asian lineage-derived ZIKV isolates in the same cell line have also yielded conflicting

findings where one study revealed that these isolates replicate similarly while another found that an epidemic strain replicates better than a pre-epidemic strain (241, 242). The discrepancies between these two studies may be due to differences in the source of the virus stocks used. Despite these discrepancies, these results suggest that genetic differences between the two lineages and between epidemic and pre-epidemic Asian lineage isolates may contribute to replicative differences. Studies have implicated genetic differences in the structural proteins as a determinant of viral virulence where a chimeric African lineage virus expressing specific residues of the E protein of an epidemic ZIKV variant was shown to exhibit enhanced viral fusion in the endosome (243). Furthermore, studies have shown that chimeric African lineage viruses expressing the structural proteins of epidemic ZIKV variants exhibit impaired cell attachment, suggesting that sequence differences in the structural proteins affect cell binding (237, 244). Together, these findings reveal lineage-dependent differences in ZIKV replication properties and highlight the replicative differences between epidemic and pre-epidemic Asian lineage-derived strains that may contribute to the severe pathogenesis observed during the recent outbreaks.

Previous studies have additionally identified and characterized several ZIKV genetic determinants of viral replicative fitness. Liu et al. identified four aa substitutions (C protein T106A, prM V1A, NS1 A188V, and NS5 M872V) in emerging ZIKV strains that represent direct reversions to those present in African lineage viruses and enhance viral fitness *in vivo* (245). Substitution of T106A in the C protein and of A188V in NS1 alone in pre-epidemic Asian lineage strains respectively enhance viral infectivity *in vitro* and increase mosquito infectivity and transmissivity (134, 246). Remarkably,

introduction of the valine at position 1 of prM alone in an epidemic ZIKV isolate enhanced *in vivo* pathogenesis, suggesting that the reduction in viral fitness associated with the prM V1A mutation is masked by the other direct aa reversions identified by Liu et al. to enhance the viral fitness of Asian lineage-derived epidemic strains (245, 247). Other mutations within NS1 and NS3 that arose during the recent ZIKV epidemics or represent reversions to aa residues encoded by ancestral Asian lineage ZIKV have been additionally shown to impact infectivity in mosquito and mammalian cell lines, highlighting the impact of genomic differences on viral replicative fitness (247).

### 1.4.3 Viral pathogenesis

*In vitro studies*

*In vitro* studies of ZIKV variants of distinct lineages have shed light on possible mechanisms underlying differential disease severity. African lineage viruses induced more CPE than Asian lineage viruses during infection of various mammalian cell lines, including neuronal and placental cells (46, 226, 231–233, 235–237, 240, 248, 249). The lower rate of cell death observed during infection with Asian lineage viruses suggests that infection with these strains may facilitate survival and persistence in infected cells, whereas the higher CPE induced by African lineage viruses may result in severe fetal or placental damage and subsequent fetal loss instead of congenital abnormalities. However, studies in NPCs and organotypic brain slices from mice with variants from either lineage have observed no differences in the levels of CPE induced upon infection, suggesting that other factors also contribute to lineage-dependent ZIKV pathogenesis (250, 251). Indeed, Rosenfeld et al. demonstrated that neural migration was impaired in organotypic brain slices from mice infected with African and Asian lineage variants,

indicating that ZIKV-induced disruption of neuronal processes contributes to ZIKV neuropathogenesis (250). Similarly, infection of neural stem cells revealed that both ZIKV lineages inhibit neurodevelopment via distinct mechanisms with the African lineage strain inducing cell death and the Asian lineage virus arresting cell cycling (249). Emerging ZIKV variants have also been demonstrated to impair NPC proliferation, migration, and maturation and induce premature NPC differentiation with some studies showing that African lineage variants induce premature NPC differentiation to a greater extent (46, 236, 252). In doing so, ZIKV depletes the NPC pool needed for proper neurodevelopment. Together, these findings suggest that ZIKV generally impairs neurodevelopment, but the lower rate of cell death induced by Asian lineage ZIKV strains allows infected neuronal cells to persist and drive sustained impairment of neuronal functions.

*In vivo studies*

*In vivo* studies of ZIKV infection have built upon results from *in vitro* studies to provide a deeper understanding of ZIKV pathogenesis. However, as immunocompetent mice do not exhibit clinical symptoms upon ZIKV infection, *in vivo* studies of ZIKV have relied on immunocompromised mouse models (253). Using these immunocompromised mouse models, studies have provided evidence for vertical transmission of both ZIKV lineages (224, 254). Comparisons of Asian lineage-derived pre-epidemic and epidemic strains have shown that pre-epidemic variants also cross the maternal-fetal barrier to infect the fetus (241, 255). These results indicate that differences in ZIKV-induced pathogenesis following *in utero* infection likely occur downstream of vertical transmission as both lineages are vertically transmitted but only infection with emerging

Asian lineage viruses has been linked to congenital disease. Infection of embryonic stem cell-derived trophoblasts and IFNAR KO mice has revealed that African lineage viruses cause more structural damage to the placental architecture than Asian lineage variants, suggesting that infection with African lineage strains may result in fetal loss instead (248, 254). Moreover, infection with African lineage variants has shown that they cause higher rates of mortality than Asian lineage strains (103, 224, 226, 227, 233, 254, 256, 257). The higher lethality associated with African lineage ZIKV variants may result in the termination of pregnancy such that any fetal damage caused by *in utero* ZIKV infection is missed. Pre-epidemic and epidemic Asian lineage variants have also been shown to induce fetal resorption and placental damage, with epidemic ZIKV variants causing less placental damage and additionally restricting intrauterine growth (258). These findings suggest that infection with emerging ZIKV variants does not result in spontaneous termination of pregnancy, but rather restricts intrauterine growth, leading to congenital abnormalities.

*In vivo* studies have also evaluated the neurovirulence of ZIKV variants of either lineage. Intracranial infection of mice revealed that Asian lineage-derived epidemic ZIKV variants are more neurovirulent, causing more severe microcephaly and more neuronal cell death than pre-epidemic Asian lineage strains (255, 259). These findings suggest that the increased incidence of CZS observed during the 2015 ZIKV outbreak may be due to the combined effects of the increased neurovirulence and CPE of emerging strains. As intracranial infection is not a natural route of ZIKV infection, other studies have compared the neurovirulence of African and Asian lineage viruses using a subcutaneous route of infection, mimicking local viral replication followed by

dissemination to the brain during natural ZIKV infection. Subcutaneous infection of immunocompromised mice with African lineage variants caused acute episodes of severe neurological symptoms and increased neuroinvasion whereas infection with Asian lineage strains, including emerging variants, induced persistent and less severe neurological disease (103, 257, 260). Combined with the results from *in vivo* studies assessing placental and fetal damage, these findings suggest that the more pathogenic nature of African lineage viruses results in fetal loss instead, thereby obscuring their ability to cause neurological disease.

Several studies have evaluated and defined the impact of genomic differences on *in vivo* ZIKV pathogenesis. These studies have implicated the structural proteins in ZIKV virulence as chimeric Asian lineage viruses expressing African lineage structural proteins or prM alone exhibit significantly enhanced viral virulence and lethality compared to the WT viruses (103, 256). Specific residues within C, prM, and E proteins (C protein T106A, prM A1V, and E V473M) have been shown to increase the lethality of ZIKV variants (246, 247, 255). Another mutation in prM, S17N, has been demonstrated to contribute to severe microcephaly, providing further evidence of the role of structural proteins in ZIKV pathogenesis (102). However, this mutation is absent in a ZIKV isolate from a microcephalic human fetus, suggesting that there are other viral genetic determinants of pathogenesis (22). Indeed, Collette et al. identified NS1 G100A, a mutation that arose during the 2015 ZIKV epidemic, as another major genetic determinant of ZIKV virulence in IFNAR KO mice (247).

A caveat to using mouse models is that they must be immunocompromised and that their placental architecture is significantly different from that of humans, highlighting

the need for NHP models to evaluate lineage-dependent differences in ZIKV pathogenesis (261). Using pregnant rhesus macaques subcutaneously infected with ZIKV strains of either lineage, Crooks et al. did not observe any fetal damage upon infection with African lineage viruses or Asian lineage-derived epidemic strains (262). Subcutaneous infection of pregnant pigtail macaques with pre-epidemic or epidemic Asian lineage variants, however, revealed that both strains were capable of inducing fetal brain lesions to the same severity (39). The discrepancies between these two studies may be due to differences in the NHP species or ZIKV strains used, but these studies highlight the significant knowledge gap in our understanding of ZIKV-induced fetal pathology in NHP models.

## 1.5 Innate immunity to ZIKV infection

Vertebrate host innate immunity is critical for protecting the host against RNA viruses, such as ZIKV (263–266). To combat viral infection, host-encoded pattern recognition receptors (PRRs) distinguish between host and viral genomes by recognizing a wide array of pathogen-associated molecular patterns (PAMPs) (263, 266). The major species of PAMP sensed by the host during ZIKV infection is the viral RNA. Upon recognition of viral PAMPs, PRRs initiate antiviral immune responses by upregulating the expression of antiviral, immunomodulatory, and inflammatory factors to induce an antiviral state within cells to restrict viral replication and spread (263, 266, 267). Innate immune sensors in the retinoic acid-inducible gene-I- (RIG-I) like receptor (RLR) and toll-like receptor (TLR) families detect ZIKV infection (242, 268–270).

### 1.5.1 RLR signaling

RLRs are crucial for directing antiviral responses to viral infection. The RLR family consists of RIG-I, melanoma-associated gene 5 (MDA5), and laboratory of genetics and physiology 2 (LGP2) though only RIG-I and MDA5 are capable of signaling (271). Cells lacking RIG-I, MDA5, or both have higher viral loads than WT cells as they are unable to mount an antiviral response to effectively control flavivirus replication (242, 268, 269, 272). Moreover, tissues that express RLRs at low basal levels, such as the female reproductive tract, are more susceptible to ZIKV infection due to limited viral sensing and weak activation of innate immunity (273). Mice lacking various effectors downstream of RLR signaling are also unable to control WNV and ZIKV replication; these mice have high viral burdens in peripheral tissues, exhibit early viral entry into the central nervous system, and develop severe neurological symptoms (253, 274). These studies provide compelling evidence for the significance of RLRs and RLR-mediated antiviral signaling for the control of flavivirus infection. For ZIKV infection, studies have now identified RIG-I as the primary sensor of ZIKV in human cells (242, 269). As RIG-I and MDA5 activate the same signaling cascade, the rest of this section will focus on RIG-I signaling, RIG-I ligands, and regulation of RIG-I signaling (271).

RIG-I is primarily localized in the microsome and cytoplasm (265, 275). Its C-terminal domain recognizes and binds to its cognate ligands, which are short blunt-ended dsRNAs with an exposed 5’ triphosphate group (276–281). Treatment of viral RNA with phosphatases to remove the 5’ triphosphate moiety abolishes recognition by RIG-I, emphasizing the importance of the exposed 5’ triphosphate group in RIG-I ligand recognition (276, 282, 283). RIG-I, however, also exhibits some sequence specificity as

it is able to bind to a polyU/UC motif in the hepatitis C virus PAMP near the 3’ end of the viral genome in the absence of a 5’ triphosphate moiety (284–286). As ZIKV replication occurs in the cytoplasmic replication compartments along the ER membrane, RIG-I is poised to detect ZIKV PAMP (50, 57). Indeed, the 5’ end of the ZIKV genome is recognized and bound by RIG-I to induce RIG-I-mediated signaling in human cells (242, 268, 269, 282).

Upon recognition of its ligand, RIG-I autoinhibition is relieved, exposing its caspase activation and recruitment domains (CARDs) in an ATP-dependent manner (281, 287). Exposure and subsequent multimerization of RIG-I CARDs along with ubiquitination by tripartite motif-containing protein 25 (TRIM25) enable interactions between RIG-I and the adaptor protein mitochondrial antiviral-signaling protein (MAVS) on the mitochondrial-associated membranes (MAM) to establish a signaling scaffold that activates downstream effectors (263, 265, 266, 275, 288–293). 14-3-3ε facilitates the translocation of RIG-I from the cytoplasm to the MAM (294). RIG-I signals through MAVS to activate interferon regulatory factor (IRF) 3, IRF7, and nuclear factor kappa B (NFκB) transcription factors to drive the production of type I and III IFNs (Fig. 1-12) (295–298). Signaling through TANK-binding kinase 1 (TBK1) and inhibitor of NFκB (IκB) kinase ε (IKKε) leads to the phosphorylation, activation, and nuclear translocation of IRF3 and IRF7 while signaling through IKKα, IKKβ, and IKKγ results in the phosphorylation and degradation of IκB and subsequent nuclear translocation of NFκB that together induce the expression of IFNs (263, 265, 271, 290–292, 295, 299, 300). As IRF7 is constitutively expressed only in plasmacytoid DCs, IRF7-mediated induction of IFNs in other cell types occurs only after IRF7 is upregulated in response to IFN

signaling and amplifies IFN production in infected and uninfected bystander cells (263, 301). Activation of NFκB via RIG-I signaling drives the production of inflammatory cytokines in addition to IFNs to prime adaptive immune responses (266, 291, 292). IRF3 activation downstream of RIG-I signaling induces apoptosis to clear infected cells and prevent viral spread and upregulates the expression of IRF3-target genes that exert antiviral and immunomodulatory functions (266, 290, 291, 302).

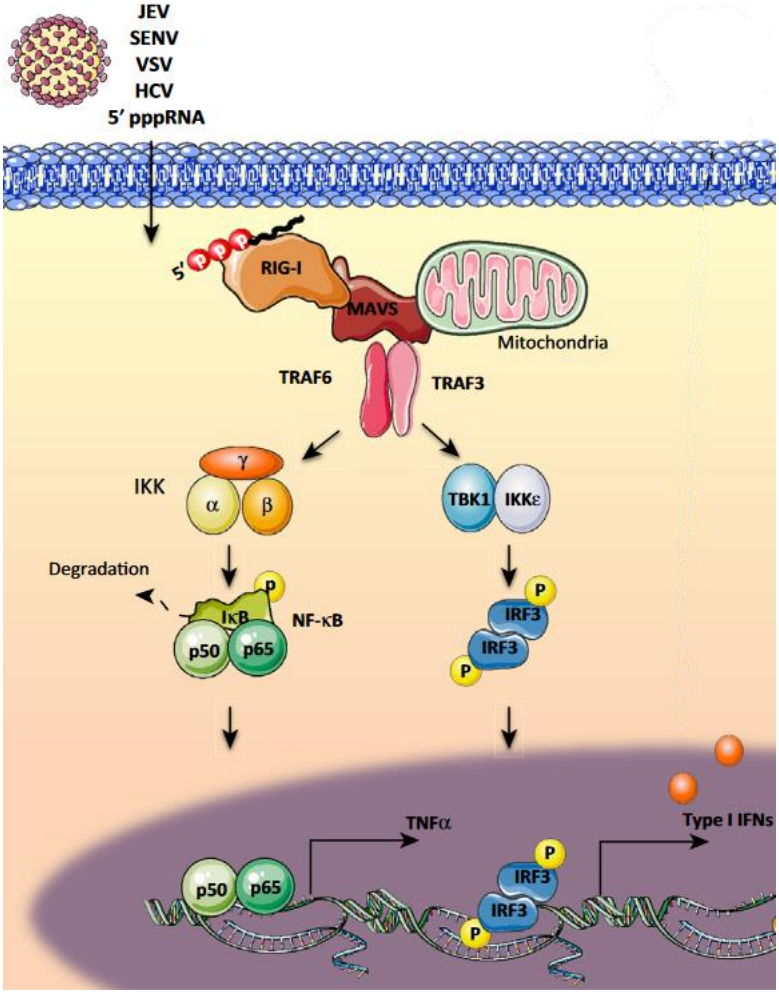


Fig. 1-12 RIG-I signaling pathway in virally infected cells. RIG-I detects short blunt-ended dsRNA. Upon ligand binding, RIG-I undergoes conformational changes and ubiquitination by TRIM25 (not shown here) that enables interactions with MAVS via their CARDs at the MAM. RIG-I signals through MAVS to activate IRF3, IRF7 (not shown here), and NFκB to induce IFN expression. NFκB additionally induces the expression of pro-inflammatory cytokines. Image adapted from Zevini et al., 2017 (299).

RIG-I signaling primes cross-talk between innate and adaptive immunity through the induction of inflammatory cytokines (263, 265, 266, 290, 291). As RIG-I is upregulated by IFN, RIG-I-mediated induction of IFN production and response drives a

positive feedback loop that amplifies RIG-I signaling (263, 265, 290, 291). Given that RIG-I signaling plays a critical role in activating innate immunity and orchestrating the adaptive immune response, RIG-I activation must be strictly regulated. The C-terminal domain of RIG-I contains a repressor region that masks and autoinhibits RIG-I CARDs in the absence of viral pathogens (281, 284). In addition to this, LGP2 serves as a negative regulator of RIG-I signaling by interacting with TRIM25 and MAVS during the resting state to block their interaction with RIG-I, and relocates upon activation of RIG-I during infection (275, 284, 303).

### 1.5.2 TLR signaling

TLR3, TLR7, and TLR8 are the TLRs that sense viral RNA; specifically, TLR3 recognizes dsRNA while TLR7 and TLR8 detect single-stranded RNA (266, 304). TLRs play an important role in mounting an effective antiviral response to control flavivirus replication as depletion of TLRs increases viral burden *in vitro* and *in vivo* (54, 305, 306). ZIKV infection has been demonstrated to upregulate TLR3 and trigger downstream signaling, but no studies have yet shown activation of TLR7 or TLR8 signaling upon ZIKV infection (45, 54, 270, 307). As such, this section will focus on TLR3 signaling.

TLR3 is expressed in the endosome though some cell types also express TLR3 on their surface (308). Surface expression of TLR3 is dependent on an ER accessory protein (309). As ZIKV enters cells through clathrin-mediated endocytosis, it must escape the endosome to replicate in the cytoplasm (50, 51). As such, secondary structures within the viral genome may be detected by endosomal TLR3 during viral uncoating. For TLR3 to transduce signals, its ectodomain, located in the endosome,

must be cleaved to enable receptor dimerization following ligand binding (304, 308). The TLR3 ectodomain recognizes dsRNA in a sequence-independent manner as the interaction between the receptor and RNA ligand relies primarily on electrostatic interactions (310–314). Upon ligand binding, TLR3 dimerizes and signals via its cytosolic toll/interleukin-1 receptor (TIR) domain through TIR-domain-containing adapter-inducing IFNβ (TRIF) to activate IRF3 and NFκB (Fig. 1-13) (310, 315–317). TLR3-induced IRF3 and NFκB activation occurs in a manner similar to RIG-I-induced IRF3 and NFκB activation (300, 304). IFNβ is also the direct product of IRF3 and NFκB activation downstream of TLR3 signaling with activation of NFκB further inducing the expression of inflammatory cytokines (300, 308, 311, 316, 317).

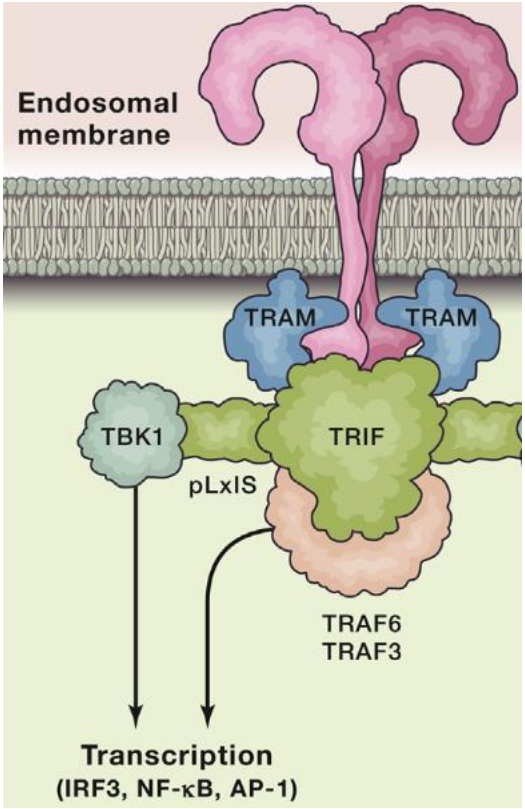


Fig. 1-13 TLR3 signaling pathway in infected cells. TLR3 ectodomain detects dsRNA. Upon ligand recognition, TLR3 dimerizes and signals through its cytosolic TIR domain to activate IRF3 and NFκB transcription factors to induce the expression of IFN, IRF3-target genes, and inflammatory cytokines. Image adapted from Fitzgerald and Kagan, 2020 (304).

As TLR3 plays an important role in initiating an antiviral response and inflammation upon detection of viral nucleic acids, TLR3 signaling is regulated on many

levels to avoid detection of and response to host nucleic acids. TLR3 is primarily localized in the endosome where host nucleic acids are not found (266). In order for TLR3 to signal, its ectodomain must be cleaved by endosomal proteases (304, 308). Moreover, studies have shown that binding of dsRNA ligands to TLR3 and TLR3 dimerization are dependent on acidic pH similar to that found in the endosome (310, 312, 315). Recognition of dsRNA ligands by cell surface TLR3 does not activate downstream signaling at the cell surface; instead, cell surface TLR3 signals from the endosome like its endosomal counterpart (310, 314). Together, these mechanisms limit aberrant endosomal TLR3 signaling in the absence of viral pathogens and reinforce distinction between host and viral nucleic acids.

### 1.5.3 IFN signaling

Activation of RIG-I and TLR3 induces type I IFN production in infected cells as well as type III IFN production in infected epithelial cells (63, 318, 319). Type I IFN binds to IFNAR1/2 whereas type III IFN binds to the IFNλ receptor (IFNLR), which consists of IFNLR and interleukin-10 receptor 2 (IL-10R2), and both signal in an autocrine or paracrine manner (63, 320, 321). Binding of IFNs to host cell receptors induces receptor heterodimerization, activating the Janus kinase/signal transducers and activators of transcription (JAK/STAT) signaling pathway (63, 322) (Fig. 1-14). Types I and III IFNs activate the same downstream effectors to upregulate similar transcriptional profiles (323). Heterodimerization of IFN receptors induces autophosphorylation and activation of the receptor-associated kinases, JAK1 and tyrosine kinase 2 (Tyk2), followed by receptor phosphorylation by JAK1 and Tyk2 (63, 105, 319, 320, 324, 325). Phosphorylation of IFN receptors recruits STAT1 and STAT2, allowing JAK1 and Tyk2

to phosphorylate STAT1 and STAT2 (63, 105, 320, 326–328). Phosphorylation of STAT1 and STAT2 leads to their heterodimerization, interaction with IRF9 to form the interferon stimulated gene factor 3 (ISGF3) complex, and the nuclear translocation of the ISGF3 complex (327, 329, 330). In the nucleus, ISGF3 binds to IFN-stimulated response elements (ISREs) in the promoters of hundreds of genes to induce the expression of a suite of genes known collectively as IFN stimulated genes (ISGs) (63, 105, 319, 321, 328, 331). These ISGs exert antiviral and immunomodulatory functions to restrict viral replication and spread (63, 105, 319, 328, 332). Moreover, this suite of genes includes PRRs, like RIG-I and TLR3, that are upregulated to further amplify IFN production and host antiviral programs (63, 263, 319). The result of IFN signaling is the induction of an antiviral state and the upregulation of ISGs within infected cells to restrict viral replication and, more importantly, in neighbouring uninfected cells to render them less susceptible to infection, limiting viral spread (328). Additionally, IFN signaling promotes antigen presentation and immune cell functions and orchestrates an adaptive immune response aimed at eradicating the viral pathogen (328). Specifically, upregulation of ISGs in antigen presenting cells is critical for proper and efficient activation of B and T cells to restrict viral spread and to eliminate infected cells (105).

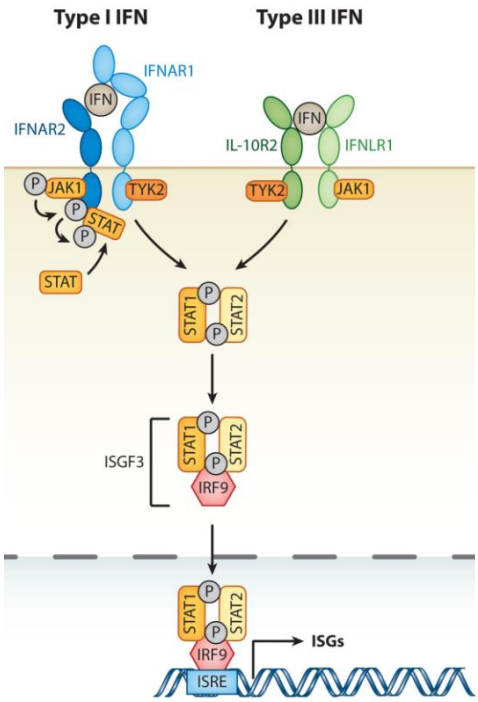


Fig. 1-14 Types I and III IFN signaling pathway. Binding of types I and III IFNs to their cognate receptors activates the JAK/STAT signaling pathway through a series of phosphorylation events that results in the nuclear translocation of the ISGF3 complex. Binding of the ISGF3 complex to ISREs in the promoters of target genes induces the expression of hundreds of ISGs that exert antiviral and immunomodulatory functions. Image adapted from Schneider et al., 2014 (321).

IFN is essential for restricting ZIKV replication and spread. Immunocompetent mice do not display overt clinical symptoms upon ZIKV infection. However, mice lacking IFNAR, STAT2, or both IFNAR and the IFNγ receptor are highly susceptible to ZIKV infection, display severe clinical disease, and exhibit enhanced viral dissemination, indicating that IFN signaling is indispensable for restricting ZIKV infection (253, 257, 273, 333, 334). Several studies have identified specific ISGs that limit ZIKV infection in various cell types by targeting viral proteins for degradation, blocking early viral replication, or driving a positive feedback loop for IFN production and signaling (335–343). Upregulation of ISGs in bystander uninfected cells is sufficient to protect them from acute ZIKV infection (344, 345). These studies demonstrate that ISGs employ distinct mechanisms to limit ZIKV infection and further highlight the critical role that the IFN response and ISGs play in restricting ZIKV replication.

As IFN signaling widely induces an antiviral state in both infected and bystander cells and activates adaptive immunity, uncontrolled IFN signaling following clearance of viral pathogens is deleterious to the host. As such, the host employs multiple mechanisms to restore homeostasis once the pathogen is eliminated (Fig. 1-15). Downregulation and internalization of surface IFN receptors play a role in suppressing further IFN signaling (324). IFN signaling also upregulates the expression of negative regulators of JAK/STAT signaling that terminate the IFN response by inhibiting the functions of JAKs and STATs and by disrupting interactions between JAK/STAT signaling components (346–356). Moreover, IFN signaling upregulates miRNAs that target the 3' UTR of JAK and STAT transcripts, leading to their degradation and preventing further translation of these key players in the IFN response (320). Upregulation of these distinct negative regulators of JAK/STAT signaling ensures return to homeostasis through various mechanisms following clearance of the viral pathogen.

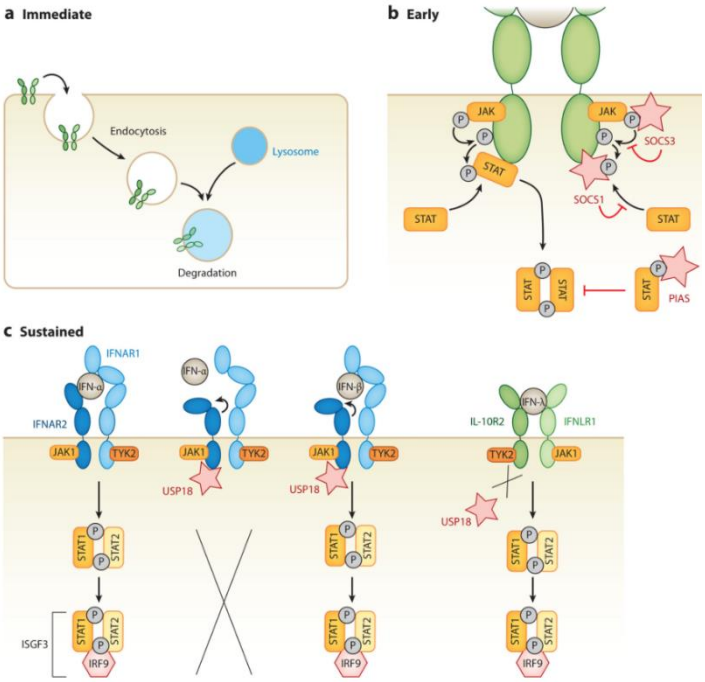


Fig. 1-15 Regulation of IFN signaling. Following clearance of the viral pathogen, IFN signaling is shut off via multiple distinct mechanisms. Internalization and degradation of IFNAR immediately terminate IFN signaling. Negative regulators, such as suppressor of cytokine signaling proteins (SOCS), protein inhibitor of activated STAT (PIAS), and phosphatases, are upregulated by IFN signaling to drive a negative feedback loop, dampening the IFN response and restoring homeostasis. Image adopted from Schneider et al., 2014 (321).

### 1.5.4 Immune-mediated ZIKV pathology

ZIKV-induced activation of innate immunity and production of inflammatory cytokines are essential for controlling viral replication and spread, but studies have demonstrated a pathological impact of innate immune activation and inflammation in response to flaviviruses. TLR3-driven induction of inflammatory cytokines has been shown to break down the blood-brain barrier during WNV infection, facilitating viral spread to the brain and infection of neurons (357). Studies in brain organoids have identified TLR3-target genes involved in neurogenesis and apoptosis that are dysregulated upon ZIKV infection, contributing to reduced brain organoid sizes and potentially microcephaly (45). *In vitro* studies in NPCs and astrocytes have also shown that ZIKV infection activates TLR3 signaling and upregulates the expression of inflammatory cytokines (270, 307). However, Plociennikowska et al. demonstrated that ZIKV activation of TLR3 signaling upregulates negative regulators of IFN signaling, suppressing the IFN response and allowing ZIKV to replicate unrestrained (270). In each of these studies, inhibition of TLR3 restricts viral replication and ameliorates neuropathogenesis, indicating that TLR3 activation during ZIKV infection can drive an ineffective antiviral response and contribute to immunopathology (45, 270, 307).

Type I IFN signaling has also been implicated in ZIKV pathogenesis. Cytokine profiling of confirmed ZIKV-induced human microcephaly cases revealed that these infants exhibit chronic inflammation in the central nervous system characterized by high levels of IFNs and inflammatory cytokines (358). These findings suggest that sustained inflammation in the central nervous system may contribute to fetal brain damage, resulting in microcephaly. Studies in pregnant mouse models have highlighted the

immunopathologic effects of robust IFN signaling on the placental tissue during *in utero* ZIKV infection; high levels of IFNs produced during ZIKV infection induce inflammation, which inhibits placental development and disrupts placental architecture, leading to enhanced fetal resorption or intrauterine growth restriction (359, 360). These studies suggest that a strong IFN response to *in utero* ZIKV infection aimed at restricting viral replication may additionally result in fetal damage or fetal demise. Together, these findings reveal a role for the innate immune response in mediating ZIKV pathology.

### 1.5.5 Lineage-dependent differences in innate immune responses

Comparative analyses of the host innate immune response to infection with African and Asian lineage ZIKV strains have revealed lineage-dependent differences in the host immune response that, along with differences in viral replication kinetics and CPE, may contribute to differential viral pathogenesis. In primary astrocytes, infection with an epidemic variant induced the host antiviral response faster, which correlated with lower viral RNA levels, compared to infection with an African lineage virus (234). These findings suggest that the kinetics of the innate immune response to ZIKV infection is crucial in restricting viral replication early in acute infection. Studies in human lung epithelial cells, however, revealed that an epidemic ZIKV strain exhibited delayed innate immune activation compared to African and pre-epidemic Asian lineage variants, suggesting that there may be cell type-specific differences in the antiviral response elicited upon ZIKV infection (242). This delayed innate immune activation by the epidemic ZIKV variant correlated with a weak IFN response (242). This observation is consistent with those from other *in vitro* studies where Asian lineage-derived epidemic ZIKV variants induce weaker innate immune responses than African lineage and pre-

epidemic Asian lineage strains and skew infected monocytes towards an immunosuppressive phenotype (60, 61, 235, 242, 244, 358). Along with the delayed activation of host innate immunity, a dampened IFN response may enhance the spread of epidemic ZIKV variants and promote viral persistence in infected hosts.

*In vitro* and *in vivo* studies have shown that infection with African and endemic Asian lineage variants induces high levels of inflammatory cytokines and chemokines (61, 235, 257, 361). The prevalence of inflammatory cytokines and chemokines can drive excessive inflammation and immune cell infiltration to mediate immunopathology, potentially inducing severe fetal damage or fetal demise during *in utero* infection with these variants. However, *in vitro* comparative analyses of epidemic ZIKV strains with African lineage or pre-epidemic Asian lineage variants have demonstrated that epidemic strains induce higher levels of inflammatory cytokines (238, 259, 307). The high levels of inflammatory cytokines produced during infection with epidemic ZIKV variants may drive immune-mediated pathology. Robust activation of TLR3 signaling in astrocytes not only induces high levels of inflammatory cytokines, but also other TLR3-target genes that disrupt neurogenesis, suggesting that TLR3-mediated inflammatory responses to *in utero* infection with epidemic ZIKV strains can cause fetal brain damage (307). *In vivo* studies comparing epidemic and pre-epidemic Asian lineage strains have additionally revealed that epidemic ZIKV strains induce more inflammation and immune cell recruitment (362). As CD14+ monocytes were identified as a major target of ZIKV infection, a greater abundance of inflammatory cytokines and chemokines can recruit more immune cells to the site of infection to serve as ZIKV targets or increase inflammation and immunopathology (61). Indeed, de Alwis et al. observed that infection

with epidemic ZIKV variants induces greater recruitment of CD14+ monocytes and DCs, which may have contributed to the enhanced viral dissemination and inflammation observed during infection with these strains (362). These findings indicate that an inflammatory response to infection with epidemic ZIKV variants to clear viral infection may additionally promote viral dissemination, inflammation, and immunopathology.

In addition to lineage-dependent differences in the host innate immune response to infection, studies have also identified differences in the IFN sensitivity of ZIKV lineages. African lineage viruses and Asian lineage-derived epidemic strains have been shown to exhibit enhanced resistance to IFN, suggesting that they are able to overcome host antiviral responses (242, 363). The increased resistance to IFN signaling of these variants may further contribute to their increased virulence compared to pre-epidemic Asian lineage strains.

## 1.6 ZIKV-mediated antagonism of innate immunity

ZIKV infection induces innate immune activation and signaling, upregulating the expression of IFNs, inflammatory cytokines, and ISGs (86, 105). Like other closely related flaviviruses, ZIKV employs multiple mechanisms to subvert host innate immune activation and signaling (63, 66, 364–367). The various ways in which ZIKV antagonizes host innate immune activation and signaling are discussed below.

### 1.6.1 Antagonism of innate immune activation

As innate immune activation is critical for restricting ZIKV replication and spread, ZIKV uses distinct mechanisms to target different steps of innate immune activation to inhibit IFN production. The C protein has been shown to interact with TRIM25 to block

TRIM25-mediated ubiquitination of RIG-I, which is required for the interaction between RIG-I and MAVS (288, 368). NS4A and NS5 have also been shown to block the interaction between RIG-I and MAVS at the MAM by binding to RIG-I CARDs (369, 370). To prevent the translocation of RIG-I to the MAM for assembly of the MAVS signalosome, NS3 binds to 14-3-3ε to sequester it from RIG-I (371). Moreover, several studies have demonstrated that ZIKV targets MAVS and the downstream effector proteins to inhibit their activation. NS2B, NS3, and NS4A interact with MAVS or target MAVS for degradation, thereby shutting down RLR signal transduction through MAVS (372–374). The kinases TBK1 and IKKε are also directly targeted by ZIKV NS1, NS2A, NS2B, NS4A, NS4B, and NS5 to prevent their phosphorylation, activation, and kinase activities (374–378). The NS1 A188V mutation present in epidemic Asian lineage-derived viruses and African lineage strains confers enhanced ability to interact with TBK1 to inhibit TBK1 phosphorylation (377). Additionally, NS3 was shown to indirectly destabilize TBK1, leading to TBK1 degradation and inhibition of downstream signaling (379). At the level of IRF3 transcriptional activity, studies have shown that NS1, NS4A, and NS5 antagonize IRF3-driven promoter activity (377, 380, 381). Nuclear localization of NS5 appears to be critical in suppressing the induction of IRF3-target genes (380). Studies have also found that ZIKV infection disrupts NFκB-driven promoter activity and weakly induces inflammatory cytokines, suggesting that ZIKV broadly antagonizes innate immune activation and modulates IRF3 and NFκB transcriptional activities (244, 382). NS1 secreted from infected cells can bind to cell surface CD303 to activate CD303 signaling in plasmacytoid DCs, which suppresses the production of inflammatory cytokines, including type I IFN (383). The consequence of these interactions between

ZIKV proteins and host factors involved in RLR signaling is the blockade of types I and III IFN production (378).

### 1.6.2 Antagonism of IFN signaling

IFN signaling is crucial for restricting ZIKV replication. As such, ZIKV antagonizes IFN signaling via multiple distinct mechanisms to block the host IFN response and downstream induction of antiviral effectors. NS5 has been identified as a major antagonist of IFN signaling for several flaviviruses, including ZIKV (364, 384–388). Specifically, ZIKV NS5 targets STAT2 for proteasomal degradation to suppress types I and III IFN signaling (386). ZIKV NS5, however, along with other flavivirus NS5 proteins, has also been shown to sequester the host chaperone HSP90 from cellular kinases to broadly antagonize JAK/STAT signaling downstream of different cytokine stimuli (387). Consequently, kinases, such as JAKs, are destabilized and degraded by the proteasome, effectively inhibiting JAK/STAT signaling (387). A recent study revealed that sfRNA binds to and stabilizes ZIKV NS5 to prevent STAT1 phosphorylation and downstream induction of ISGs, providing further insight into NS5-mediated suppression of IFN signaling (84). Other studies have also shown that NS2A targets STAT1 and STAT2 for degradation to block the host cell response to IFNα and that NS4B inhibits STAT1 phosphorylation and the nuclear translocation of phosphorylated STAT2 to block IFN signaling (389, 390). Additionally, one of the entry receptors identified for ZIKV, AXL, was demonstrated to facilitate ZIKV infection by interfering with IFN signaling through the upregulation of SOCS (53, 391). Upregulation of SOCS upon viral entry ensures effective blockade of IFN signaling early in ZIKV infection. Together, these

studies reveal the mechanisms by which ZIKV antagonizes IFN signaling to promote viral replication.

## 1.7 Premise of this dissertation

It is still not fully understood how ZIKV infection was suddenly associated with severe clinical manifestations characterized by neurological symptoms during the recent outbreaks. Previous studies have demonstrated that both ZIKV lineages can cross the maternal-fetal interface during *in utero* infection; more importantly, these studies have indicated that endemic Asian lineage variants can also cross the maternal-fetal barrier to infect and damage the fetus (224, 241, 254, 255). Indeed, countries in Southeast Asia have reported cases of microcephaly following *in utero* ZIKV infection with endemic ZIKV variants, highlighting the danger that endemic Asian lineage viruses pose on pregnant women and their fetuses (22, 23). The mechanisms underlying these differences in ZIKV pathogenesis between endemic African or Asian lineage viruses and epidemic Asian lineage strains, however, are not well-understood. Comparative analyses of African or endemic Asian lineage strains with epidemic Asian lineage-derived variants have provided evidence that viral genetics and replication kinetics contribute to differences in viral pathogenesis (227, 237, 239, 245). Evaluation of host innate immune responses to infection with ZIKV variants from either lineage has also implicated differential innate immune responses to infection in ZIKV pathogenesis (61, 259, 358, 362). Yet, the consequences of these differences in viral replication kinetics on the extent of host innate immune responses and the impact of antiviral actions across different stages of the ZIKV life cycle remain poorly understood. In this work, we comparatively assessed the replication properties of and the host innate immune

responses to two prototypic ZIKV variants from the African and Asian lineages. We hypothesized that differences in viral sequences impact viral replication kinetics to drive distinct innate immune responses to infection with the ZIKV variants. We demonstrate that RIG-I-mediated antiviral signaling restricts viral protein accumulation, genome replication, and virus spread during late stages of acute infection. We found that early accumulation of viral proteins in infected cells is linked with greater ability to antagonize IFN signaling, promoting ZIKV genome replication and cell-to-cell spread. Hence, RIG-I-driven innate immune responses impart control of ZIKV fitness by restricting the accumulation of viral proteins to enhance IFN signaling to limit ZIKV replication and spread.

# Chapter 2. Materials and methods

## 2.1 Cell line maintenance

A549 (ATCC, Manassas, VA, USA), Vero WHO (Vero; WHO, Geneva, Switzerland), and HEK293T cells (ATCC) were maintained in complete Dulbecco's modified Eagle medium (cDMEM) (10% fetal bovine serum (FBS; Hyclone, Logan, UT, USA), 10mM L-glutamine, 5mM sodium pyruvate (Corning, NY, USA), 0.5X non-essential amino acids (Corning), 10mM HEPES (Corning), and 1X antibiotics/antimycotics (Corning)). A549 non-targeting control (NTC) and RIG-I KO cells were generated by CRISPR-Cas9 as previously described and were maintained in cDMEM containing 10µg/ml puromycin (Invivogen, San Diego, CA, USA) (242). ZV-13 hybridomas 8A3.C1 were kindly gifted by Michael Diamond (Washington University in

St. Louis, St. Louis, MO, USA) and were cultured in Iscove's modified Dulbecco's medium (Thermofisher-Life Technologies, Waltham, MA, USA) supplemented with 20% FBS, 1mM sodium pyruvate, and 1X penicillin-streptomycin (Fisher Scientific, Hampton, NH, USA). All cell lines were free of mycoplasma contamination.

## 2.2 Generation of ZIKV stocks

ZIKV/Dakar/1984/ArD41519 (ZIKV/Dakar) was a kind gift from Michael Diamond (Washington University in St. Louis) and ZIKV/Malaysia/1966/P6740 (ZIKV/Malaysia) was kindly provided by Robert Tesh (University of Texas Medical Branch, Galveston, TX, USA). For each strain, plaque-picked isolates were passaged twice in Vero cells and then used to infect Vero cells to generate working ZIKV stocks. Vero cells were infected at a multiplicity of infection (MOI) of 0.05 PFU/cell at 37$^{o}$C for 2 hours rocking. Inoculums were then removed and fresh DMEM supplemented with 5% FBS (5% DMEM) was added. At 48 hours post-infection (hpi), media was replaced with fresh 5% DMEM. ZIKV working stocks were harvested 48 hours after the media change and titered via focus-forming unit (FFU) assays.

## 2.3 Deep sequencing and sequence alignment of ZIKV stocks

ZIKV RNA was extracted from working stocks using the QIAmp viral RNA minikit (Qiagen, Hilden, Germany). Isolated RNA was then digested with DNase I and purified using the Qiagen RNeasy kit (Qiagen). RNA quality was analyzed on the Agilent 2100 bioanalyzer (Agilent, Santa Clara, CA, USA) using the Agilent RNA 6000 Pico assay (Agilent). RNA concentrations were quantified on a Qubit fluorometer (Invitrogen, Carlsbad, CA, USA) prior to rRNA depletion and library prep using the KAPA HyperPrep

kit (Roche Diagnostics Corporation, Indianapolis, IN, USA). cDNA library qualities were evaluated on the Agilent 2100 bioanalyzer and quantified with the Qubit fluorometer prior to sequencing on a NextSeq 500 Illumina sequencing platform (Illumina, San Diego, USA). 2x76 nucleotide stranded paired-end reads were generated with approximately 25 million raw reads per sample. Adapters, low quality bases, and human reads were removed from the raw RNAseq data before sequencing files were loaded onto the *de novo* assembler Trinity (version 2.9.0), and viral consensus sequences assembled and aligned as previously described (242, 392). Viral sequence alignments were loaded into the JALView software (version 2.11.0) to identify amino acid differences between ZIKV strains (393).

## 2.4 ZV-13 antibody purification and quantification

Supernatant from ZV-13 hybridomas was harvested once approximately 95% cell death was observed and was clarified by centrifuging for 10 minutes at 400xg at 4$^{o}$C. The clarified supernatant was filtered through a 0.22µm filter. ZV-13 antibody was purified from the clarified supernatant using the Pierce Protein A IgG purification kit and NAb Protein A Plus Spin Columns (both from ThermoFisher-Life Technologies). Purified ZV-13 antibody was concentrated and buffer-exchanged into 1X phosphate buffered saline (PBS; Fisher Scientific) using Amicon Ultra-0.5 100kDa Centrifugal Filter units (Sigma-Aldrich, St. Louis, MO, USA) for quantification by ELISA. 96-well Nunc ELISA plates (Fisher Scientific) were coated with goat anti-mouse IgG2c (Jackson ImmunoResearch, West Grove, PA, USA) at a concentration of 500ng/ml in 1X PBS and incubated overnight at 4$^{o}$C. Coated plates were washed with PBS plus Tween-20 (PBST; Fisher Scientific) and blocked for 1 hour at room temperature with 1% bovine

serum albumin in PBS (PBSA; Sigma-Aldrich) containing 2% normal goat serum (NGS; Jackson ImmunoResearch). Serial dilutions of hybridoma supernatant and purified ZV-13 antibody were then added and incubated for 1 hour at 37$^{o}$C. Following washes, biotin-conjugated anti-mouse IgG2c secondary antibody (Jackson ImmunoResearch) was diluted 1:5000 in PBSA, added to plates, and incubated for 1 hour at room temperature. Plates were then washed, and streptavidin-horseradish peroxide (HRP) (ThermoFisher-Life Technologies) diluted 1:20,000 in PBSA was added and incubated for 30 minutes at room temperature. Plates were washed, developed by adding 3,3',5,5'-tetramethylbenzinide (TMB; Surmodics, Eden Prairie, MN, USA), and incubated in the dark until the reaction was stopped by adding 1M $H_2SO_4$. Absorbance was measured at 450nm using a microplate reader (BioLegend, San Diego, CA, USA). Serial dilutions of known concentrations of mouse IgG2c (Southern Biotech, Birmingham, AL, USA) were used to generate a standard curve. OD values for the standard curve were plotted against concentration in GraphPad Prism (version 9, GraphPad, La Jolla, CA, USA), and the linear portion of the curve was used to derive a least squares equation to determine the concentration of purified ZV-13 antibody.

## 2.5 Titering of ZIKV stocks by FFU assays

A549 cells were seeded at a density of 2x10$^4$ cells per well in 96-well plates. ZIKV stocks were serially diluted in DMEM supplemented with 2% FBS (2% DMEM). Cells were inoculated with virus dilutions in triplicate and incubated at 37$^{o}$C for 2 hours. Following adsorption, a methylcellulose overlay (DMEM supplemented with 1% carboxymethylcellulose (Fisher Scientific), 2% FBS, 10mM HEPES, and 1X penicillin/streptomycin) was added to cells. At 48 hpi, the methylcellulose overlay and

media were removed. Cells were fixed with 4% paraformaldehyde (Fisher Scientific) for 20 minutes at room temperature and then washed with 1X PBS. ZV-13 antibody was diluted 1:250 in permeabilization/wash/block buffer (2.5% NGS, 2.5% normal donkey serum (Sigma-Aldrich), 0.2% BSA, and 0.1% Triton X-100 (Fisher Scientific) in 1X PBS), added to each well, and incubated for 2 hours rocking at room temperature. Cells were then washed with 1X PBS, and donkey anti-mouse HRP secondary antibody (Jackson ImmunoResearch) diluted 1:3000 in permeabilization/wash/block buffer was added and incubated rocking for 1 hour in the dark. Following washes, TrueBlue peroxidase substrate (VWR, Radnor, PA, USA) was added and incubated until foci of infected cells were observed. $dH_2O$ was added to stop the enzymatic reaction and removed prior to imaging. Plates were imaged on a BioSpot plate reader (Cellular Technology Limited, Cleveland, OH, USA), and foci of infected cells were manually counted using the multi-point tool in Fiji (version 2.1.0, NIH, USA) to determine the titer of ZIKV stocks (394).

## 2.6 Measuring viral spread by FFU assays

A549 cells were seeded at a density of $6x10^5$ cells per well in 6-well plates. ZIKV stocks were serially diluted in 2% DMEM, and cells were inoculated and fixed as described above (see 2.5 Titering of ZIKV stocks by FFU assays). Fixed cells were washed with 1X PBS and stained with an anti-flavivirus envelope antibody, 4G2 (Ab00230-2.0; Absolute Antibody, Oxford, UK), diluted 1:500 in permeabilization/wash/block buffer (see recipe in 2.5). Following incubation with primary antibody, donkey anti-mouse HRP secondary antibody diluted 1:1000 in permeabilization/wash/block buffer was added to plates and incubated rocking for 1

hour in the dark. Foci were developed and imaged as described above (see 2.5). The diameter of foci was measured in Fiji.

## 2.7 ZIKV infection

A549 cells were seeded at a density of $3x10^5$ cells per well in 12-well plates. Virus inoculums were prepared in DMEM, and cells were uninfected, mock-infected, or infected with ZIKV variants at a MOI of 5 FFU/cell for 2 hours, rocking, at 37ºC. Uninfected samples are seeded cells that remained untouched throughout the infection time-course while mock-infected samples were inoculated with DMEM. The inoculums were removed following adsorption, and cells were washed with 1X PBS. Fresh cDMEM was added to plates, and plates were returned to 37ºC until the appropriate time points.

## 2.8 Synchronized ZIKV attachment and entry

A549 cells were seeded as described above (see 2.7 ZIKV infection). Viral inoculums were prepared in ice-cold DMEM. Cells were pre-cooled at 4ºC prior to the addition of ice-cold inoculums. Viral inoculums were allowed to adsorb for 1 hour at 4ºC. The inoculums were removed after adsorption, and cells were washed with ice-cold 1X PBS. Fresh pre-warmed cDMEM was added to cells, and cells were returned to 37ºC until 1 hpi to evaluate viral entry or until appropriate time points to evaluate genome replication and virion production. For viral attachment assays, RNA lysates were harvested immediately following ice-cold 1X PBS washes using the Qiagen RNeasy kit followed by DNase I digestion.

## 2.9 Quantification of extracellular and intracellular vRNA

RNA lysates harvested with the Qiagen RNeasy kit were used to extract intracellular vRNA. To evaluate genome replication following synchronized ZIKV infections, 1ml of cell culture supernatants was harvested at appropriate time points and centrifuged at 2000rpm at 4$^{o}$C for 10 minutes. Extracellular vRNA was extracted from the clarified supernatants using the QIAmp viral RNA minikit to quantify extracellular viral copy numbers. Cells were washed with ice-cold stringent wash buffer (1M NaCl, 50mM sodium bicarbonate, pH 9.5) for 3 minutes to remove cell surface-associated viruses. After ice-cold 1X PBS washes, cells were harvested using the Qiagen RNeasy kit to extract intracellular vRNA to quantify intracellular viral copy numbers.

## 2.10 Quantification of extracellular and intracellular virus

1ml of cell culture supernatants was harvested at appropriate time points and centrifuged at 2000rpm for 10 minutes at 4$^{o}$C. The clarified supernatants were used to quantify extracellular virions via plaque assays. To evaluate intracellular virion production following synchronized ZIKV infections, cells were washed with ice-cold stringent wash buffer as described above (2.9 Quantification of extracellular and intracellular vRNA). Cells were then detached with 0.05% trypsin-EDTA (Fisher Scientific), resuspended in 1ml cDMEM, and centrifuged at 300xg for 5 minutes at 4$^{o}$C. Supernatants were discarded, and cell pellets were resuspended in 0.5-1ml of cDMEM and stored at -80$^{o}$C. Cell pellets were thawed at 37$^{o}$C, and cellular debris removed by centrifuging at 3200xg for 5 minutes at 4$^{o}$C. The clarified supernatants were used for plaque assays to quantify intracellular viral titers.

## 2.11 Plaque assays

Vero cells were seeded at a density of $1.85x10^5$ cells per well in 6-well plates. Supernatants from infection experiments were serially diluted in DMEM containing 1% FBS. Vero cells were incubated with virus dilutions in duplicate at 37°C for 1 hour rocking. Following adsorption, 2X DMEM (Fisher Scientific) containing 1% low-melt agarose (Fisher Scientific), 5% sodium bicarbonate (Fisher Scientific), and 5% FBS was added to cells as an overlay. 4-5 days later, 1% low-melt agarose overlay containing 3% Neutral Red (Sigma-Aldrich), 10% 10X PBS (Fisher Scientific), and $dH_2O$ was added to the primary overlay to visualize plaques.

## 2.12 Quantification of ZIKV copy number

For each sample, cDNA was synthesized from RNA samples using the iScript Select cDNA Synthesis Kit (BioRad, Hercules, CA, USA). cDNA was diluted to a final concentration of 2.5ng/µl for Taqman qRT-PCR on the QuantStudio 5 real-time PCR system (ThermoFisher) using the TaqMan Universal PCR master mix (Fisher Scientific) and primers and probe targeting ZIKV NS3 (Table 1; IDT, Coralville, IA). The ZIKV NS3-specific probe contains a 5' FAM reporter dye and a 3' Iowa Black FQ quencher. ZIKV NS3-specific primers and probe target a conserved 88 base pair region in NS3. The ZIKV NS3 amplicon was amplified from ZIKV cDNA and cloned into the multiple cloning site in the pEF mammalian expression plasmid containing a N-terminal FLAG tag (pEF NS3 N-FLAG) using the Takara In-Fusion cloning kit (Table 1; Takara Bio, Kusatsu, Japan) following the manufacturer's instructions. For Taqman qRT-PCR, each sample was run in triplicate, and dilutions of known concentrations of pEF NS3 N-FLAG were

run in triplicate and used to generate a standard curve with copy number values plotted against Ct values to derive a semi-log equation in GraphPad Prism. This equation was used to determine the viral copy number of each sample. Serial dilutions of cDNA of RNA extracted from ZIKV stocks using the QIAmp viral RNA minikit were run in triplicate and used to derive a log-log equation in GraphPad Prism to convert viral copy numbers to their FFU equivalent.

## 2.13 Transcript analysis by qRT-PCR

cDNA for each sample was synthesized as described above (see 2.12 Quantification of ZIKV copy number). For each sample, cDNA was diluted to a final concentration of 2.5ng/µl for SYBR green qRT-PCR on the QuantStudio 5 real-time PCR system using the SYBR Green Master Mix (ThermoFisher) and gene-specific primers (Table 1; Qiagen; IDT). Each sample was run in triplicate.

## 2.14 Transcript analysis by Nanostring

For each sample, RNA was diluted to a final concentration of 20ng/µl and hybridized to reporters and capture probes from a custom-generated innate immunity probe set (Nanostring, Seattle, WA, USA). Samples were hybridized for 16 hours at 65$^{o}$C. Sample preparation was completed on a nCounter MAX prep station (Nanostring) according to manufacturer's protocol. Absolute RNA transcript counts were quantified on a Nanostring nCounter (Nanostring) according to manufacturer's instructions.

## 2.15 Bioinformatics analyses of Nanostring data

Raw reads were assessed for technical quality control flags using the nSolver software (Nanostring) prior to being transferred into Rstudio (RStudio, Boston, MA,

USA). As the design of our probe set was non-random, the differences in the number of observed counts for each gene were large between mock-infected and ZIKV-infected samples. To address these differences, we developed a custom approach for data analysis (395). We used count data within each sample vector as an internal reference, against which we compared genes of interest (GOIs). To identify reference genes, we measured the coefficient of variation (CV) for all genes in the probe set, including GOIs, housekeeping (HK) genes, and positive and negative controls, to select the HK genes with the lowest variability. We then determined the geometric mean of the selected HK genes to obtain our within-sample reference value and "anchored" all count data from each sample to its within-sample reference in ratio form to derive anchored gene counts (AGCs). We took the ratio of the AGC for each GOI against its values from mock-infected samples at each time point and took the log2 of these values, which were used to generate principal component analysis (PCA) plots and line graphs.

## 2.16 Protein lysate quantification and immunoblot analysis

Cells were washed with 1X PBS and lysed on ice with radioimmunoprecipitation assay (RIPA) buffer (50mM Tris pH 7.6, 150mM NaCl, 1% Triton X-100, 0.5% sodium deoxycholate). Phosphatase inhibitors (1:100; VWR), protease inhibitors (1:100; Sigma-Aldrich), and 250nM okadaic acid (1:1000; Fisher Scientific) were freshly added to the RIPA buffer. Cell lysates were collected and stored at -80$^{o}$C. Lysates were then thawed on ice and sonicated in an ice slurry bath for three 30 second bursts on the highest setting with two 20 second pauses in between. Sonicated lysates were centrifuged at 14,000rpm for 15 minutes at 4$^{o}$C to pellet cellular debris. The clarified lysates were collected and quantified using a BioRad protein assay kit (BioRad). For immunoblot

analysis, protein lysates were incubated with 4X Laemmli buffer (BioRad) containing 10% β-mercaptoethanol (ThermoFisher-Life Technologies) at 95$^{o}$C for 3 minutes. For each sample, approximately 7-10µg of protein was loaded per lane onto 4-20% Criterion TGX gradient gels (BioRad) and electrophoresed at 96V in 1X sodium dodecyl sulfate (SDS) running buffer (25mM Tris, 192mM glycine, 0.1% SDS). Proteins were then transferred onto nitrocellulose membranes (Fisher Scientific) at 90V for 1 hour at 4$^{o}$C in 1X Towbins transfer buffer (25mM Tris, 192mM glycine, 0.01% SDS, 20% methanol). Following transfer, membranes were blocked for 1 hour at room temperature in Tris-buffer saline (TBS)-based LI-COR Intercept blocking buffer (LI-COR, Lincoln, NE, USA) and stained overnight at 4$^{o}$C with primary antibodies (Table 2) diluted in blocking buffer. Alexa Fluor 680- (715-625-151 or 711-625-152) or Alexa Fluor 790-conjugated secondary antibodies (711-655-152 or 715-655-150) (all from Jackson ImmunoResearch) were diluted 1:10,000 in blocking buffer and added to membranes after membranes were washed with TBS containing Tween-20 (TBST). Secondary antibodies were incubated for 1 hour at room temperature. Membranes were washed with TBST followed by 1X TBS prior to imaging on an Odyssey CLx imager (LI-COR). If necessary, membranes were stripped with 5X NewBlot IR Stripping Buffer (LI-COR) diluted 1:5 in $dH_2O$ and reprobed with appropriate primary and secondary antibodies as described above. Protein abundance was quantified in Fiji and normalized to actin abundance.

## 2.17 Recombinant DNA construct generation and plasmid transfections

ZIKV/Dakar and ZIKV/Malaysia NS5 sequences were amplified from ZIKV/Dakar or ZIKV/Malaysia cDNA and cloned into the multiple cloning site in the mammalian expression plasmid pcDNA3.1+ (Table 1) using the Takara In-Fusion cloning kit. HEK293T cells were seeded at a density of $4x10^5$ cells per well in a 6-well plate. Cells were transfected the following day with 2.5µg of the empty pcDNA3.1+, pcDNA3.1+ ZIKV/Dakar NS5, or pcDNA3.1+ ZIKV/Malaysia NS5 plasmids using Lipofectamine 3000 (ThermoFisher-Life Technologies) according to the manufacturer's protocol. The ratio of plasmid DNA (µg): lipofectamine 3000 (µl): P3000 reagent (µl): Opti-MEM (µl) (Fisher Scientific) used was 1:3:2:50.

## 2.18 IFNβ treatment

A549 NTC and RIG-I KO cells were seeded on No. 1 glass coverslips (Electron Microscopy Sciences, Hatfield, PA, USA) at a density of $1x10^5$ cells per well in a 24-well plate. The next day, cells were mock-infected or infected with ZIKV variants. 100IU/ml of IFNβ (Toray, Tokyo, Japan) was prepared in cDMEM. At 18 or 40 hpi, A549 NTC and RIG-I KO cells were treated with IFNβ for 1 hour for immunofluorescence analysis. For flow cytometry analysis, A549 RIG-I KO cells were seeded at a density of $4x10^6$ cells/dish in 10cm dishes and mock-infected or infected with ZIKV variants the next day. At appropriate time points, cells were detached with 0.05% trypsin-EDTA, pelleted, resuspended in media containing 100IU/ml of IFNβ, and incubated at 37$^o$C for 30 minutes rocking. HEK293T cells were seeded and transfected as described above (see

2.17 Recombinant DNA construct generation and plasmid transfections). The following day, cells were detached with 0.05% trypsin-EDTA, pelleted, resuspended in media containing 1000IU/ml of IFNβ, and incubated at 37$^{o}$C for 8 hours rocking for flow cytometry analysis.

## 2.19 Immunofluorescence analysis

A549 cells were seeded on No. 1 glass coverslips at a density of 1x10$^{5}$ cells per well in a 24-well plate. The next day, cells were mock-infected or infected with ZIKV strains. At appropriate time points, cells were fixed with 4% formaldehyde (Fisher Scientific) in filtered 1X TBS for 30 minutes at room temperature. Cells were then washed with filtered 1X TBS and permeabilized and blocked in 5% NGS in 1X TBS (5% NGS/TBS) containing 0.1% Triton X-100 for 30 minutes at 4$^{o}$C. For pSTAT1 staining, cells were permeabilized with 100% ice-cold methanol (Fisher Scientific) for 10 minutes at -20$^{o}$C. Cells were then washed in 1X TBS for 5 minutes and blocked in 5% NGS/TBS for 30 minutes at room temperature. For all immunofluorescence staining, cells were stained for 1 hour at room temperature or overnight at 4$^{o}$C with the following primary antibodies diluted in 5% NGS/TBS: mouse anti-dsRNA (J2, no. 10010500; 1:800; Scicons, Budapest, Hungary), rabbit anti-ZIKV NS5 (GTX133327; 1:500; GeneTex), and rabbit anti-pSTAT1 (no. 7649; 1:400; CST). Cells were washed with filtered 1X TBS, and isotype-specific and fluorophore-conjugated secondary antibodies (A-21131, A-11036, A-11008, or A-21241; ThermoFisher-Life Technologies) diluted 1:1000 in 5% NGS/TBS containing 4', 6-diamidino-2-phenylindole dihydrochloride (DAPI; 1:10,000; ThermoFisher-Life Technologies) to stain cell nuclei were added and incubated for 1 hour at room temperature. Cells were then washed with filtered 1X TBS followed by

$dH_2O$. Excess water was removed from coverslips before coverslips were mounted onto glass slides (VWR) using ProLong Gold mounting media (ThermoFisher-Life Technologies). Coverslips were dried overnight at room temperature. Images and Z-stacks with 2.5µm step sizes were acquired on a Nikon Eclipse Ti confocal microscope (Nikon, Tokyo, Japan) with a 60x oil immersion objective. Images were merged and processed using the Nikon confocal analysis software (NIS Elements AR 5.11.03; Nikon), and further image analyses were performed in Fiji as indicated in the figure legends.

## 2.20 Flow cytometry analysis

A549 RIG-I KO and HEK293T cells treated with IFNβ were pelleted and fixed with 4% formaldehyde in 1X PBS at room temperature for 15 minutes. Following fixation, cells were washed with excess 1X PBS, pelleted, and resuspended in 1X PBS and stored at $4^oC$. Cells were permeabilized with 90% ice-cold methanol in 1X PBS for at least 10 minutes on ice and then washed with excess 1X PBS. The following fluorescently conjugated antibodies were prepared in 0.5% PBSA: pSTAT1-PE (no. 8062, 1:50, CST) and ZIKV NS5 AF647 (1:2000, conjugated in house). ZIKV NS5 was conjugated to AF647 using an Alexa Fluor 647 antibody labeling kit (ThermoFisher Scientific) according to the manufacturer's instructions. Cells were incubated in the dark with antibodies for 1 hour at room temperature. Following staining, cells were washed with 1X PBS, and data was acquired on a Canto II flow cytometer (BD Biosciences, Franklin Lakes, NJ, USA). Flow cytometry data were analyzed in FlowJo (BD Biosciences).

## 2.21 Statistical analyses

Statistical analyses were carried out as indicated in the figure legends. Statistical analyses were performed in GraphPad Prism and in RStudio.

## 2.22 Data availability

Deep sequencing data were deposited in GenBank under these accession numbers: ZIKV/Dakar GenBank OQ180929; ZIKV/Malaysia GenBank OQ165285. Raw and processed Nanostring transcript expression data are presented in Tables 4-6.

## 2.23 Acknowledgements

We thank members of the University of Washington and the Center for Innate Immunity and Immune Disease for helpful discussions and advice throughout the course of this study. We thank Michael Diamond (Washington University in St. Louis) and Robert Tesh (University of Texas Medical Branch) for providing hybridomas and ZIKV isolates. We are grateful to the Seattle Genomics sequencing group for sequencing ZIKV stocks and to the University of Washington Cell Analysis Facility for technical assistance. This work was supported by National Institutes of Health grants AI143265, AI145296, and AI151698.

Table 1. Primer sequences for cloning and qRT-PCR.

| **Primers for cloning** | **Sequence (5’ to 3’)** | **Source** |
|---|---|---|
| pEF N-FLAG vector forward (F) | AAACCCGCTGATCAGCCT | This paper |
| pEF N-FLAG vector reverse (R) | GCTGAATTCCTTGTCATCGTCATCC | This paper |
| ZIKV NS3 F | GACAAGGAATTCAGCGAGGGAGAGTTCAAGCTTAGGACG | This paper |
| ZIKV NS3 R | CTGATCAGCGGGTTTGATAGGCCAGCCAAACAGGAAGA | This paper |
| pcDNA3.1+ ZIKV/Dakar and ZIKV/Malaysia NS5 vector F | GTTTAAACCCGCTGATCAGCCT | This paper |
| pcDNA3.1+ ZIKV/Dakar and ZIKV/Malaysia NS5 vector R | CAGCTTGGGTCTCCCTATAGTGAG | This paper |
| pcDNA3.1+ ZIKV/Dakar NS5 F | GGGAGACCCAAGCTGATGGAGGTGGAACGGGAGAG | This paper |
| pcDNA3.1+ ZIKV/Dakar NS5 R | TCAGCGGGTTTAAACTTACAGCACTCCAGGTGTGGAC | This paper |
| pcDNA3.1+ ZIKV/Malaysia NS5 F | GGGAGACCCAAGCTGATGGAGGTGGA | This paper |
| pcDNA3.1+ ZIKV/Malaysia NS5 R | TCAGCGGGTTTAAACTTATAACACTCCAGGTGTGGACCC | This paper |
| **Primers for TaqMan qRT-PCR** | **Sequence (5’ to 3’)** | **Source** |
| ZIKV NS3 F | GAGGGAGAGTTCAAGCT | This paper |

| | | |
|---|---|---|
| ZIKV NS3 R | GATAGGCCAGCCAAAC | This paper |
| ZIKV NS3 probe (with quencher) | 56-FAM/ TTC ATG AGT TCC ACA AAG GTC TTC CTT TGC /3IABkFQ | This paper |
| **Primers for SYBR Green qRT-PCR** | **Sequence (5' to 3')** | **Source** |
| IFNB | N/A | PPH00384F; Qiagen |
| TNF | N/A | PPH00341F; Qiagen |
| IL6 | N/A | PPH00560C-200; Qiagen |
| MX1 | N/A | PPH01325A; Qiagen |
| IFITM1 | N/A | PPH05981C; Qiagen |
| DDX58 | N/A | PPH20774A-200; Qiagen |
| OAS1 | N/A | PPH01324A-200; Qiagen |
| RPL13A F | GCCCTACGACAAGAAAAAGCG | (242) |
| RPL13A R | TACTTCCAGCCAACCTCGTGA | (242) |

Table 2. Primary antibodies for immunoblot analysis.

| Antigen | Catalog # | Source | Host | Concentration |
|---|---|---|---|---|
| pIRF3 S386 | ab76493 | Abcam, Cambridge, UK | Rabbit | 1:1000 |
| pIRF3 S396 | 4947 | Cell Signaling Technology (CST), Danvers, MA, USA | Rabbit | 1:1000 |
| IRF3 | 4302 | CST | Rabbit | 1:1000 |
| IκBα | 4814 | CST | Mouse | 1:1000 |
| IFIT1 | 971 | In house | Rabbit | 1:1000 |
| ZIKV NS5 | GTX133327 | GeneTex, Irvine, CA, USA | Rabbit | 1:2500 |
| ZIKV NS1 | ARG65781 | Arigo Biolaboratories, Hsinchu City, Taiwan | Mouse | 1:1000 |
| ZIKV capsid | GTX133317 | GeneTex | Rabbit | 1:1000 |
| pSTAT1 | 7649 | CST | Rabbit | 1:1000 |
| STAT1 | 9172 | CST | Rabbit | 1:1000 |
| STAT2 | 72604 | CST | Rabbit | 1:1000 |
| IFITM1 | 60074-1-1g | ProteinTech Group, Rosemont, IL, USA | Mouse | 1:1000 |
| OAS1 | 14498 | CST | Rabbit | 1:1000 |
| Mx1 | 340B | In house | Rabbit | 1:500 |
| RIG-I | AG-20B-0009-C100 | Adipogen, San Diego, CA, USA | Mouse | 1:1000 |
| Actin | MAB 1501 | Sigma-Aldrich | Mouse | 1:1000 |

# Chapter 3. Genomic differences between prototypic ZIKV variants link with differential replication kinetics and innate immune responses

*This chapter is combined with chapter 4 as a manuscript.*

## 3.1 Introduction

The 2013 and 2015 ZIKV outbreaks marked the emergence of severe clinical manifestations following ZIKV infection and of mosquito-independent transmission routes, highlighting the global threat ZIKV poses. Since these outbreaks, previous studies have comparatively assessed the replication properties of African and Asian lineage strains and have revealed that African lineage strains replicate to higher levels and induce more cell death (46, 226, 227, 230–237, 249). As the recently emerging ZIKV variants belong to the Asian lineage, it is likely that ZIKV has evolved to become more pathogenic than pre-epidemic Asian lineage viruses (3, 10–13, 396). Indeed, comparative analyses of viral replication kinetics between pre-epidemic and epidemic Asian lineage variants have demonstrated that epidemic strains exhibit enhanced viral replicative fitness compared to pre-epidemic Asian lineage viruses (242, 245). Moreover, studies have identified specific aa residues between epidemic and pre-epidemic Asian lineage strains that differentially impact fetal brain damage, viral infectivity, and viral transmissibility (102, 134, 245–247, 397). These findings provide evidence that viral genetics plays a crucial role in ZIKV replication, transmission, and disease.

The innate immune response to ZIKV infection is differentially modulated by ZIKV variants as studies have shown that Asian lineage-derived epidemic strains induce weaker antiviral and IFN responses than African lineage or pre-epidemic Asian lineage viruses (61, 235, 242, 244, 358). Furthermore, African and Asian lineage-derived epidemic strains have been shown to be less sensitive to the antiviral effects of IFN (242, 363). Dampened antiviral and IFN responses along with a decrease in IFN sensitivity can promote efficient replication and cell-to-cell spread and facilitate persistence of epidemic ZIKV strains, highlighting the crucial role that host antiviral signaling plays in controlling ZIKV replication and spread. Additionally, high levels of TLR3 and IFN signaling induce severe damage to the fetal brain and the placenta, implicating the innate immune response in ZIKV pathogenesis (45, 307, 358–360, 398). Other *in vitro* and *in vivo* studies have demonstrated that epidemic ZIKV variants induce more robust inflammatory responses than African lineage and pre-epidemic Asian lineage-derived strains, increasing viral pathogenesis of emerging variants (259, 307, 362). Together, these studies indicate a contribution of the host inflammatory response to ZIKV infection in viral pathogenesis.

As previous studies predominantly compared African or pre-epidemic Asian lineage viruses with emerging strains, our understanding of the replication properties of and host innate immune responses to prototypic African and Asian lineage strains remains limited. Since viral genetics is a determinant of viral fitness, we hypothesized that changes in ZIKV genome sequences between prototypic African and Asian lineage strains impact viral replication and innate immune actions to drive differential control of ZIKV infection. Hence, we carried out a comprehensive virologic and host innate

immune analysis of the prototypic African and Asian lineage viruses, ZIKV/Dakar/1984/ArD41519 (ZIKV/Dakar) and ZIKV/Malaysia/1966/P6740 (ZIKV/Malaysia), respectively, in an immunocompetent human epithelial cell infection model. We assessed viral replication kinetics and the innate immune activation and response profiles induced by infection with these variants to evaluate how ZIKV sequences link with virologic differences and innate immune responses. *De novo* sequence determination identified aa changes within the ZIKV/Dakar genome compared to ZIKV/Malaysia. One-step viral growth analyses revealed that ZIKV/Malaysia accumulated viral proteins and RNA faster and to higher levels and exhibited a higher infection efficiency than ZIKV/Dakar. We demonstrate that despite robust activation of RIG-I signaling during acute infection with either ZIKV variant, ZIKV/Malaysia, but not ZIKV/Dakar, potently blocked IFN signaling. These findings reveal that ZIKV/Malaysia exhibits higher replicative fitness and induces a weaker IFN response than ZIKV/Dakar contrary to findings from previous studies, demonstrating that the prototypic Asian lineage virus may be more virulent than the prototypic African lineage isolate.

## 3.2 Results

### Prototypic ZIKV variants encode genomic differences associated with viral fitness

To evaluate how changes in ZIKV genome sequences contribute to viral fitness, we first sequenced two prototypic ZIKV strains from distinct lineages, African lineage ZIKV/Dakar (GenBank OQ180929) and Asian lineage ZIKV/Malaysia (GenBank OQ165285). Although the original ZIKV strain isolated in Uganda in 1947 is the prototypic African lineage strain, it has been passaged extensively in mice prior to its distribution for research, whereas ZIKV/Dakar has undergone only limited passaging in

cell culture since its original isolation in 1984 (1, 3, 399). We note that ZIKV/Malaysia is the prototypic Asian lineage virus and was thus included in our analyses with ZIKV/Dakar (4). We also included the sequence of a reference Asian lineage strain (GenBank KX377336) in our genomic analysis and determined the percent aa divergence of our ZIKV variants compared to the reference Asian lineage strain and to one another (400). Compared to the Asian lineage reference strain, we found that ZIKV/Malaysia displays 0.029% aa sequence divergence. Importantly, ZIKV/Dakar exhibits increased aa sequence divergence from the Asian lineage reference strain compared to ZIKV/Malaysia with 2.48% aa divergence (Fig. 3-1A).

**A.**

| AA % divergence | **ZIKV/Malaysia/1966/P6740 (KX377336)** | **ZIKV/Malaysia/1966/P6740 (ZIKV/Malaysia)** |
|---|---|---|
| **ZIKV/Dakar/1984/ArD41519 (ZIKV/Dakar)** | 2.48 | 2.45 |
| **ZIKV/Malaysia/1966/P6740 (ZIKV/Malaysia)** | 0.029 | |

**B.**

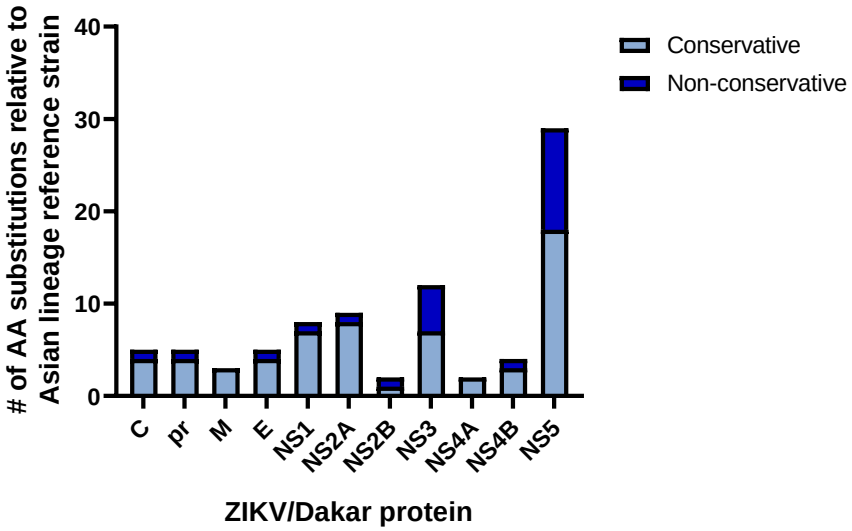

Figure 3-1. Prototypic ZIKV variants encode sequence differences associated with viral fitness. Viral stocks were sequenced, and consensus sequences were assembled *de novo*. (A) The matrix depicts the percent divergence of aa sequences of prototypic ZIKV variants compared to an Asian lineage reference genome (GenBank KX377336). (B) The total number of aa substitutions in each ZIKV/Dakar protein compared to an Asian lineage reference strain is presented and categorized as conservative or non-conservative.

We also identified non-conservative and conservative aa substitutions in each of the ZIKV/Dakar structural and non-structural proteins compared to the Asian lineage reference strain with the greatest number of substitutions located in NS5 (Fig. 3-1B and Table 3). We found that ZIKV/Dakar and ZIKV/Malaysia both encode an alanine at position 106 of the C protein. The alanine at this position is conserved in all epidemic strains and has been shown to increase viral infectivity and fitness in the mosquito vector and in mammalian hosts (245, 246). Our sequencing analysis also revealed that ZIKV/Dakar encodes the V1A mutation in prM, which is found in epidemic strains and has been associated with reduced viral fitness and virulence in mammalian hosts (247). Neither ZIKV/Dakar nor ZIKV/Malaysia encode the S17N mutation in prM linked with enhanced infectivity in NPCs and increased microcephaly severity (102). Both ZIKV variants retain the E protein glycosylation site at position 154, which has been demonstrated to enhance viral infectivity and virulence in mosquitoes and IFNAR KO mice (102, 109, 110). Furthermore, ZIKV/Dakar encodes the A188V mutation in NS1, which enhances infectivity in mosquitoes and confers enhanced blockade of innate immune activation and IFNβ induction through the interaction between NS1 and TBK1 (134, 377). Importantly, this mutation is absent in ZIKV/Malaysia but present in all

African lineage variants and emerging Asian lineage-derived strains (134, 242, 377). We also identified several other aa substitutions in the remaining structural and non-structural proteins in the ZIKV/Dakar genome that have not been previously reported to contribute to viral fitness or host interactions.

**ZIKV strains exhibit replication differences in immunocompetent cells**

To evaluate strain-specific differences on viral replication, we carried out analyses to examine viral protein accumulation, genome replication, virus secretion, and spread of the ZIKV variants in an established immunocompetent human epithelial cell (A549) infection model (242, 269, 387). We performed immunoblot analyses to evaluate the accumulation of viral proteins over a 48-hour acute infection time-course and found that samples infected with ZIKV/Malaysia accumulated detectable levels of the C protein, NS1, and NS5 by 8 hpi (Fig. 3-2A). On the other hand, samples infected with ZIKV/Dakar did not accumulate detectable levels of these viral proteins until 24 hpi. We also observed that samples infected with ZIKV/Malaysia had a greater abundance of the C protein, NS1, and NS5 throughout the infection time-course compared to samples infected with ZIKV/Dakar. Next, we conducted one-step viral growth analyses to characterize the growth kinetics of these variants during acute infection at a high MOI. We observed that ZIKV/Malaysia replicated to significantly higher levels with vRNA levels peaking at 24 hpi and plateauing throughout the remainder of the time-course (Fig. 3-2B). ZIKV/Dakar, however, did not reach the exponential phase of genome replication until 8 hpi, likely due to the slower rate of viral protein accumulation, and accumulated significantly fewer copies of genomic RNA.

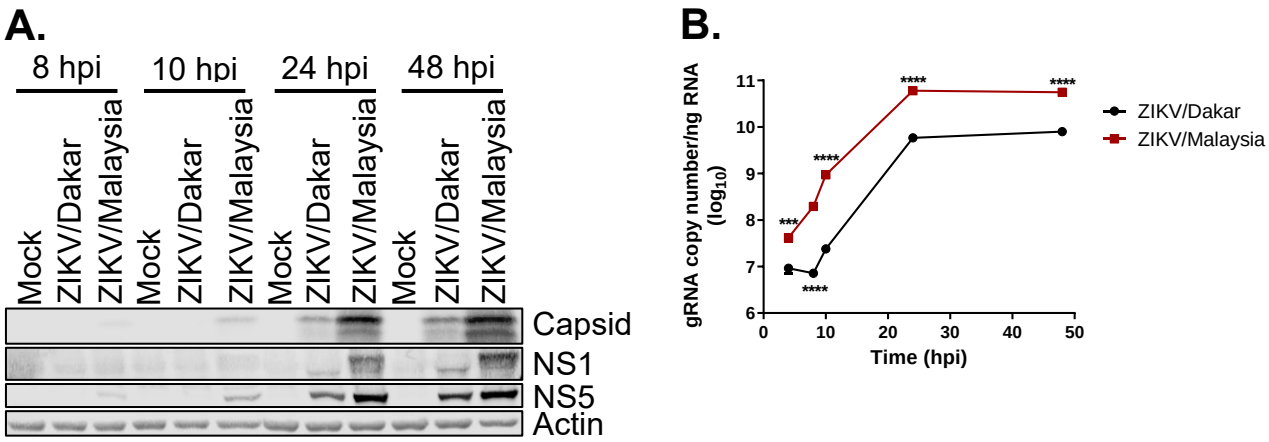


Figure 3-2. ZIKV/Malaysia accumulates viral proteins and genome copies faster and to higher levels than ZIKV/Dakar during acute infection. A549 cells were mock-infected or infected with ZIKV/Dakar or ZIKV/Malaysia over a 48-hour time-course at a MOI of 5. (A) Cell lysates were analyzed via immunoblotting. One immunoblot representative of three independent experiments (n = 3) is presented. (B) Viral copy numbers were determined from RNA lysates by qRT-PCR. Depicted are means from three biological and technical replicates that were pooled for statistical analysis; error bars represent SEM. Statistical analyses were performed with a two-tailed unpaired t-test at each time point (***p<0.001; ****p<0.0001).

Given the differences in the accumulation of viral protein and intracellular vRNA between cells infected with these ZIKV variants, we investigated whether ZIKV/Dakar and ZIKV/Malaysia exhibited differences in viral attachment and entry that could possibly link with these outcomes (Fig. 3-3A). Cell binding analyses revealed that ZIKV/Dakar and ZIKV/Malaysia exhibited similar efficiency of cell attachment, indicating that differences in viral attachment to cells do not contribute to differences in the accumulation of viral proteins and intracellular genome copies in A549 cells (Fig. 3-3B). We then quantified the intracellular vRNA levels at 1 hpi to assess viral entry and observed that they were comparable between the ZIKV variants, indicating that ZIKV/Dakar and ZIKV/Malaysia do not exhibit differences in viral entry in A549 cells (Fig. 3-3C). Analysis of genome replication over this 24-hour infection time-course

demonstrated that ZIKV/Malaysia replicated viral genome to higher levels compared to ZIKV/Dakar, indicating that ZIKV/Malaysia is more efficient at genome replication than ZIKV/Dakar (Fig. 3-3D).

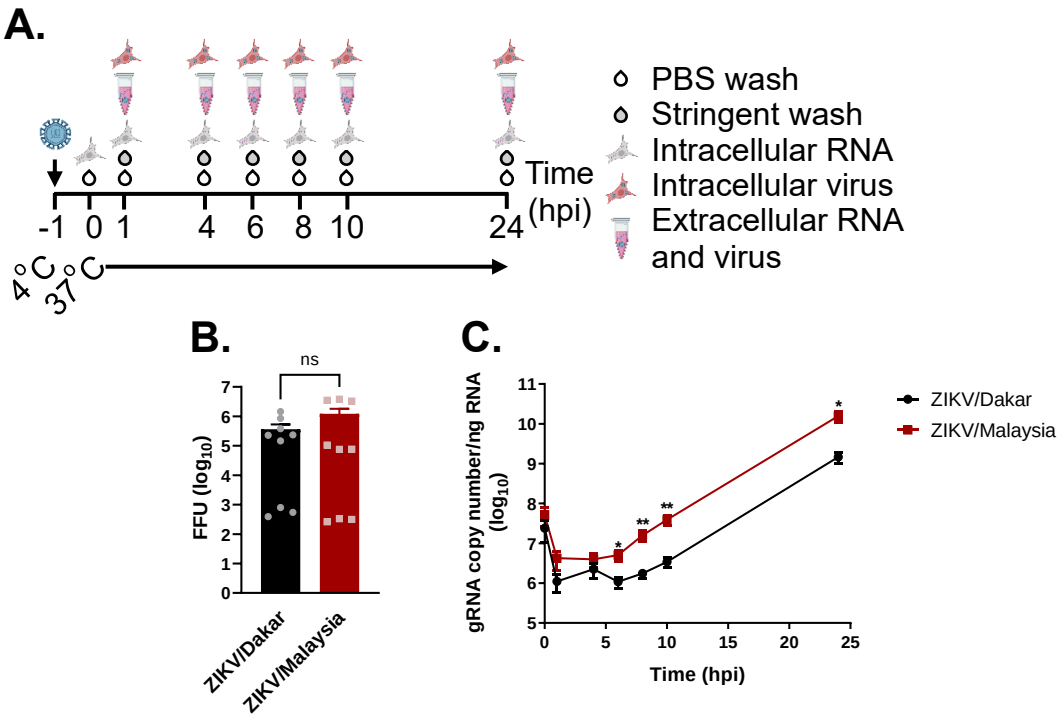


Figure 3-3. ZIKV variants exhibit similar cell attachment and entry efficiencies, but ZIKV/Malaysia is more efficient at genome replication. A549 cells were mock-infected or infected with ZIKV variants over a 24-hour time-course at a MOI of 5. Results are representative of three independent experiments (n = 3). (A) Schematic of experimental setup. Illustrations were generated in BioRender. (B) RNA lysates were harvested at 0 hpi, and viral copy numbers were determined by qRT-PCR and converted to FFUs. Results depict means from three biological and technical replicates that were pooled for statistical analysis. (C) Intracellular viral copy numbers were quantified from RNA lysates by qRT-PCR. Depicted are means from three biological and technical replicates that were pooled for statistical analysis. For all figures, error bars represent SEM. All statistical analyses were performed with a two-tailed unpaired t-test at each time point (ns: not significant; *p<0.05; **p<0.005).

Next, we compared virion production between the ZIKV variants and found that cells infected with either variant released similar amounts of infectious virions despite the significant differences in the levels of intracellular viral genome copies (Fig. 3-4).

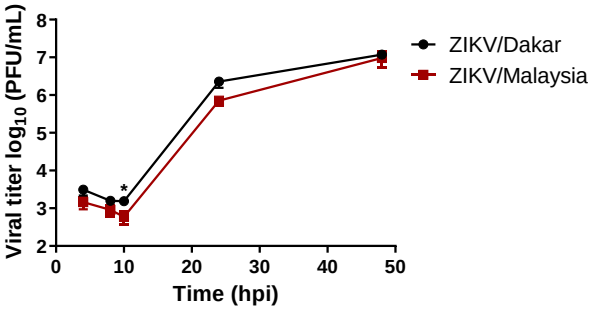


Figure 3-4. Cells infected with either ZIKV variant secrete similar amounts of infectious virions. A549 cells were mock-infected or infected with ZIKV/Dakar or ZIKV/Malaysia over a 48-hour time-course at a MOI of 5. Cell culture supernatants were titered by plaque assay. Results are depicted as means; error bars represent SEM. Results are representative of three independent experiments (n = 3). Statistical analyses were performed with a two-tailed unpaired t-test at each time point (*p<0.05).

To determine whether differences in virion assembly or secretion kinetics could account for this discrepancy, we employed a synchronous infection analysis as outlined in Fig. 3-3A. We observed that cells synchronously infected with ZIKV/Dakar or ZIKV/Malaysia had similar amounts of intracellular infectious particles at 24 hpi despite significant differences in the levels of intracellular vRNA observed at this time point (Fig. 3-3C, Fig. 3-5A). Given this observation, we calculated the intracellular RNA:PFU ratios to evaluate the virion assembly efficiency of these ZIKV variants and revealed that ZIKV/Dakar was more efficient at virion assembly than ZIKV/Malaysia (Fig. 3-5B). When we quantified the amounts of extracellular infectious virions over the 24-hour infection time-course, we observed no differences in the abundance of extracellular vRNA and infectious particles (Fig. 3-5C, D). Comparisons of extracellular RNA:PFU ratios to assess the infectivity of progeny virions revealed no differences in the infectivity of progeny produced by ZIKV/Dakar- and ZIKV/Malaysia-infected cells (Fig. 3-2E). These findings demonstrate that the ZIKV variants do not differ in the kinetics of virion

secretion nor in the infectivity of progeny virus. Instead, ZIKV/Dakar and ZIKV/Malaysia differ in virion assembly efficiency, with ZIKV/Dakar exhibiting greater virion assembly efficiency.

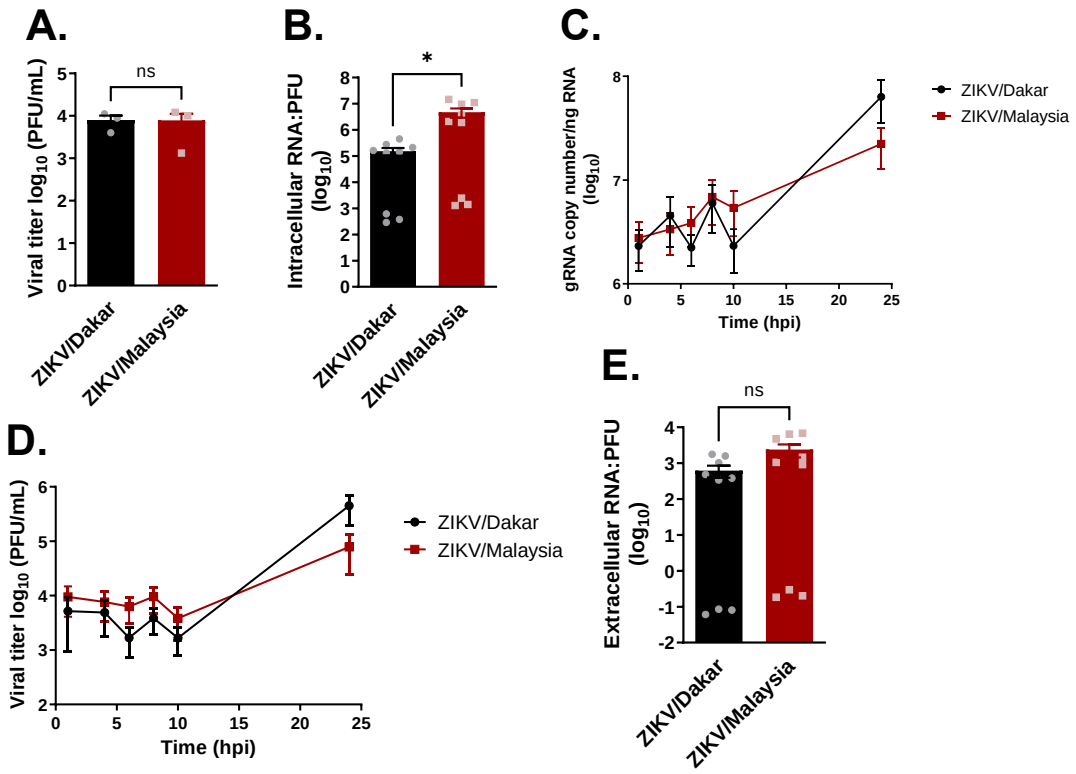


Figure 3-5. ZIKV/Dakar exhibits greater virion assembly efficiency. A549 cells were mock-infected or infected with ZIKV variants over a 24-hour time-course at a MOI of 5. Results are representative of three independent experiments (n = 3). (A) Cell pellets were collected at 24 hpi, and intracellular viral titers were determined by plaque assay. Results are depicted as means. (B) Intracellular RNA:PFU ratios were calculated for ZIKV variants. Results represent means from three biological and technical replicates. (C, D) Cell culture supernatants were collected at the indicated time points to quantify (C) extracellular viral copy number via qRT-PCR and (D) extracellular viral titers by plaque assay. Results depict means from (C) three biological and technical replicates that were pooled for statistical analysis and (D) means from three independent experiments (n = 3). (E) Extracellular RNA:PFU ratios were calculated for ZIKV variants. Results are depicted as means from three biological and technical replicates. For all figures, error bars represent SEM. All statistical analyses were performed with a two-tailed unpaired t-test at each time point (ns: not significant; *p<0.05).

Lastly, we evaluated spread of ZIKV/Dakar and ZIKV/Malaysia over a 48-hour acute infection time-course at a high MOI. We stained cells with antibodies specific to dsRNA (a marker for viral replication) and ZIKV NS5 protein for immunofluorescence analyses to compare the infection efficiency of these variants. At both 24 and 48 hpi, ZIKV/Malaysia infected a significantly higher percentage of cells than ZIKV/Dakar (Fig. 3-6A, B). We did not observe a significant increase in the percentage of infected cells for either ZIKV strain between 24 and 48 hpi, suggesting that there was limited viral spread between these two time points (Fig. 3-6B). As the infection efficiency of these ZIKV variants differed by only two-fold, it is likely that this difference contributes only minimally to the 10-fold difference in intracellular viral genome copies observed between ZIKV/Dakar and ZIKV/Malaysia (see Fig. 3-2B), suggesting that the ZIKV variants may additionally differ in their interactions with host factors critical for viral control. Together, our data clearly demonstrate that ZIKV/Dakar and ZIKV/Malaysia exhibit unique replication differences in immunocompetent A549 cells, specifically at the stages of viral protein accumulation, genome replication, and virion assembly that together impact viral spread.

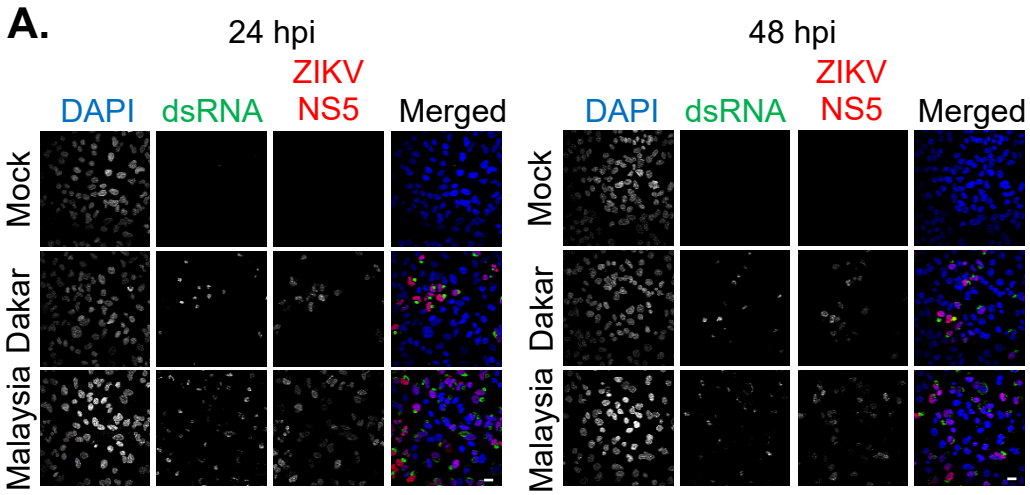

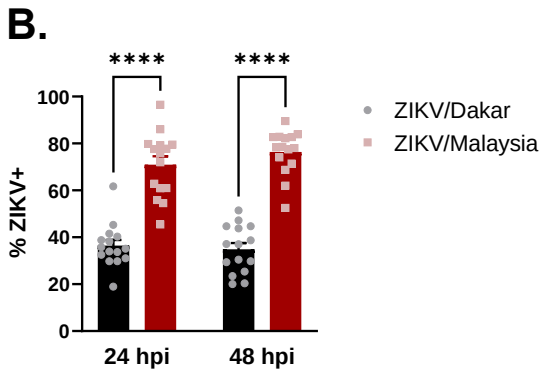


Figure 3-6. ZIKV/Malaysia exhibits enhanced cell-to-cell spread compared to ZIKV/Dakar. A549 cells were infected with ZIKV strains at a MOI of 5, and the percentage of infected cells at each time point was quantified by immunofluorescence analysis. (A) For each sample, five randomly selected fields of view representing at least 190 cells total were analyzed. Scale bar represents 10μm. (B) Images were manually analyzed in Fiji using the multipoint tool. The percentages of ZIKV+ cells are presented after normalizing to the total number of cells as determined by DAPI staining. Depicted are means from five randomly selected fields of view across three independent experiments (n = 3) that were pooled for statistical analysis. Error bars represent SEM. Statistical analyses were performed with a two-tailed unpaired t-test at each time point (****p<0.0001).

**ZIKV variants induce robust innate immune activation**

To investigate the contribution of innate immunity on the replication differences observed between the ZIKV variants, we evaluated activation of RLR signaling and response over a 48-hour acute infection time-course. We carried out immunoblot analyses and probed for phospho-IRF3 (pIRF3) S386 and S396 and IκB as markers of IRF3 and NFκB activation, respectively. We observed that ZIKV variants induced IRF3 and NFκB activation to a similar extent at 24 hpi (Fig. 3-7A). At 48 hpi, however, ZIKV/Malaysia induced RLR activation to a greater extent as indicated by the increased abundance of pIRF3 S386 and S396 and decreased levels of IκB. Thus, both

ZIKV/Dakar and ZIKV/Malaysia activate RLR signaling with ZIKV/Malaysia inducing increased RLR signaling late in acute infection.

RLR activation triggers a signaling cascade that results in the expression of IFNβ and inflammatory cytokines (263, 266, 291, 401). As such, we used a custom Nanostring innate immunity gene panel that includes target genes of IRF3, NFκB, IFN, and inflammatory cytokine signaling marking activation of these pathways to analyze a select cytokine mRNA expression profile induced in response to infection with ZIKV/Dakar or ZIKV/Malaysia. Nanostring analysis provides a direct measure of the absolute counts of the target mRNAs noted (402). PCA revealed that ZIKV/Dakar- and ZIKV/Malaysia-infected samples clustered with mock-infected samples prior to 24 hpi (Fig. 3-7B). At 24 and 48 hpi, infected samples clustered away from the mock-infected samples with infected samples clustering together at these time points. This indicates that our samples clustered by infection condition and time post-infection. To define the cytokine-specific transcriptional profiles induced by infection with the ZIKV variants, we visualized fold change in the expression levels of cytokines over the 48-hour acute infection time-course (Fig. 3-7C; Table 5). Compared to mock-infected samples, samples infected with the ZIKV variants similarly induced the expression of several cytokines, especially types I and III IFNs, indicating innate immune activation of IRF3 and NFκB signaling. To validate the results from our Nanostring analysis, we quantified the relative transcript levels of *IFNB*, *TNF*, and *IL6* genes by qRT-PCR (Fig. 3-7D). Consistent with our Nanostring results, infection with ZIKV/Dakar and ZIKV/Malaysia induced the expression of these cytokines to similar levels. Hence, our analyses of RLR signaling in response to infection with ZIKV/Dakar and ZIKV/Malaysia demonstrate that

the ZIKV variants activate RLR signaling to the same extent to induce similar innate immune activation gene expression profiles.

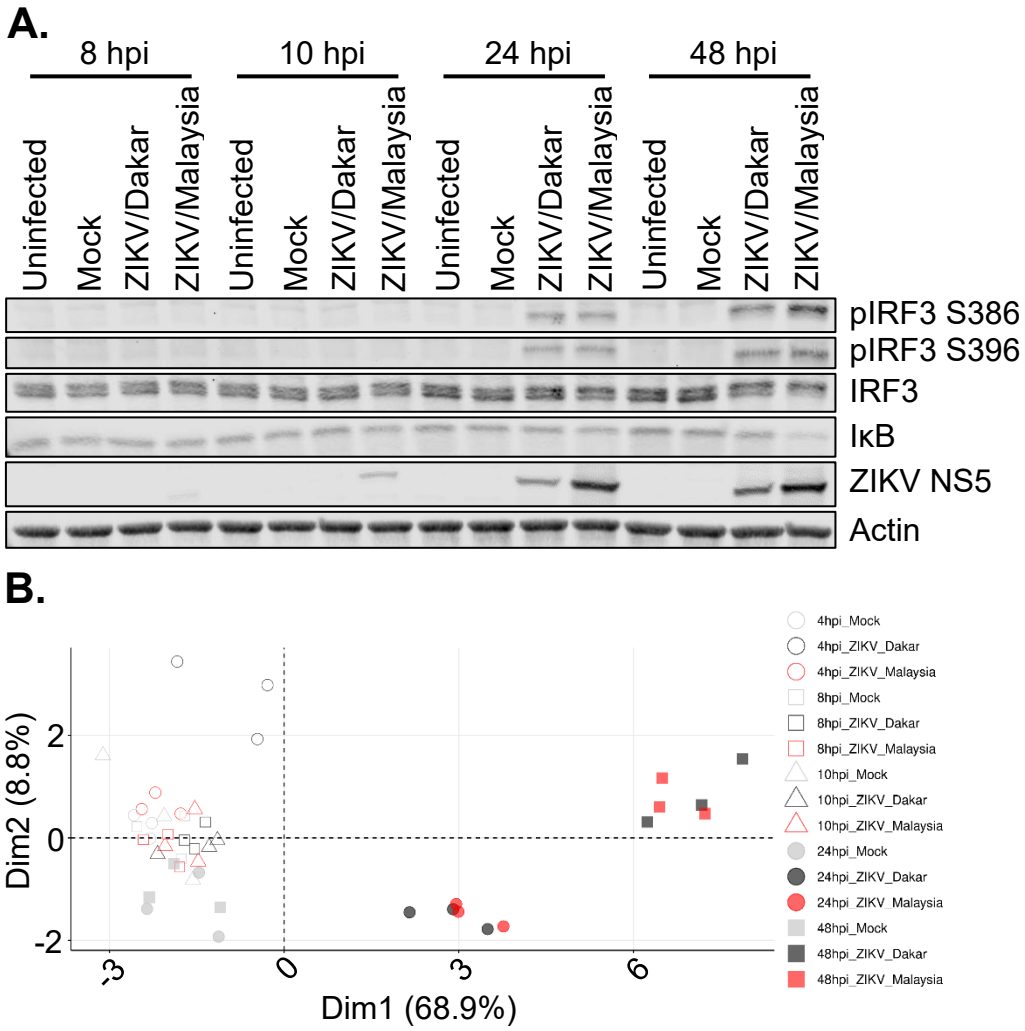

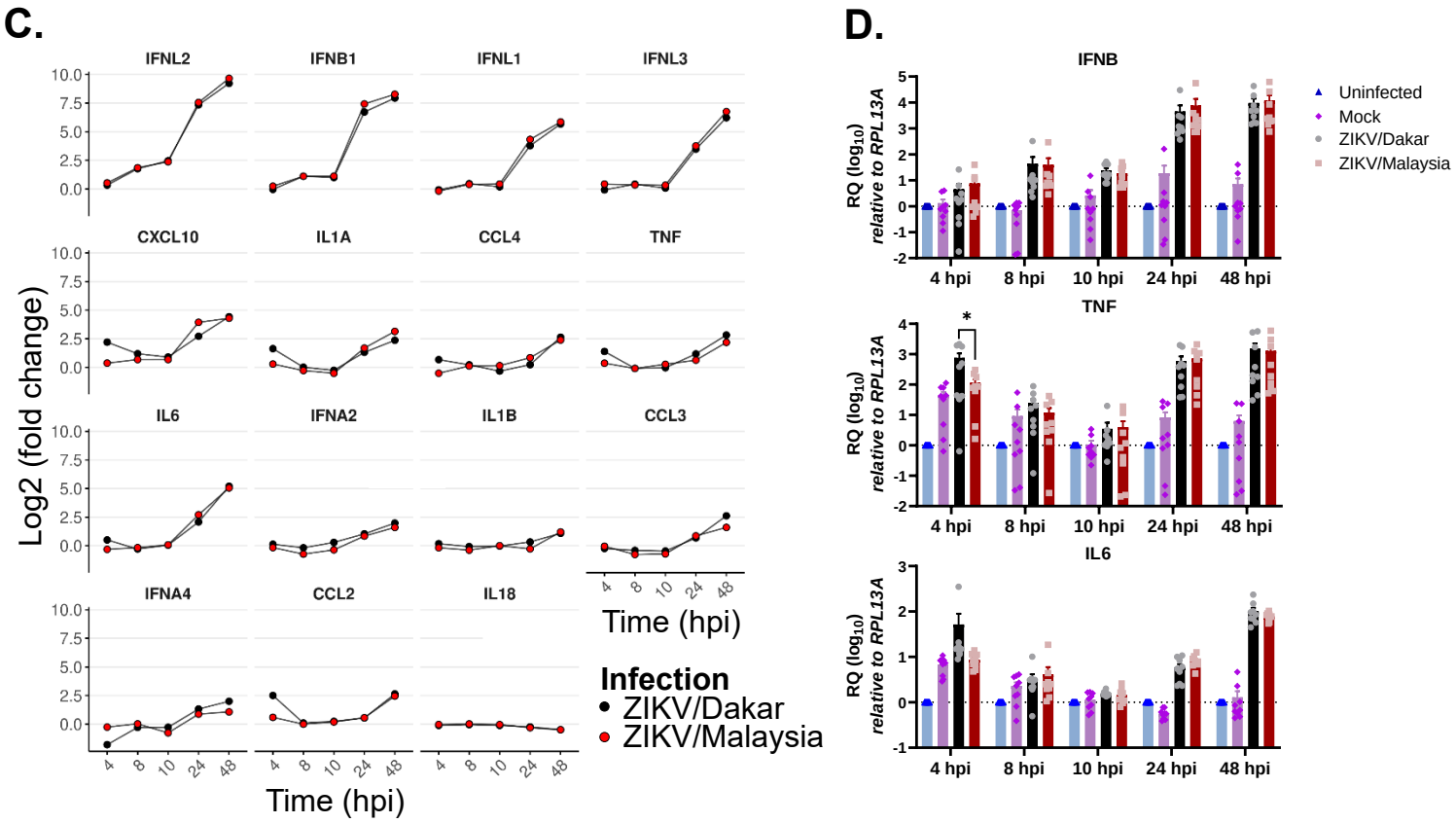


Figure 3-7. ZIKV/Dakar and ZIKV/Malaysia activate RLR signaling to the same extent. (A, D) A549 cells were uninfected, mock-infected, or infected with ZIKV variants over a 48-hour time-course at a MOI of 5. (A) Cell lysates were analyzed via immunoblotting. Depicted is an immunoblot representative of three independent experiments (n = 3). (B, C) A549 cells were mock-infected or infected with ZIKV/Dakar or ZIKV/Malaysia over a 48-hour time-course at a MOI of 5. RNA lysates were collected and raw mRNA transcript levels of cytokines and IFNs were quantified on the Nanostring nCounter. Raw and processed gene expression data are presented in Tables 4 and 5, respectively. Results are representative of three independent experiments (n = 3). (B) PCA plot of GOIs depicts changes in the cytokine transcriptional profiles over the infection time-course. (C) Log2 fold change over mock infection of the transcript levels of GOIs are depicted individually for each gene. Statistical analysis was performed with two-tailed t-test followed by Benjamini-Hochberg (BH) correction for each time point. (D) RNA lysates were collected and analyzed via qRT-PCR. *IFNB, TNF,* and *IL6* transcript levels were normalized to the *RPL13A* HK gene of uninfected samples at each time point. Results depict means from three biological and technical replicates, which were pooled for statistical analysis; error bars represent SEMs. Statistical analysis was performed with a one-way ANOVA followed by Tukey's multiple comparison test for each time point.

**ZIKV/Malaysia blocks IFN signaling to suppress induction of ISGs**

Given the robust induction of IFNs in response to acute infection with the ZIKV variants, we assessed the activation status of the JAK/STAT signaling pathway and the expression of ISGs at the protein level using an immunoblot assay. At 24 hpi, we observed that infection with the ZIKV variants induced STAT1 phosphorylation (pSTAT1) to similar levels (Fig. 3-8A). At 48 hpi, however, the levels of pSTAT1 induced by infection with ZIKV/Dakar or ZIKV/Malaysia diverged; specifically, the levels of pSTAT1 detected were lower during infection with ZIKV/Malaysia but higher during infection with ZIKV/Dakar. To evaluate whether the differential activation of STAT1 observed at 48 hpi impacts downstream induction of ISGs, we probed for several canonical ISGs: STAT1, RIG-I, IFITM1, OAS1, Mx1, and IFIT1. We observed that the expression of these ISGs at the protein level were lower during infection with ZIKV/Malaysia compared to infection with ZIKV/Dakar, indicating that lower pSTAT1 levels correlate with a reduction in ISG induction (Fig. 3-8A). As ZIKV is known to target STAT2 for proteasomal degradation as a mechanism of antagonizing JAK/STAT signaling, we additionally assessed STAT2 abundance (386, 389). We found that STAT2 levels were consistently lower throughout the acute ZIKV/Malaysia infection time-course (Fig. 3-8A). In fact, we observed STAT2 reduction as early as 8 hpi, which coincided with detection of ZIKV/Malaysia NS5 protein. Thus, although both ZIKV variants acutely induced robust levels of IFNs during infection, we found that infection with ZIKV/Malaysia elicits a weak IFN response compared to ZIKV/Dakar, indicating that ZIKV/Malaysia can more efficiently block IFN signaling than ZIKV/Dakar.

To further delineate the effects of innate immune activation and differential regulation of JAK/STAT signaling on downstream gene expression during acute ZIKV infection, we evaluated the IRF3-target gene and ISG transcriptional profiles induced by infection with ZIKV/Dakar and ZIKV/Malaysia using our custom Nanostring innate immunity gene panel. PCA indicated that infected samples clustered with mock-infected samples prior to 24 hpi before clustering away from mock-infected samples (Fig. 3-8B). At 24 and 48 hpi, we observed that samples infected with ZIKV/Dakar and ZIKV/Malaysia clustered based on ZIKV variant and time. Compared to mock infection, infection with the ZIKV variants induced initial upregulation of the transcript levels of IRF3-target genes and ISGs in our panel at early time points post-infection (Fig. 3-8C; Table 6). In accordance with our immunoblot results, we observed that infection with ZIKV/Malaysia suppressed the transcriptional induction of a majority of ISGs in our panel by 24 hpi compared to infection with ZIKV/Dakar, which induced ISGs to higher levels overall. To validate the results from our Nanostring analysis, we quantified the transcript levels of canonical ISGs, *MX1*, *IFITM1*, *DDX58*, and *OAS1*, via qRT-PCR (Fig. 3-8D). We observed that infection with ZIKV/Dakar induced the expression of these ISGs to significantly higher levels compared to infection with ZIKV/Malaysia, verifying our results from our Nanostring analysis. Together, our data reveal a unique immunophenotype where the prototypic African and Asian lineage ZIKV strains induce similar IRF3 and NFκB signaling profiles but differentially regulate IFN signaling to modulate downstream ISG expression, driving distinct innate immune signatures.

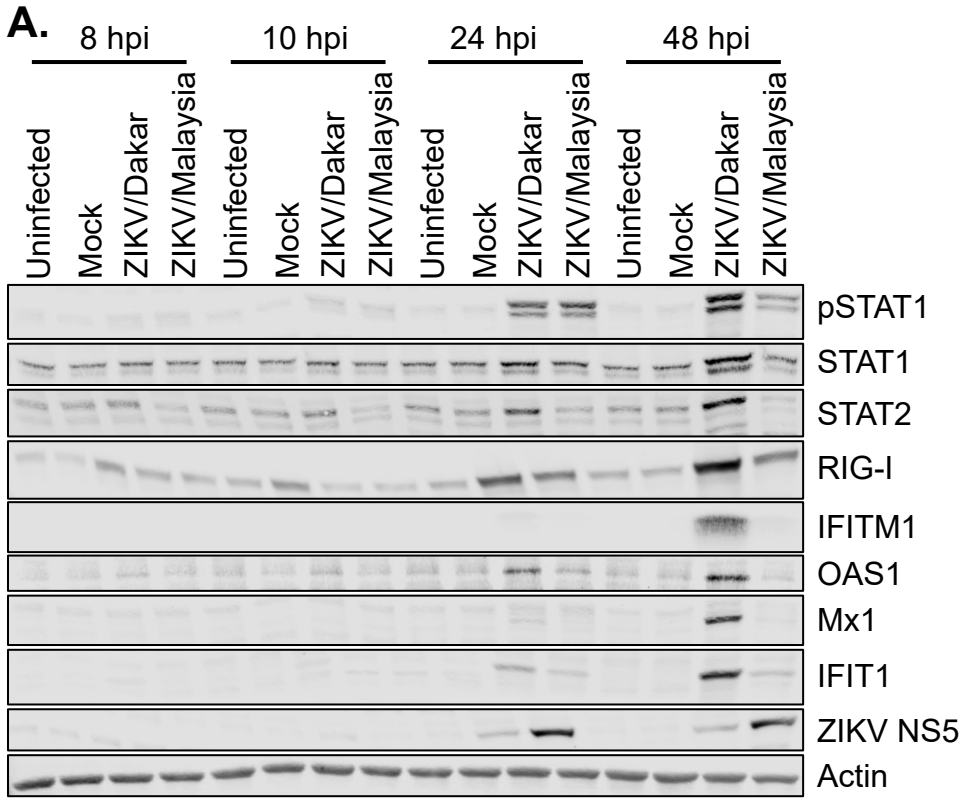
A.
8 hpi
10 hpi
24 hpi
48 hpi
Uninfected
Mock
ZIKV/Dakar
ZIKV/Malaysia
pSTAT1
STAT1
STAT2
RIG-I
IFITM1
OAS1
Mx1
IFIT1
ZIKV NS5
Actin

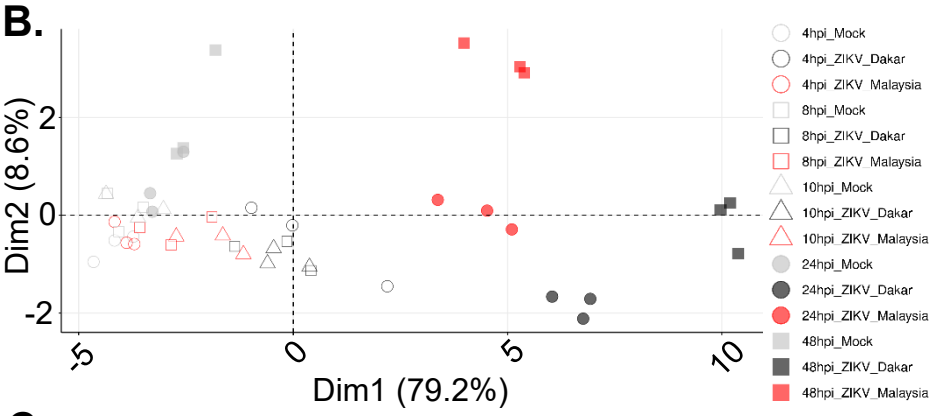
B.
Dim2 (8.6%)
Dim1 (79.2%)
4hpi_Mock
4hpi_ZIKV_Dakar
4hpi_ZIKV_Malaysia
8hpi_Mock
8hpi_ZIKV_Dakar
8hpi_ZIKV_Malaysia
10hpi_Mock
10hpi_ZIKV_Dakar
10hpi_ZIKV_Malaysia
24hpi_Mock
24hpi_ZIKV_Dakar
24hpi_ZIKV_Malaysia
48hpi_Mock
48hpi_ZIKV_Dakar
48hpi_ZIKV_Malaysia

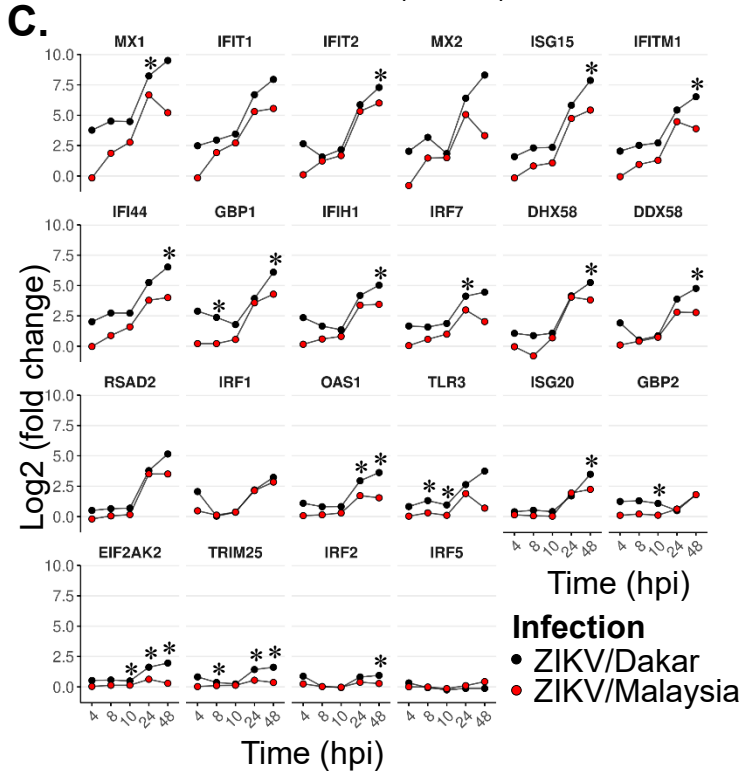
C.
MX1
IFIT1
IFIT2
MX2
ISG15
IFITM1
IFI44
GBP1
IFIH1
IRF7
DHX58
DDX58
RSAD2
IRF1
OAS1
TLR3
ISG20
GBP2
EIF2AK2
TRIM25
IRF2
IRF5
Log2 (fold change)
Time (hpi)
Infection
ZIKV/Dakar
ZIKV/Malaysia

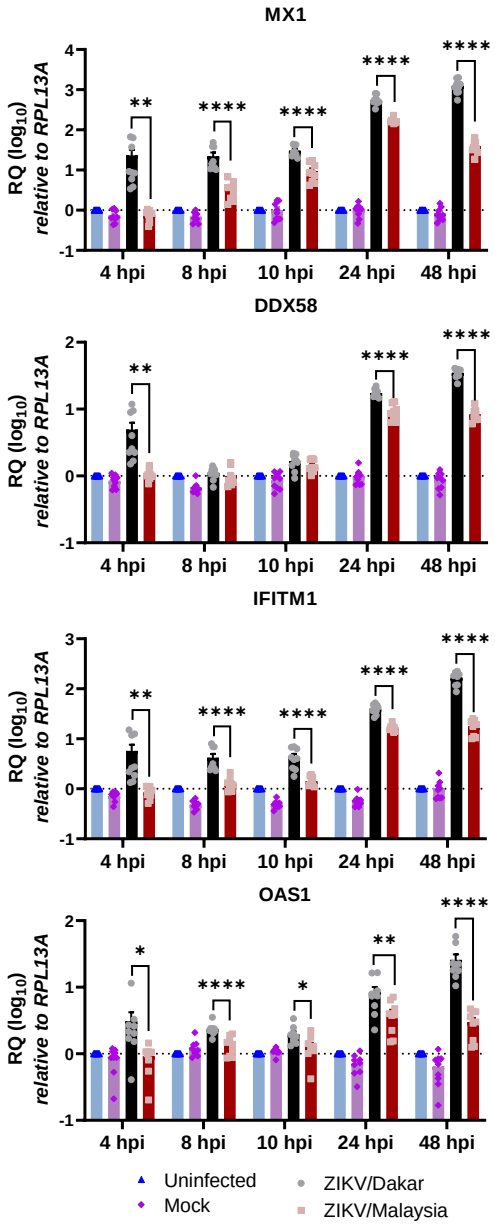
D.
MX1
DDX58
IFITM1
OAS1
RQ (log10) relative to RPL13A
4 hpi
8 hpi
10 hpi
24 hpi
48 hpi
Uninfected
Mock
ZIKV/Dakar
ZIKV/Malaysia

Figure 3-8. ZIKV/Malaysia blocks IFN signaling to suppress induction of ISGs. (A, D) A549 cells were uninfected, mock-infected, or infected with ZIKV/Dakar or ZIKV/Malaysia over a 48-hour time-course at a MOI of 5. (A) Cell lysates were analyzed by immunoblotting. Depicted is an immunoblot representative of three independent experiments (n = 3). (B, C) A549 cells were mock-infected or infected with ZIKV variants over a 48-hour time-course at a MOI of 5. RNA lysates were collected and RNA transcript levels of a select panel of ISGs were quantified on the Nanostring nCounter. Raw and processed expression data are presented in Tables 4 and 6, respectively. Results are representative of three independent experiments (n = 3). (B) PCA plot depicts changes in ISG transcriptome under each infection condition over the infection time-course. (C) Log2 fold change of ISG transcript levels is depicted. Statistical analysis was performed with two-tailed t-test followed by BH correction for each time point (*p<0.05). (D) RNA lysates were collected for qRT-PCR analysis. *MX1, IFITM1, DDX58,* and *OAS1* transcript levels were normalized to the *RPL13A* HK gene of uninfected samples at each time point. Depicted are means from three biological and technical replicates that were pooled for statistical analysis; error bars represent SEMs. Statistical analysis was performed with a one-way ANOVA followed by Tukey's multiple comparison test (*p<0.05; **p<0.005; ****p<0.0001).

## 3.3 Summary of results

In this chapter, we sought to evaluate the impact of viral genomic differences on viral replication kinetics and host innate immune responses to two prototypic ZIKV variants, African lineage ZIKV/Dakar and Asian lineage ZIKV/Malaysia. Our sequencing analysis identified several aa differences between each viral protein of ZIKV/Dakar compared to a reference Asian lineage strain and further revealed that ZIKV/Dakar and ZIKV/Malaysia share some known genetic determinants of viral fitness (Fig. 3-1B, Table 3). We found that ZIKV/Dakar encodes the V1A mutation in prM and the A188V mutation in NS1 while ZIKV/Malaysia does not, suggesting that these ZIKV variants may exhibit differences in viral fitness, virulence, and IFN induction (247, 377). We also

identified several aa differences in the structural and non-structural proteins in the ZIKV/Dakar genome, but their impact on viral fitness remains uncharacterized.

Evaluation of replication kinetics of these prototypic strains revealed lineage-dependent differences in specific stages of the viral life cycle. We observed that samples infected with ZIKV/Malaysia accumulated viral proteins and genome copies earlier and to higher levels compared to samples infected with ZIKV/Dakar but was less efficient at infectious virion assembly (Fig. 3-2A, B, Fig. 3-4H). These discrepancies were not due to differences in cell attachment or viral entry but were rather attributed to differences in genome replication efficiencies (Fig. 3-3C). We also found that ZIKV/Malaysia exhibited a higher infection efficiency than ZIKV/Dakar (Fig. 3-6). Cells infected with either ZIKV variant secreted similar amounts of infectious particles despite the significantly lower infection efficiency observed for ZIKV/Dakar (Fig. 3-4). This observation indicates that ZIKV/Dakar-infected cells secrete more infectious virions per infected cell, possibly due to the higher efficiency of infectious particle assembly observed for ZIKV/Dakar (Fig. 3-5B).

Comparative analyses of the innate immune response to ZIKV/Dakar and ZIKV/Malaysia demonstrated that the ZIKV variants activate RLR signaling and induce similar transcriptional upregulation of inflammatory cytokines, particularly types I and III IFNs (Fig. 3-7). Despite the robust acute induction of IFNs, we observed a striking immunophenotype between the ZIKV variants where ZIKV/Malaysia, but not ZIKV/Dakar, effectively blocked JAK/STAT signaling and the downstream expression of ISGs at the transcriptional and protein levels during acute infection (Fig. 3-8). RIG-I-

mediated antiviral signaling observed during infection with ZIKV/Dakar likely restricts the replication and spread of ZIKV/Dakar over an acute infection time-course.

# Chapter 4. RIG-I drives a critical innate immune response that regulates the kinetics of viral protein accumulation to permit IFN signaling for control of ZIKV replication and spread

*This chapter is combined with chapter 3 as a manuscript.*

## 4.1 Introduction

Host innate immune activation and signaling is the first line cell-intrinsic defense mechanism against viral pathogens (263–266). RIG-I serves as the primary PRR that recognizes ZIKV in human cells (242, 268, 269, 282). Binding of ZIKV PAMP to RIG-I triggers a signaling cascade that activates IRF3 and NFκB transcription factors to induce their translocation into the nucleus where they bind to the IFNβ promoter to upregulate expression of IFNβ (295–298). In the absence of RIG-I, IRF3 phosphorylation is abrogated and subsequently IFNβ production is severely blunted in response to ZIKV infection (242, 269). Consequently, ZIKV replicates to higher titers in RIG-I KO cells than in WT cells, underscoring the crucial role that RIG-I signaling plays in restricting ZIKV replication (242, 269).

Following RIG-I-mediated induction of IFNβ, IFNβ signals through IFNAR in an autocrine and paracrine manner, activating JAK/STAT signaling to upregulate ISGs in

infected and neighbouring uninfected cells (63, 105, 319, 321, 328). Upregulation of ISGs in infected cells restricts further viral replication while the expression of ISGs in uninfected cells induces an antiviral state that renders them less susceptible to infection, thereby limiting viral spread (328, 344, 345). IFN signaling is essential for restricting ZIKV spread as ZIKV dissemination and overt clinical disease are observed in immunocompromised mice lacking components of the IFN response pathway (253, 257, 273, 333).

In the previous chapter, we observed that ZIKV/Malaysia accumulated viral proteins earlier in acute infection and to a greater abundance than ZIKV/Dakar in immunocompetent A549 cells. Evaluation of the IFN response following acute ZIKV infection revealed a unique immunophenotype where infection with ZIKV/Malaysia elicited a weak IFN response despite the robust induction of IFNs downstream of RIG-I activation. In this chapter, we aimed to define the impact of RIG-I-mediated antiviral signaling on distinct stages of the ZIKV life cycle given the crucial role that RIG-I signaling plays in controlling ZIKV replication. As previous studies have provided evidence for a correlation between the rate of accumulation of viral innate immune antagonists and the host IFN response, we also sought to investigate how the kinetics of ZIKV protein accumulation regulates host IFN signaling (384, 403, 404). Paired analyses in control and RIG-I KO cells infected with ZIKV/Dakar or ZIKV/Malaysia revealed that RIG-I signaling is critical for restricting ZIKV protein accumulation and genome replication late in acute infection that together limit virus spread. We demonstrate for the first time for ZIKV that early accumulation of viral proteins in infected cells confers enhanced ability to restrict IFN signaling. The studies presented in

this chapter reveal that RIG-I directs an innate immune response that controls viral replicative fitness by limiting viral protein accumulation, which permits IFN signaling to restrict ZIKV genome replication and spread.

## 4.2 Results

### RIG-I-mediated signaling differentially restricts the accumulation of ZIKV/Dakar proteins and viral genome and suppresses spread of ZIKV variants late in acute infection

To elucidate the role of RIG-I in host innate immune control of prototypic ZIKV variants, we utilized A549 RIG-I KO cells to assess the contribution of RIG-I-driven antiviral actions on distinct stages of the ZIKV life cycle. A549 RIG-I KO cells have been previously shown to be defective in RLR signaling and do not produce IFN in response to ZIKV infection (242). As a control, we assessed ZIKV infection in A549 non-targeting control (NTC) cells that were transduced with a lentivirus expressing a non-targeting guide RNA. We infected NTC and RIG-I KO cells with ZIKV/Dakar or ZIKV/Malaysia over a 48-hour infection time-course at a high MOI to evaluate viral protein accumulation, genome replication, infectious virion release, and viral spread. Immunoblot analyses revealed that ZIKV/Malaysia-infected samples accumulated higher levels of NS5 in both NTC and RIG-I KO cells at 24 hpi compared to ZIKV/Dakar-infected samples (Fig. 4-1A). The discrepancy in viral protein accumulation in the absence of innate immune pressures indicates that cells infected with ZIKV/Dakar and ZIKV/Malaysia exhibit intrinsic differences in the rate of viral protein translation and accumulation early in infection. At 48 hpi, however, the levels of NS5 across the ZIKV variants were comparable in RIG-I KO cells, whereas NTC cells infected with

ZIKV/Dakar had a lower abundance of NS5 than cells infected with ZIKV/Malaysia. Our findings demonstrate that RIG-I-mediated antiviral signaling directs an innate immune response that restricts ZIKV/Dakar, but not ZIKV/Malaysia, protein accumulation at late time points of acute infection.

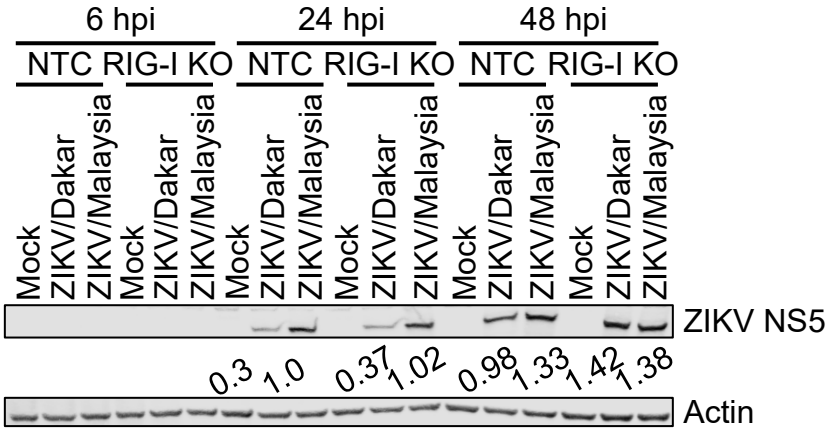


Figure 4-1. RIG-I signaling restricts ZIKV/Dakar protein accumulation. A549 NTC and RIG-I KO cells were mock-infected or infected with the ZIKV variants over a 48-hour time-course at a MOI of 5. Cell lysates were analyzed via immunoblotting. Depicted is one representative immunoblot from three independent experiments (n = 3). Immunoblot band intensities were quantified in Fiji and indicated beneath the corresponding bands.

Next, we carried out paired one-step viral growth analyses of the ZIKV variants in NTC and RIG-I KO cells to determine the impact of RIG-I signaling on viral genome replication and virion release. For each ZIKV strain, we observed that the levels of intracellular vRNA were similar between NTC and RIG-I KO cells at 6 and 24 hpi (Fig. 4-2A, B). However, at 48 hpi, we found significantly more ZIKV/Dakar RNA in RIG-I KO cells than in NTC cells, indicating that RIG-I signaling is crucial for restricting ZIKV/Dakar genome replication as observed previously with ZIKV and other flaviviruses (242, 269, 272). In contrast, we did not observe any differences in ZIKV/Malaysia RNA levels between NTC and RIG-I KO cells at 48 hpi, suggesting that RIG-I signaling

cannot restrict replication of this variant at the high MOI used (Fig. 4-2B). When we quantified the amounts of infectious particles released, we found no differences in infectious viral titers between ZIKV variants across cell types (Fig. 4-2C, D). Hence, our results demonstrate that ZIKV/Dakar, but not ZIKV/Malaysia, genome replication is restricted by RIG-I-mediated antiviral signaling at late time points in acute infection and further reveal that infectious virion release by cells infected with the ZIKV variants is insensitive to RIG-I signaling.

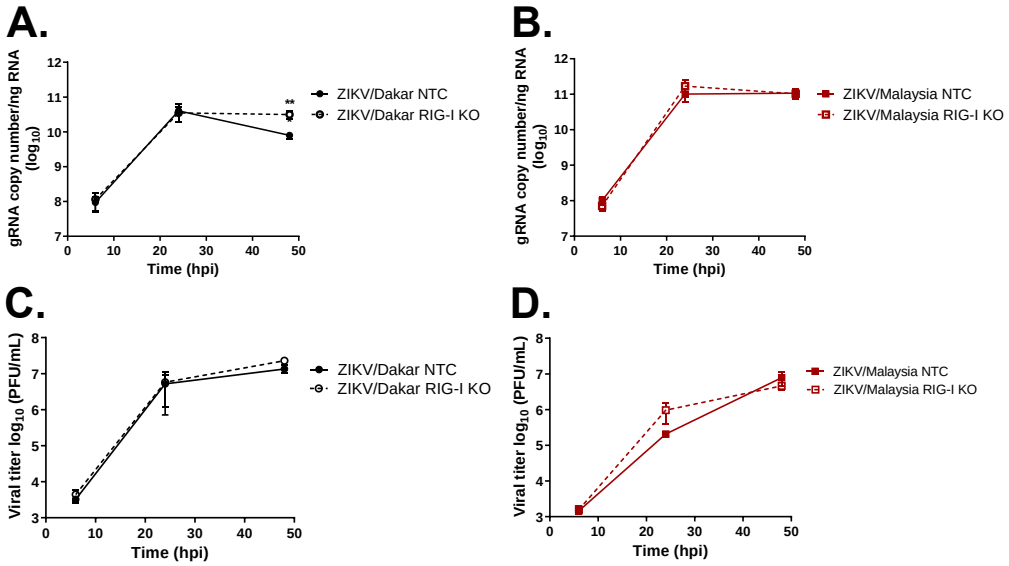


Figure 4-2. RIG-I signaling restricts ZIKV/Dakar genome accumulation. (A – D) A549 NTC and RIG-I KO cells were infected with (A, C) ZIKV/Dakar or (B, D) ZIKV/Malaysia over a 48-hour time-course at a MOI of 5. (A, B) RNA lysates were analyzed by qRT-PCR to quantify viral copy numbers. Depicted are means from three biological and technical replicates that were pooled for statistical analysis. (C, D) Cell culture supernatants were analyzed by plaque assay to quantify viral titers. Depicted are means from two to three independent experiments (n = 2-3). Statistical analyses were performed with a two-tailed unpaired t-test at each time point (**p<0.005).

Lastly, we assessed the impact of RIG-I signaling on virus spread. We infected NTC and RIG-I KO cells at a high MOI and quantified the percentage of infected cells at

24 and 48 hpi. At 24 hpi, ZIKV/Malaysia infected a significantly higher percentage of NTC and RIG-I KO cells compared to ZIKV/Dakar (Fig. 4-3A, B). These observations are similar to what we observed in WT cells (see Chapter 3, Fig. 3-6). We also found that ZIKV/Malaysia infected a significantly higher percentage of RIG-I KO cells compared to NTC cells at 24 hpi, suggesting that RIG-I signaling can restrict ZIKV/Malaysia spread early in acute infection under these high MOI conditions. We did not observe any differences in the percentages of ZIKV/Malaysia-infected NTC and RIG-I KO cells at 48 hpi during acute infection at a high MOI. Remarkably, however, ZIKV/Dakar infected significantly more cells at 48 hpi in RIG-I KO cultures compared to NTC cultures, reaching a similar infection efficiency as ZIKV/Malaysia in RIG-I KO cultures. This observation highlights the importance of RIG-I signaling in restricting ZIKV/Dakar spread at late time points in acute infection. To further evaluate the impact of RIG-I signaling on ZIKV spread, we infected NTC and RIG-I KO cells using serial virus dilutions that yielded isolated foci and measured the diameters of foci as a proxy of viral spread over a 96-hour infection time-course. At 48 hpi, the diameters of foci formed following infection with ZIKV/Dakar and ZIKV/Malaysia were similar between NTC and RIG-I KO cells (Fig. 4-3C, D). However, at 72 and 96 hpi, we observed that the diameters of foci formed by infection with ZIKV/Dakar and ZIKV/Malaysia were significantly increased in RIG-I KO cells compared to NTC cells, indicating that viral spread was enhanced in the absence of RIG-I particularly at late time points in acute infection. Our findings establish RIG-I-mediated innate immune activation as critical in restricting ZIKV infection by limiting viral protein accumulation and genome replication at late time points in acute infection to control viral spread.

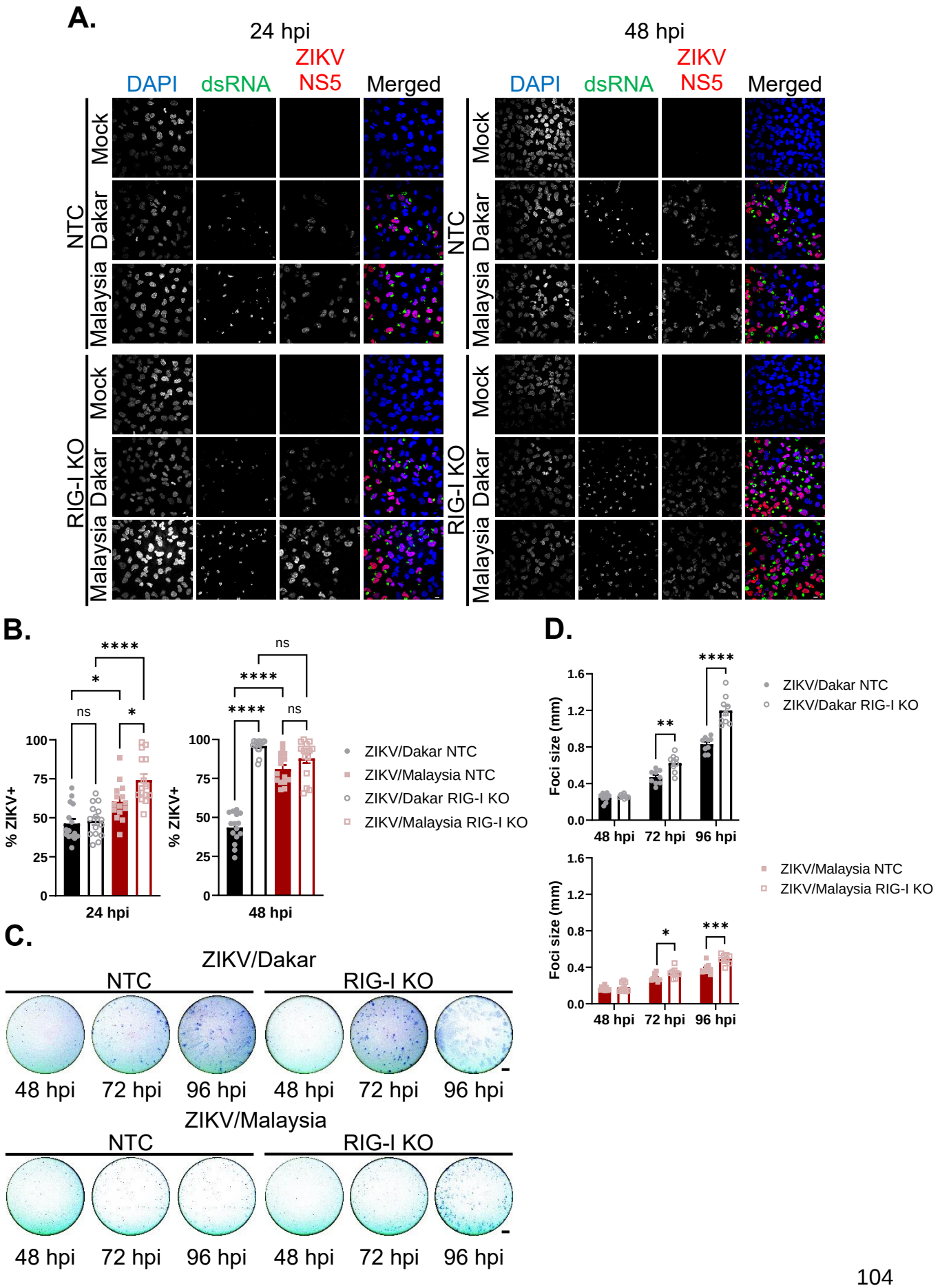
A.
24 hpi
48 hpi
DAPI
dsRNA
ZIKV NS5
Merged
NTC
RIG-I KO
Mock
Dakar
Malaysia
B.
% ZIKV+
24 hpi
48 hpi
ns
*
****
ZIKV/Dakar NTC
ZIKV/Malysia NTC
ZIKV/Dakar RIG-I KO
ZIKV/Malysia RIG-I KO
C.
ZIKV/Dakar
ZIKV/Malaysia
NTC
RIG-I KO
48 hpi
72 hpi
96 hpi
D.
Foci size (mm)
**
***

Figure 4-3. RIG-I signaling universally suppresses ZIKV spread. (A, B) A549 NTC and RIG-I KO cells were infected with ZIKV/Dakar or ZIKV/Malaysia at a MOI of 5. Samples were analyzed by immunofluorescence staining for dsRNA and ZIKV NS5. Scale bar represents 10μm. Five randomly selected fields of view representing at least 300 cells total were analyzed per sample. Images were manually analyzed using the multipoint tool in Fiji. The percent of ZIKV+ cells is presented after normalizing to the total number of cells as determined by DAPI staining. Depicted are means of five randomly selected fields across three independent experiments that were pooled for statistical analysis. Statistical analysis was performed with a one-way ANOVA followed by Tukey's multiple comparison test (ns: not significant; *p<0.05; ****p<0.0001). (C, D) A549 NTC and RIG-I KO cells were infected with serial dilutions of ZIKV/Dakar or ZIKV/Malaysia over a 96-hour time-course. Cells were fixed and stained for ZIKV E protein to detect foci of infection. Depicted are representative images of foci from three independent experiments (n = 3). Scale bar represents 1mm. Diameter of ten randomly selected foci were measured for each of the three technical replicates. Presented are means of ten randomly selected foci from each of the three technical replicates across three independent experiments. Statistical analysis was performed with a two-tailed unpaired t-test for each time point (*p<0.05; **p<0.005; ***p<0.001; ****p<0.0001). For all figures, error bars represent SEM.

**Early accumulation of ZIKV NS5 during ZIKV/Malaysia infection confers enhanced ability to block IFNβ signaling**

To determine how differences in the rate of viral protein accumulation affect the response to IFN in ZIKV-infected cells, we assessed the IFN response of RIG-I KO cells infected with ZIKV/Dakar and ZIKV/Malaysia. As RIG-I KO cells lack the ability to produce IFNβ in response to ZIKV infection, this approach allowed us to introduce exogenous IFNβ to comparatively assess ZIKV-mediated JAK/STAT blockade across the ZIKV variants in the absence of RIG-I-mediated innate immune activation. We infected RIG-I KO cells with ZIKV/Dakar or ZIKV/Malaysia and mock-treated or IFNβ-treated cells early (at 18 hpi) or late (at 40 hpi) in infection and quantified the

percentage of IFN responsive cells via immunofluorescence assays. To exclude any possible IFN response from uninfected or bystander cells in the culture, we quantified only the percentage of ZIKV-infected cells (defined as dsRNA+ cells) that had nuclear pSTAT1 signal. At both 18 and 40 hpi, the percentages of ZIKV/Dakar- and ZIKV/Malaysia-infected cells that were responsive to exogenous IFNβ stimulus were comparable, indicating that the ZIKV variants do not exhibit differences in their ability to antagonize IFNβ signaling (Fig. 4-4). The percentages of infected cells responsive to IFNβ stimulus were significantly lower at 40 hpi compared to 18 hpi. This reduction in IFN responsiveness coincided with an increased abundance in viral proteins, suggesting that viral protein accumulation during acute infection regulates the extent and ability of ZIKV-mediated blockade of IFN signaling (see Fig. 4-1A).

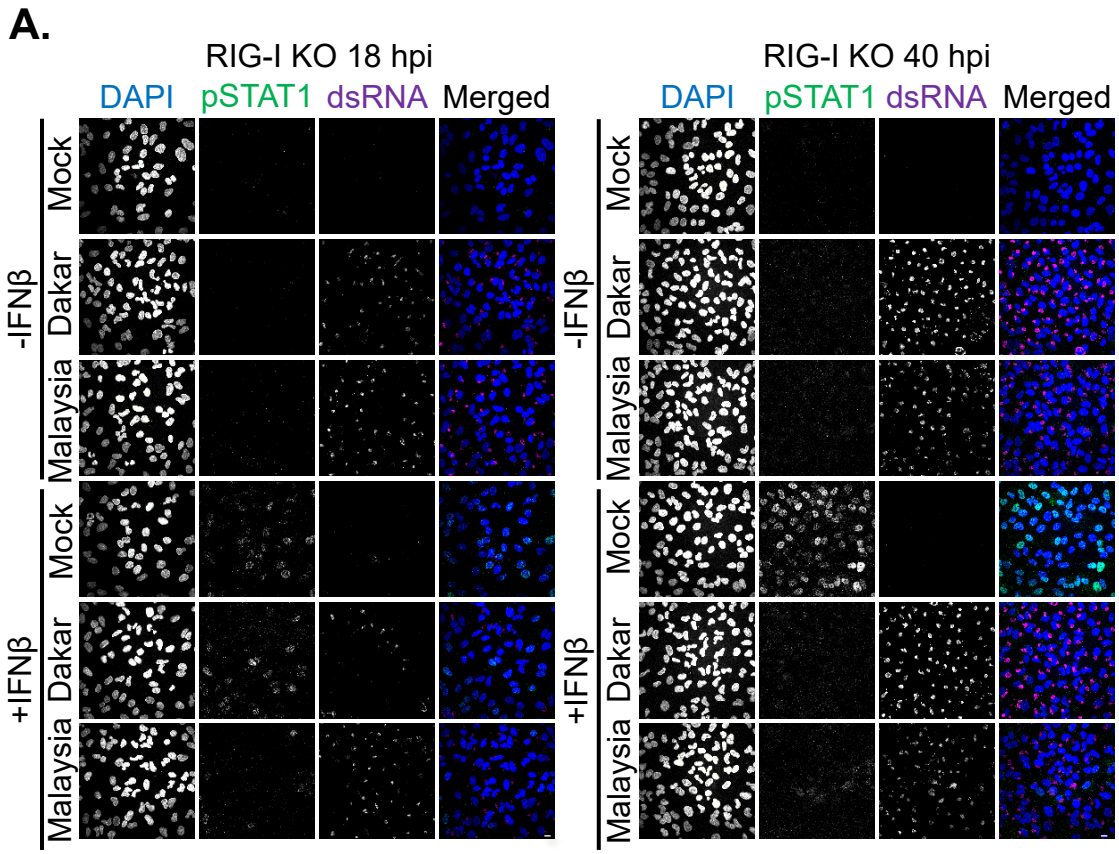

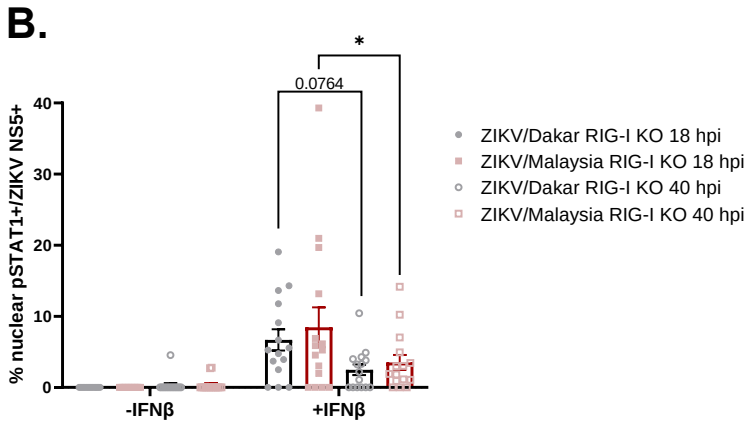


Figure 4-4. ZIKV variants block IFN signaling to the same extent in the absence of RIG-I signaling. A549 RIG-I KO cells were mock-infected or infected with ZIKV variants at a MOI of 5 then mock-treated or treated with 100IU/ml of IFNβ for immunofluorescence analysis. (A) Five randomly selected fields of view representing at least 310 cells total were analyzed for each sample. Z-stacks with a 2.5μm step size were acquired and maximum Z-projections were generated in Fiji for manual analysis with the multipoint tool in Fiji. Scale bar represents 10μm. (B) The percentage of nuclear pSTAT1+ cells is presented after normalizing to the number of infected cells (defined as dsRNA+). Depicted are means of five randomly selected fields of view from three independent experiments (n = 3), which were pooled for statistical analysis; error bars represent SEM. Statistical analysis was performed with a two-way ANOVA followed by Tukey's multiple comparison test (*p<0.05).

Previous studies have demonstrated that ZIKV NS5 is a potent IFN antagonist (364, 386, 387, 405). Since we identified 29 substitutions between ZIKV/Dakar and ZIKV/Malaysia NS5 proteins in our genomic analysis (see Chapter 3, Fig. 3-1B), we tested whether these divergent NS5 proteins differ in their ability to modulate IFN signaling when expressed alone to determine whether sequence differences in NS5 are responsible for the immunophenotype uncovered in Chapter 3 (see Fig. 3-8). We transfected HEK293T cells with an empty pcDNA3.1+ vector or with plasmids expressing either ZIKV/Dakar NS5 or ZIKV/Malaysia NS5 and subsequently mock-

treated or treated them with a high dose of IFNβ. To identify transfected cells and IFN responsive cells, we stained cells for NS5 and pSTAT1, respectively (Fig. 4-5A). To account for differences in transfection efficiency between samples, we measured pSTAT1 median fluorescence intensities (MFIs) of only the NS5+ population. We found that cells expressing ZIKV/Dakar NS5 or ZIKV/Malaysia NS5 and treated with IFNβ both suppressed pSTAT1 accumulation. We observed that ZIKV/Malaysia NS5 trended towards greater suppression of pSTAT1 accumulation compared to ZIKV/Dakar NS5, but this difference was not statistically significant (Fig. 4-5B). Thus, the divergent NS5 proteins from ZIKV variants of distinct lineages can both suppress the JAK/STAT pathway. Our results demonstrate that the divergent NS5 proteins do not contribute to the differential modulation of IFN signaling observed during acute ZIKV/Dakar and ZIKV/Malaysia infections in immunocompetent cells (see Chapter 3, Fig. 3-8).

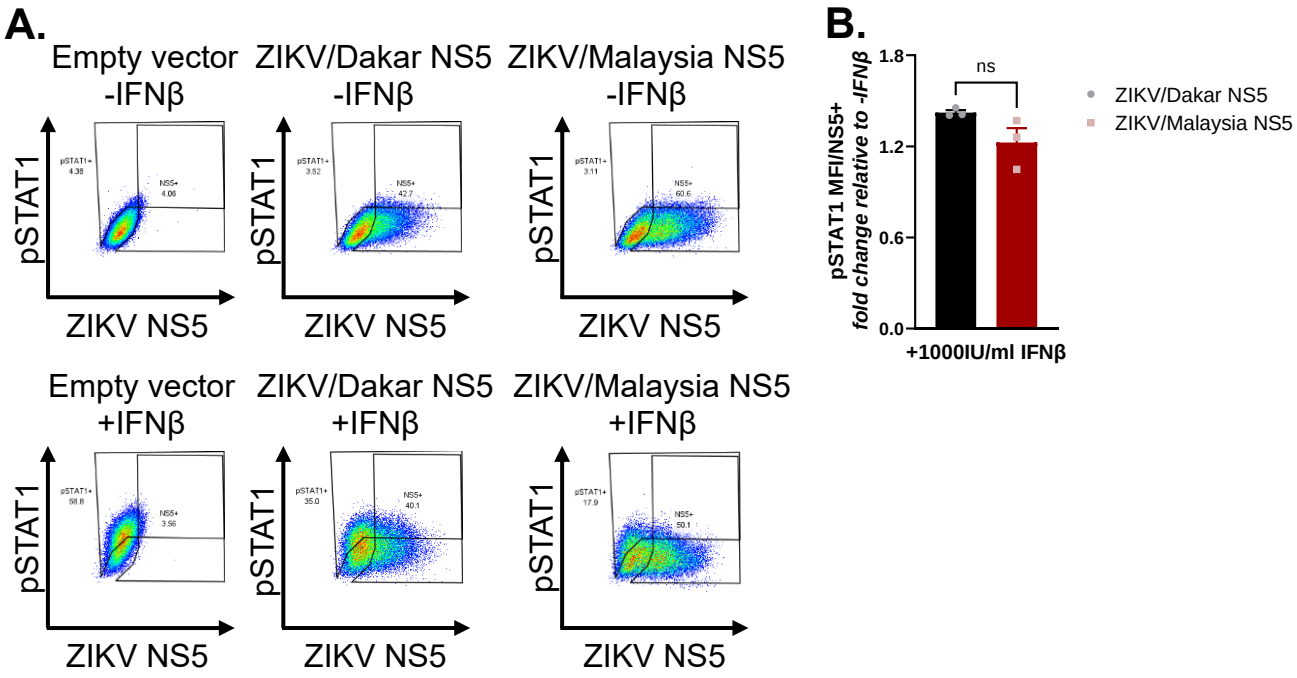

Figure 4-5. Divergent ZIKV NS5 proteins antagonize IFN signaling to the same extent. HEK293T cells were transfected with an empty plasmid, ZIKV/Dakar NS5, or ZIKV/Malaysia NS5 and treated with 1000IU/ml of IFNβ. (A) Gating strategy to identify transfected cells (NS5+) and IFN responsive cells (pSTAT1+). (B) pSTAT1 MFI of transfected cells treated with IFNβ are normalized to that of transfected, mock-treated cells. Depicted are means from three independent experiments (n = 3); error bars represent SEM. Statistical analysis was performed with a two-tailed unpaired t-test (ns: not significant).

Since ZIKV/Dakar- and ZIKV/Malaysia-infected cells and cells expressing ZIKV/Dakar and ZIKV/Malaysia NS5 proteins blocked IFN signaling to the same extent, we hypothesized that the ability of cells to respond to IFN is dependent on the rate of ZIKV protein accumulation. To test this hypothesis, we mock-infected or infected A549 RIG-I KO cells with the ZIKV variants to exclude the production of endogenous IFN during infection that otherwise occurs in immunocompetent cells. At various time points throughout a 30-hour infection time-course, we mock-treated or IFNβ-treated the RIG-I KO cells to evaluate the ability of both the total and infected cell populations to respond to exogenous IFNβ via flow cytometry analysis. To identify infected cells and IFN responsive cells, we stained cells for NS5 and pSTAT1, respectively (Fig. 4-6A). We observed that the percentage of infected RIG-I KO cells increased over the course of infection for both ZIKV variants with ZIKV/Malaysia infecting a significantly higher percentage of cells than ZIKV/Dakar prior to 24 hpi (Fig. 4-6B). However, at both 24 and 30 hpi, the percentages of infected cells were similar between samples infected with either ZIKV variant. When we quantified the percentage of IFN responsive cells over time, we observed a decrease in the percentage of pSTAT1+ cells in infected RIG-I KO cultures compared to mock-infected cultures (Fig. 4-6C). Remarkably, RIG-I KO

cultures infected with ZIKV/Malaysia exhibited a reduction in the percentage of pSTAT1+ cells as early as 4 hpi compared to mock-infected and ZIKV/Dakar-infected cultures even though ZIKV/Malaysia-infected cells express levels of NS5 below the limit of detection at this time point. Compared to ZIKV/Dakar, ZIKV/Malaysia-infected RIG-I KO cultures had fewer pSTAT1+ cells up to 24 hpi. The percentages of pSTAT1+ cells between ZIKV/Dakar- and ZIKV/Malaysia-infected RIG-I KO cultures were only significantly different at 8 hpi. At 24 and 30 hpi, when the percentages of infected RIG-I KO cells were comparable between the two variants, both ZIKV/Dakar- and ZIKV/Malaysia-infected samples had significantly lower percentages of pSTAT1+ cells following IFNβ treatment compared to mock-infected samples. At these time points, we did not observe any differences in the percentages of pSTAT1+ cells between RIG-I KO cultures infected with ZIKV/Dakar and ZIKV/Malaysia. Similar trends were observed when we plotted NS5 and pSTAT1 MFIs of the total cell population where NS5 MFI increased over time during infection with either ZIKV strain while pSTAT1 MFI decreased over the course of both ZIKV/Dakar and ZIKV/Malaysia infections in the RIG-I KO cultures (Fig. 4-6D). Of note, in ZIKV/Dakar-infected RIG-I KO cultures, there was a delayed increase in NS5 MFIs at 4, 8, and 10 hpi compared to ZIKV/Malaysia-infected samples. This delayed increase in NS5 MFIs coincided with a delayed decrease in pSTAT1 MFI at these time points. At 24 and 30 hpi, NS5 and pSTAT1 MFIs were comparable between samples infected with either ZIKV variant, indicating that ZIKV/Dakar and ZIKV/Malaysia can block IFN signaling to a similar extent in the absence of RIG-I only when the levels of NS5 are equivalent. Our findings demonstrate

that the IFN responsiveness of ZIKV-infected cultures is inversely correlated with the levels of ZIKV NS5 over the infection time-course.

We next evaluated whether ZIKV NS5 levels within infected cells predict the IFN responsiveness of infected cells. We normalized NS5 and pSTAT1 MFIs of ZIKV/Dakar- and ZIKV/Malaysia-infected cells that were treated with IFNβ to those of mock-infected IFNβ-treated samples for each time point and plotted these normalized values against each other (Fig. 4-6E). NS5 MFIs between ZIKV/Dakar- and ZIKV/Malaysia-infected cells were similar at 4 hpi but differed between 8 and 24 hpi with higher NS5 MFIs observed for ZIKV/Malaysia-infected cells between these time points. At 24 and 30 hpi, NS5 MFIs were similar between cells infected with either ZIKV variant, indicating that levels of NS5 within ZIKV/Dakar- and ZIKV/Malaysia-infected cells were comparable at these time points. When we evaluated pSTAT1 MFIs in cells infected with the ZIKV variants, we observed that ZIKV/Malaysia-infected cells had lower pSTAT1 MFIs than ZIKV/Dakar-infected cells as early as 4 hpi and up to 24 hpi. These observations demonstrate that differences in the rate of NS5 accumulation in infected cells early in infection contribute to the differential ability of the ZIKV variants to block IFNβ signaling at these early time points in infection. When NS5 levels were similar between ZIKV/Dakar- and ZIKV/Malaysia-infected RIG-I KO cells at 24 and 30 hpi, pSTAT1 MFIs were comparable between cells infected with either variant. Linear regression analyses confirmed that NS5 MFI of infected cells is inversely correlated with pSTAT1 MFI of infected cells and revealed that NS5 MFI significantly predicts pSTAT1 MFI in cells infected with the ZIKV variants. When we compared the regression slopes, we found that they were significantly different between the ZIKV variants, indicating that

ZIKV/Dakar and ZIKV/Malaysia differ in their rate of NS5 accumulation and regulation of IFNβ signaling (Fig. 4-6E). Together, our results clearly demonstrate that the rate and levels of ZIKV NS5 accumulation in infected cells significantly determine the extent of ZIKV-mediated IFN blockade, such that ZIKV/Dakar and ZIKV/Malaysia antagonize IFN signaling to the same extent when levels of NS5 are comparable in infected cells.

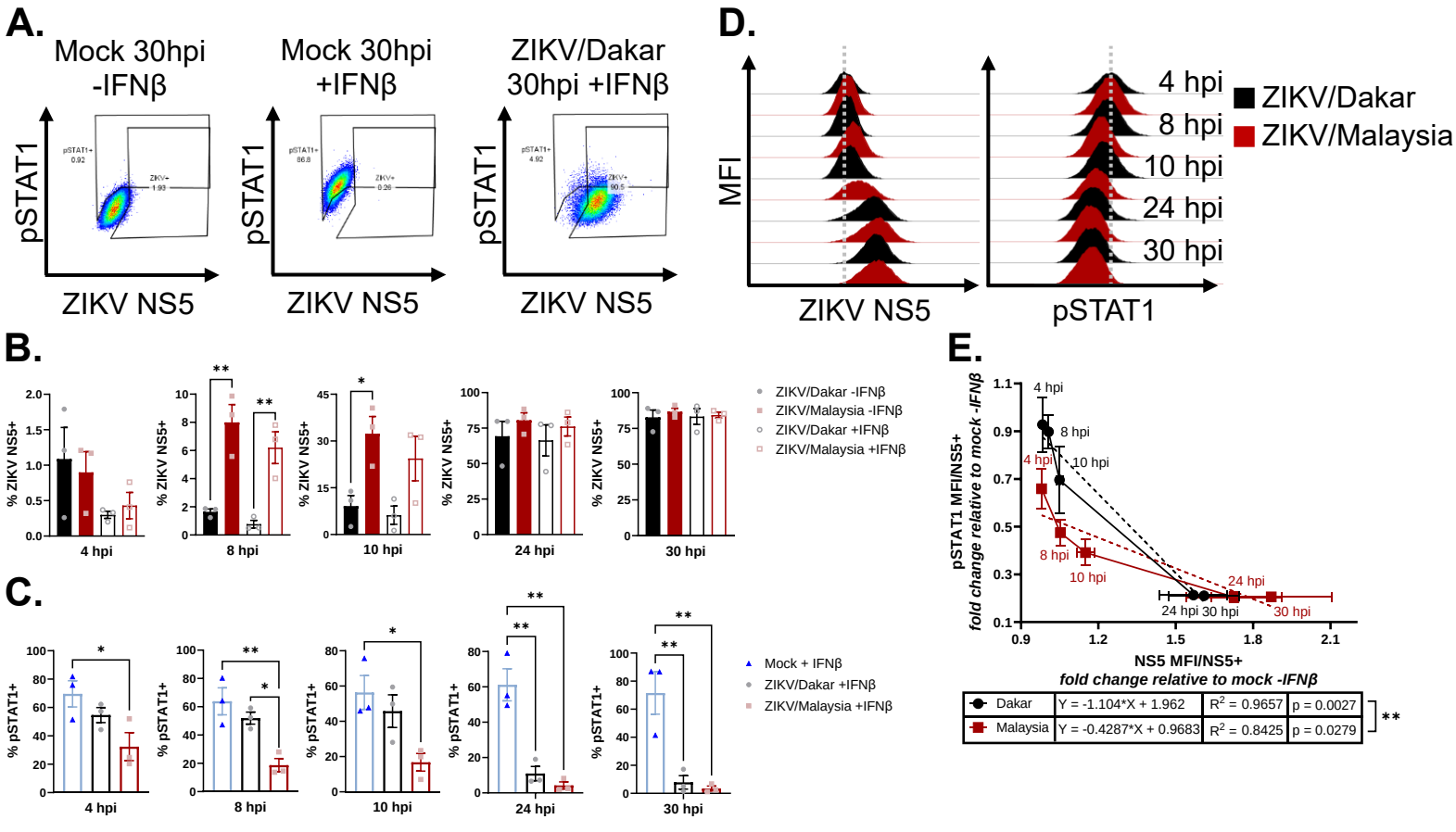

Figure 4-6. Early accumulation of ZIKV/Malaysia NS5 links with enhanced IFN antagonism. A549 RIG-I KO cells were mock-infected or infected with the ZIKV variants at a MOI of 5 over a 30-hour infection time-course then mock-treated or treated with 100IU/ml of IFNβ. Results are representative of three independent experiments (n = 3). (A) Gating strategy to identify infected cells (ZIKV NS5+) and IFN responsive cells (pSTAT1+). (B) Depicted is the mean percentage of infected cells. Statistical analysis was performed with a one-way ANOVA followed by Tukey's multiple comparison test (*p<0.05; **p<0.005). (C) The mean percentage of pSTAT1+ cells of the total cell population is presented. Statistical analysis was performed with a one-way ANOVA followed by Tukey's multiple comparison test (*p<0.05; **p<0.005). (D) Depicted are representative histograms of ZIKV NS5 and pSTAT1 MFIs of the total cell population over the infection time-course. Gray dotted lines indicate the centers of the histograms for ZIKV/Dakar-infected samples at 4 hpi and serve as a reference point for visualizing the shift in histograms. (E) Depicted are the mean NS5 and pSTAT1 MFIs of the infected cell population over each infection time-course. Statistical analysis was performed with linear regressions (**p<0.005). For all figures, error bars represent SEM.

## 4.3 Summary of results

Our paired analyses in NTC and RIG-I KO cells reveal the interplay between RIG-I-mediated antiviral signaling and the rate of ZIKV NS5 accumulation and its impact on host immune control of ZIKV replication. We found that RIG-I is required for limiting ZIKV protein accumulation, genome replication, and virus spread late in acute infection (Fig. 4-1 – 3). Specifically, in the absence of RIG-I-imposed innate immune pressures, the levels of NS5 in ZIKV/Dakar-infected cells reached levels comparable to those in ZIKV/Malaysia-infected cells late in acute infection (Fig. 4-1A, Fig. 4-4B). Interestingly, we observed that both NTC and RIG-I KO cells infected with ZIKV/Dakar displayed a delay in viral protein accumulation at early time points in acute infection, indicating that the ZIKV variants exhibit intrinsic differences in the rate of viral protein translation and accumulation. Consequently, we found that the ability of ZIKV-infected cells to respond

to IFN is differentially impaired at early time points during acute infection. ZIKV/Malaysia-infected cells accumulated NS5 earlier and to a greater abundance than ZIKV/Dakar-infected cells prior to 24 hpi (Fig. 4-6E). The early accumulation of NS5 linked with an increased ability to block IFN signaling. However, once the levels of NS5 in cells infected with either ZIKV variant were equivalent at late time points in acute infection, the IFN responsiveness of infected cells are similarly abrogated regardless of ZIKV variant. In the studies presented in this chapter, we probed for ZIKV NS5 as a marker of infection. Since NS5 is a potent IFN antagonist, we evaluated whether the aa differences that we identified in the NS5 proteins of these prototypic ZIKV strains contribute to differential modulation of the host IFN response. We observed that the divergent NS5 proteins do not differ in their ability to block IFN signaling though there was a trend for ZIKV/Malaysia NS5 to impart greater suppression of pSTAT1 accumulation (Fig. 4-5) (364, 386, 387, 405). These findings demonstrate that the rate of ZIKV NS5 accumulation is the major determinant of the IFN responsiveness of infected cells where early accumulation of viral innate immune antagonists confers enhanced ability to antagonize IFN signaling.

# Chapter 5. Discussion

## 5.1 Discussion

In this dissertation, we conducted virologic and host innate immune analyses comparing prototypic African and Asian lineage strains to gain a deeper understanding of differences between ZIKV variants that might impart disease. Genomic analyses of ZIKV/Dakar and ZIKV/Malaysia revealed that these variants share some previously

identified genetic determinants of viral fitness but not others. One-step viral growth analyses demonstrated that cells infected with ZIKV/Malaysia accumulated viral proteins and genome earlier and to higher levels than cells infected with ZIKV/Dakar. Evaluation of the innate immune response profiles initiated upon infection with the ZIKV variants revealed that both variants induced innate immune activation marked by expression of IRF3 and NFκB target genes, including IFNβ. Despite robust IFN induction, we observed that ZIKV/Malaysia, but not ZIKV/Dakar, robustly blocked IFN signaling and downstream induction of ISGs. Our subsequent analyses in NTC and RIG-I KO cells revealed that RIG-I mediates a crucial innate immune response that restricts ZIKV protein accumulation late in acute infection, such that early accumulation of viral proteins confers enhanced antagonism of IFN signaling to support efficient genome replication and viral spread late in acute infection. Based on our results, we propose a model of RIG-I action during acute ZIKV infection where RIG-I recognition of ZIKV PAMPs activates IRF3 and NFκB, leading to innate immune activation to drive IFNβ production and response (268). The IFN response is subjected to differential regulation across viral variants through the variable rate and levels of NS5 accumulation within infected cells. RIG-I and rapid accumulation of NS5 are key features of this model that respectively drive acute innate immune activation and an antiviral response that are necessary for limiting ZIKV replication and spread and suppress IFN signaling to support overall infection progression (Fig. 5-1). Our proposed model highlights the arms race between ZIKV and the host to control infection outcome. The results from our comparative analyses indicate that the early rapid accumulation of NS5 in ZIKV/Malaysia-infected cells renders ZIKV/Malaysia more successful in the arms race

than ZIKV/Dakar as ZIKV/Malaysia can effectively suppress IFN signaling earlier in acute infection. Thus, infection with ZIKV/Malaysia may link with worse disease outcome than infection with ZIKV/Dakar.

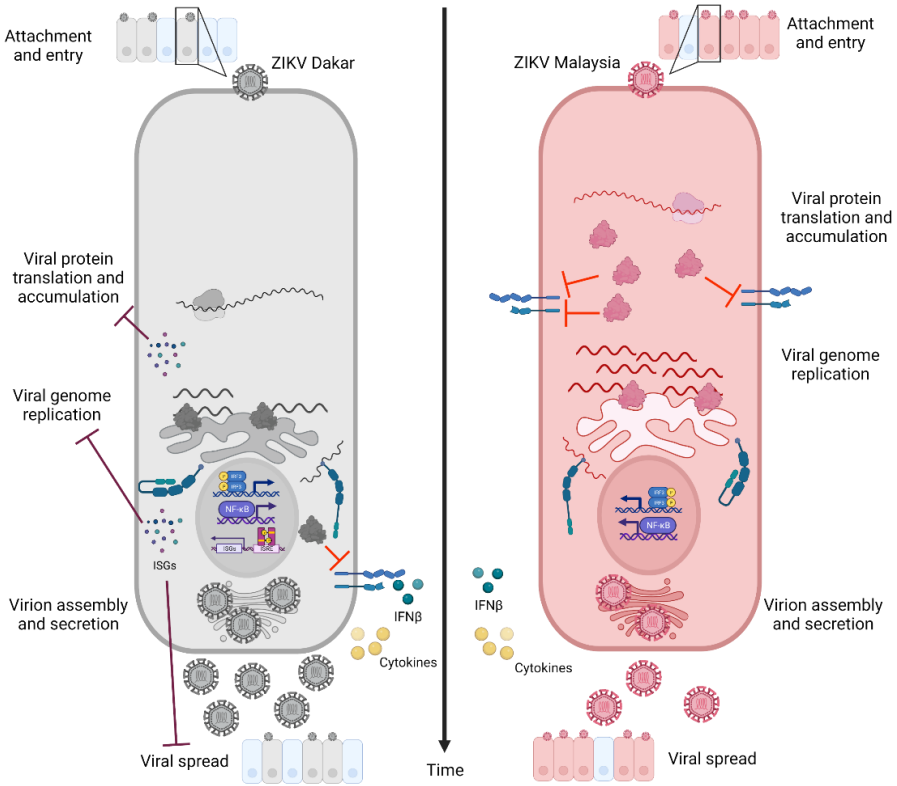


Figure 5-1. Early accumulation of ZIKV proteins confers enhanced ability to suppress host innate immune responses to overcome host control of viral replication and spread. The model figure highlights the evolutionary arms race between ZIKV/Dakar (left) or ZIKV/Malaysia (right) and the host for control of infection outcome. Early accumulation of ZIKV/Malaysia proteins links with an enhanced ability to block IFNβ signaling, rendering ZIKV/Malaysia more successful than ZIKV/Dakar in overcoming host antiviral actions.

Other comparative studies have previously demonstrated that African lineage strains replicate to higher levels than Asian lineage variants, indicating that ZIKV isolates of the African lineage generally exhibit higher viral fitness than those of the Asian lineage (227, 230, 232–235, 237, 242, 406). Comparative analyses of a pre-

epidemic Asian lineage variant (ZIKV/Cambodia/2010/FSS13025; ZIKV/Cambodia) with African lineage viruses and epidemic strains have shown that both epidemic variants and African lineage viruses exhibit higher replicative fitness than ZIKV/Cambodia, suggesting that Asian lineage ZIKV strains isolated prior to the epidemics may be less fit (242, 245). Remarkably, we found that ZIKV/Malaysia, the pre-epidemic prototypic Asian lineage virus, exhibits enhanced early replicative fitness relative to the prototypic African lineage strain, ZIKV/Dakar, in our A549 epithelial cell infection model (Fig. 3-1B). These results were unexpected and contrary to those from previous reports, suggesting that the replicative fitness of the prototypic Asian lineage strain differs from that of later pre-epidemic Asian lineage strains and of emerging ZIKV variants. Since ZIKV/Cambodia was isolated several decades after ZIKV/Malaysia, it is likely that genetic changes arose during the time between the isolation of these two Asian lineage variants to facilitate adaptation to the mosquito vectors and mammalian hosts in southeast Asia. Liu et al. have previously identified four aa substitutions (T106A in C, V1A in prM, A188V in NS1, and M872V in NS5) present in Asian lineage-derived epidemic strains, but absent in ZIKV/Cambodia, that represent direct reversions to those encoded by African lineage viruses and have demonstrated that these genetic changes were sufficient to restore viral fitness of emerging ZIKV variants (245). Our sequencing analysis revealed that ZIKV/Malaysia encodes the alanine at position 106 of C and the valine at position 872 of NS5 (Table 1). As these two residues are shared with ZIKV/Dakar, they likely contribute to the enhanced replicative fitness of ZIKV/Malaysia that we observed relative to ZIKV/Cambodia, which lacks these residues. Although we found that ZIKV/Malaysia additionally encodes the alanine at

position 188 of NS1 linked with reduced viral fitness, the presence of the alanine at position 106 of C, which exerts a strong effect on viral fitness, may be sufficient to overcome the impairment associated with the V188A mutation in NS1, thereby increasing the overall replicative fitness of ZIKV/Malaysia compared to ZIKV/Cambodia (245). Interestingly, a comparative study of ZIKV/Dakar and ZIKV/Malaysia in DCs revealed that cells infected with ZIKV/Dakar produce higher viral titers over an acute infection time-course than ZIKV/Malaysia-infected cells (231). The discrepancies observed between that study and ours suggest that the replicative fitness of ZIKV/Dakar and ZIKV/Malaysia may exhibit cell type-dependent differences. As such, future studies should assess the viral replicative fitness of these prototypic ZIKV variants in cell types targeted by ZIKV infection, such as those from the reproductive and nervous systems.

As we observed that ZIKV/Malaysia exhibited greater genome replication efficiency than ZIKV/Dakar, there must be other uncharacterized genetic differences between these two variants that contribute to the replication discrepancies observed in this study. Our sequencing analysis identified several aa differences in each of the structural and non-structural proteins. As these substitutions have not been previously characterized, it is possible that they may impact viral replicative fitness. Additionally, we identified sequence differences in NS5, including within the RdRp domain. Since the NS5 RdRp domain carries out viral polymerase activity, it is possible that specific sequence differences that we identified within NS5 could differentially affect RdRp activity, conferring replication differences between these two prototypic ZIKV variants (201, 202). Given the contribution of genomic differences in viral replicative fitness,

future comparative studies of these prototypic African and Asian lineage strains should define these genetic determinants of viral fitness.

Evaluation of the innate immune response elicited upon infection with ZIKV/Dakar and ZIKV/Malaysia revealed that the ZIKV variants acutely induced RLR activation and induction of antiviral and inflammatory cytokine expression, including IFNβ, to the same extent (Fig. 3-7). This robust induction of IFNβ during acute infection with the ZIKV variants was unexpected as previous studies have shown that ZIKV variants of both lineages block IFN induction during acute infection, suggesting that this discrepancy may be ZIKV strain- and/or cell type-dependent (61, 231, 370, 371, 373, 375, 383). It was additionally surprising that infection with ZIKV/Dakar induced IFNβ to a similar extent as infection with ZIKV/Malaysia since ZIKV/Dakar encodes a valine at position 188 of NS1, which has been demonstrated to enhance ZIKV-mediated blockade of IFNβ induction compared to NS1 proteins encoding an alanine at this position (377). Since infection with ZIKV/Dakar and ZIKV/Malaysia, which encodes an alanine at this position, similarly induced IFNβ expression, our findings suggest that the valine at this position in NS1 is not sufficient to abolish IFN induction during *in vitro* infection in our A549 epithelial cell infection model.

When we assessed the IFN response following infection with the ZIKV variants, we observed a striking and unique immunophenotype where ZIKV/Malaysia robustly blocked IFN signaling and the downstream induction of ISGs while ZIKV/Dakar did not (Fig. 3-8). These findings suggest that, compared to ZIKV/Dakar, ZIKV/Malaysia exhibits enhanced ability to restrict IFN signaling. We evaluated whether ZIKV/Dakar and ZIKV/Malaysia NS5 proteins alone differentially block IFN signaling and observed

that these divergent viral proteins antagonized IFN signaling to a similar extent though there was a trend for ZIKV/Malaysia to impart greater suppression of pSTAT1 accumulation (Fig. 4-3B). These results indicate that the aa differences that we identified within NS5 proteins encoded by prototypic African and Asian lineage variants have limited impact on NS5-mediated blockade of IFN signaling (Fig. 4-3B). We revealed that the differential regulation of IFN signaling observed at late time points in acute infection with the ZIKV variants was due to differences in the rate of accumulation of viral proteins in infected cells early in infection (Fig. 4-4). As ZIKV/Malaysia-infected cells accumulated NS5 earlier and to higher levels in acute infection, they were significantly less responsive to IFN stimulus compared to ZIKV/Dakar-infected cells, which accumulated NS5 slower and to lower levels. Similar findings have also been observed in studies of other flaviviruses as well as SARS-CoV-2 where they demonstrated a clear association between the rate of accumulation of virally-encoded innate immune antagonists and host innate immune responses (384, 403, 404, 407). Our study is the first to describe this relationship in the context of ZIKV infection and identifies the kinetics of ZIKV protein accumulation as a major regulator of host innate immunity and an important viral feature that can be used to predict the IFN sensitivity of emerging strains.

Our linear regression analyses revealed that the correlations between pSTAT1 and ZIKV NS5 levels were different between ZIKV/Dakar- and ZIKV/Malaysia-infected cells, which is likely driven by differences in the rate of NS5 accumulation in infected cells observed for each ZIKV variant (Fig. 4-4E). As ZIKV NS5 interacts with STAT2 and HSP90 to suppress IFN signaling, differences in the rate of NS5 accumulation may alter

the kinetics of interactions between NS5 and these host factors critical for productive IFN signaling (386, 387, 405). ZIKV NS5 has also been demonstrated to interact with sfRNA, which stabilizes NS5 to facilitate NS5-mediated antagonism of IFN signaling (84). As such, rapid accumulation of ZIKV NS5 can drive these interactions early in acute infection to efficiently dampen the IFN response in infected cells to promote viral replication. Since sfRNA is a byproduct of incomplete degradation of the flavivirus genome generated when XRN1 is stalled on the secondary structures in the 3' UTR, genomic differences within the 3' UTR of ZIKV/Dakar and ZIKV/Malaysia may affect the generation of sfRNA and, subsequently, the accumulation of ZIKV NS5 (66, 82, 83). Whether differences in the abundance of sfRNA generated during infection with ZIKV/Dakar and ZIKV/Malaysia contribute to the differential rate of NS5 accumulation observed in this study remains unclear. A simple future experiment comparing the abundance of sfRNA generated during infection with the ZIKV variants will address this outstanding question. Additionally, as both the 5' and 3' UTRs of the ZIKV variants were not fully sequenced in our study, it is unclear whether there are nucleotide differences within these regions between the ZIKV variants. As the UTRs play important roles in genome translation, initiation of genome replication, and sfRNA generation that together impact viral virulence, it would be imperative to fully sequence the 5' and 3' UTRs of ZIKV/Dakar and ZIKV/Malaysia and evaluate the contribution of any nucleotide differences within these regions on viral replicative fitness, NS5 accumulation, and JAK/STAT regulation (57, 65, 66).

Prior to the 2013 and 2015 ZIKV outbreaks in French Polynesia and the Americas, respectively, infection with ZIKV was not associated with severe clinical

manifestations (32, 42). The sudden change in viral pathogenesis, particularly during *in utero* ZIKV infection, raised the question as to why infection with emerging ZIKV variants was associated with more severe disease, such as CZS. Comparative studies of African and Asian lineage viruses *in vitro* and *in vivo* have demonstrated in many experimental systems that African lineage strains are generally more virulent and more cytopathic, such that *in utero* infection with these viruses would result in fetal demise or resorption rather than congenital defects (224, 230, 248). In this study, we observed that Asian lineage ZIKV/Malaysia replicated to higher levels than African lineage ZIKV/Dakar, suggesting that *in utero* infection with ZIKV/Malaysia may similarly cause severe fetal damage. As ZIKV/Dakar additionally exhibited increased sensitivity to the antiviral actions of RIG-I signaling compared to ZIKV/Malaysia, ZIKV/Dakar would be acutely restricted by the innate immune response during *in utero* infection and likely not confer congenital infection. Other *in vivo* studies have shown that high levels of IFNs produced during *in utero* ZIKV infection with African and Asian lineage strains can also inflict severe damage on the placenta and the fetus, leading to fetal demise or resorption (359, 360). The distinct differences in viral replicative fitness and unique JAK/STAT immunophenotype observed in our study raise new questions regarding the mechanisms underlying lineage-specific differences on fetal pathology and warrant further examination of ZIKV/Dakar and ZIKV/Malaysia in an established pregnant pigtail macaque model to understand lineage-dependent differences on fetal pathology and define the underlying mechanisms (40).

We observed that ZIKV/Malaysia exhibited enhanced blockade of IFN signaling compared to ZIKV/Dakar, suggesting that the dampened IFN response elicited during

acute ZIKV/Malaysia infection can promote persistence in infected hosts and facilitate viral dissemination to and persistence in immune-privileged sites, such as the reproductive tissues and brain (43, 199, 344, 408). ZIKV isolates endemic to southeast Asia have been detected in the placenta and fetal brain several weeks following the onset of symptoms in the infected pregnant woman, indicating that endemic ZIKV variants can disseminate to and persist within these tissues (22, 23). Since ZIKV/Malaysia robustly blocked IFN signaling compared to ZIKV/Dakar, it is possible that ZIKV/Malaysia-mediated antagonism of IFN signaling may facilitate viral spread to and persistence in reproductive tissues and the fetal brain. The unique immunophenotypes uncovered in our study emphasize the need for surveillance of endemic ZIKV variants.

In this study, we utilized RIG-I KO cells to evaluate the impact of host innate immune responses on ZIKV infection. However, RIG-I KO cells are deficient in both RIG-I and endogenous IFN signaling, raising the question as to whether the restriction of ZIKV dissemination and spread is dependent on both intact RIG-I and IFN signaling. Future studies using STAT1 KO cells or animal models fully ablated of IFN signaling are warranted to define the innate immune requirements for restricting ZIKV dissemination and spread.

## 5.2 Concluding remarks

In conclusion, our comparative analysis of prototypic African lineage ZIKV/Dakar and Asian lineage ZIKV/Malaysia revealed that cells acutely infected with ZIKV/Malaysia accumulated viral proteins and genome earlier and to higher levels than cells acutely infected with ZIKV/Dakar despite releasing similar levels of mature virions.

Early accumulation of viral proteins in ZIKV/Malaysia-infected cells during acute infection linked with enhanced antagonism of IFN signaling and suppression of ISG expression at late time points in acute infection, allowing ZIKV/Malaysia to overcome the robust activation of RIG-I signaling and IFN production initiated upon infection. Together, our findings reveal that RIG-I drives an innate immune response that is critical for imparting control of ZIKV replicative fitness and implicate RIG-I signaling in limiting the epidemic potential of ZIKV variants. Specifically, RIG-I-mediated innate immune responses restrict ZIKV protein accumulation to enhance IFN signaling, which limits viral genome replication and cell-to-cell spread. Our study identifies the window prior to the accumulation of ZIKV innate immune antagonists as crucial for ZIKV sensitivity to host innate immune restriction. As such, early administration of RIG-I-targeting immunotherapeutics could drive innate immune suppression of ZIKV during acute infection.

# Appendix

Table 3. AA differences between ZIKV/Dakar and an Asian lineage reference strain.

| Position | Substitution | Type of substitution | Protein |
|---|---|---|---|
| 7 | K to N | Non-conservative | Capsid |
| 25 | S to N | Conservative | Capsid |
| 27 | F to L | Conservative | Capsid |
| 101 | K to R | Conservative | Capsid |
| 110 | V to I | Conservative | Capsid |
| 123 | V to A | Conservative | pr |
| 125 | V to I | Conservative | pr |
| 148 | P to A | Conservative | pr |
| 157 | Y to H | Non-conservative | pr |
| 158 | I to V | Conservative | pr |
| 246 | R to K | Conservative | M |
| 260 | A to L | Conservative | M |
| 262 | A to V | Conservative | M |
| 575 | S to F | Non-conservative | E |
| 607 | I to V | Conservative | E |
| 727 | A to V | Conservative | E |
| 728 | L to F | Conservative | E |
| 785 | L to M | Conservative | E |
| 846 | D to E | Conservative | NS1 |

| | | | |
|---|---|---|---|
| 863 | R to K | Conservative | NS1 |
| 926 | S to R | Non-conservative | NS1 |
| 956 | V to I | Conservative | NS1 |
| 982 | A to V | Conservative | NS1 |
| 988 | V to A | Conservative | NS1 |
| 1007 | K to R | Conservative | NS1 |
| 1030 | I to V | Conservative | NS1 |
| 1180 | I to M | Conservative | NS2A |
| 1191 | I to V | Conservative | NS2A |
| 1204 | A to V | Conservative | NS2A |
| 1226 | I to V | Conservative | NS2A |
| 1263 | V to A | Conservative | NS2A |
| 1270 | D to E | Conservative | NS2A |
| 1275 | I to V | Conservative | NS2A |
| 1297 | T to A | Non-conservative | NS2A |
| 1354 | L to I | Conservative | NS2A |
| 1461 | D to E | Conservative | NS2B |
| 1477 | T to A | Non-conservative | NS2B |
| 1553 | H to Q | Non-conservative | NS3 |
| 1558 | S to A | Non-conservative | NS3 |
| 1594 | H to L | Non-conservative | NS3 |
| 1620 | T to K | Non-conservative | NS3 |
| 1671 | R to K | Conservative | NS3 |

| | | | |
|---|---|---|---|
| 1676 | T to A | Conservative | NS3 |
| 1687 | K to R | Conservative | NS3 |
| 1717 | T to K | Non-conservative | NS3 |
| 1862 | V to I | Conservative | NS3 |
| 1909 | V to I | Conservative | NS3 |
| 1962 | I to V | Conservative | NS3 |
| 2085 | R to K | Conservative | NS3 |
| 2123 | F to L | Conservative | NS4A |
| 2127 | E to D | Conservative | NS4A |
| 2282 | L to I | Conservative | NS4B |
| 2283 | G to A | Conservative | NS4B |
| 2289 | R to K | Conservative | NS4B |
| 2293 | A to T | Non-conservative | NS4B |
| 2594 | Y to H | Non-conservative | NS5 |
| 2598 | I to V | Conservative | NS5 |
| 2621 | K to R | Conservative | NS5 |
| 2634 | T to M | Non-conservative | NS5 |
| 2659 | S to P | Non-conservative | NS5 |
| 2679 | A to T | Non-conservative | NS5 |
| 2715 | L to M | Conservative | NS5 |
| 2722 | Y to H | Non-conservative | NS5 |
| 2765 | D to E | Conservative | NS5 |
| 2795 | L to M | Conservative | NS5 |

| | | | |
|---|---|---|---|
| 2800 | N to R | Non-conservative | NS5 |
| 2802 | V to I | Conservative | NS5 |
| 2807 | S to N | Conservative | NS5 |
| 2842 | I to V | Conservative | NS5 |
| 2909 | H to R | Conservative | NS5 |
| 2969 | Q to H | Non-conservative | NS5 |
| 3039 | V to I | Conservative | NS5 |
| 3044 | S to N | Conservative | NS5 |
| 3046 | T to A | Non-conservative | NS5 |
| 3154 | Q to H | Non-conservative | NS5 |
| 3161 | R to K | Conservative | NS5 |
| 3167 | S to R | Non-conservative | NS5 |
| 3239 | Y to H | Non-conservative | NS5 |
| 3257 | I to F | Conservative | NS5 |
| 3304 | S to A | Non-conservative | NS5 |
| 3307 | V to I | Conservative | NS5 |
| 3333 | V to M | Conservative | NS5 |
| 3335 | W to C | Conservative | NS5 |
| 3402 | Y to F | Non-conservative | NS5 |

Table 4. Raw transcript counts and fold change of genes in Nanostring panel.

| Sample | Gene | Raw counts | AGCs | Ratio | FC (over mock) | Log2 FC (over mock) |
|---|---|---|---|---|---|---|
| ZIKV/Dakar 4 hpi_1 | IRF5 | 299 | 21745.79117 | 0.013749787 | 1.282677764 | 0.35915878 |
| ZIKV/Dakar 8 hpi_1 | IRF5 | 237 | 17326.69644 | 0.013678314 | 0.961425628 | -0.056752834 |
| ZIKV/Dakar 10 hpi_1 | IRF5 | 224 | 17513.91951 | 0.012789827 | 0.870033812 | -0.200856626 |
| ZIKV/Dakar 24 hpi_1 | IRF5 | 182 | 12050.24737 | 0.015103424 | 0.956588042 | -0.064030338 |
| ZIKV/Dakar 48 hpi_1 | IRF5 | 304 | 14705.51891 | 0.020672511 | 1.063246409 | 0.088475982 |
| ZIKV/Dakar 4 hpi_2 | IRF5 | 139 | 10431.40144 | 0.013325151 | 1.243064696 | 0.313901384 |
| ZIKV/Dakar 8 hpi_2 | IRF5 | 176 | 12658.05148 | 0.013904 | 0.977302311 | -0.03312 |
| ZIKV/Dakar 10 hpi_2 | IRF5 | 162 | 13088.28841 | 0.012377 | 0.841983576 | -0.24814 |
| ZIKV/Dakar 24 hpi_2 | IRF5 | 138 | 9702.067847 | 0.014224 | 0.900874515 | -0.1506 |
| ZIKV/Dakar 48 hpi_2 | IRF5 | 127 | 7275.616586 | 0.017456 | 0.897789685 | -0.15555 |
| ZIKV/Dakar 4 hpi_3 | IRF5 | 137 | 10334.87659 | 0.013256 | 1.236621699 | 0.306404 |
| ZIKV/Dakar 8 hpi_3 | IRF5 | 134 | 10124.86039 | 0.013235 | 0.930248268 | -0.10431 |
| ZIKV/Dakar 10 hpi_3 | IRF5 | 104 | 8611.388976 | 0.012077 | 0.82154545 | -0.28359 |
| ZIKV/Dakar 24 hpi_3 | IRF5 | 132 | 9356.243092 | 0.014108 | 0.893556372 | -0.16237 |
| ZIKV/Dakar 48 hpi_3 | IRF5 | 124 | 7898.825141 | 0.015699 | 0.807420701 | -0.30861 |
| ZIKV/Dakar 4 hpi_1 | IFNB1 | 16 | 21745.79117 | 0.000736 | 0.787427858 | -0.34478 |
| ZIKV/Dakar 8 hpi_1 | IFNB1 | 38 | 17326.69644 | 0.002193 | 2.302933644 | 1.203473 |
| ZIKV/Dakar 10 hpi_1 | IFNB1 | 34 | 17513.91951 | 0.001941 | 1.668340497 | 0.738414 |
| ZIKV/Dakar 24 hpi_1 | IFNB1 | 1029 | 12050.24737 | 0.085392 | 115.3089179 | 6.84936 |
| ZIKV/Dakar 48 hpi_1 | IFNB1 | 3561 | 14705.51891 | 0.242154 | 266.7003159 | 8.059076 |
| ZIKV/Dakar 4 hpi_2 | IFNB1 | 11 | 10431.40144 | 0.001055 | 1.128537598 | 0.174454 |

| | | | | | | |
|---|---|---|---|---|---|---|
| ZIKV/Dakar 8 hpi_2 | IFNB1 | 22 | 12658.05148 | 0.001738 | 1.825027521 | 0.867918 |
| ZIKV/Dakar 10 hpi_2 | IFNB1 | 28 | 13088.28841 | 0.002139 | 1.838502816 | 0.878531 |
| ZIKV/Dakar 24 hpi_2 | IFNB1 | 849 | 9702.067847 | 0.087507 | 118.164458 | 6.884652 |
| ZIKV/Dakar 48 hpi_2 | IFNB1 | 2225 | 7275.616586 | 0.305816 | 336.8155404 | 8.395815 |
| ZIKV/Dakar 4 hpi_3 | IFNB1 | 10 | 10334.87659 | 0.000968 | 1.035525293 | 0.050363 |
| ZIKV/Dakar 8 hpi_3 | IFNB1 | 23 | 10124.86039 | 0.002272 | 2.385351513 | 1.254202 |
| ZIKV/Dakar 10 hpi_3 | IFNB1 | 26 | 8611.388976 | 0.003019 | 2.59471263 | 1.375575 |
| ZIKV/Dakar 24 hpi_3 | IFNB1 | 600 | 9356.243092 | 0.064128 | 86.59508397 | 6.436213 |
| ZIKV/Dakar 48 hpi_3 | IFNB1 | 1186 | 7898.825141 | 0.150149 | 165.3689998 | 7.369545 |
| ZIKV/Dakar 4 hpi_1 | MX1 | 2346 | 21745.79117 | 0.107883 | 9.804884373 | 3.293501 |
| ZIKV/Dakar 8 hpi_1 | MX1 | 3133 | 17326.69644 | 0.180819 | 19.17270925 | 4.260982 |
| ZIKV/Dakar 10 hpi_1 | MX1 | 2866 | 17513.91951 | 0.163641 | 15.23414621 | 3.929237 |
| ZIKV/Dakar 24 hpi_1 | MX1 | 38886 | 12050.24737 | 3.226988 | 305.4307255 | 8.254701 |
| ZIKV/Dakar 48 hpi_1 | MX1 | 89927 | 14705.51891 | 6.115187 | 662.2660902 | 9.371267 |
| ZIKV/Dakar 4 hpi_2 | MX1 | 705 | 10431.40144 | 0.067584 | 6.142372352 | 2.618796 |
| ZIKV/Dakar 8 hpi_2 | MX1 | 1574 | 12658.05148 | 0.124348 | 13.18489661 | 3.720814 |
| ZIKV/Dakar 10 hpi_2 | MX1 | 2515 | 13088.28841 | 0.192157 | 17.88876734 | 4.160982 |
| ZIKV/Dakar 24 hpi_2 | MX1 | 25966 | 9702.067847 | 2.676337 | 253.3122309 | 7.984773 |
| ZIKV/Dakar 48 hpi_2 | MX1 | 40411 | 7275.616586 | 5.554306 | 601.5234465 | 9.232477 |
| ZIKV/Dakar 4 hpi_3 | MX1 | 4789 | 10334.87659 | 0.463382 | 42.11426482 | 5.396237 |
| ZIKV/Dakar 8 hpi_3 | MX1 | 4462 | 10124.86039 | 0.440697 | 46.72823535 | 5.546223 |
| ZIKV/Dakar 10 hpi_3 | MX1 | 3767 | 8611.388976 | 0.437444 | 40.72374378 | 5.347798 |
| ZIKV/Dakar 24 hpi_3 | MX1 | 35217 | 9356.243092 | 3.764011 | 356.2593528 | 8.476784 |
| ZIKV/Dakar 48 hpi_3 | MX1 | 70724 | 7898.825141 | 8.953737 | 969.6769734 | 9.92136 |
| ZIKV/Dakar 4 hpi_1 | IFNL3 | 20 | 21745.79117 | 0.00092 | 0.740765932 | -0.43291 |

| | | | | | | |
|---|---|---|---|---|---|---|
| ZIKV/Dakar 8 hpi_1 | IFNL3 | 27 | 17326.69644 | 0.001558 | 1.057209449 | 0.080261 |
| ZIKV/Dakar 10 hpi_1 | IFNL3 | 30 | 17513.91951 | 0.001713 | 1.195641488 | 0.257785 |
| ZIKV/Dakar 24 hpi_1 | IFNL3 | 227 | 12050.24737 | 0.018838 | 11.77929762 | 3.558182 |
| ZIKV/Dakar 48 hpi_1 | IFNL3 | 1075 | 14705.51891 | 0.073102 | 72.73183964 | 6.184515 |
| ZIKV/Dakar 4 hpi_2 | IFNL3 | 19 | 10431.40144 | 0.001821 | 1.467023803 | 0.552892 |
| ZIKV/Dakar 8 hpi_2 | IFNL3 | 24 | 12658.05148 | 0.001896 | 1.286344881 | 0.363277 |
| ZIKV/Dakar 10 hpi_2 | IFNL3 | 25 | 13088.28841 | 0.00191 | 1.333276497 | 0.414976 |
| ZIKV/Dakar 24 hpi_2 | IFNL3 | 179 | 9702.067847 | 0.01845 | 11.53661033 | 3.528147 |
| ZIKV/Dakar 48 hpi_2 | IFNL3 | 822 | 7275.616586 | 0.11298 | 112.4083247 | 6.812605 |
| ZIKV/Dakar 4 hpi_3 | IFNL3 | 10 | 10334.87659 | 0.000968 | 0.779329154 | -0.3597 |
| ZIKV/Dakar 8 hpi_3 | IFNL3 | 26 | 10124.86039 | 0.002568 | 1.742197326 | 0.800908 |
| ZIKV/Dakar 10 hpi_3 | IFNL3 | 9 | 8611.388976 | 0.001045 | 0.729511889 | -0.455 |
| ZIKV/Dakar 24 hpi_3 | IFNL3 | 152 | 9356.243092 | 0.016246 | 10.15854693 | 3.344622 |
| ZIKV/Dakar 48 hpi_3 | IFNL3 | 405 | 7898.825141 | 0.051273 | 51.01395392 | 5.67282 |
| ZIKV/Dakar 4 hpi_1 | IFIH1 | 575 | 21745.79117 | 0.026442 | 4.184950648 | 2.065211 |
| ZIKV/Dakar 8 hpi_1 | IFIH1 | 342 | 17326.69644 | 0.019738 | 3.039659008 | 1.603909 |
| ZIKV/Dakar 10 hpi_1 | IFIH1 | 287 | 17513.91951 | 0.016387 | 2.32384228 | 1.216512 |
| ZIKV/Dakar 24 hpi_1 | IFIH1 | 1791 | 12050.24737 | 0.148628 | 19.80202963 | 4.307576 |
| ZIKV/Dakar 48 hpi_1 | IFIH1 | 4296 | 14705.51891 | 0.292135 | 32.3670711 | 5.016455 |
| ZIKV/Dakar 4 hpi_2 | IFIH1 | 238 | 10431.40144 | 0.022816 | 3.611037574 | 1.852413 |
| ZIKV/Dakar 8 hpi_2 | IFIH1 | 212 | 12658.05148 | 0.016748 | 2.579191155 | 1.366919 |
| ZIKV/Dakar 10 hpi_2 | IFIH1 | 233 | 13088.28841 | 0.017802 | 2.524533665 | 1.336017 |
| ZIKV/Dakar 24 hpi_2 | IFIH1 | 1152 | 9702.067847 | 0.118738 | 15.8197004 | 3.98365 |
| ZIKV/Dakar 48 hpi_2 | IFIH1 | 2150 | 7275.616586 | 0.295508 | 32.74071343 | 5.033014 |
| ZIKV/Dakar 4 hpi_3 | IFIH1 | 580 | 10334.87659 | 0.056121 | 8.882197131 | 3.150917 |

| | | | | | | |
|---|---|---|---|---|---|---|
| ZIKV/Dakar 8 hpi_3 | IFIH1 | 265 | 10124.86039 | 0.026173 | 4.030615381 | 2.011 |
| ZIKV/Dakar 10 hpi_3 | IFIH1 | 174 | 8611.388976 | 0.020206 | 2.865392655 | 1.518733 |
| ZIKV/Dakar 24 hpi_3 | IFIH1 | 1348 | 9356.243092 | 0.144075 | 19.19545796 | 4.262693 |
| ZIKV/Dakar 48 hpi_3 | IFIH1 | 2331 | 7898.825141 | 0.295107 | 32.69634873 | 5.031058 |
| ZIKV/Dakar 4 hpi_1 | IL1B | 54 | 21745.79117 | 0.002483 | 1.353099035 | 0.436267 |
| ZIKV/Dakar 8 hpi_1 | IL1B | 31 | 17326.69644 | 0.001789 | 1.011749276 | 0.016852 |
| ZIKV/Dakar 10 hpi_1 | IL1B | 28 | 17513.91951 | 0.001599 | 0.972366163 | -0.04043 |
| ZIKV/Dakar 24 hpi_1 | IL1B | 39 | 12050.24737 | 0.003236 | 1.469103431 | 0.554936 |
| ZIKV/Dakar 48 hpi_1 | IL1B | 83 | 14705.51891 | 0.005644 | 1.826936781 | 0.869427 |
| ZIKV/Dakar 4 hpi_2 | IL1B | 23 | 10431.40144 | 0.002205 | 1.201423755 | 0.264745 |
| ZIKV/Dakar 8 hpi_2 | IL1B | 18 | 12658.05148 | 0.001422 | 0.804141773 | -0.31448 |
| ZIKV/Dakar 10 hpi_2 | IL1B | 23 | 13088.28841 | 0.001757 | 1.068809081 | 0.096004 |
| ZIKV/Dakar 24 hpi_2 | IL1B | 23 | 9702.067847 | 0.002371 | 1.076086684 | 0.105794 |
| ZIKV/Dakar 48 hpi_2 | IL1B | 64 | 7275.616586 | 0.008797 | 2.847317849 | 1.509604 |
| ZIKV/Dakar 4 hpi_3 | IL1B | 17 | 10334.87659 | 0.001645 | 0.896302615 | -0.15794 |
| ZIKV/Dakar 8 hpi_3 | IL1B | 19 | 10124.86039 | 0.001877 | 1.061186051 | 0.085678 |
| ZIKV/Dakar 10 hpi_3 | IL1B | 13 | 8611.388976 | 0.00151 | 0.918174657 | -0.12316 |
| ZIKV/Dakar 24 hpi_3 | IL1B | 26 | 9356.243092 | 0.002779 | 1.261407995 | 0.335035 |
| ZIKV/Dakar 48 hpi_3 | IL1B | 45 | 7898.825141 | 0.005697 | 1.844063173 | 0.882888 |
| ZIKV/Dakar 4 hpi_1 | GBP1 | 433 | 21745.79117 | 0.019912 | 8.326417727 | 3.057696 |
| ZIKV/Dakar 8 hpi_1 | GBP1 | 328 | 17326.69644 | 0.01893 | 6.081800195 | 2.604498 |
| ZIKV/Dakar 10 hpi_1 | GBP1 | 225 | 17513.91951 | 0.012847 | 3.910128892 | 1.967216 |
| ZIKV/Dakar 24 hpi_1 | GBP1 | 631 | 12050.24737 | 0.052364 | 18.65650781 | 4.221607 |
| ZIKV/Dakar 48 hpi_1 | GBP1 | 2172 | 14705.51891 | 0.1477 | 65.06647791 | 6.023843 |
| ZIKV/Dakar 4 hpi_2 | GBP1 | 124 | 10431.40144 | 0.011887 | 4.970779954 | 2.313472 |

| | | | | | | |
|---|---|---|---|---|---|---|
| ZIKV/Dakar 8 hpi_2 | GBP1 | 168 | 12658.05148 | 0.013272 | 4.263993121 | 2.092205 |
| ZIKV/Dakar 10 hpi_2 | GBP1 | 117 | 13088.28841 | 0.008939 | 2.720789296 | 1.444025 |
| ZIKV/Dakar 24 hpi_2 | GBP1 | 341 | 9702.067847 | 0.035147 | 12.52238434 | 3.646437 |
| ZIKV/Dakar 48 hpi_2 | GBP1 | 1290 | 7275.616586 | 0.177305 | 78.10839927 | 6.287406 |
| ZIKV/Dakar 4 hpi_3 | GBP1 | 243 | 10334.87659 | 0.023513 | 9.832104604 | 3.2975 |
| ZIKV/Dakar 8 hpi_3 | GBP1 | 170 | 10124.86039 | 0.01679 | 5.394285756 | 2.431432 |
| ZIKV/Dakar 10 hpi_3 | GBP1 | 109 | 8611.388976 | 0.012658 | 3.85252261 | 1.945803 |
| ZIKV/Dakar 24 hpi_3 | GBP1 | 400 | 9356.243092 | 0.042752 | 15.23194812 | 3.929029 |
| ZIKV/Dakar 48 hpi_3 | GBP1 | 1133 | 7898.825141 | 0.143439 | 63.18954697 | 5.981614 |
| ZIKV/Dakar 4 hpi_1 | IFITM1 | 663 | 21745.79117 | 0.030489 | 4.081302403 | 2.02903 |
| ZIKV/Dakar 8 hpi_1 | IFITM1 | 795 | 17326.69644 | 0.045883 | 6.194658812 | 2.631025 |
| ZIKV/Dakar 10 hpi_1 | IFITM1 | 842 | 17513.91951 | 0.048076 | 5.518459657 | 2.464266 |
| ZIKV/Dakar 24 hpi_1 | IFITM1 | 10041 | 12050.24737 | 0.833261 | 45.03327164 | 5.492919 |
| ZIKV/Dakar 48 hpi_1 | IFITM1 | 121959 | 14705.51891 | 8.293417 | 93.4956134 | 6.546827 |
| ZIKV/Dakar 4 hpi_2 | IFITM1 | 132 | 10431.40144 | 0.012654 | 1.693915461 | 0.760362 |
| ZIKV/Dakar 8 hpi_2 | IFITM1 | 279 | 12658.05148 | 0.022041 | 2.975797504 | 1.573276 |
| ZIKV/Dakar 10 hpi_2 | IFITM1 | 489 | 13088.28841 | 0.037362 | 4.288595966 | 2.100505 |
| ZIKV/Dakar 24 hpi_2 | IFITM1 | 5847 | 9702.067847 | 0.602655 | 32.57026418 | 5.025484 |
| ZIKV/Dakar 48 hpi_2 | IFITM1 | 50706 | 7275.616586 | 6.969306 | 78.56828658 | 6.295875 |
| ZIKV/Dakar 4 hpi_3 | IFITM1 | 784 | 10334.87659 | 0.07586 | 10.15479656 | 3.344089 |
| ZIKV/Dakar 8 hpi_3 | IFITM1 | 770 | 10124.86039 | 0.07605 | 10.26757091 | 3.360023 |
| ZIKV/Dakar 10 hpi_3 | IFITM1 | 916 | 8611.388976 | 0.106371 | 12.20988004 | 3.609977 |
| ZIKV/Dakar 24 hpi_3 | IFITM1 | 9455 | 9356.243092 | 1.010555 | 54.61507456 | 5.771227 |
| ZIKV/Dakar 48 hpi_3 | IFITM1 | 73844 | 7898.825141 | 9.348732 | 105.39268 | 6.719631 |
| ZIKV/Dakar 4 hpi_1 | TLR3 | 248 | 21745.79117 | 0.011405 | 1.45836342 | 0.54435 |

| | | | | | | |
|---|---|---|---|---|---|---|
| ZIKV/Dakar 8 hpi_1 | TLR3 | 256 | 17326.69644 | 0.014775 | 2.301035282 | 1.202283 |
| ZIKV/Dakar 10 hpi_1 | TLR3 | 212 | 17513.91951 | 0.012105 | 1.741001558 | 0.799917 |
| ZIKV/Dakar 24 hpi_1 | TLR3 | 682 | 12050.24737 | 0.056596 | 6.37480091 | 2.67238 |
| ZIKV/Dakar 48 hpi_1 | TLR3 | 1483 | 14705.51891 | 0.100846 | 11.24253 | 3.490895 |
| ZIKV/Dakar 4 hpi_2 | TLR3 | 148 | 10431.40144 | 0.014188 | 1.814296869 | 0.859411 |
| ZIKV/Dakar 8 hpi_2 | TLR3 | 217 | 12658.05148 | 0.017143 | 2.669881312 | 1.416776 |
| ZIKV/Dakar 10 hpi_2 | TLR3 | 193 | 13088.28841 | 0.014746 | 2.120904439 | 1.08468 |
| ZIKV/Dakar 24 hpi_2 | TLR3 | 513 | 9702.067847 | 0.052875 | 5.955678856 | 2.574266 |
| ZIKV/Dakar 48 hpi_2 | TLR3 | 815 | 7275.616586 | 0.112018 | 12.48794744 | 3.642464 |
| ZIKV/Dakar 4 hpi_3 | TLR3 | 170 | 10334.87659 | 0.016449 | 2.103453524 | 1.07276 |
| ZIKV/Dakar 8 hpi_3 | TLR3 | 163 | 10124.86039 | 0.016099 | 2.50725 | 1.326106 |
| ZIKV/Dakar 10 hpi_3 | TLR3 | 119 | 8611.388976 | 0.013819 | 1.987560711 | 0.990999 |
| ZIKV/Dakar 24 hpi_3 | TLR3 | 520 | 9356.243092 | 0.055578 | 6.260082553 | 2.646182 |
| ZIKV/Dakar 48 hpi_3 | TLR3 | 1213 | 7898.825141 | 0.153567 | 17.11991322 | 4.097603 |
| ZIKV/Dakar 4 hpi_1 | CCL3 | 16 | 21745.79117 | 0.000736 | 0.960979151 | -0.05742 |
| ZIKV/Dakar 8 hpi_1 | CCL3 | 9 | 17326.69644 | 0.000519 | 0.657642482 | -0.60462 |
| ZIKV/Dakar 10 hpi_1 | CCL3 | 12 | 17513.91951 | 0.000685 | 0.685765061 | -0.54421 |
| ZIKV/Dakar 24 hpi_1 | CCL3 | 14 | 12050.24737 | 0.001162 | 1.870193243 | 0.903187 |
| ZIKV/Dakar 48 hpi_1 | CCL3 | 58 | 14705.51891 | 0.003944 | 5.328293698 | 2.413674 |
| ZIKV/Dakar 4 hpi_2 | CCL3 | 8 | 10431.40144 | 0.000767 | 1.001651219 | 0.00238 |
| ZIKV/Dakar 8 hpi_2 | CCL3 | 13 | 12658.05148 | 0.001027 | 1.300288172 | 0.378831 |
| ZIKV/Dakar 10 hpi_2 | CCL3 | 7 | 13088.28841 | 0.000535 | 0.535294328 | -0.9016 |
| ZIKV/Dakar 24 hpi_2 | CCL3 | 7 | 9702.067847 | 0.000721 | 1.161416905 | 0.215886 |
| ZIKV/Dakar 48 hpi_2 | CCL3 | 39 | 7275.616586 | 0.00536 | 7.241613107 | 2.856311 |
| ZIKV/Dakar 4 hpi_3 | CCL3 | 5 | 10334.87659 | 0.000484 | 0.631878975 | -0.66228 |

| | | | | | | |
|---|---|---|---|---|---|---|
| ZIKV/Dakar 8 hpi_3 | CCL3 | 4 | 10124.86039 | 0.000395 | 0.500188917 | -0.99946 |
| ZIKV/Dakar 10 hpi_3 | CCL3 | 9 | 8611.388976 | 0.001045 | 1.046036312 | 0.064933 |
| ZIKV/Dakar 24 hpi_3 | CCL3 | 11 | 9356.243092 | 0.001176 | 1.892542315 | 0.920326 |
| ZIKV/Dakar 48 hpi_3 | CCL3 | 35 | 7898.825141 | 0.004431 | 5.986128843 | 2.581623 |
| ZIKV/Dakar 4 hpi_1 | IL18 | 1303 | 21745.79117 | 0.05992 | 0.812389328 | -0.29976 |
| ZIKV/Dakar 8 hpi_1 | IL18 | 1078 | 17326.69644 | 0.062216 | 0.875458564 | -0.19189 |
| ZIKV/Dakar 10 hpi_1 | IL18 | 1060 | 17513.91951 | 0.060523 | 0.849347694 | -0.23557 |
| ZIKV/Dakar 24 hpi_1 | IL18 | 535 | 12050.24737 | 0.044397 | 0.751826799 | -0.41153 |
| ZIKV/Dakar 48 hpi_1 | IL18 | 776 | 14705.51891 | 0.052769 | 0.647808844 | -0.62636 |
| ZIKV/Dakar 4 hpi_2 | IL18 | 770 | 10431.40144 | 0.073816 | 1.000790268 | 0.00114 |
| ZIKV/Dakar 8 hpi_2 | IL18 | 937 | 12658.05148 | 0.074024 | 1.041610465 | 0.058816 |
| ZIKV/Dakar 10 hpi_2 | IL18 | 928 | 13088.28841 | 0.070903 | 0.995011536 | -0.00721 |
| ZIKV/Dakar 24 hpi_2 | IL18 | 501 | 9702.067847 | 0.051638 | 0.874446817 | -0.19356 |
| ZIKV/Dakar 48 hpi_2 | IL18 | 440 | 7275.616586 | 0.060476 | 0.742417802 | -0.4297 |
| ZIKV/Dakar 4 hpi_3 | IL18 | 750 | 10334.87659 | 0.07257 | 0.983900033 | -0.02342 |
| ZIKV/Dakar 8 hpi_3 | IL18 | 726 | 10124.86039 | 0.071705 | 1.008974472 | 0.01289 |
| ZIKV/Dakar 10 hpi_3 | IL18 | 580 | 8611.388976 | 0.067353 | 0.945187094 | -0.08133 |
| ZIKV/Dakar 24 hpi_3 | IL18 | 514 | 9356.243092 | 0.054937 | 0.930296966 | -0.10424 |
| ZIKV/Dakar 48 hpi_3 | IL18 | 486 | 7898.825141 | 0.061528 | 0.755334418 | -0.40481 |
| ZIKV/Dakar 4 hpi_1 | CXCL10 | 16 | 21745.79117 | 0.000736 | 3.1417981 | 1.65159 |
| ZIKV/Dakar 8 hpi_1 | CXCL10 | 9 | 17326.69644 | 0.000519 | 1.745165193 | 0.803364 |
| ZIKV/Dakar 10 hpi_1 | CXCL10 | 11 | 17513.91951 | 0.000628 | 2.292984104 | 1.197226 |
| ZIKV/Dakar 24 hpi_1 | CXCL10 | 26 | 12050.24737 | 0.002158 | 6.115856802 | 2.612555 |
| ZIKV/Dakar 48 hpi_1 | CXCL10 | 116 | 14705.51891 | 0.007888 | 24.14091874 | 4.593409 |
| ZIKV/Dakar 4 hpi_2 | CXCL10 | 14 | 10431.40144 | 0.001342 | 5.730847872 | 2.518749 |

| | | | | | | |
|---|---|---|---|---|---|---|
| ZIKV/Dakar 8 hpi_2 | CXCL10 | 7 | 12658.05148 | 0.000553 | 1.857979775 | 0.893735 |
| ZIKV/Dakar 10 hpi_2 | CXCL10 | 4 | 13088.28841 | 0.000306 | 1.115755004 | 0.15802 |
| ZIKV/Dakar 24 hpi_2 | CXCL10 | 25 | 9702.067847 | 0.002577 | 7.303913547 | 2.86867 |
| ZIKV/Dakar 48 hpi_2 | CXCL10 | 68 | 7275.616586 | 0.009346 | 28.60324244 | 4.838107 |
| ZIKV/Dakar 4 hpi_3 | CXCL10 | 13 | 10334.87659 | 0.001258 | 5.371202924 | 2.425245 |
| ZIKV/Dakar 8 hpi_3 | CXCL10 | 11 | 10124.86039 | 0.001086 | 3.650172941 | 1.867965 |
| ZIKV/Dakar 10 hpi_3 | CXCL10 | 6 | 8611.388976 | 0.000697 | 2.543722621 | 1.346941 |
| ZIKV/Dakar 24 hpi_3 | CXCL10 | 21 | 9356.243092 | 0.002244 | 6.362059411 | 2.669494 |
| ZIKV/Dakar 48 hpi_3 | CXCL10 | 37 | 7898.825141 | 0.004684 | 14.33558378 | 3.841529 |
| ZIKV/Dakar 4 hpi_1 | IFNA4 | 7 | 21745.79117 | 0.000322 | 1.300336122 | 0.378885 |
| ZIKV/Dakar 8 hpi_1 | IFNA4 | 5 | 17326.69644 | 0.000289 | 0.626790884 | -0.67394 |
| ZIKV/Dakar 10 hpi_1 | IFNA4 | 3 | 17513.91951 | 0.000171 | 0.428002891 | -1.22431 |
| ZIKV/Dakar 24 hpi_1 | IFNA4 | 17 | 12050.24737 | 0.001411 | 3.231751543 | 1.692316 |
| ZIKV/Dakar 48 hpi_1 | IFNA4 | 22 | 14705.51891 | 0.001496 | 3.571997758 | 1.836731 |
| ZIKV/Dakar 4 hpi_2 | IFNA4 | 5 | 10431.40144 | 0.000479 | 1.93624427 | 0.953261 |
| ZIKV/Dakar 8 hpi_2 | IFNA4 | 4 | 12658.05148 | 0.000316 | 0.686375175 | -0.54293 |
| ZIKV/Dakar 10 hpi_2 | IFNA4 | 6 | 13088.28841 | 0.000458 | 1.145452781 | 0.195918 |
| ZIKV/Dakar 24 hpi_2 | IFNA4 | 12 | 9702.067847 | 0.001237 | 2.833361214 | 1.502515 |
| ZIKV/Dakar 48 hpi_2 | IFNA4 | 10 | 7275.616586 | 0.001374 | 3.281701279 | 1.714444 |
| ZIKV/Dakar 4 hpi_3 | IFNA4 | 0.024417492 | 10334.87659 | 2.36E-06 | 0.009543959 | -6.7112 |
| ZIKV/Dakar 8 hpi_3 | IFNA4 | 6 | 10124.86039 | 0.000593 | 1.287154386 | 0.364185 |
| ZIKV/Dakar 10 hpi_3 | IFNA4 | 4 | 8611.388976 | 0.000465 | 1.160634783 | 0.214914 |
| ZIKV/Dakar 24 hpi_3 | IFNA4 | 7 | 9356.243092 | 0.000748 | 1.713884491 | 0.77727 |
| ZIKV/Dakar 48 hpi_3 | IFNA4 | 18 | 7898.825141 | 0.002279 | 5.441001629 | 2.443872 |
| ZIKV/Dakar 4 hpi_1 | IRF1 | 940 | 21745.79117 | 0.043227 | 3.741819459 | 1.90374 |

| | | | | | | |
|---|---|---|---|---|---|---|
| ZIKV/Dakar 8 hpi_1 | IRF1 | 207 | 17326.69644 | 0.011947 | 0.99401595 | -0.00866 |
| ZIKV/Dakar 10 hpi_1 | IRF1 | 202 | 17513.91951 | 0.011534 | 1.186839589 | 0.247125 |
| ZIKV/Dakar 24 hpi_1 | IRF1 | 615 | 12050.24737 | 0.051036 | 4.597661175 | 2.2009 |
| ZIKV/Dakar 48 hpi_1 | IRF1 | 1447 | 14705.51891 | 0.098398 | 8.096579219 | 3.017313 |
| ZIKV/Dakar 4 hpi_2 | IRF1 | 690 | 10431.40144 | 0.066146 | 5.725805885 | 2.517479 |
| ZIKV/Dakar 8 hpi_2 | IRF1 | 136 | 12658.05148 | 0.010744 | 0.893945053 | -0.16174 |
| ZIKV/Dakar 10 hpi_2 | IRF1 | 186 | 13088.28841 | 0.014211 | 1.462359303 | 0.548298 |
| ZIKV/Dakar 24 hpi_2 | IRF1 | 521 | 9702.067847 | 0.0537 | 4.837614144 | 2.274296 |
| ZIKV/Dakar 48 hpi_2 | IRF1 | 1007 | 7275.616586 | 0.138408 | 11.3886713 | 3.509528 |
| ZIKV/Dakar 4 hpi_3 | IRF1 | 402 | 10334.87659 | 0.038897 | 3.367060707 | 1.75149 |
| ZIKV/Dakar 8 hpi_3 | IRF1 | 148 | 10124.86039 | 0.014617 | 1.216218055 | 0.282402 |
| ZIKV/Dakar 10 hpi_3 | IRF1 | 101 | 8611.388976 | 0.011729 | 1.206902457 | 0.271309 |
| ZIKV/Dakar 24 hpi_3 | IRF1 | 446 | 9356.243092 | 0.047669 | 4.294288036 | 2.102419 |
| ZIKV/Dakar 48 hpi_3 | IRF1 | 856 | 7898.825141 | 0.108371 | 8.917120945 | 3.156578 |
| ZIKV/Dakar 4 hpi_1 | IFI44 | 295 | 21745.79117 | 0.013566 | 3.657353092 | 1.8708 |
| ZIKV/Dakar 8 hpi_1 | IFI44 | 441 | 17326.69644 | 0.025452 | 7.142698762 | 2.836469 |
| ZIKV/Dakar 10 hpi_1 | IFI44 | 357 | 17513.91951 | 0.020384 | 5.754252525 | 2.524629 |
| ZIKV/Dakar 24 hpi_1 | IFI44 | 2448 | 12050.24737 | 0.203149 | 42.39754426 | 5.405909 |
| ZIKV/Dakar 48 hpi_1 | IFI44 | 6783 | 14705.51891 | 0.461255 | 102.6658639 | 6.681813 |
| ZIKV/Dakar 4 hpi_2 | IFI44 | 87 | 10431.40144 | 0.00834 | 2.248519619 | 1.168975 |
| ZIKV/Dakar 8 hpi_2 | IFI44 | 189 | 12658.05148 | 0.014931 | 4.190197161 | 2.067018 |
| ZIKV/Dakar 10 hpi_2 | IFI44 | 250 | 13088.28841 | 0.019101 | 5.392140535 | 2.430858 |
| ZIKV/Dakar 24 hpi_2 | IFI44 | 1384 | 9702.067847 | 0.14265 | 29.77124755 | 4.895848 |
| ZIKV/Dakar 48 hpi_2 | IFI44 | 2492 | 7275.616586 | 0.342514 | 76.23648011 | 6.25241 |
| ZIKV/Dakar 4 hpi_3 | IFI44 | 311 | 10334.87659 | 0.030092 | 8.112882413 | 3.020215 |

| | | | | | | |
|---|---|---|---|---|---|---|
| ZIKV/Dakar 8 hpi_3 | IFI44 | 357 | 10124.86039 | 0.03526 | 9.895065748 | 3.306709 |
| ZIKV/Dakar 10 hpi_3 | IFI44 | 286 | 8611.388976 | 0.033212 | 9.375552646 | 3.228904 |
| ZIKV/Dakar 24 hpi_3 | IFI44 | 1972 | 9356.243092 | 0.210768 | 43.98764027 | 5.459026 |
| ZIKV/Dakar 48 hpi_3 | IFI44 | 3534 | 7898.825141 | 0.447408 | 99.5837894 | 6.637839 |
| ZIKV/Dakar 4 hpi_1 | IL1A | 67 | 21745.79117 | 0.003081 | 3.053676323 | 1.610547 |
| ZIKV/Dakar 8 hpi_1 | IL1A | 17 | 17326.69644 | 0.000981 | 0.743094402 | -0.42838 |
| ZIKV/Dakar 10 hpi_1 | IL1A | 19 | 17513.91951 | 0.001085 | 0.663900022 | -0.59096 |
| ZIKV/Dakar 24 hpi_1 | IL1A | 38 | 12050.24737 | 0.003153 | 2.498625764 | 1.321135 |
| ZIKV/Dakar 48 hpi_1 | IL1A | 135 | 14705.51891 | 0.00918 | 4.869720366 | 2.283839 |
| ZIKV/Dakar 4 hpi_2 | IL1A | 63 | 10431.40144 | 0.006039 | 5.985787607 | 2.581541 |
| ZIKV/Dakar 8 hpi_2 | IL1A | 22 | 12658.05148 | 0.001738 | 1.316335696 | 0.396527 |
| ZIKV/Dakar 10 hpi_2 | IL1A | 19 | 13088.28841 | 0.001452 | 0.888389008 | -0.17074 |
| ZIKV/Dakar 24 hpi_2 | IL1A | 44 | 9702.067847 | 0.004535 | 3.593370091 | 1.845338 |
| ZIKV/Dakar 48 hpi_2 | IL1A | 102 | 7275.616586 | 0.014019 | 7.436712227 | 2.894665 |
| ZIKV/Dakar 4 hpi_3 | IL1A | 17 | 10334.87659 | 0.001645 | 1.63029816 | 0.705136 |
| ZIKV/Dakar 8 hpi_3 | IL1A | 14 | 10124.86039 | 0.001383 | 1.047248694 | 0.066604 |
| ZIKV/Dakar 10 hpi_3 | IL1A | 14 | 8611.388976 | 0.001626 | 0.994917937 | -0.00735 |
| ZIKV/Dakar 24 hpi_3 | IL1A | 20 | 9356.243092 | 0.002138 | 1.693721803 | 0.760197 |
| ZIKV/Dakar 48 hpi_3 | IL1A | 56 | 7898.825141 | 0.00709 | 3.760764477 | 1.911026 |
| ZIKV/Dakar 4 hpi_1 | IFIT1 | 1814 | 21745.79117 | 0.083418 | 3.914637794 | 1.968879 |
| ZIKV/Dakar 8 hpi_1 | IFIT1 | 2604 | 17326.69644 | 0.150288 | 9.673629424 | 3.274057 |
| ZIKV/Dakar 10 hpi_1 | IFIT1 | 2989 | 17513.91951 | 0.170664 | 9.204019963 | 3.202264 |
| ZIKV/Dakar 24 hpi_1 | IFIT1 | 46725 | 12050.24737 | 3.877514 | 115.3874469 | 6.850342 |
| ZIKV/Dakar 48 hpi_1 | IFIT1 | 88916 | 14705.51891 | 6.046437 | 249.8713602 | 7.965042 |
| ZIKV/Dakar 4 hpi_2 | IFIT1 | 432 | 10431.40144 | 0.041413 | 1.94343761 | 0.958611 |

| | | | | | | |
|---|---|---|---|---|---|---|
| ZIKV/Dakar 8 hpi_2 | IFIT1 | 740 | 12658.05148 | 0.058461 | 3.762955612 | 1.911866 |
| ZIKV/Dakar 10 hpi_2 | IFIT1 | 2469 | 13088.28841 | 0.188642 | 10.17356631 | 3.346754 |
| ZIKV/Dakar 24 hpi_2 | IFIT1 | 26521 | 9702.067847 | 2.733541 | 81.34498897 | 6.345982 |
| ZIKV/Dakar 48 hpi_2 | IFIT1 | 33645 | 7275.616586 | 4.62435 | 191.1030621 | 7.578207 |
| ZIKV/Dakar 4 hpi_3 | IFIT1 | 5090 | 10334.87659 | 0.492507 | 23.11223806 | 4.530585 |
| ZIKV/Dakar 8 hpi_3 | IFIT1 | 2013 | 10124.86039 | 0.198818 | 12.79731808 | 3.67777 |
| ZIKV/Dakar 10 hpi_3 | IFIT1 | 2241 | 8611.388976 | 0.260237 | 14.03471624 | 3.810928 |
| ZIKV/Dakar 24 hpi_3 | IFIT1 | 36651 | 9356.243092 | 3.917277 | 116.5707385 | 6.865062 |
| ZIKV/Dakar 48 hpi_3 | IFIT1 | 60203 | 7898.825141 | 7.621766 | 314.9724373 | 8.299082 |
| ZIKV/Dakar 4 hpi_1 | IFIT2 | 1005 | 21745.79117 | 0.046216 | 6.258739657 | 2.645872 |
| ZIKV/Dakar 8 hpi_1 | IFIT2 | 488 | 17326.69644 | 0.028165 | 4.681393758 | 2.226938 |
| ZIKV/Dakar 10 hpi_1 | IFIT2 | 488 | 17513.91951 | 0.027864 | 4.524147131 | 2.177646 |
| ZIKV/Dakar 24 hpi_1 | IFIT2 | 9587 | 12050.24737 | 0.795585 | 74.60786903 | 6.221256 |
| ZIKV/Dakar 48 hpi_1 | IFIT2 | 23908 | 14705.51891 | 1.625784 | 163.2435997 | 7.350883 |
| ZIKV/Dakar 4 hpi_2 | IFIT2 | 292 | 10431.40144 | 0.027992 | 3.790846774 | 1.92252 |
| ZIKV/Dakar 8 hpi_2 | IFIT2 | 125 | 12658.05148 | 0.009875 | 1.641399406 | 0.714926 |
| ZIKV/Dakar 10 hpi_2 | IFIT2 | 337 | 13088.28841 | 0.025748 | 4.180683518 | 2.063739 |
| ZIKV/Dakar 24 hpi_2 | IFIT2 | 4973 | 9702.067847 | 0.512571 | 48.06755398 | 5.586991 |
| ZIKV/Dakar 48 hpi_2 | IFIT2 | 10693 | 7275.616586 | 1.469704 | 147.5716836 | 7.205272 |
| ZIKV/Dakar 4 hpi_3 | IFIT2 | 801 | 10334.87659 | 0.077505 | 10.49598639 | 3.391766 |
| ZIKV/Dakar 8 hpi_3 | IFIT2 | 208 | 10124.86039 | 0.020543 | 3.414643809 | 1.771735 |
| ZIKV/Dakar 10 hpi_3 | IFIT2 | 258 | 8611.388976 | 0.02996 | 4.864595649 | 2.28232 |
| ZIKV/Dakar 24 hpi_3 | IFIT2 | 5486 | 9356.243092 | 0.586346 | 54.98600624 | 5.780993 |
| ZIKV/Dakar 48 hpi_3 | IFIT2 | 12417 | 7898.825141 | 1.572006 | 157.8437721 | 7.302354 |
| ZIKV/Dakar 4 hpi_1 | DHX58 | 12 | 21745.79117 | 0.000552 | 1.55504996 | 0.636961 |

| | | | | | | |
|---|---|---|---|---|---|---|
| ZIKV/Dakar 8 hpi_1 | DHX58 | 12 | 17326.69644 | 0.000693 | 1.52500718 | 0.608816 |
| ZIKV/Dakar 10 hpi_1 | DHX58 | 17 | 17513.91951 | 0.000971 | 2.025711308 | 1.018429 |
| ZIKV/Dakar 24 hpi_1 | DHX58 | 72 | 12050.24737 | 0.005975 | 14.83370063 | 3.890807 |
| ZIKV/Dakar 48 hpi_1 | DHX58 | 365 | 14705.51891 | 0.024821 | 33.42769195 | 5.062972 |
| ZIKV/Dakar 4 hpi_2 | DHX58 | 10 | 10431.40144 | 0.000959 | 2.701442044 | 1.43373 |
| ZIKV/Dakar 8 hpi_2 | DHX58 | 9 | 12658.05148 | 0.000711 | 1.5656045 | 0.64672 |
| ZIKV/Dakar 10 hpi_2 | DHX58 | 11 | 13088.28841 | 0.00084 | 1.753968581 | 0.810623 |
| ZIKV/Dakar 24 hpi_2 | DHX58 | 74 | 9702.067847 | 0.007627 | 18.93565744 | 4.243034 |
| ZIKV/Dakar 48 hpi_2 | DHX58 | 233 | 7275.616586 | 0.032025 | 43.13005356 | 5.430622 |
| ZIKV/Dakar 4 hpi_3 | DHX58 | 8 | 10334.87659 | 0.000774 | 2.181338202 | 1.125213 |
| ZIKV/Dakar 8 hpi_3 | DHX58 | 12 | 10124.86039 | 0.001185 | 2.609748229 | 1.383911 |
| ZIKV/Dakar 10 hpi_3 | DHX58 | 11 | 8611.388976 | 0.001277 | 2.665823912 | 1.414581 |
| ZIKV/Dakar 24 hpi_3 | DHX58 | 75 | 9356.243092 | 0.008016 | 19.90090114 | 4.314762 |
| ZIKV/Dakar 48 hpi_3 | DHX58 | 223 | 7898.825141 | 0.028232 | 38.02211263 | 5.248767 |
| ZIKV/Dakar 4 hpi_1 | MX2 | 22 | 21745.79117 | 0.001012 | 7.117126256 | 2.831295 |
| ZIKV/Dakar 8 hpi_1 | MX2 | 20 | 17326.69644 | 0.001154 | 10.76552409 | 3.428347 |
| ZIKV/Dakar 10 hpi_1 | MX2 | 16 | 17513.91951 | 0.000914 | 3.185658087 | 1.671591 |
| ZIKV/Dakar 24 hpi_1 | MX2 | 394 | 12050.24737 | 0.032696 | 108.7582456 | 6.764981 |
| ZIKV/Dakar 48 hpi_1 | MX2 | 1948 | 14705.51891 | 0.132467 | 379.2629619 | 8.567055 |
| ZIKV/Dakar 4 hpi_2 | MX2 | 1 | 10431.40144 | 9.59E-05 | 0.674395313 | -0.56833 |
| ZIKV/Dakar 8 hpi_2 | MX2 | 6 | 12658.05148 | 0.000474 | 4.420845537 | 2.144322 |
| ZIKV/Dakar 10 hpi_2 | MX2 | 9 | 13088.28841 | 0.000688 | 2.397850937 | 1.261742 |
| ZIKV/Dakar 24 hpi_2 | MX2 | 162 | 9702.067847 | 0.016697 | 55.54086526 | 5.795478 |
| ZIKV/Dakar 48 hpi_2 | MX2 | 564 | 7275.616586 | 0.077519 | 221.9428371 | 7.794044 |
| ZIKV/Dakar 4 hpi_3 | MX2 | 21 | 10334.87659 | 0.002032 | 14.2945735 | 3.837396 |

| | | | | | | |
|---|---|---|---|---|---|---|
| ZIKV/Dakar 8 hpi_3 | MX2 | 17 | 10124.86039 | 0.001679 | 15.65960582 | 3.968976 |
| ZIKV/Dakar 10 hpi_3 | MX2 | 15 | 8611.388976 | 0.001742 | 6.074081026 | 2.602666 |
| ZIKV/Dakar 24 hpi_3 | MX2 | 280 | 9356.243092 | 0.029927 | 99.54477478 | 6.637274 |
| ZIKV/Dakar 48 hpi_3 | MX2 | 1040 | 7898.825141 | 0.131665 | 376.966427 | 8.558292 |
| ZIKV/Dakar 4 hpi_1 | IRF2 | 1873 | 21745.79117 | 0.086132 | 1.750783097 | 0.808 |
| ZIKV/Dakar 8 hpi_1 | IRF2 | 1205 | 17326.69644 | 0.069546 | 1.175986248 | 0.233871 |
| ZIKV/Dakar 10 hpi_1 | IRF2 | 1171 | 17513.91951 | 0.066861 | 1.034019224 | 0.048263 |
| ZIKV/Dakar 24 hpi_1 | IRF2 | 1587 | 12050.24737 | 0.131699 | 1.888430289 | 0.917188 |
| ZIKV/Dakar 48 hpi_1 | IRF2 | 2833 | 14705.51891 | 0.192649 | 1.992934648 | 0.994894 |
| ZIKV/Dakar 4 hpi_2 | IRF2 | 903 | 10431.40144 | 0.086566 | 1.759603723 | 0.815251 |
| ZIKV/Dakar 8 hpi_2 | IRF2 | 753 | 12658.05148 | 0.059488 | 1.005909898 | 0.008501 |
| ZIKV/Dakar 10 hpi_2 | IRF2 | 744 | 13088.28841 | 0.056845 | 0.879113899 | -0.18588 |
| ZIKV/Dakar 24 hpi_2 | IRF2 | 1064 | 9702.067847 | 0.109667 | 1.572524114 | 0.653082 |
| ZIKV/Dakar 48 hpi_2 | IRF2 | 1315 | 7275.616586 | 0.180741 | 1.869746744 | 0.902843 |
| ZIKV/Dakar 4 hpi_3 | IRF2 | 1028 | 10334.87659 | 0.099469 | 2.021890354 | 1.015705 |
| ZIKV/Dakar 8 hpi_3 | IRF2 | 536 | 10124.86039 | 0.052939 | 0.895172452 | -0.15976 |
| ZIKV/Dakar 10 hpi_3 | IRF2 | 549 | 8611.388976 | 0.063753 | 0.985948442 | -0.02042 |
| ZIKV/Dakar 24 hpi_3 | IRF2 | 1196 | 9356.243092 | 0.127829 | 1.832946023 | 0.874164 |
| ZIKV/Dakar 48 hpi_3 | IRF2 | 1456 | 7898.825141 | 0.184331 | 1.906890312 | 0.931222 |
| ZIKV/Dakar 4 hpi_1 | IFNL1 | 52 | 21745.79117 | 0.002391 | 1.193065647 | 0.254673 |
| ZIKV/Dakar 8 hpi_1 | IFNL1 | 33 | 17326.69644 | 0.001905 | 1.100556061 | 0.138233 |
| ZIKV/Dakar 10 hpi_1 | IFNL1 | 46 | 17513.91951 | 0.002626 | 1.439679806 | 0.525748 |
| ZIKV/Dakar 24 hpi_1 | IFNL1 | 314 | 12050.24737 | 0.026058 | 13.85213249 | 3.792036 |
| ZIKV/Dakar 48 hpi_1 | IFNL1 | 1657 | 14705.51891 | 0.112679 | 49.60845201 | 5.632514 |
| ZIKV/Dakar 4 hpi_2 | IFNL1 | 14 | 10431.40144 | 0.001342 | 0.66960947 | -0.57861 |

| | | | | | | |
|---|---|---|---|---|---|---|
| ZIKV/Dakar 8 hpi_2 | IFNL1 | 36 | 12658.05148 | 0.002844 | 1.643424056 | 0.716705 |
| ZIKV/Dakar 10 hpi_2 | IFNL1 | 24 | 13088.28841 | 0.001834 | 1.005124401 | 0.007374 |
| ZIKV/Dakar 24 hpi_2 | IFNL1 | 278 | 9702.067847 | 0.028654 | 15.23222828 | 3.929055 |
| ZIKV/Dakar 48 hpi_2 | IFNL1 | 1355 | 7275.616586 | 0.186239 | 81.99417713 | 6.35745 |
| ZIKV/Dakar 4 hpi_3 | IFNL1 | 22 | 10334.87659 | 0.002129 | 1.062071111 | 0.08688 |
| ZIKV/Dakar 8 hpi_3 | IFNL1 | 25 | 10124.86039 | 0.002469 | 1.426806114 | 0.512789 |
| ZIKV/Dakar 10 hpi_3 | IFNL1 | 16 | 8611.388976 | 0.001858 | 1.018446469 | 0.02637 |
| ZIKV/Dakar 24 hpi_3 | IFNL1 | 214 | 9356.243092 | 0.022872 | 12.15892634 | 3.603944 |
| ZIKV/Dakar 48 hpi_3 | IFNL1 | 589 | 7898.825141 | 0.074568 | 32.82965478 | 5.036928 |
| ZIKV/Dakar 4 hpi_1 | EIF2AK2 | 8933 | 21745.79117 | 0.410792 | 1.378523961 | 0.463124 |
| ZIKV/Dakar 8 hpi_1 | EIF2AK2 | 8231 | 17326.69644 | 0.475047 | 1.461202766 | 0.547156 |
| ZIKV/Dakar 10 hpi_1 | EIF2AK2 | 8201 | 17513.91951 | 0.468256 | 1.348501305 | 0.431357 |
| ZIKV/Dakar 24 hpi_1 | EIF2AK2 | 13861 | 12050.24737 | 1.150267 | 3.255992146 | 1.703097 |
| ZIKV/Dakar 48 hpi_1 | EIF2AK2 | 20424 | 14705.51891 | 1.388866 | 4.071596061 | 2.025594 |
| ZIKV/Dakar 4 hpi_2 | EIF2AK2 | 3742 | 10431.40144 | 0.358725 | 1.203797183 | 0.267592 |
| ZIKV/Dakar 8 hpi_2 | EIF2AK2 | 5581 | 12658.05148 | 0.440905 | 1.356184622 | 0.439554 |
| ZIKV/Dakar 10 hpi_2 | EIF2AK2 | 6222 | 13088.28841 | 0.475387 | 1.369036601 | 0.453161 |
| ZIKV/Dakar 24 hpi_2 | EIF2AK2 | 9365 | 9702.067847 | 0.965258 | 2.732298992 | 1.450115 |
| ZIKV/Dakar 48 hpi_2 | EIF2AK2 | 8459 | 7275.616586 | 1.162651 | 3.408422772 | 1.769104 |
| ZIKV/Dakar 4 hpi_3 | EIF2AK2 | 5569 | 10334.87659 | 0.538855 | 1.808273514 | 0.854613 |
| ZIKV/Dakar 8 hpi_3 | EIF2AK2 | 5379 | 10124.86039 | 0.531267 | 1.634128301 | 0.708521 |
| ZIKV/Dakar 10 hpi_3 | EIF2AK2 | 4467 | 8611.388976 | 0.518732 | 1.493862599 | 0.579047 |
| ZIKV/Dakar 24 hpi_3 | EIF2AK2 | 10797 | 9356.243092 | 1.153989 | 3.26652775 | 1.707758 |
| ZIKV/Dakar 48 hpi_3 | EIF2AK2 | 11490 | 7898.825141 | 1.454647 | 4.264437625 | 2.092355 |
| ZIKV/Dakar 4 hpi_1 | GBP2 | 606 | 21745.79117 | 0.027867 | 2.978537831 | 1.574604 |

| | | | | | | |
|---|---|---|---|---|---|---|
| ZIKV/Dakar 8 hpi_1 | GBP2 | 445 | 17326.69644 | 0.025683 | 3.07625533 | 1.621175 |
| ZIKV/Dakar 10 hpi_1 | GBP2 | 396 | 17513.91951 | 0.022611 | 2.374967371 | 1.247908 |
| ZIKV/Dakar 24 hpi_1 | GBP2 | 287 | 12050.24737 | 0.023817 | 1.719909294 | 0.782332 |
| ZIKV/Dakar 48 hpi_1 | GBP2 | 1418 | 14705.51891 | 0.096426 | 3.824503721 | 1.935273 |
| ZIKV/Dakar 4 hpi_2 | GBP2 | 242 | 10431.40144 | 0.023199 | 2.479581667 | 1.310097 |
| ZIKV/Dakar 8 hpi_2 | GBP2 | 227 | 12658.05148 | 0.017933 | 2.148014133 | 1.103003 |
| ZIKV/Dakar 10 hpi_2 | GBP2 | 258 | 13088.28841 | 0.019712 | 2.070535402 | 1.050004 |
| ZIKV/Dakar 24 hpi_2 | GBP2 | 190 | 9702.067847 | 0.019583 | 1.414193714 | 0.49998 |
| ZIKV/Dakar 48 hpi_2 | GBP2 | 734 | 7275.616586 | 0.100885 | 4.001340099 | 2.000483 |
| ZIKV/Dakar 4 hpi_3 | GBP2 | 174 | 10334.87659 | 0.016836 | 1.799490933 | 0.847589 |
| ZIKV/Dakar 8 hpi_3 | GBP2 | 191 | 10124.86039 | 0.018864 | 2.259552615 | 1.176037 |
| ZIKV/Dakar 10 hpi_3 | GBP2 | 158 | 8611.388976 | 0.018348 | 1.927212888 | 0.946516 |
| ZIKV/Dakar 24 hpi_3 | GBP2 | 148 | 9356.243092 | 0.015818 | 1.142299081 | 0.19194 |
| ZIKV/Dakar 48 hpi_3 | GBP2 | 555 | 7898.825141 | 0.070264 | 2.786824976 | 1.478622 |
| ZIKV/Dakar 4 hpi_1 | TNF | 29 | 21745.79117 | 0.001334 | 2.626004961 | 1.39287 |
| ZIKV/Dakar 8 hpi_1 | TNF | 11 | 17326.69644 | 0.000635 | 0.724978938 | -0.46399 |
| ZIKV/Dakar 10 hpi_1 | TNF | 22 | 17513.91951 | 0.001256 | 1.764354584 | 0.819141 |
| ZIKV/Dakar 24 hpi_1 | TNF | 33 | 12050.24737 | 0.002739 | 2.770610079 | 1.470204 |
| ZIKV/Dakar 48 hpi_1 | TNF | 85 | 14705.51891 | 0.00578 | 8.107353293 | 3.019231 |
| ZIKV/Dakar 4 hpi_2 | TNF | 21 | 10431.40144 | 0.002013 | 3.964143737 | 1.987009 |
| ZIKV/Dakar 8 hpi_2 | TNF | 14 | 12658.05148 | 0.001106 | 1.263018318 | 0.336876 |
| ZIKV/Dakar 10 hpi_2 | TNF | 6 | 13088.28841 | 0.000458 | 0.643894822 | -0.6351 |
| ZIKV/Dakar 24 hpi_2 | TNF | 23 | 9702.067847 | 0.002371 | 2.398396386 | 1.26207 |
| ZIKV/Dakar 48 hpi_2 | TNF | 49 | 7275.616586 | 0.006735 | 9.446410245 | 3.239766 |
| ZIKV/Dakar 4 hpi_3 | TNF | 9 | 10334.87659 | 0.000871 | 1.714786168 | 0.778029 |

| | | | | | | |
|---|---|---|---|---|---|---|
| ZIKV/Dakar 8 hpi_3 | TNF | 8 | 10124.86039 | 0.00079 | 0.902296795 | -0.14833 |
| ZIKV/Dakar 10 hpi_3 | TNF | 5 | 8611.388976 | 0.000581 | 0.815536375 | -0.29418 |
| ZIKV/Dakar 24 hpi_3 | TNF | 16 | 9356.243092 | 0.00171 | 1.730118771 | 0.790871 |
| ZIKV/Dakar 48 hpi_3 | TNF | 26 | 7898.825141 | 0.003292 | 4.616909641 | 2.206927 |
| ZIKV/Dakar 4 hpi_1 | RSAD2 | 81 | 21745.79117 | 0.003725 | 1.105577986 | 0.144801 |
| ZIKV/Dakar 8 hpi_1 | RSAD2 | 97 | 17326.69644 | 0.005598 | 1.7076161 | 0.771984 |
| ZIKV/Dakar 10 hpi_1 | RSAD2 | 80 | 17513.91951 | 0.004568 | 1.367353389 | 0.451386 |
| ZIKV/Dakar 24 hpi_1 | RSAD2 | 555 | 12050.24737 | 0.046057 | 13.47567209 | 3.752285 |
| ZIKV/Dakar 48 hpi_1 | RSAD2 | 1784 | 14705.51891 | 0.121315 | 30.2248216 | 4.917662 |
| ZIKV/Dakar 4 hpi_2 | RSAD2 | 28 | 10431.40144 | 0.002684 | 0.796700242 | -0.32789 |
| ZIKV/Dakar 8 hpi_2 | RSAD2 | 47 | 12658.05148 | 0.003713 | 1.132570574 | 0.179601 |
| ZIKV/Dakar 10 hpi_2 | RSAD2 | 68 | 13088.28841 | 0.005195 | 1.555249929 | 0.637146 |
| ZIKV/Dakar 24 hpi_2 | RSAD2 | 448 | 9702.067847 | 0.046176 | 13.51036619 | 3.755995 |
| ZIKV/Dakar 48 hpi_2 | RSAD2 | 1322 | 7275.616586 | 0.181703 | 45.27004236 | 5.500485 |
| ZIKV/Dakar 4 hpi_3 | RSAD2 | 113 | 10334.87659 | 0.010934 | 3.245284124 | 1.698345 |
| ZIKV/Dakar 8 hpi_3 | RSAD2 | 67 | 10124.86039 | 0.006617 | 2.018459465 | 1.013255 |
| ZIKV/Dakar 10 hpi_3 | RSAD2 | 57 | 8611.388976 | 0.006619 | 1.981416535 | 0.986532 |
| ZIKV/Dakar 24 hpi_3 | RSAD2 | 459 | 9356.243092 | 0.049058 | 14.35372437 | 3.843353 |
| ZIKV/Dakar 48 hpi_3 | RSAD2 | 1047 | 7898.825141 | 0.132551 | 33.02428563 | 5.045455 |
| ZIKV/Dakar 4 hpi_1 | DDX58 | 4019 | 21745.79117 | 0.184817 | 3.128346605 | 1.6454 |
| ZIKV/Dakar 8 hpi_1 | DDX58 | 2018 | 17326.69644 | 0.116468 | 1.74260934 | 0.801249 |
| ZIKV/Dakar 10 hpi_1 | DDX58 | 2324 | 17513.91951 | 0.132694 | 1.885657039 | 0.915067 |
| ZIKV/Dakar 24 hpi_1 | DDX58 | 14613 | 12050.24737 | 1.212672 | 16.88028066 | 4.077267 |
| ZIKV/Dakar 48 hpi_1 | DDX58 | 29089 | 14705.51891 | 1.978101 | 28.07256655 | 4.811089 |
| ZIKV/Dakar 4 hpi_2 | DDX58 | 1492 | 10431.40144 | 0.14303 | 2.421019212 | 1.275615 |

| | | | | | | |
|---|---|---|---|---|---|---|
| ZIKV/Dakar 8 hpi_2 | DDX58 | 916 | 12658.05148 | 0.072365 | 1.082737699 | 0.114684 |
| ZIKV/Dakar 10 hpi_2 | DDX58 | 1604 | 13088.28841 | 0.122552 | 1.741531925 | 0.800357 |
| ZIKV/Dakar 24 hpi_2 | DDX58 | 8430 | 9702.067847 | 0.868887 | 12.09482276 | 3.596318 |
| ZIKV/Dakar 48 hpi_2 | DDX58 | 12518 | 7275.616586 | 1.720541 | 24.41736668 | 4.609836 |
| ZIKV/Dakar 4 hpi_3 | DDX58 | 4380 | 10334.87659 | 0.423808 | 7.173661614 | 2.84271 |
| ZIKV/Dakar 8 hpi_3 | DDX58 | 1060 | 10124.86039 | 0.104693 | 1.566431702 | 0.647482 |
| ZIKV/Dakar 10 hpi_3 | DDX58 | 1102 | 8611.388976 | 0.12797 | 1.818520999 | 0.862766 |
| ZIKV/Dakar 24 hpi_3 | DDX58 | 10616 | 9356.243092 | 1.134643 | 15.79412803 | 3.981316 |
| ZIKV/Dakar 48 hpi_3 | DDX58 | 16250 | 7898.825141 | 2.057268 | 29.19608019 | 4.867703 |
| ZIKV/Dakar 4 hpi_1 | TRIM25 | 8274 | 21745.79117 | 0.380487 | 1.635475352 | 0.70971 |
| ZIKV/Dakar 8 hpi_1 | TRIM25 | 5341 | 17326.69644 | 0.308253 | 1.276937943 | 0.352688 |
| ZIKV/Dakar 10 hpi_1 | TRIM25 | 5108 | 17513.91951 | 0.291654 | 1.196503985 | 0.258825 |
| ZIKV/Dakar 24 hpi_1 | TRIM25 | 7919 | 12050.24737 | 0.657165 | 2.810253589 | 1.4907 |
| ZIKV/Dakar 48 hpi_1 | TRIM25 | 8648 | 14705.51891 | 0.588079 | 3.040932443 | 1.604514 |
| ZIKV/Dakar 4 hpi_2 | TRIM25 | 3289 | 10431.40144 | 0.315298 | 1.355267159 | 0.438577 |
| ZIKV/Dakar 8 hpi_2 | TRIM25 | 3801 | 12658.05148 | 0.300283 | 1.243924416 | 0.314899 |
| ZIKV/Dakar 10 hpi_2 | TRIM25 | 3879 | 13088.28841 | 0.296372 | 1.215859895 | 0.281977 |
| ZIKV/Dakar 24 hpi_2 | TRIM25 | 5584 | 9702.067847 | 0.575547 | 2.461230186 | 1.29938 |
| ZIKV/Dakar 48 hpi_2 | TRIM25 | 4196 | 7275.616586 | 0.576721 | 2.982202432 | 1.576378 |
| ZIKV/Dakar 4 hpi_3 | TRIM25 | 6009 | 10334.87659 | 0.581429 | 2.499197679 | 1.321465 |
| ZIKV/Dakar 8 hpi_3 | TRIM25 | 3288 | 10124.86039 | 0.324745 | 1.345258503 | 0.427883 |
| ZIKV/Dakar 10 hpi_3 | TRIM25 | 2391 | 8611.388976 | 0.277656 | 1.13907673 | 0.187865 |
| ZIKV/Dakar 24 hpi_3 | TRIM25 | 6167 | 9356.243092 | 0.659132 | 2.818665773 | 1.495012 |
| ZIKV/Dakar 48 hpi_3 | TRIM25 | 4846 | 7898.825141 | 0.613509 | 3.172432241 | 1.665589 |
| ZIKV/Dakar 4 hpi_1 | CCL2 | 11229 | 21745.79117 | 0.516376 | 4.54375704 | 2.183886 |

| | | | | | | |
|---|---|---|---|---|---|---|
| ZIKV/Dakar 8 hpi_1 | CCL2 | 2706 | 17326.69644 | 0.156175 | 1.095803222 | 0.131989 |
| ZIKV/Dakar 10 hpi_1 | CCL2 | 2488 | 17513.91951 | 0.142058 | 1.215756687 | 0.281855 |
| ZIKV/Dakar 24 hpi_1 | CCL2 | 856 | 12050.24737 | 0.071036 | 1.321503851 | 0.402181 |
| ZIKV/Dakar 48 hpi_1 | CCL2 | 2668 | 14705.51891 | 0.181428 | 6.233934493 | 2.640143 |
| ZIKV/Dakar 4 hpi_2 | CCL2 | 9608 | 10431.40144 | 0.921065 | 8.10474897 | 3.018768 |
| ZIKV/Dakar 8 hpi_2 | CCL2 | 2044 | 12658.05148 | 0.161478 | 1.133012187 | 0.180163 |
| ZIKV/Dakar 10 hpi_2 | CCL2 | 1842 | 13088.28841 | 0.140737 | 1.204443439 | 0.268367 |
| ZIKV/Dakar 24 hpi_2 | CCL2 | 883 | 9702.067847 | 0.091012 | 1.693117221 | 0.759682 |
| ZIKV/Dakar 48 hpi_2 | CCL2 | 1806 | 7275.616586 | 0.248226 | 8.529129424 | 3.092398 |
| ZIKV/Dakar 4 hpi_3 | CCL2 | 5880 | 10334.87659 | 0.568947 | 5.006350633 | 2.323759 |
| ZIKV/Dakar 8 hpi_3 | CCL2 | 1437 | 10124.86039 | 0.141928 | 0.995837031 | -0.00602 |
| ZIKV/Dakar 10 hpi_3 | CCL2 | 1143 | 8611.388976 | 0.132731 | 1.135932864 | 0.183878 |
| ZIKV/Dakar 24 hpi_3 | CCL2 | 689 | 9356.243092 | 0.073641 | 1.369961479 | 0.454135 |
| ZIKV/Dakar 48 hpi_3 | CCL2 | 1054 | 7898.825141 | 0.133438 | 4.584952852 | 2.196907 |
| ZIKV/Dakar 4 hpi_1 | CCL4 | 19 | 21745.79117 | 0.000874 | 1.223011194 | 0.290438 |
| ZIKV/Dakar 8 hpi_1 | CCL4 | 15 | 17326.69644 | 0.000866 | 1.466844739 | 0.552716 |
| ZIKV/Dakar 10 hpi_1 | CCL4 | 7 | 17513.91951 | 0.0004 | 0.532699776 | -0.90861 |
| ZIKV/Dakar 24 hpi_1 | CCL4 | 20 | 12050.24737 | 0.00166 | 1.651999124 | 0.724213 |
| ZIKV/Dakar 48 hpi_1 | CCL4 | 91 | 14705.51891 | 0.006188 | 6.438472512 | 2.686718 |
| ZIKV/Dakar 4 hpi_2 | CCL4 | 14 | 10431.40144 | 0.001342 | 1.878613423 | 0.909668 |
| ZIKV/Dakar 8 hpi_2 | CCL4 | 8 | 12658.05148 | 0.000632 | 1.070857751 | 0.098767 |
| ZIKV/Dakar 10 hpi_2 | CCL4 | 6 | 13088.28841 | 0.000458 | 0.610992977 | -0.71077 |
| ZIKV/Dakar 24 hpi_2 | CCL4 | 15 | 9702.067847 | 0.001546 | 1.538872828 | 0.621874 |
| ZIKV/Dakar 48 hpi_2 | CCL4 | 60 | 7275.616586 | 0.008247 | 8.580315426 | 3.101031 |
| ZIKV/Dakar 4 hpi_3 | CCL4 | 13 | 10334.87659 | 0.001258 | 1.760719206 | 0.816165 |

| | | | | | | |
|---|---|---|---|---|---|---|
| ZIKV/Dakar 8 hpi_3 | CCL4 | 6 | 10124.86039 | 0.000593 | 1.004085885 | 0.005883 |
| ZIKV/Dakar 10 hpi_3 | CCL4 | 10 | 8611.388976 | 0.001161 | 1.547727921 | 0.630152 |
| ZIKV/Dakar 24 hpi_3 | CCL4 | 6 | 9356.243092 | 0.000641 | 0.638301012 | -0.64769 |
| ZIKV/Dakar 48 hpi_3 | CCL4 | 33 | 7898.825141 | 0.004178 | 4.346835924 | 2.119966 |
| ZIKV/Dakar 4 hpi_1 | OAS1 | 5381 | 21745.79117 | 0.24745 | 1.801051811 | 0.84884 |
| ZIKV/Dakar 8 hpi_1 | OAS1 | 5952 | 17326.69644 | 0.343516 | 1.879013119 | 0.909975 |
| ZIKV/Dakar 10 hpi_1 | OAS1 | 5237 | 17513.91951 | 0.299019 | 1.671229186 | 0.74091 |
| ZIKV/Dakar 24 hpi_1 | OAS1 | 15519 | 12050.24737 | 1.287857 | 8.084203521 | 3.015106 |
| ZIKV/Dakar 48 hpi_1 | OAS1 | 34508 | 14705.51891 | 2.346602 | 12.28932157 | 3.619333 |
| ZIKV/Dakar 4 hpi_2 | OAS1 | 2364 | 10431.40144 | 0.226623 | 1.649465517 | 0.721999 |
| ZIKV/Dakar 8 hpi_2 | OAS1 | 3212 | 12658.05148 | 0.253752 | 1.388005974 | 0.473014 |
| ZIKV/Dakar 10 hpi_2 | OAS1 | 3735 | 13088.28841 | 0.28537 | 1.594940686 | 0.673503 |
| ZIKV/Dakar 24 hpi_2 | OAS1 | 10514 | 9702.067847 | 1.083687 | 6.80257178 | 2.76608 |
| ZIKV/Dakar 48 hpi_2 | OAS1 | 15163 | 7275.616586 | 2.084085 | 10.91449895 | 3.448174 |
| ZIKV/Dakar 4 hpi_3 | OAS1 | 4682 | 10334.87659 | 0.453029 | 3.297346154 | 1.721305 |
| ZIKV/Dakar 8 hpi_3 | OAS1 | 3828 | 10124.86039 | 0.378079 | 2.068071463 | 1.048286 |
| ZIKV/Dakar 10 hpi_3 | OAS1 | 3214 | 8611.388976 | 0.373227 | 2.085976698 | 1.060723 |
| ZIKV/Dakar 24 hpi_3 | OAS1 | 12434 | 9356.243092 | 1.328952 | 8.342166118 | 3.060422 |
| ZIKV/Dakar 48 hpi_3 | OAS1 | 21053 | 7898.825141 | 2.665333 | 13.95853897 | 3.803076 |
| ZIKV/Dakar 4 hpi_1 | ISG20 | 673 | 21745.79117 | 0.030949 | 1.176003761 | 0.233893 |
| ZIKV/Dakar 8 hpi_1 | ISG20 | 593 | 17326.69644 | 0.034225 | 1.434199337 | 0.520246 |
| ZIKV/Dakar 10 hpi_1 | ISG20 | 497 | 17513.91951 | 0.028377 | 1.179595197 | 0.238292 |
| ZIKV/Dakar 24 hpi_1 | ISG20 | 1577 | 12050.24737 | 0.130869 | 3.416407223 | 1.77248 |
| ZIKV/Dakar 48 hpi_1 | ISG20 | 7478 | 14705.51891 | 0.508517 | 9.973067849 | 3.318037 |
| ZIKV/Dakar 4 hpi_2 | ISG20 | 298 | 10431.40144 | 0.028568 | 1.085531586 | 0.118402 |

| | | | | | | |
|---|---|---|---|---|---|---|
| ZIKV/Dakar 8 hpi_2 | ISG20 | 359 | 12658.05148 | 0.028361 | 1.188497251 | 0.249139 |
| ZIKV/Dakar 10 hpi_2 | ISG20 | 356 | 13088.28841 | 0.0272 | 1.130647165 | 0.177149 |
| ZIKV/Dakar 24 hpi_2 | ISG20 | 1212 | 9702.067847 | 0.124922 | 3.261160797 | 1.705386 |
| ZIKV/Dakar 48 hpi_2 | ISG20 | 4152 | 7275.616586 | 0.570673 | 11.19209034 | 3.484408 |
| ZIKV/Dakar 4 hpi_3 | ISG20 | 485 | 10334.87659 | 0.046928 | 1.783221547 | 0.834486 |
| ZIKV/Dakar 8 hpi_3 | ISG20 | 420 | 10124.86039 | 0.041482 | 1.738324445 | 0.797697 |
| ZIKV/Dakar 10 hpi_3 | ISG20 | 364 | 8611.388976 | 0.04227 | 1.757066236 | 0.813169 |
| ZIKV/Dakar 24 hpi_3 | ISG20 | 1115 | 9356.243092 | 0.119172 | 3.111052004 | 1.637403 |
| ZIKV/Dakar 48 hpi_3 | ISG20 | 5065 | 7898.825141 | 0.641235 | 12.57594463 | 3.652595 |
| ZIKV/Dakar 4 hpi_1 | IRF7 | 155 | 21745.79117 | 0.007128 | 2.639569222 | 1.400303 |
| ZIKV/Dakar 8 hpi_1 | IRF7 | 105 | 17326.69644 | 0.00606 | 2.462965915 | 1.300397 |
| ZIKV/Dakar 10 hpi_1 | IRF7 | 134 | 17513.91951 | 0.007651 | 2.82053304 | 1.495968 |
| ZIKV/Dakar 24 hpi_1 | IRF7 | 635 | 12050.24737 | 0.052696 | 18.58233951 | 4.21586 |
| ZIKV/Dakar 48 hpi_1 | IRF7 | 1401 | 14705.51891 | 0.09527 | 22.5336408 | 4.494009 |
| ZIKV/Dakar 4 hpi_2 | IRF7 | 59 | 10431.40144 | 0.005656 | 2.094526809 | 1.066624 |
| ZIKV/Dakar 8 hpi_2 | IRF7 | 64 | 12658.05148 | 0.005056 | 2.054934511 | 1.039092 |
| ZIKV/Dakar 10 hpi_2 | IRF7 | 119 | 13088.28841 | 0.009092 | 3.351767207 | 1.744922 |
| ZIKV/Dakar 24 hpi_2 | IRF7 | 405 | 9702.067847 | 0.041744 | 14.72018756 | 3.879724 |
| ZIKV/Dakar 48 hpi_2 | IRF7 | 550 | 7275.616586 | 0.075595 | 17.87995703 | 4.160271 |
| ZIKV/Dakar 4 hpi_3 | IRF7 | 162 | 10334.87659 | 0.015675 | 5.804787023 | 2.537243 |
| ZIKV/Dakar 8 hpi_3 | IRF7 | 133 | 10124.86039 | 0.013136 | 5.338846897 | 2.416528 |
| ZIKV/Dakar 10 hpi_3 | IRF7 | 123 | 8611.388976 | 0.014283 | 5.265524615 | 2.396577 |
| ZIKV/Dakar 24 hpi_3 | IRF7 | 514 | 9356.243092 | 0.054937 | 19.37243667 | 4.275934 |
| ZIKV/Dakar 48 hpi_3 | IRF7 | 875 | 7898.825141 | 0.110776 | 26.20107673 | 4.711554 |
| ZIKV/Dakar 4 hpi_1 | ISG15 | 784 | 21745.79117 | 0.036053 | 2.387892388 | 1.255738 |

| | | | | | | |
|---|---|---|---|---|---|---|
| ZIKV/Dakar 8 hpi_1 | ISG15 | 1107 | 17326.69644 | 0.06389 | 4.964508712 | 2.311651 |
| ZIKV/Dakar 10 hpi_1 | ISG15 | 1192 | 17513.91951 | 0.06806 | 4.257988003 | 2.090172 |
| ZIKV/Dakar 24 hpi_1 | ISG15 | 11768 | 12050.24737 | 0.976577 | 62.01250068 | 5.954487 |
| ZIKV/Dakar 48 hpi_1 | ISG15 | 45102 | 14705.51891 | 3.067012 | 243.2579121 | 7.926343 |
| ZIKV/Dakar 4 hpi_2 | ISG15 | 203 | 10431.40144 | 0.01946 | 1.288923911 | 0.366167 |
| ZIKV/Dakar 8 hpi_2 | ISG15 | 416 | 12658.05148 | 0.032864 | 2.553705995 | 1.352592 |
| ZIKV/Dakar 10 hpi_2 | ISG15 | 729 | 13088.28841 | 0.055699 | 3.484626215 | 1.801004 |
| ZIKV/Dakar 24 hpi_2 | ISG15 | 6808 | 9702.067847 | 0.701706 | 44.55821526 | 5.47762 |
| ZIKV/Dakar 48 hpi_2 | ISG15 | 17721 | 7275.616586 | 2.43567 | 193.1834641 | 7.593828 |
| ZIKV/Dakar 4 hpi_3 | ISG15 | 1383 | 10334.87659 | 0.133819 | 8.863204838 | 3.147828 |
| ZIKV/Dakar 8 hpi_3 | ISG15 | 1253 | 10124.86039 | 0.123755 | 9.61626561 | 3.265477 |
| ZIKV/Dakar 10 hpi_3 | ISG15 | 1244 | 8611.388976 | 0.14446 | 9.037716235 | 3.175958 |
| ZIKV/Dakar 24 hpi_3 | ISG15 | 9638 | 9356.243092 | 1.030114 | 65.41208199 | 6.031485 |
| ZIKV/Dakar 48 hpi_3 | ISG15 | 27018 | 7898.825141 | 3.420509 | 271.2952723 | 8.08372 |
| ZIKV/Dakar 4 hpi_1 | IL6 | 1022 | 21745.79117 | 0.046998 | 2.984054263 | 1.577274 |
| ZIKV/Dakar 8 hpi_1 | IL6 | 158 | 17326.69644 | 0.009119 | 1.792982568 | 0.842361 |
| ZIKV/Dakar 10 hpi_1 | IL6 | 114 | 17513.91951 | 0.006509 | 1.8204796 | 0.864319 |
| ZIKV/Dakar 24 hpi_1 | IL6 | 290 | 12050.24737 | 0.024066 | 7.300306666 | 2.867957 |
| ZIKV/Dakar 48 hpi_1 | IL6 | 4762 | 14705.51891 | 0.323824 | 58.52157365 | 5.870897 |
| ZIKV/Dakar 4 hpi_2 | IL6 | 157 | 10431.40144 | 0.015051 | 0.955626154 | -0.06548 |
| ZIKV/Dakar 8 hpi_2 | IL6 | 25 | 12658.05148 | 0.001975 | 0.388336219 | -1.36462 |
| ZIKV/Dakar 10 hpi_2 | IL6 | 24 | 13088.28841 | 0.001834 | 0.512852764 | -0.96338 |
| ZIKV/Dakar 24 hpi_2 | IL6 | 114 | 9702.067847 | 0.01175 | 3.564344006 | 1.833637 |
| ZIKV/Dakar 48 hpi_2 | IL6 | 1645 | 7275.616586 | 0.226098 | 40.86044166 | 5.352633 |
| ZIKV/Dakar 4 hpi_3 | IL6 | 164 | 10334.87659 | 0.015869 | 1.007556912 | 0.010861 |

| | | | | | | |
|---|---|---|---|---|---|---|
| ZIKV/Dakar 8 hpi_3 | IL6 | 41 | 10124.86039 | 0.004049 | 0.796213543 | -0.32877 |
| ZIKV/Dakar 10 hpi_3 | IL6 | 37 | 8611.388976 | 0.004297 | 1.201691066 | 0.265066 |
| ZIKV/Dakar 24 hpi_3 | IL6 | 90 | 9356.243092 | 0.009619 | 2.917965017 | 1.544963 |
| ZIKV/Dakar 48 hpi_3 | IL6 | 906 | 7898.825141 | 0.114701 | 20.72872818 | 4.37356 |
| ZIKV/Dakar 4 hpi_1 | IFNL2 | 23 | 21745.79117 | 0.001058 | 1.584614492 | 0.664132 |
| ZIKV/Dakar 8 hpi_1 | IFNL2 | 57 | 17326.69644 | 0.00329 | 4.167866067 | 2.059309 |
| ZIKV/Dakar 10 hpi_1 | IFNL2 | 69 | 17513.91951 | 0.00394 | 5.891130006 | 2.558544 |
| ZIKV/Dakar 24 hpi_1 | IFNL2 | 2188 | 12050.24737 | 0.181573 | 172.2112232 | 7.428035 |
| ZIKV/Dakar 48 hpi_1 | IFNL2 | 12464 | 14705.51891 | 0.847573 | 638.3000806 | 9.318091 |
| ZIKV/Dakar 4 hpi_2 | IFNL2 | 6 | 10431.40144 | 0.000575 | 0.861746627 | -0.21466 |
| ZIKV/Dakar 8 hpi_2 | IFNL2 | 28 | 12658.05148 | 0.002212 | 2.802501408 | 1.486715 |
| ZIKV/Dakar 10 hpi_2 | IFNL2 | 46 | 13088.28841 | 0.003515 | 5.25542498 | 2.393807 |
| ZIKV/Dakar 24 hpi_2 | IFNL2 | 1920 | 9702.067847 | 0.197896 | 187.6925426 | 7.552228 |
| ZIKV/Dakar 48 hpi_2 | IFNL2 | 8828 | 7275.616586 | 1.213368 | 913.7772323 | 9.835699 |
| ZIKV/Dakar 4 hpi_3 | IFNL2 | 10 | 10334.87659 | 0.000968 | 1.449658497 | 0.535713 |
| ZIKV/Dakar 8 hpi_3 | IFNL2 | 27 | 10124.86039 | 0.002667 | 3.378542498 | 1.756401 |
| ZIKV/Dakar 10 hpi_3 | IFNL2 | 31 | 8611.388976 | 0.0036 | 5.382962482 | 2.4284 |
| ZIKV/Dakar 24 hpi_3 | IFNL2 | 1317 | 9356.243092 | 0.140762 | 133.5040296 | 7.060739 |
| ZIKV/Dakar 48 hpi_3 | IFNL2 | 3884 | 7898.825141 | 0.491719 | 370.3092277 | 8.532587 |
| ZIKV/Dakar 4 hpi_1 | IFNA2 | 13 | 21745.79117 | 0.000598 | 1.085384324 | 0.118206 |
| ZIKV/Dakar 8 hpi_1 | IFNA2 | 7 | 17326.69644 | 0.000404 | 0.58572273 | -0.77171 |
| ZIKV/Dakar 10 hpi_1 | IFNA2 | 17 | 17513.91951 | 0.000971 | 1.407425589 | 0.493059 |
| ZIKV/Dakar 24 hpi_1 | IFNA2 | 17 | 12050.24737 | 0.001411 | 2.216260437 | 1.148127 |
| ZIKV/Dakar 48 hpi_1 | IFNA2 | 48 | 14705.51891 | 0.003264 | 3.443868126 | 1.78403 |
| ZIKV/Dakar 4 hpi_2 | IFNA2 | 5 | 10431.40144 | 0.000479 | 0.870247434 | -0.2005 |

| | | | | | | |
|---|---|---|---|---|---|---|
| ZIKV/Dakar 8 hpi_2 | IFNA2 | 12 | 12658.05148 | 0.000948 | 1.37443496 | 0.458839 |
| ZIKV/Dakar 10 hpi_2 | IFNA2 | 10 | 13088.28841 | 0.000764 | 1.10783993 | 0.147749 |
| ZIKV/Dakar 24 hpi_2 | IFNA2 | 12 | 9702.067847 | 0.001237 | 1.943053567 | 0.958326 |
| ZIKV/Dakar 48 hpi_2 | IFNA2 | 23 | 7275.616586 | 0.003161 | 3.335367257 | 1.737846 |
| ZIKV/Dakar 4 hpi_3 | IFNA2 | 8 | 10334.87659 | 0.000774 | 1.40540048 | 0.490981 |
| ZIKV/Dakar 8 hpi_3 | IFNA2 | 6 | 10124.86039 | 0.000593 | 0.859155969 | -0.21901 |
| ZIKV/Dakar 10 hpi_3 | IFNA2 | 7 | 8611.388976 | 0.000813 | 1.178649576 | 0.237135 |
| ZIKV/Dakar 24 hpi_3 | IFNA2 | 12 | 9356.243092 | 0.001283 | 2.014872567 | 1.010689 |
| ZIKV/Dakar 48 hpi_3 | IFNA2 | 40 | 7898.825141 | 0.005064 | 5.342974739 | 2.417643 |
| ZIKV/Dakar 4 hpi_1 | POS_C | 3767 | 21745.79117 | 0.173229 | 0.93992416 | -0.08938 |
| ZIKV/Dakar 8 hpi_1 | POS_C | 3196 | 17326.69644 | 0.184455 | 0.769888578 | -0.37728 |
| ZIKV/Dakar 10 hpi_1 | POS_C | 3188 | 17513.91951 | 0.182027 | 0.797433229 | -0.32656 |
| ZIKV/Dakar 24 hpi_1 | POS_C | 3705 | 12050.24737 | 0.307463 | 1.159870464 | 0.213964 |
| ZIKV/Dakar 48 hpi_1 | POS_C | 4036 | 14705.51891 | 0.274455 | 0.987567996 | -0.01805 |
| ZIKV/Dakar 4 hpi_2 | POS_C | 2899 | 10431.40144 | 0.277911 | 1.507918823 | 0.592559 |
| ZIKV/Dakar 8 hpi_2 | POS_C | 3098 | 12658.05148 | 0.244745 | 1.021530713 | 0.030733 |
| ZIKV/Dakar 10 hpi_2 | POS_C | 2860 | 13088.28841 | 0.218516 | 0.95728784 | -0.06298 |
| ZIKV/Dakar 24 hpi_2 | POS_C | 2988 | 9702.067847 | 0.307976 | 1.161805759 | 0.216369 |
| ZIKV/Dakar 48 hpi_2 | POS_C | 3072 | 7275.616586 | 0.422232 | 1.519314248 | 0.60342 |
| ZIKV/Dakar 4 hpi_3 | POS_C | 2514 | 10334.87659 | 0.243254 | 1.319873728 | 0.4004 |
| ZIKV/Dakar 8 hpi_3 | POS_C | 3027 | 10124.86039 | 0.298967 | 1.247843871 | 0.319437 |
| ZIKV/Dakar 10 hpi_3 | POS_C | 2155 | 8611.388976 | 0.25025 | 1.096310146 | 0.132656 |
| ZIKV/Dakar 24 hpi_3 | POS_C | 2322 | 9356.243092 | 0.248177 | 0.936220093 | -0.09508 |
| ZIKV/Dakar 48 hpi_3 | POS_C | 2623 | 7898.825141 | 0.332075 | 1.194901192 | 0.256891 |
| ZIKV/Dakar 4 hpi_1 | POS_A | 44611 | 21745.79117 | 2.051477 | 0.926701344 | -0.10982 |

| | | | | | | |
|---|---|---|---|---|---|---|
| ZIKV/Dakar 8 hpi_1 | POS_A | 37496 | 17326.69644 | 2.164059 | 0.750358248 | -0.41435 |
| ZIKV/Dakar 10 hpi_1 | POS_A | 40200 | 17513.91951 | 2.295317 | 0.82679311 | -0.2744 |
| ZIKV/Dakar 24 hpi_1 | POS_A | 43750 | 12050.24737 | 3.630631 | 1.184079283 | 0.243766 |
| ZIKV/Dakar 48 hpi_1 | POS_A | 47320 | 14705.51891 | 3.21784 | 0.999451897 | -0.00079 |
| ZIKV/Dakar 4 hpi_2 | POS_A | 35817 | 10431.40144 | 3.433575 | 1.551027849 | 0.633225 |
| ZIKV/Dakar 8 hpi_2 | POS_A | 38556 | 12658.05148 | 3.045966 | 1.056147562 | 0.078811 |
| ZIKV/Dakar 10 hpi_2 | POS_A | 34176 | 13088.28841 | 2.611189 | 0.940573026 | -0.08839 |
| ZIKV/Dakar 24 hpi_2 | POS_A | 35195 | 9702.067847 | 3.627577 | 1.183083371 | 0.242552 |
| ZIKV/Dakar 48 hpi_2 | POS_A | 37432 | 7275.616586 | 5.144856 | 1.597977803 | 0.676247 |
| ZIKV/Dakar 4 hpi_3 | POS_A | 30676 | 10334.87659 | 2.968202 | 1.340807658 | 0.423102 |
| ZIKV/Dakar 8 hpi_3 | POS_A | 35520 | 10124.86039 | 3.508197 | 1.216419576 | 0.282641 |
| ZIKV/Dakar 10 hpi_3 | POS_A | 26230 | 8611.388976 | 3.045966 | 1.097183402 | 0.133805 |
| ZIKV/Dakar 24 hpi_3 | POS_A | 26644 | 9356.243092 | 2.847724 | 0.928745272 | -0.10665 |
| ZIKV/Dakar 48 hpi_3 | POS_A | 30064 | 7898.825141 | 3.806136 | 1.182175018 | 0.241444 |
| ZIKV/Dakar 4 hpi_1 | POS_F | 67 | 21745.79117 | 0.003081 | 0.827547958 | -0.27309 |
| ZIKV/Dakar 8 hpi_1 | POS_F | 56 | 17326.69644 | 0.003232 | 0.624046218 | -0.68028 |
| ZIKV/Dakar 10 hpi_1 | POS_F | 80 | 17513.91951 | 0.004568 | 0.935237881 | -0.09659 |
| ZIKV/Dakar 24 hpi_1 | POS_F | 111 | 12050.24737 | 0.009211 | 1.770928292 | 0.824506 |
| ZIKV/Dakar 48 hpi_1 | POS_F | 81 | 14705.51891 | 0.005508 | 0.921052256 | -0.11865 |
| ZIKV/Dakar 4 hpi_2 | POS_F | 59 | 10431.40144 | 0.005656 | 1.519157963 | 0.603272 |
| ZIKV/Dakar 8 hpi_2 | POS_F | 73 | 12658.05148 | 0.005767 | 1.113526348 | 0.155136 |
| ZIKV/Dakar 10 hpi_2 | POS_F | 62 | 13088.28841 | 0.004737 | 0.969894027 | -0.0441 |
| ZIKV/Dakar 24 hpi_2 | POS_F | 87 | 9702.067847 | 0.008967 | 1.723966828 | 0.785732 |
| ZIKV/Dakar 48 hpi_2 | POS_F | 64 | 7275.616586 | 0.008797 | 1.470922446 | 0.556721 |
| ZIKV/Dakar 4 hpi_3 | POS_F | 59 | 10334.87659 | 0.005709 | 1.533346472 | 0.616684 |

| | | | | | | |
|---|---|---|---|---|---|---|
| ZIKV/Dakar 8 hpi_3 | POS_F | 69 | 10124.86039 | 0.006815 | 1.315844417 | 0.395989 |
| ZIKV/Dakar 10 hpi_3 | POS_F | 46 | 8611.388976 | 0.005342 | 1.093704695 | 0.129223 |
| ZIKV/Dakar 24 hpi_3 | POS_F | 47 | 9356.243092 | 0.005023 | 0.965762462 | -0.05026 |
| ZIKV/Dakar 48 hpi_3 | POS_F | 69 | 7898.825141 | 0.008735 | 1.46071738 | 0.546677 |
| ZIKV/Dakar 4 hpi_1 | POS_D | 925 | 21745.79117 | 0.042537 | 0.938808776 | -0.0911 |
| ZIKV/Dakar 8 hpi_1 | POS_D | 799 | 17326.69644 | 0.046114 | 0.781354829 | -0.35595 |
| ZIKV/Dakar 10 hpi_1 | POS_D | 859 | 17513.91951 | 0.049047 | 0.840763084 | -0.25023 |
| ZIKV/Dakar 24 hpi_1 | POS_D | 892 | 12050.24737 | 0.074023 | 1.123849638 | 0.168449 |
| ZIKV/Dakar 48 hpi_1 | POS_D | 1020 | 14705.51891 | 0.069362 | 0.98692786 | -0.01898 |
| ZIKV/Dakar 4 hpi_2 | POS_D | 679 | 10431.40144 | 0.065092 | 1.4366062 | 0.522665 |
| ZIKV/Dakar 8 hpi_2 | POS_D | 750 | 12658.05148 | 0.059251 | 1.003949097 | 0.005686 |
| ZIKV/Dakar 10 hpi_2 | POS_D | 668 | 13088.28841 | 0.051038 | 0.874898005 | -0.19281 |
| ZIKV/Dakar 24 hpi_2 | POS_D | 744 | 9702.067847 | 0.076685 | 1.164254556 | 0.219407 |
| ZIKV/Dakar 48 hpi_2 | POS_D | 689 | 7275.616586 | 0.0947 | 1.347457291 | 0.43024 |
| ZIKV/Dakar 4 hpi_3 | POS_D | 667 | 10334.87659 | 0.064539 | 1.424397359 | 0.510352 |
| ZIKV/Dakar 8 hpi_3 | POS_D | 712 | 10124.86039 | 0.070322 | 1.191538935 | 0.252826 |
| ZIKV/Dakar 10 hpi_3 | POS_D | 569 | 8611.388976 | 0.066075 | 1.132668649 | 0.179726 |
| ZIKV/Dakar 24 hpi_3 | POS_D | 569 | 9356.243092 | 0.060815 | 0.923315417 | -0.1151 |
| ZIKV/Dakar 48 hpi_3 | POS_D | 589 | 7898.825141 | 0.074568 | 1.061007334 | 0.085435 |
| ZIKV/Dakar 4 hpi_1 | POS_B | 13619 | 21745.79117 | 0.626282 | 0.947929598 | -0.07715 |
| ZIKV/Dakar 8 hpi_1 | POS_B | 11568 | 17326.69644 | 0.66764 | 0.777322354 | -0.36342 |
| ZIKV/Dakar 10 hpi_1 | POS_B | 12286 | 17513.91951 | 0.701499 | 0.839758542 | -0.25195 |
| ZIKV/Dakar 24 hpi_1 | POS_B | 13657 | 12050.24737 | 1.133338 | 1.188622352 | 0.24929 |
| ZIKV/Dakar 48 hpi_1 | POS_B | 14434 | 14705.51891 | 0.981536 | 0.996030772 | -0.00574 |
| ZIKV/Dakar 4 hpi_2 | POS_B | 10478 | 10431.40144 | 1.004467 | 1.520343817 | 0.604398 |

| | | | | | | |
|---|---|---|---|---|---|---|
| ZIKV/Dakar 8 hpi_2 | POS_B | 11472 | 12658.05148 | 0.906301 | 1.055190627 | 0.077504 |
| ZIKV/Dakar 10 hpi_2 | POS_B | 10338 | 13088.28841 | 0.789866 | 0.945542252 | -0.08079 |
| ZIKV/Dakar 24 hpi_2 | POS_B | 10669 | 9702.067847 | 1.099662 | 1.153304413 | 0.205773 |
| ZIKV/Dakar 48 hpi_2 | POS_B | 10758 | 7275.616586 | 1.478638 | 1.50047286 | 0.585417 |
| ZIKV/Dakar 4 hpi_3 | POS_B | 8988 | 10334.87659 | 0.869677 | 1.31632717 | 0.396518 |
| ZIKV/Dakar 8 hpi_3 | POS_B | 10630 | 10124.86039 | 1.049891 | 1.222370513 | 0.289682 |
| ZIKV/Dakar 10 hpi_3 | POS_B | 8045 | 8611.388976 | 0.934228 | 1.118356099 | 0.16138 |
| ZIKV/Dakar 24 hpi_3 | POS_B | 8527 | 9356.243092 | 0.91137 | 0.955827039 | -0.06518 |
| ZIKV/Dakar 48 hpi_3 | POS_B | 9269 | 7898.825141 | 1.173466 | 1.190794421 | 0.251924 |
| ZIKV/Dakar 4 hpi_1 | POS_E | 143 | 21745.79117 | 0.006576 | 1.049230206 | 0.069331 |
| ZIKV/Dakar 8 hpi_1 | POS_E | 139 | 17326.69644 | 0.008022 | 0.944151662 | -0.08291 |
| ZIKV/Dakar 10 hpi_1 | POS_E | 116 | 17513.91951 | 0.006623 | 0.707690463 | -0.49881 |
| ZIKV/Dakar 24 hpi_1 | POS_E | 157 | 12050.24737 | 0.013029 | 1.360977405 | 0.444643 |
| ZIKV/Dakar 48 hpi_1 | POS_E | 200 | 14705.51891 | 0.0136 | 1.466836917 | 0.552708 |
| ZIKV/Dakar 4 hpi_2 | POS_E | 118 | 10431.40144 | 0.011312 | 1.804884058 | 0.851906 |
| ZIKV/Dakar 8 hpi_2 | POS_E | 118 | 12658.05148 | 0.009322 | 1.097129463 | 0.133734 |
| ZIKV/Dakar 10 hpi_2 | POS_E | 107 | 13088.28841 | 0.008175 | 0.873513507 | -0.1951 |
| ZIKV/Dakar 24 hpi_2 | POS_E | 122 | 9702.067847 | 0.012575 | 1.313538324 | 0.393458 |
| ZIKV/Dakar 48 hpi_2 | POS_E | 123 | 7275.616586 | 0.016906 | 1.823339318 | 0.866583 |
| ZIKV/Dakar 4 hpi_3 | POS_E | 88 | 10334.87659 | 0.008515 | 1.358586634 | 0.442107 |
| ZIKV/Dakar 8 hpi_3 | POS_E | 104 | 10124.86039 | 0.010272 | 1.208890665 | 0.273684 |
| ZIKV/Dakar 10 hpi_3 | POS_E | 80 | 8611.388976 | 0.00929 | 0.992625628 | -0.01068 |
| ZIKV/Dakar 24 hpi_3 | POS_E | 88 | 9356.243092 | 0.009405 | 0.982490591 | -0.02548 |
| ZIKV/Dakar 48 hpi_3 | POS_E | 72 | 7898.825141 | 0.009115 | 0.983110165 | -0.02458 |
| ZIKV/Dakar 4 hpi_1 | NEG_C | 16 | 21745.79117 | 0.000736 | 1.640135932 | 0.713815 |

| | | | | | | |
|---|---|---|---|---|---|---|
| ZIKV/Dakar 8 hpi_1 | NEG_C | 8 | 17326.69644 | 0.000462 | 0.771406341 | -0.37444 |
| ZIKV/Dakar 10 hpi_1 | NEG_C | 8 | 17513.91951 | 0.000457 | 0.536098322 | -0.89943 |
| ZIKV/Dakar 24 hpi_1 | NEG_C | 7 | 12050.24737 | 0.000581 | 1.193953745 | 0.255747 |
| ZIKV/Dakar 48 hpi_1 | NEG_C | 15 | 14705.51891 | 0.00102 | 2.383144245 | 1.252866 |
| ZIKV/Dakar 4 hpi_2 | NEG_C | 5 | 10431.40144 | 0.000479 | 1.068470213 | 0.095547 |
| ZIKV/Dakar 8 hpi_2 | NEG_C | 6 | 12658.05148 | 0.000474 | 0.791942001 | -0.33653 |
| ZIKV/Dakar 10 hpi_2 | NEG_C | 5 | 13088.28841 | 0.000382 | 0.448358036 | -1.15728 |
| ZIKV/Dakar 24 hpi_2 | NEG_C | 12 | 9702.067847 | 0.001237 | 2.542156969 | 1.346053 |
| ZIKV/Dakar 48 hpi_2 | NEG_C | 10 | 7275.616586 | 0.001374 | 3.211216748 | 1.68312 |
| ZIKV/Dakar 4 hpi_3 | NEG_C | 8 | 10334.87659 | 0.000774 | 1.725519079 | 0.78703 |
| ZIKV/Dakar 8 hpi_3 | NEG_C | 9 | 10124.86039 | 0.000889 | 1.485123088 | 0.570583 |
| ZIKV/Dakar 10 hpi_3 | NEG_C | 2 | 8611.388976 | 0.000232 | 0.272580384 | -1.87525 |
| ZIKV/Dakar 24 hpi_3 | NEG_C | 2 | 9356.243092 | 0.000214 | 0.439353331 | -1.18655 |
| ZIKV/Dakar 48 hpi_3 | NEG_C | 13 | 7898.825141 | 0.001646 | 3.845211895 | 1.943063 |
| ZIKV/Dakar 4 hpi_1 | NEG_D | 11 | 21745.79117 | 0.000506 | 1.364122661 | 0.447973 |
| ZIKV/Dakar 8 hpi_1 | NEG_D | 7 | 17326.69644 | 0.000404 | 0.728589297 | -0.45682 |
| ZIKV/Dakar 10 hpi_1 | NEG_D | 6 | 17513.91951 | 0.000343 | 1.010342076 | 0.014844 |
| ZIKV/Dakar 24 hpi_1 | NEG_D | 7 | 12050.24737 | 0.000581 | 1.231974197 | 0.300972 |
| ZIKV/Dakar 48 hpi_1 | NEG_D | 29 | 14705.51891 | 0.001972 | 2.903936354 | 1.53801 |
| ZIKV/Dakar 4 hpi_2 | NEG_D | 1 | 10431.40144 | 9.59E-05 | 0.258519491 | -1.95166 |
| ZIKV/Dakar 8 hpi_2 | NEG_D | 5 | 12658.05148 | 0.000395 | 0.712366783 | -0.48931 |
| ZIKV/Dakar 10 hpi_2 | NEG_D | 1 | 13088.28841 | 7.64E-05 | 0.225329308 | -2.14989 |
| ZIKV/Dakar 24 hpi_2 | NEG_D | 5 | 9702.067847 | 0.000515 | 1.092962424 | 0.128244 |
| ZIKV/Dakar 48 hpi_2 | NEG_D | 16 | 7275.616586 | 0.002199 | 3.238319 | 1.695245 |
| ZIKV/Dakar 4 hpi_3 | NEG_D | 4 | 10334.87659 | 0.000387 | 1.043735962 | 0.061757 |

| | | | | | | |
|---|---|---|---|---|---|---|
| ZIKV/Dakar 8 hpi_3 | NEG_D | 8 | 10124.86039 | 0.00079 | 1.424956009 | 0.510917 |
| ZIKV/Dakar 10 hpi_3 | NEG_D | 4 | 8611.388976 | 0.000465 | 1.369895135 | 0.454065 |
| ZIKV/Dakar 24 hpi_3 | NEG_D | 9 | 9356.243092 | 0.000962 | 2.040048755 | 1.028604 |
| ZIKV/Dakar 48 hpi_3 | NEG_D | 13 | 7898.825141 | 0.001646 | 2.423540614 | 1.277116 |
| ZIKV/Dakar 4 hpi_1 | NEG_E | 13 | 21745.79117 | 0.000598 | 0.470202943 | -1.08864 |
| ZIKV/Dakar 8 hpi_1 | NEG_E | 11 | 17326.69644 | 0.000635 | 0.57395913 | -0.80098 |
| ZIKV/Dakar 10 hpi_1 | NEG_E | 10 | 17513.91951 | 0.000571 | 0.458167751 | -1.12605 |
| ZIKV/Dakar 24 hpi_1 | NEG_E | 8 | 12050.24737 | 0.000664 | 0.492614963 | -1.02147 |
| ZIKV/Dakar 48 hpi_1 | NEG_E | 21 | 14705.51891 | 0.001428 | 1.181338947 | 0.240423 |
| ZIKV/Dakar 4 hpi_2 | NEG_E | 14 | 10431.40144 | 0.001342 | 1.055607775 | 0.078074 |
| ZIKV/Dakar 8 hpi_2 | NEG_E | 12 | 12658.05148 | 0.000948 | 0.857074233 | -0.22251 |
| ZIKV/Dakar 10 hpi_2 | NEG_E | 19 | 13088.28841 | 0.001452 | 1.164873087 | 0.220173 |
| ZIKV/Dakar 24 hpi_2 | NEG_E | 13 | 9702.067847 | 0.00134 | 0.994243178 | -0.00833 |
| ZIKV/Dakar 48 hpi_2 | NEG_E | 12 | 7275.616586 | 0.001649 | 1.36441669 | 0.448284 |
| ZIKV/Dakar 4 hpi_3 | NEG_E | 13 | 10334.87659 | 0.001258 | 0.98936208 | -0.01543 |
| ZIKV/Dakar 8 hpi_3 | NEG_E | 16 | 10124.86039 | 0.00158 | 1.428680079 | 0.514683 |
| ZIKV/Dakar 10 hpi_3 | NEG_E | 12 | 8611.388976 | 0.001394 | 1.118190778 | 0.161166 |
| ZIKV/Dakar 24 hpi_3 | NEG_E | 10 | 9356.243092 | 0.001069 | 0.793071015 | -0.33448 |
| ZIKV/Dakar 48 hpi_3 | NEG_E | 11 | 7898.825141 | 0.001393 | 1.152035247 | 0.204185 |
| ZIKV/Dakar 4 hpi_1 | NEG_A | 17 | 21745.79117 | 0.000782 | 1.304036324 | 0.382984 |
| ZIKV/Dakar 8 hpi_1 | NEG_A | 16 | 17326.69644 | 0.000923 | 1.044678781 | 0.063059 |
| ZIKV/Dakar 10 hpi_1 | NEG_A | 12 | 17513.91951 | 0.000685 | 0.880875046 | -0.18299 |
| ZIKV/Dakar 24 hpi_1 | NEG_A | 14 | 12050.24737 | 0.001162 | 1.404179991 | 0.489728 |
| ZIKV/Dakar 48 hpi_1 | NEG_A | 21 | 14705.51891 | 0.001428 | 1.37898433 | 0.463606 |
| ZIKV/Dakar 4 hpi_2 | NEG_A | 10 | 10431.40144 | 0.000959 | 1.599091525 | 0.677253 |

| | | | | | | |
|---|---|---|---|---|---|---|
| ZIKV/Dakar 8 hpi_2 | NEG_A | 15 | 12658.05148 | 0.001185 | 1.340611558 | 0.422891 |
| ZIKV/Dakar 10 hpi_2 | NEG_A | 7 | 13088.28841 | 0.000535 | 0.687593233 | -0.54037 |
| ZIKV/Dakar 24 hpi_2 | NEG_A | 13 | 9702.067847 | 0.00134 | 1.619458234 | 0.695511 |
| ZIKV/Dakar 48 hpi_2 | NEG_A | 17 | 7275.616586 | 0.002337 | 2.25631384 | 1.173968 |
| ZIKV/Dakar 4 hpi_3 | NEG_A | 3 | 10334.87659 | 0.00029 | 0.484207977 | -1.0463 |
| ZIKV/Dakar 8 hpi_3 | NEG_A | 13 | 10124.86039 | 0.001284 | 1.452555939 | 0.538594 |
| ZIKV/Dakar 10 hpi_3 | NEG_A | 9 | 8611.388976 | 0.001045 | 1.343648629 | 0.426156 |
| ZIKV/Dakar 24 hpi_3 | NEG_A | 8 | 9356.243092 | 0.000855 | 1.033425555 | 0.047434 |
| ZIKV/Dakar 48 hpi_3 | NEG_A | 16 | 7898.825141 | 0.002026 | 1.956040637 | 0.967936 |
| ZIKV/Dakar 4 hpi_1 | NEG_H | 11 | 21745.79117 | 0.000506 | 1.694324616 | 0.76071 |
| ZIKV/Dakar 8 hpi_1 | NEG_H | 3 | 17326.69644 | 0.000173 | 1.68399739 | 0.75189 |
| ZIKV/Dakar 10 hpi_1 | NEG_H | 7 | 17513.91951 | 0.0004 | 4.314314926 | 2.109131 |
| ZIKV/Dakar 24 hpi_1 | NEG_H | 6 | 12050.24737 | 0.000498 | 1.850756671 | 0.888115 |
| ZIKV/Dakar 48 hpi_1 | NEG_H | 15 | 14705.51891 | 0.00102 | 5.548766541 | 2.472167 |
| ZIKV/Dakar 4 hpi_2 | NEG_H | 3 | 10431.40144 | 0.000288 | 0.963291536 | -0.05396 |
| ZIKV/Dakar 8 hpi_2 | NEG_H | 0.039552527 | 12658.05148 | 3.12E-06 | 0.030390882 | -5.04022 |
| ZIKV/Dakar 10 hpi_2 | NEG_H | 3 | 13088.28841 | 0.000229 | 2.474204266 | 1.306965 |
| ZIKV/Dakar 24 hpi_2 | NEG_H | 4 | 9702.067847 | 0.000412 | 1.532462018 | 0.615851 |
| ZIKV/Dakar 48 hpi_2 | NEG_H | 4 | 7275.616586 | 0.00055 | 2.990719859 | 1.580493 |
| ZIKV/Dakar 4 hpi_3 | NEG_H | 4 | 10334.87659 | 0.000387 | 1.296384544 | 0.374494 |
| ZIKV/Dakar 8 hpi_3 | NEG_H | 6 | 10124.86039 | 0.000593 | 5.763657068 | 2.526984 |
| ZIKV/Dakar 10 hpi_3 | NEG_H | 2 | 8611.388976 | 0.000232 | 2.506997737 | 1.325961 |
| ZIKV/Dakar 24 hpi_3 | NEG_H | 8 | 9356.243092 | 0.000855 | 3.178209529 | 1.668214 |
| ZIKV/Dakar 48 hpi_3 | NEG_H | 7 | 7898.825141 | 0.000886 | 4.820821905 | 2.269279 |
| ZIKV/Dakar 4 hpi_1 | NEG_G | 11 | 21745.79117 | 0.000506 | 0.943907997 | -0.08328 |

| | | | | | | |
|---|---|---|---|---|---|---|
| ZIKV/Dakar 8 hpi_1 | NEG_G | 9 | 17326.69644 | 0.000519 | 1.746720517 | 0.804649 |
| ZIKV/Dakar 10 hpi_1 | NEG_G | 9 | 17513.91951 | 0.000514 | 1.70671581 | 0.771223 |
| ZIKV/Dakar 24 hpi_1 | NEG_G | 9 | 12050.24737 | 0.000747 | 1.589185303 | 0.668287 |
| ZIKV/Dakar 48 hpi_1 | NEG_G | 18 | 14705.51891 | 0.001224 | 2.168424149 | 1.116647 |
| ZIKV/Dakar 4 hpi_2 | NEG_G | 4 | 10431.40144 | 0.000383 | 0.715532766 | -0.48291 |
| ZIKV/Dakar 8 hpi_2 | NEG_G | 8 | 12658.05148 | 0.000632 | 2.125297876 | 1.087665 |
| ZIKV/Dakar 10 hpi_2 | NEG_G | 6 | 13088.28841 | 0.000458 | 1.52254608 | 0.606486 |
| ZIKV/Dakar 24 hpi_2 | NEG_G | 4 | 9702.067847 | 0.000412 | 0.877250606 | -0.18894 |
| ZIKV/Dakar 48 hpi_2 | NEG_G | 6 | 7275.616586 | 0.000825 | 1.460943868 | 0.546901 |
| ZIKV/Dakar 4 hpi_3 | NEG_G | 4 | 10334.87659 | 0.000387 | 0.722215641 | -0.4695 |
| ZIKV/Dakar 8 hpi_3 | NEG_G | 5 | 10124.86039 | 0.000494 | 1.660648202 | 0.731746 |
| ZIKV/Dakar 10 hpi_3 | NEG_G | 3 | 8611.388976 | 0.000348 | 1.157044599 | 0.210444 |
| ZIKV/Dakar 24 hpi_3 | NEG_G | 6 | 9356.243092 | 0.000641 | 1.364513216 | 0.448386 |
| ZIKV/Dakar 48 hpi_3 | NEG_G | 5 | 7898.825141 | 0.000633 | 1.121397513 | 0.165298 |
| ZIKV/Dakar 4 hpi_1 | NEG_F | 25 | 21745.79117 | 0.00115 | 1.056454827 | 0.079231 |
| ZIKV/Dakar 8 hpi_1 | NEG_F | 26 | 17326.69644 | 0.001501 | 0.883390361 | -0.17888 |
| ZIKV/Dakar 10 hpi_1 | NEG_F | 37 | 17513.91951 | 0.002113 | 1.267436667 | 0.341914 |
| ZIKV/Dakar 24 hpi_1 | NEG_F | 25 | 12050.24737 | 0.002075 | 1.544359554 | 0.627009 |
| ZIKV/Dakar 48 hpi_1 | NEG_F | 50 | 14705.51891 | 0.0034 | 1.831731049 | 0.873208 |
| ZIKV/Dakar 4 hpi_2 | NEG_F | 17 | 10431.40144 | 0.00163 | 1.497588163 | 0.582641 |
| ZIKV/Dakar 8 hpi_2 | NEG_F | 25 | 12658.05148 | 0.001975 | 1.162701482 | 0.217481 |
| ZIKV/Dakar 10 hpi_2 | NEG_F | 29 | 13088.28841 | 0.002216 | 1.32930009 | 0.410667 |
| ZIKV/Dakar 24 hpi_2 | NEG_F | 23 | 9702.067847 | 0.002371 | 1.764687875 | 0.819413 |
| ZIKV/Dakar 48 hpi_2 | NEG_F | 19 | 7275.616586 | 0.002611 | 1.406876104 | 0.492495 |
| ZIKV/Dakar 4 hpi_3 | NEG_F | 16 | 10334.87659 | 0.001548 | 1.422659027 | 0.50859 |

| | | | | | | |
|---|---|---|---|---|---|---|
| ZIKV/Dakar 8 hpi_3 | NEG_F | 27 | 10124.86039 | 0.002667 | 1.569892069 | 0.650665 |
| ZIKV/Dakar 10 hpi_3 | NEG_F | 24 | 8611.388976 | 0.002787 | 1.672037169 | 0.741607 |
| ZIKV/Dakar 24 hpi_3 | NEG_F | 18 | 9356.243092 | 0.001924 | 1.432106715 | 0.518139 |
| ZIKV/Dakar 48 hpi_3 | NEG_F | 20 | 7898.825141 | 0.002532 | 1.364079093 | 0.447927 |
| ZIKV/Dakar 4 hpi_1 | NEG_B | 11 | 21745.79117 | 0.000506 | 0.948395082 | -0.07644 |
| ZIKV/Dakar 8 hpi_1 | NEG_B | 13 | 17326.69644 | 0.00075 | 0.754486805 | -0.40643 |
| ZIKV/Dakar 10 hpi_1 | NEG_B | 15 | 17513.91951 | 0.000856 | 1.120676406 | 0.16437 |
| ZIKV/Dakar 24 hpi_1 | NEG_B | 12 | 12050.24737 | 0.000996 | 1.787458862 | 0.83791 |
| ZIKV/Dakar 48 hpi_1 | NEG_B | 29 | 14705.51891 | 0.001972 | 1.901219178 | 0.926925 |
| ZIKV/Dakar 4 hpi_2 | NEG_B | 6 | 10431.40144 | 0.000575 | 1.078401325 | 0.108894 |
| ZIKV/Dakar 8 hpi_2 | NEG_B | 6 | 12658.05148 | 0.000474 | 0.476659723 | -1.06897 |
| ZIKV/Dakar 10 hpi_2 | NEG_B | 4 | 13088.28841 | 0.000306 | 0.399898204 | -1.3223 |
| ZIKV/Dakar 24 hpi_2 | NEG_B | 7 | 9702.067847 | 0.000721 | 1.295043941 | 0.373001 |
| ZIKV/Dakar 48 hpi_2 | NEG_B | 11 | 7275.616586 | 0.001512 | 1.457596857 | 0.543592 |
| ZIKV/Dakar 4 hpi_3 | NEG_B | 10 | 10334.87659 | 0.000968 | 1.81412215 | 0.859272 |
| ZIKV/Dakar 8 hpi_3 | NEG_B | 9 | 10124.86039 | 0.000889 | 0.893876519 | -0.16185 |
| ZIKV/Dakar 10 hpi_3 | NEG_B | 8 | 8611.388976 | 0.000929 | 1.215595544 | 0.281663 |
| ZIKV/Dakar 24 hpi_3 | NEG_B | 6 | 9356.243092 | 0.000641 | 1.151066793 | 0.202972 |
| ZIKV/Dakar 48 hpi_3 | NEG_B | 16 | 7898.825141 | 0.002026 | | |
| ZIKV/Dakar 4 hpi_1 | ACTB | 163101 | 21745.79117 | 7.500348 | 0.874346728 | -0.19372 |
| ZIKV/Dakar 8 hpi_1 | ACTB | 134828 | 17326.69644 | 7.781518 | 0.870903776 | -0.19941 |
| ZIKV/Dakar 10 hpi_1 | ACTB | 139078 | 17513.91951 | 7.940998 | 0.905234431 | -0.14364 |
| ZIKV/Dakar 24 hpi_1 | ACTB | 92021 | 12050.24737 | 7.636441 | 0.961114493 | -0.05722 |
| ZIKV/Dakar 48 hpi_1 | ACTB | 96426 | 14705.51891 | 6.55713 | 0.856437629 | -0.22358 |
| ZIKV/Dakar 4 hpi_2 | ACTB | 93725 | 10431.40144 | 8.984891 | 1.047406028 | 0.066821 |

| | | | | | | |
|---|---|---|---|---|---|---|
| ZIKV/Dakar 8 hpi_2 | ACTB | 115679 | 12658.05148 | 9.138768 | 1.022806587 | 0.032533 |
| ZIKV/Dakar 10 hpi_2 | ACTB | 114617 | 13088.28841 | 8.757218 | 0.998279511 | -0.00248 |
| ZIKV/Dakar 24 hpi_2 | ACTB | 78941 | 9702.067847 | 8.136513 | 1.024053053 | 0.03429 |
| ZIKV/Dakar 48 hpi_2 | ACTB | 55692 | 7275.616586 | 7.654609 | 0.99978117 | -0.00032 |
| ZIKV/Dakar 4 hpi_3 | ACTB | 94353 | 10334.87659 | 9.129572 | 1.064272148 | 0.089867 |
| ZIKV/Dakar 8 hpi_3 | ACTB | 94177 | 10124.86039 | 9.30156 | 1.041026192 | 0.058006 |
| ZIKV/Dakar 10 hpi_3 | ACTB | 80525 | 8611.388976 | 9.350989 | 1.065966371 | 0.092162 |
| ZIKV/Dakar 24 hpi_3 | ACTB | 75079 | 9356.243092 | 8.024482 | 1.009952905 | 0.014288 |
| ZIKV/Dakar 48 hpi_3 | ACTB | 55348 | 7898.825141 | 7.007118 | 0.915211303 | -0.12782 |
| ZIKV/Dakar 4 hpi_1 | GADPH | 277453 | 21745.79117 | 12.75893 | 1.052472648 | 0.073783 |
| ZIKV/Dakar 8 hpi_1 | GADPH | 235337 | 17326.69644 | 13.58234 | 1.111798387 | 0.152895 |
| ZIKV/Dakar 10 hpi_1 | GADPH | 233929 | 17513.91951 | 13.35675 | 1.048807002 | 0.068749 |
| ZIKV/Dakar 24 hpi_1 | GADPH | 172132 | 12050.24737 | 14.28452 | 1.006897691 | 0.009917 |
| ZIKV/Dakar 48 hpi_1 | GADPH | 219591 | 14705.51891 | 14.93256 | 1.006906686 | 0.00993 |
| ZIKV/Dakar 4 hpi_2 | GADPH | 119770 | 10431.40144 | 11.48168 | 0.947113435 | -0.07839 |
| ZIKV/Dakar 8 hpi_2 | GADPH | 147936 | 12658.05148 | 11.68711 | 0.956662185 | -0.06392 |
| ZIKV/Dakar 10 hpi_2 | GADPH | 154785 | 13088.28841 | 11.82622 | 0.928626084 | -0.10683 |
| ZIKV/Dakar 24 hpi_2 | GADPH | 128796 | 9702.067847 | 13.27511 | 0.935745528 | -0.09581 |
| ZIKV/Dakar 48 hpi_2 | GADPH | 99026 | 7275.616586 | 13.61067 | 0.917771304 | -0.12379 |
| ZIKV/Dakar 4 hpi_3 | GADPH | 115383 | 10334.87659 | 11.16443 | 0.92094382 | -0.11881 |
| ZIKV/Dakar 8 hpi_3 | GADPH | 120482 | 10124.86039 | 11.89962 | 0.974057777 | -0.03792 |
| ZIKV/Dakar 10 hpi_3 | GADPH | 102861 | 8611.388976 | 11.94476 | 0.937934258 | -0.09244 |
| ZIKV/Dakar 24 hpi_3 | GADPH | 115174 | 9356.243092 | 12.30986 | 0.86770609 | -0.20472 |
| ZIKV/Dakar 48 hpi_3 | GADPH | 98926 | 7898.825141 | 12.52414 | 0.84450649 | -0.24382 |
| ZIKV/Dakar 4 hpi_1 | HPRT1 | 15701 | 21745.79117 | 0.722025 | 0.969962977 | -0.044 |

| | | | | | | |
|---|---|---|---|---|---|---|
| ZIKV/Dakar 8 hpi_1 | HPRT1 | 13300 | 17326.69644 | 0.767602 | 1.074123922 | 0.10316 |
| ZIKV/Dakar 10 hpi_1 | HPRT1 | 12974 | 17513.91951 | 0.740782 | 1.030164958 | 0.042875 |
| ZIKV/Dakar 24 hpi_1 | HPRT1 | 9356 | 12050.24737 | 0.776416 | 0.992818304 | -0.0104 |
| ZIKV/Dakar 48 hpi_1 | HPRT1 | 11349 | 14705.51891 | 0.771751 | 1.00664558 | 0.009556 |
| ZIKV/Dakar 4 hpi_2 | HPRT1 | 7558 | 10431.40144 | 0.724543 | 0.973346084 | -0.03898 |
| ZIKV/Dakar 8 hpi_2 | HPRT1 | 8829 | 12658.05148 | 0.697501 | 0.976030016 | -0.035 |
| ZIKV/Dakar 10 hpi_2 | HPRT1 | 9556 | 13088.28841 | 0.730118 | 1.015335366 | 0.021956 |
| ZIKV/Dakar 24 hpi_2 | HPRT1 | 7120 | 9702.067847 | 0.733864 | 0.93840694 | -0.09171 |
| ZIKV/Dakar 48 hpi_2 | HPRT1 | 4836 | 7275.616586 | 0.664686 | 0.86699349 | -0.20591 |
| ZIKV/Dakar 4 hpi_3 | HPRT1 | 7113 | 10334.87659 | 0.688252 | 0.924592935 | -0.11311 |
| ZIKV/Dakar 8 hpi_3 | HPRT1 | 7129 | 10124.86039 | 0.704108 | 0.985276412 | -0.0214 |
| ZIKV/Dakar 10 hpi_3 | HPRT1 | 6206 | 8611.388976 | 0.720674 | 1.002200912 | 0.003172 |
| ZIKV/Dakar 24 hpi_3 | HPRT1 | 7221 | 9356.243092 | 0.771784 | 0.986895964 | -0.01903 |
| ZIKV/Dakar 48 hpi_3 | HPRT1 | 5967 | 7898.825141 | 0.755429 | 0.985355368 | -0.02128 |
| ZIKV/Dakar 4 hpi_1 | ABCF1 | 4885 | 21745.79117 | 0.224641 | 1.06021454 | 0.084356 |
| ZIKV/Dakar 8 hpi_1 | ABCF1 | 3565 | 17326.69644 | 0.205752 | 1.019643005 | 0.028064 |
| ZIKV/Dakar 10 hpi_1 | ABCF1 | 3495 | 17513.91951 | 0.199556 | 1.000402724 | 0.000581 |
| ZIKV/Dakar 24 hpi_1 | ABCF1 | 2218 | 12050.24737 | 0.184063 | 1.028431589 | 0.040446 |
| ZIKV/Dakar 48 hpi_1 | ABCF1 | 2765 | 14705.51891 | 0.188025 | 1.227893986 | 0.296186 |
| ZIKV/Dakar 4 hpi_2 | ABCF1 | 2226 | 10431.40144 | 0.213394 | 1.007133176 | 0.010254 |
| ZIKV/Dakar 8 hpi_2 | ABCF1 | 2652 | 12658.05148 | 0.209511 | 1.038271753 | 0.054184 |
| ZIKV/Dakar 10 hpi_2 | ABCF1 | 2604 | 13088.28841 | 0.198956 | 0.997399529 | -0.00376 |
| ZIKV/Dakar 24 hpi_2 | ABCF1 | 1876 | 9702.067847 | 0.193361 | 1.080384525 | 0.111545 |
| ZIKV/Dakar 48 hpi_2 | ABCF1 | 1400 | 7275.616586 | 0.192424 | 1.256621025 | 0.32955 |
| ZIKV/Dakar 4 hpi_3 | ABCF1 | 2259 | 10334.87659 | 0.21858 | 1.031609509 | 0.044897 |

| | | | | | | |
|---|---|---|---|---|---|---|
| ZIKV/Dakar 8 hpi_3 | ABCF1 | 2125 | 10124.86039 | 0.209879 | 1.040098015 | 0.056719 |
| ZIKV/Dakar 10 hpi_3 | ABCF1 | 1706 | 8611.388976 | 0.19811 | 0.993154593 | -0.00991 |
| ZIKV/Dakar 24 hpi_3 | ABCF1 | 1783 | 9356.243092 | 0.190568 | 1.064779484 | 0.090555 |
| ZIKV/Dakar 48 hpi_3 | ABCF1 | 1553 | 7898.825141 | 0.196612 | 1.283970503 | 0.360612 |
| ZIKV/Dakar 4 hpi_1 | SDHA | 1401 | 21745.79117 | 0.064426 | 1.050765843 | 0.071441 |
| ZIKV/Dakar 8 hpi_1 | SDHA | 1038 | 17326.69644 | 0.059908 | 0.938528561 | -0.09153 |
| ZIKV/Dakar 10 hpi_1 | SDHA | 1117 | 17513.91951 | 0.063778 | 1.016394854 | 0.023461 |
| ZIKV/Dakar 24 hpi_1 | SDHA | 773 | 12050.24737 | 0.064148 | 1.00149872 | 0.002161 |
| ZIKV/Dakar 48 hpi_1 | SDHA | 1035 | 14705.51891 | 0.070382 | 0.917223812 | -0.12465 |
| ZIKV/Dakar 4 hpi_2 | SDHA | 654 | 10431.40144 | 0.062695 | 1.02253484 | 0.03215 |
| ZIKV/Dakar 8 hpi_2 | SDHA | 811 | 12658.05148 | 0.06407 | 1.00373693 | 0.005381 |
| ZIKV/Dakar 10 hpi_2 | SDHA | 870 | 13088.28841 | 0.066472 | 1.059324532 | 0.083145 |
| ZIKV/Dakar 24 hpi_2 | SDHA | 633 | 9702.067847 | 0.065244 | 1.018606093 | 0.026596 |
| ZIKV/Dakar 48 hpi_2 | SDHA | 546 | 7275.616586 | 0.075045 | 0.977998443 | -0.0321 |
| ZIKV/Dakar 4 hpi_3 | SDHA | 674 | 10334.87659 | 0.065216 | 1.063647261 | 0.08902 |
| ZIKV/Dakar 8 hpi_3 | SDHA | 619 | 10124.86039 | 0.061137 | 0.957783855 | -0.06223 |
| ZIKV/Dakar 10 hpi_3 | SDHA | 540 | 8611.388976 | 0.062708 | 0.999339807 | -0.00095 |
| ZIKV/Dakar 24 hpi_3 | SDHA | 644 | 9356.243092 | 0.068831 | 1.07461089 | 0.103814 |
| ZIKV/Dakar 48 hpi_3 | SDHA | 606 | 7898.825141 | 0.07672 | 0.999828355 | -0.00025 |
| ZIKV/Dakar 4 hpi_1 | PGK1 | 64196 | 21745.79117 | 2.952111 | 1.134257623 | 0.181748 |
| ZIKV/Dakar 8 hpi_1 | PGK1 | 56013 | 17326.69644 | 3.232757 | 1.211652547 | 0.276976 |
| ZIKV/Dakar 10 hpi_1 | PGK1 | 57635 | 17513.91951 | 3.290811 | 1.146058561 | 0.196681 |
| ZIKV/Dakar 24 hpi_1 | PGK1 | 50015 | 12050.24737 | 4.150537 | 1.164609988 | 0.219847 |
| ZIKV/Dakar 48 hpi_1 | PGK1 | 94426 | 14705.51891 | 6.421127 | 1.188378683 | 0.248995 |

| | | | | | | |
|---|---|---|---|---|---|---|
| ZIKV/Dakar 4 hpi_2 | PGK1 | 26803 | 10431.40144 | 2.569453 | 0.98723308 | -0.01854 |
| ZIKV/Dakar 8 hpi_2 | PGK1 | 32007 | 12658.05148 | 2.528588 | 0.947726763 | -0.07746 |
| ZIKV/Dakar 10 hpi_2 | PGK1 | 35850 | 13088.28841 | 2.73909 | 0.953916071 | -0.06807 |
| ZIKV/Dakar 24 hpi_2 | PGK1 | 33226 | 9702.067847 | 3.424631 | 0.960926019 | -0.0575 |
| ZIKV/Dakar 48 hpi_2 | PGK1 | 39889 | 7275.616586 | 5.482559 | 1.014674996 | 0.021018 |
| ZIKV/Dakar 4 hpi_3 | PGK1 | 25599 | 10334.87659 | 2.476953 | 0.951692522 | -0.07143 |
| ZIKV/Dakar 8 hpi_3 | PGK1 | 25874 | 10124.86039 | 2.555492 | 0.957810432 | -0.06219 |
| ZIKV/Dakar 10 hpi_3 | PGK1 | 22678 | 8611.388976 | 2.633489 | 0.917139516 | -0.12479 |
| ZIKV/Dakar 24 hpi_3 | PGK1 | 29086 | 9356.243092 | 3.108726 | 0.872285599 | -0.19713 |
| ZIKV/Dakar 48 hpi_3 | PGK1 | 42359 | 7898.825141 | 5.362696 | 0.992491539 | -0.01087 |
| ZIKV/Malaysia 4 hpi_1 | IRF5 | 201 | 18941.07792 | 0.010612 | 0.989949311 | -0.01457 |
| ZIKV/Malaysia 8 hpi_1 | IRF5 | 267 | 16004.07538 | 0.016683 | 1.172637527 | 0.229757 |
| ZIKV/Malaysia 10 hpi_1 | IRF5 | 268 | 20365.09781 | 0.01316 | 0.895199345 | -0.15972 |
| ZIKV/Malaysia 24 hpi_1 | IRF5 | 268 | 16824.24388 | 0.015929 | 1.008901484 | 0.012785 |
| ZIKV/Malaysia 48 hpi_1 | IRF5 | 231 | 9016.561426 | 0.02562 | 1.317685385 | 0.398006 |
| ZIKV/Malaysia 4 hpi_2 | IRF5 | 158 | 13310.81661 | 0.01187 | 1.107322126 | 0.147075 |
| ZIKV/Malaysia 8 hpi_2 | IRF5 | 205 | 15300.45305 | 0.013398 | 0.941743619 | -0.08659 |
| ZIKV/Malaysia 10 hpi_2 | IRF5 | 149 | 11873.49207 | 0.012549 | 0.853648859 | -0.22829 |
| ZIKV/Malaysia 24 hpi_2 | IRF5 | 129 | 7114.262677 | 0.018133 | 1.148442712 | 0.199679 |
| ZIKV/Malaysia 48 hpi_2 | IRF5 | 196 | 7202.033077 | 0.027215 | 1.399721568 | 0.48514 |
| ZIKV/Malaysia 4 hpi_3 | IRF5 | 79 | 8019.493292 | 0.009851 | 0.918970888 | -0.12191 |
| ZIKV/Malaysia 8 hpi_3 | IRF5 | 171 | 13577.51567 | 0.012594 | 0.885235686 | -0.17587 |
| ZIKV/Malaysia 10 hpi_3 | IRF5 | 126 | 8780.599468 | 0.01435 | 0.976152881 | -0.03482 |
| ZIKV/Malaysia 24 hpi_3 | IRF5 | 131 | 7775.628155 | 0.016848 | 1.067051386 | 0.09363 |
| ZIKV/Malaysia 48 hpi_3 | IRF5 | 141 | 5457.964761 | 0.025834 | 1.328706563 | 0.410023 |

| | | | | | | |
|---|---|---|---|---|---|---|
| ZIKV/Malaysia 4 hpi_1 | IFNB1 | 18 | 18941.07792 | 0.00095 | 1.017030133 | 0.024362 |
| ZIKV/Malaysia 8 hpi_1 | IFNB1 | 43 | 16004.07538 | 0.002687 | 2.821314248 | 1.496367 |
| ZIKV/Malaysia 10 hpi_1 | IFNB1 | 51 | 20365.09781 | 0.002504 | 2.152151303 | 1.10578 |
| ZIKV/Malaysia 24 hpi_1 | IFNB1 | 2346 | 16824.24388 | 0.139442 | 188.2937639 | 7.556841 |
| ZIKV/Malaysia 48 hpi_1 | IFNB1 | 2779 | 9016.561426 | 0.308211 | 339.4528908 | 8.407068 |
| ZIKV/Malaysia 4 hpi_2 | IFNB1 | 15 | 13310.81661 | 0.001127 | 1.2060146 | 0.270247 |
| ZIKV/Malaysia 8 hpi_2 | IFNB1 | 19 | 15300.45305 | 0.001242 | 1.303955904 | 0.382895 |
| ZIKV/Malaysia 10 hpi_2 | IFNB1 | 28 | 11873.49207 | 0.002358 | 2.026603039 | 1.019064 |
| ZIKV/Malaysia 24 hpi_2 | IFNB1 | 779 | 7114.262677 | 0.109498 | 147.860117 | 7.208089 |
| ZIKV/Malaysia 48 hpi_2 | IFNB1 | 1704 | 7202.033077 | 0.2366 | 260.5831857 | 8.0256 |
| ZIKV/Malaysia 4 hpi_3 | IFNB1 | 10 | 8019.493292 | 0.001247 | 1.334501535 | 0.416301 |
| ZIKV/Malaysia 8 hpi_3 | IFNB1 | 35 | 13577.51567 | 0.002578 | 2.706832152 | 1.436605 |
| ZIKV/Malaysia 10 hpi_3 | IFNB1 | 24 | 8780.599468 | 0.002733 | 2.348963126 | 1.232024 |
| ZIKV/Malaysia 24 hpi_3 | IFNB1 | 1060 | 7775.628155 | 0.136323 | 184.0830774 | 7.524213 |
| ZIKV/Malaysia 48 hpi_3 | IFNB1 | 1660 | 5457.964761 | 0.304143 | 334.9725899 | 8.387899 |
| ZIKV/Malaysia 4 hpi_1 | MX1 | 209 | 18941.07792 | 0.011034 | 1.002839143 | 0.00409 |
| ZIKV/Malaysia 8 hpi_1 | MX1 | 924 | 16004.07538 | 0.057735 | 6.121815567 | 2.61396 |
| ZIKV/Malaysia 10 hpi_1 | MX1 | 2353 | 20365.09781 | 0.115541 | 10.75624559 | 3.427103 |
| ZIKV/Malaysia 24 hpi_1 | MX1 | 21162 | 16824.24388 | 1.257828 | 119.0519653 | 6.895448 |
| ZIKV/Malaysia 48 hpi_1 | MX1 | 3766 | 9016.561426 | 0.417676 | 45.23370246 | 5.499326 |
| ZIKV/Malaysia 4 hpi_2 | MX1 | 125 | 13310.81661 | 0.009391 | 0.853483236 | -0.22857 |
| ZIKV/Malaysia 8 hpi_2 | MX1 | 283 | 15300.45305 | 0.018496 | 1.961196021 | 0.971734 |
| ZIKV/Malaysia 10 hpi_2 | MX1 | 480 | 11873.49207 | 0.040426 | 3.763466493 | 1.912062 |
| ZIKV/Malaysia 24 hpi_2 | MX1 | 5457 | 7114.262677 | 0.767051 | 72.60047659 | 6.181907 |
| ZIKV/Malaysia 48 hpi_2 | MX1 | 1267 | 7202.033077 | 0.175923 | 19.0521622 | 4.251883 |

| | | | | | | |
|---|---|---|---|---|---|---|
| ZIKV/Malaysia 4 hpi_3 | MX1 | 74 | 8019.493292 | 0.009228 | 0.838637877 | -0.25388 |
| ZIKV/Malaysia 8 hpi_3 | MX1 | 522 | 13577.51567 | 0.038446 | 4.076515038 | 2.027336 |
| ZIKV/Malaysia 10 hpi_3 | MX1 | 743 | 8780.599468 | 0.084618 | 7.877527529 | 2.977743 |
| ZIKV/Malaysia 24 hpi_3 | MX1 | 9965 | 7775.628155 | 1.281568 | 121.2990037 | 6.922424 |
| ZIKV/Malaysia 48 hpi_3 | MX1 | 2961 | 5457.964761 | 0.54251 | 58.75305411 | 5.876592 |
| ZIKV/Malaysia 4 hpi_1 | IFNL3 | 30 | 18941.07792 | 0.001584 | 1.275683042 | 0.35127 |
| ZIKV/Malaysia 8 hpi_1 | IFNL3 | 33 | 16004.07538 | 0.002062 | 1.39893131 | 0.484325 |
| ZIKV/Malaysia 10 hpi_1 | IFNL3 | 27 | 20365.09781 | 0.001326 | 0.925423098 | -0.11181 |
| ZIKV/Malaysia 24 hpi_1 | IFNL3 | 368 | 16824.24388 | 0.021873 | 13.6773438 | 3.773716 |
| ZIKV/Malaysia 48 hpi_1 | IFNL3 | 1208 | 9016.561426 | 0.133976 | 133.297637 | 7.058507 |
| ZIKV/Malaysia 4 hpi_2 | IFNL3 | 31 | 13310.81661 | 0.002329 | 1.875785664 | 0.907495 |
| ZIKV/Malaysia 8 hpi_2 | IFNL3 | 28 | 15300.45305 | 0.00183 | 1.241557333 | 0.312151 |
| ZIKV/Malaysia 10 hpi_2 | IFNL3 | 24 | 11873.49207 | 0.002021 | 1.410898743 | 0.496614 |
| ZIKV/Malaysia 24 hpi_2 | IFNL3 | 148 | 7114.262677 | 0.020803 | 13.00832321 | 3.701363 |
| ZIKV/Malaysia 48 hpi_2 | IFNL3 | 677 | 7202.033077 | 0.094001 | 93.5254958 | 6.547288 |
| ZIKV/Malaysia 4 hpi_3 | IFNL3 | 10 | 8019.493292 | 0.001247 | 1.004336601 | 0.006243 |
| ZIKV/Malaysia 8 hpi_3 | IFNL3 | 24 | 13577.51567 | 0.001768 | 1.199234096 | 0.262113 |
| ZIKV/Malaysia 10 hpi_3 | IFNL3 | 19 | 8780.599468 | 0.002164 | 1.510401837 | 0.594932 |
| ZIKV/Malaysia 24 hpi_3 | IFNL3 | 174 | 7775.628155 | 0.022378 | 13.99275612 | 3.806608 |
| ZIKV/Malaysia 48 hpi_3 | IFNL3 | 557 | 5457.964761 | 0.102053 | 101.5362056 | 6.66585 |
| ZIKV/Malaysia 4 hpi_1 | IFIH1 | 119 | 18941.07792 | 0.006283 | 0.994351607 | -0.00817 |
| ZIKV/Malaysia 8 hpi_1 | IFIH1 | 188 | 16004.07538 | 0.011747 | 1.80901342 | 0.855203 |
| ZIKV/Malaysia 10 hpi_1 | IFIH1 | 309 | 20365.09781 | 0.015173 | 2.15169188 | 1.105472 |
| ZIKV/Malaysia 24 hpi_1 | IFIH1 | 1702 | 16824.24388 | 0.101164 | 13.47826786 | 3.752563 |
| ZIKV/Malaysia 48 hpi_1 | IFIH1 | 1005 | 9016.561426 | 0.111462 | 12.34936421 | 3.626365 |

| | | | | | | |
|---|---|---|---|---|---|---|
| ZIKV/Malaysia 4 hpi_2 | IFIH1 | 102 | 13310.81661 | 0.007663 | 1.212811151 | 0.278355 |
| ZIKV/Malaysia 8 hpi_2 | IFIH1 | 134 | 15300.45305 | 0.008758 | 1.348699 | 0.431568 |
| ZIKV/Malaysia 10 hpi_2 | IFIH1 | 109 | 11873.49207 | 0.00918 | 1.301835569 | 0.380547 |
| ZIKV/Malaysia 24 hpi_2 | IFIH1 | 449 | 7114.262677 | 0.063113 | 8.408654866 | 3.071875 |
| ZIKV/Malaysia 48 hpi_2 | IFIH1 | 597 | 7202.033077 | 0.082893 | 9.184144382 | 3.199145 |
| ZIKV/Malaysia 4 hpi_3 | IFIH1 | 59 | 8019.493292 | 0.007357 | 1.164401597 | 0.219589 |
| ZIKV/Malaysia 8 hpi_3 | IFIH1 | 125 | 13577.51567 | 0.009206 | 1.417764925 | 0.503618 |
| ZIKV/Malaysia 10 hpi_3 | IFIH1 | 120 | 8780.599468 | 0.013666 | 1.938050908 | 0.954606 |
| ZIKV/Malaysia 24 hpi_3 | IFIH1 | 583 | 7775.628155 | 0.074978 | 9.989486256 | 3.32041 |
| ZIKV/Malaysia 48 hpi_3 | IFIH1 | 569 | 5457.964761 | 0.104251 | 11.55050632 | 3.529884 |
| ZIKV/Malaysia 4 hpi_1 | IL1B | 32 | 18941.07792 | 0.001689 | 0.920568956 | -0.1194 |
| ZIKV/Malaysia 8 hpi_1 | IL1B | 23 | 16004.07538 | 0.001437 | 0.812688704 | -0.29923 |
| ZIKV/Malaysia 10 hpi_1 | IL1B | 34 | 20365.09781 | 0.00167 | 1.015424347 | 0.022083 |
| ZIKV/Malaysia 24 hpi_1 | IL1B | 29 | 16824.24388 | 0.001724 | 0.78243122 | -0.35396 |
| ZIKV/Malaysia 48 hpi_1 | IL1B | 91 | 9016.561426 | 0.010093 | 3.266827686 | 1.70789 |
| ZIKV/Malaysia 4 hpi_2 | IL1B | 18 | 13310.81661 | 0.001352 | 0.736849584 | -0.44056 |
| ZIKV/Malaysia 8 hpi_2 | IL1B | 19 | 15300.45305 | 0.001242 | 0.702224999 | -0.50999 |
| ZIKV/Malaysia 10 hpi_2 | IL1B | 14 | 11873.49207 | 0.001179 | 0.717141285 | -0.47967 |
| ZIKV/Malaysia 24 hpi_2 | IL1B | 13 | 7114.262677 | 0.001827 | 0.829463317 | -0.26975 |
| ZIKV/Malaysia 48 hpi_2 | IL1B | 37 | 7202.033077 | 0.005137 | 1.66292397 | 0.733722 |
| ZIKV/Malaysia 4 hpi_3 | IL1B | 15 | 8019.493292 | 0.00187 | 1.019190503 | 0.027424 |
| ZIKV/Malaysia 8 hpi_3 | IL1B | 19 | 13577.51567 | 0.001399 | 0.791334798 | -0.33764 |
| ZIKV/Malaysia 10 hpi_3 | IL1B | 20 | 8780.599468 | 0.002278 | 1.385354706 | 0.470255 |
| ZIKV/Malaysia 24 hpi_3 | IL1B | 15 | 7775.628155 | 0.001929 | 0.875668049 | -0.19154 |
| ZIKV/Malaysia 48 hpi_3 | IL1B | 38 | 5457.964761 | 0.006962 | 2.253609425 | 1.172238 |

| | | | | | | |
|---|---|---|---|---|---|---|
| ZIKV/Malaysia 4 hpi_1 | GBP1 | 46 | 18941.07792 | 0.002429 | 1.015543786 | 0.022252 |
| ZIKV/Malaysia 8 hpi_1 | GBP1 | 97 | 16004.07538 | 0.006061 | 1.947220878 | 0.961417 |
| ZIKV/Malaysia 10 hpi_1 | GBP1 | 112 | 20365.09781 | 0.0055 | 1.673876559 | 0.743193 |
| ZIKV/Malaysia 24 hpi_1 | GBP1 | 738 | 16824.24388 | 0.043865 | 15.62851681 | 3.966109 |
| ZIKV/Malaysia 48 hpi_1 | GBP1 | 378 | 9016.561426 | 0.041923 | 18.46837506 | 4.206985 |
| ZIKV/Malaysia 4 hpi_2 | GBP1 | 43 | 13310.81661 | 0.00323 | 1.350856658 | 0.433875 |
| ZIKV/Malaysia 8 hpi_2 | GBP1 | 28 | 15300.45305 | 0.00183 | 0.587932966 | -0.76628 |
| ZIKV/Malaysia 10 hpi_2 | GBP1 | 36 | 11873.49207 | 0.003032 | 0.92281775 | -0.11588 |
| ZIKV/Malaysia 24 hpi_2 | GBP1 | 156 | 7114.262677 | 0.021928 | 7.812529306 | 2.96579 |
| ZIKV/Malaysia 48 hpi_2 | GBP1 | 282 | 7202.033077 | 0.039156 | 17.24931401 | 4.108467 |
| ZIKV/Malaysia 4 hpi_3 | GBP1 | 22 | 8019.493292 | 0.002743 | 1.147152786 | 0.198058 |
| ZIKV/Malaysia 8 hpi_3 | GBP1 | 58 | 13577.51567 | 0.004272 | 1.372403296 | 0.456704 |
| ZIKV/Malaysia 10 hpi_3 | GBP1 | 60 | 8780.599468 | 0.006833 | 2.079787618 | 1.056436 |
| ZIKV/Malaysia 24 hpi_3 | GBP1 | 305 | 7775.628155 | 0.039225 | 13.97530559 | 3.804808 |
| ZIKV/Malaysia 48 hpi_3 | GBP1 | 290 | 5457.964761 | 0.053133 | 23.40696481 | 4.548866 |
| ZIKV/Malaysia 4 hpi_1 | IFITM1 | 165 | 18941.07792 | 0.008711 | 1.16611052 | 0.221705 |
| ZIKV/Malaysia 8 hpi_1 | IFITM1 | 348 | 16004.07538 | 0.021744 | 2.935720363 | 1.553715 |
| ZIKV/Malaysia 10 hpi_1 | IFITM1 | 649 | 20365.09781 | 0.031868 | 3.658030536 | 1.871067 |
| ZIKV/Malaysia 24 hpi_1 | IFITM1 | 8814 | 16824.24388 | 0.523887 | 28.31326708 | 4.823406 |
| ZIKV/Malaysia 48 hpi_1 | IFITM1 | 18764 | 9016.561426 | 2.081059 | 23.46076736 | 4.552178 |
| ZIKV/Malaysia 4 hpi_2 | IFITM1 | 72 | 13310.81661 | 0.005409 | 0.724082842 | -0.46577 |
| ZIKV/Malaysia 8 hpi_2 | IFITM1 | 144 | 15300.45305 | 0.009411 | 1.270644998 | 0.345561 |
| ZIKV/Malaysia 10 hpi_2 | IFITM1 | 162 | 11873.49207 | 0.013644 | 1.566122317 | 0.647197 |
| ZIKV/Malaysia 24 hpi_2 | IFITM1 | 2070 | 7114.262677 | 0.290965 | 15.7250829 | 3.974996 |
| ZIKV/Malaysia 48 hpi_2 | IFITM1 | 4820 | 7202.033077 | 0.669255 | 7.544833514 | 2.915489 |

| | | | | | | |
|---|---|---|---|---|---|---|
| ZIKV/Malaysia 4 hpi_3 | IFITM1 | 63 | 8019.493292 | 0.007856 | 1.051608483 | 0.072598 |
| ZIKV/Malaysia 8 hpi_3 | IFITM1 | 194 | 13577.51567 | 0.014288 | 1.9290676 | 0.947904 |
| ZIKV/Malaysia 10 hpi_3 | IFITM1 | 195 | 8780.599468 | 0.022208 | 2.549174552 | 1.35003 |
| ZIKV/Malaysia 24 hpi_3 | IFITM1 | 3506 | 7775.628155 | 0.450896 | 24.36850706 | 4.606946 |
| ZIKV/Malaysia 48 hpi_3 | IFITM1 | 8943 | 5457.964761 | 1.638523 | 18.47184339 | 4.207256 |
| ZIKV/Malaysia 4 hpi_1 | TLR3 | 136 | 18941.07792 | 0.00718 | 0.918170874 | -0.12317 |
| ZIKV/Malaysia 8 hpi_1 | TLR3 | 124 | 16004.07538 | 0.007748 | 1.206674614 | 0.271037 |
| ZIKV/Malaysia 10 hpi_1 | TLR3 | 166 | 20365.09781 | 0.008151 | 1.172379555 | 0.22944 |
| ZIKV/Malaysia 24 hpi_1 | TLR3 | 669 | 16824.24388 | 0.039764 | 4.478873292 | 2.163136 |
| ZIKV/Malaysia 48 hpi_1 | TLR3 | 105 | 9016.561426 | 0.011645 | 1.298229912 | 0.376546 |
| ZIKV/Malaysia 4 hpi_2 | TLR3 | 100 | 13310.81661 | 0.007513 | 0.96069293 | -0.05785 |
| ZIKV/Malaysia 8 hpi_2 | TLR3 | 127 | 15300.45305 | 0.0083 | 1.292702265 | 0.37039 |
| ZIKV/Malaysia 10 hpi_2 | TLR3 | 83 | 11873.49207 | 0.00699 | 1.005417116 | 0.007794 |
| ZIKV/Malaysia 24 hpi_2 | TLR3 | 188 | 7114.262677 | 0.026426 | 2.976501917 | 1.573618 |
| ZIKV/Malaysia 48 hpi_2 | TLR3 | 96 | 7202.033077 | 0.01333 | 1.48600195 | 0.571436 |
| ZIKV/Malaysia 4 hpi_3 | TLR3 | 76 | 8019.493292 | 0.009477 | 1.211869788 | 0.277235 |
| ZIKV/Malaysia 8 hpi_3 | TLR3 | 106 | 13577.51567 | 0.007807 | 1.21586297 | 0.281981 |
| ZIKV/Malaysia 10 hpi_3 | TLR3 | 64 | 8780.599468 | 0.007289 | 1.048340721 | 0.068108 |
| ZIKV/Malaysia 24 hpi_3 | TLR3 | 265 | 7775.628155 | 0.034081 | 3.838739169 | 1.940633 |
| ZIKV/Malaysia 48 hpi_3 | TLR3 | 108 | 5457.964761 | 0.019788 | 2.205953157 | 1.141402 |
| ZIKV/Malaysia 4 hpi_1 | CCL3 | 13 | 18941.07792 | 0.000686 | 0.896412404 | -0.15777 |
| ZIKV/Malaysia 8 hpi_1 | CCL3 | 6 | 16004.07538 | 0.000375 | 0.474661251 | -1.07503 |
| ZIKV/Malaysia 10 hpi_1 | CCL3 | 10 | 20365.09781 | 0.000491 | 0.491463148 | -1.02484 |
| ZIKV/Malaysia 24 hpi_1 | CCL3 | 24 | 16824.24388 | 0.001427 | 2.296307778 | 1.199316 |
| ZIKV/Malaysia 48 hpi_1 | CCL3 | 28 | 9016.561426 | 0.003105 | 4.195247635 | 2.068756 |

| | | | | | | |
|---|---|---|---|---|---|---|
| ZIKV/Malaysia 4 hpi_2 | CCL3 | 7 | 13310.81661 | 0.000526 | 0.686851002 | -0.54193 |
| ZIKV/Malaysia 8 hpi_2 | CCL3 | 8 | 15300.45305 | 0.000523 | 0.661986014 | -0.59513 |
| ZIKV/Malaysia 10 hpi_2 | CCL3 | 6 | 11873.49207 | 0.000505 | 0.505766712 | -0.98346 |
| ZIKV/Malaysia 24 hpi_2 | CCL3 | 7 | 7114.262677 | 0.000984 | 1.583881018 | 0.663464 |
| ZIKV/Malaysia 48 hpi_2 | CCL3 | 16 | 7202.033077 | 0.002222 | 3.001272208 | 1.585574 |
| ZIKV/Malaysia 4 hpi_3 | CCL3 | 9 | 8019.493292 | 0.001122 | 1.46576645 | 0.551655 |
| ZIKV/Malaysia 8 hpi_3 | CCL3 | 7 | 13577.51567 | 0.000516 | 0.652740928 | -0.61542 |
| ZIKV/Malaysia 10 hpi_3 | CCL3 | 8 | 8780.599468 | 0.000911 | 0.911891732 | -0.13307 |
| ZIKV/Malaysia 24 hpi_3 | CCL3 | 8 | 7775.628155 | 0.001029 | 1.656185255 | 0.727864 |
| ZIKV/Malaysia 48 hpi_3 | CCL3 | 9 | 5457.964761 | 0.001649 | 2.227677394 | 1.15554 |
| ZIKV/Malaysia 4 hpi_1 | IL18 | 1256 | 18941.07792 | 0.066311 | 0.899041948 | -0.15354 |
| ZIKV/Malaysia 8 hpi_1 | IL18 | 1021 | 16004.07538 | 0.063796 | 0.897692828 | -0.15571 |
| ZIKV/Malaysia 10 hpi_1 | IL18 | 1286 | 20365.09781 | 0.063147 | 0.886170859 | -0.17434 |
| ZIKV/Malaysia 24 hpi_1 | IL18 | 731 | 16824.24388 | 0.043449 | 0.73576954 | -0.44267 |
| ZIKV/Malaysia 48 hpi_1 | IL18 | 508 | 9016.561426 | 0.056341 | 0.691653011 | -0.53188 |
| ZIKV/Malaysia 4 hpi_2 | IL18 | 1034 | 13310.81661 | 0.077681 | 1.053199989 | 0.074779 |
| ZIKV/Malaysia 8 hpi_2 | IL18 | 1178 | 15300.45305 | 0.076991 | 1.083362008 | 0.115515 |
| ZIKV/Malaysia 10 hpi_2 | IL18 | 887 | 11873.49207 | 0.074704 | 1.048354466 | 0.068127 |
| ZIKV/Malaysia 24 hpi_2 | IL18 | 352 | 7114.262677 | 0.049478 | 0.837862493 | -0.25521 |
| ZIKV/Malaysia 48 hpi_2 | IL18 | 428 | 7202.033077 | 0.059428 | 0.729548489 | -0.45492 |
| ZIKV/Malaysia 4 hpi_3 | IL18 | 584 | 8019.493292 | 0.072823 | 0.9873268 | -0.0184 |
| ZIKV/Malaysia 8 hpi_3 | IL18 | 1044 | 13577.51567 | 0.076892 | 1.081963942 | 0.113652 |
| ZIKV/Malaysia 10 hpi_3 | IL18 | 621 | 8780.599468 | 0.070724 | 0.992499803 | -0.01086 |
| ZIKV/Malaysia 24 hpi_3 | IL18 | 390 | 7775.628155 | 0.050157 | 0.849354723 | -0.23556 |
| ZIKV/Malaysia 48 hpi_3 | IL18 | 320 | 5457.964761 | 0.05863 | 0.719755109 | -0.47442 |

| | | | | | | |
|---|---|---|---|---|---|---|
| ZIKV/Malaysia 4 hpi_1 | CXCL10 | 7 | 18941.07792 | 0.00037 | 1.57807214 | 0.658163 |
| ZIKV/Malaysia 8 hpi_1 | CXCL10 | 8 | 16004.07538 | 0.0005 | 1.679458198 | 0.747996 |
| ZIKV/Malaysia 10 hpi_1 | CXCL10 | 9 | 20365.09781 | 0.000442 | 1.613421045 | 0.690123 |
| ZIKV/Malaysia 24 hpi_1 | CXCL10 | 68 | 16824.24388 | 0.004042 | 11.45653484 | 3.518099 |
| ZIKV/Malaysia 48 hpi_1 | CXCL10 | 42 | 9016.561426 | 0.004658 | 14.25556726 | 3.833454 |
| ZIKV/Malaysia 4 hpi_2 | CXCL10 | 4 | 13310.81661 | 0.000301 | 1.283183583 | 0.359728 |
| ZIKV/Malaysia 8 hpi_2 | CXCL10 | 5 | 15300.45305 | 0.000327 | 1.097932178 | 0.134789 |
| ZIKV/Malaysia 10 hpi_2 | CXCL10 | 5 | 11873.49207 | 0.000421 | 1.537387149 | 0.620481 |
| ZIKV/Malaysia 24 hpi_2 | CXCL10 | 50 | 7114.262677 | 0.007028 | 19.92140802 | 4.316248 |
| ZIKV/Malaysia 48 hpi_2 | CXCL10 | 47 | 7202.033077 | 0.006526 | 19.97187803 | 4.319898 |
| ZIKV/Malaysia 4 hpi_3 | CXCL10 | 2 | 8019.493292 | 0.000249 | 1.064918987 | 0.090744 |
| ZIKV/Malaysia 8 hpi_3 | CXCL10 | 9 | 13577.51567 | 0.000663 | 2.227060405 | 1.155141 |
| ZIKV/Malaysia 10 hpi_3 | CXCL10 | 4 | 8780.599468 | 0.000456 | 1.663135113 | 0.733905 |
| ZIKV/Malaysia 24 hpi_3 | CXCL10 | 43 | 7775.628155 | 0.00553 | 15.67519292 | 3.970411 |
| ZIKV/Malaysia 48 hpi_3 | CXCL10 | 47 | 5457.964761 | 0.008611 | 26.35380265 | 4.719939 |
| ZIKV/Malaysia 4 hpi_1 | IFNA4 | 6 | 18941.07792 | 0.000317 | 1.279615111 | 0.35571 |
| ZIKV/Malaysia 8 hpi_1 | IFNA4 | 7 | 16004.07538 | 0.000437 | 0.950026864 | -0.07396 |
| ZIKV/Malaysia 10 hpi_1 | IFNA4 | 7 | 20365.09781 | 0.000344 | 0.858855966 | -0.21951 |
| ZIKV/Malaysia 24 hpi_1 | IFNA4 | 12 | 16824.24388 | 0.000713 | 1.633919654 | 0.708337 |
| ZIKV/Malaysia 48 hpi_1 | IFNA4 | 9 | 9016.561426 | 0.000998 | 2.38325446 | 1.252933 |
| ZIKV/Malaysia 4 hpi_2 | IFNA4 | 3 | 13310.81661 | 0.000225 | 0.91043586 | -0.13537 |
| ZIKV/Malaysia 8 hpi_2 | IFNA4 | 7 | 15300.45305 | 0.000458 | 0.993715774 | -0.00909 |
| ZIKV/Malaysia 10 hpi_2 | IFNA4 | 4 | 11873.49207 | 0.000337 | 0.841763949 | -0.24851 |
| ZIKV/Malaysia 24 hpi_2 | IFNA4 | 5 | 7114.262677 | 0.000703 | 1.609997174 | 0.687058 |
| ZIKV/Malaysia 48 hpi_2 | IFNA4 | 9 | 7202.033077 | 0.00125 | 2.983707517 | 1.577106 |

| | | | | | | |
|---|---|---|---|---|---|---|
| ZIKV/Malaysia 4 hpi_3 | IFNA4 | 1 | 8019.493292 | 0.000125 | 0.503716146 | -0.98932 |
| ZIKV/Malaysia 8 hpi_3 | IFNA4 | 7 | 13577.51567 | 0.000516 | 1.119814693 | 0.16326 |
| ZIKV/Malaysia 10 hpi_3 | IFNA4 | 1 | 8780.599468 | 0.000114 | 0.284567062 | -1.81316 |
| ZIKV/Malaysia 24 hpi_3 | IFNA4 | 8 | 7775.628155 | 0.001029 | 2.356891061 | 1.236885 |
| ZIKV/Malaysia 48 hpi_3 | IFNA4 | 3 | 5457.964761 | 0.00055 | 1.312379319 | 0.392185 |
| ZIKV/Malaysia 4 hpi_1 | IRF1 | 282 | 18941.07792 | 0.014888 | 1.288767591 | 0.365992 |
| ZIKV/Malaysia 8 hpi_1 | IRF1 | 222 | 16004.07538 | 0.013871 | 1.15414709 | 0.206827 |
| ZIKV/Malaysia 10 hpi_1 | IRF1 | 238 | 20365.09781 | 0.011687 | 1.202581341 | 0.266134 |
| ZIKV/Malaysia 24 hpi_1 | IRF1 | 832 | 16824.24388 | 0.049452 | 4.454978172 | 2.155418 |
| ZIKV/Malaysia 48 hpi_1 | IRF1 | 801 | 9016.561426 | 0.088837 | 7.309791046 | 2.86983 |
| ZIKV/Malaysia 4 hpi_2 | IRF1 | 232 | 13310.81661 | 0.017429 | 1.508736766 | 0.593341 |
| ZIKV/Malaysia 8 hpi_2 | IRF1 | 181 | 15300.45305 | 0.01183 | 0.984267305 | -0.02288 |
| ZIKV/Malaysia 10 hpi_2 | IRF1 | 153 | 11873.49207 | 0.012886 | 1.325979986 | 0.407059 |
| ZIKV/Malaysia 24 hpi_2 | IRF1 | 295 | 7114.262677 | 0.041466 | 3.73551022 | 1.901305 |
| ZIKV/Malaysia 48 hpi_2 | IRF1 | 609 | 7202.033077 | 0.084559 | 6.957858193 | 2.798643 |
| ZIKV/Malaysia 4 hpi_3 | IRF1 | 128 | 8019.493292 | 0.015961 | 1.381634693 | 0.466376 |
| ZIKV/Malaysia 8 hpi_3 | IRF1 | 184 | 13577.51567 | 0.013552 | 1.127551235 | 0.173193 |
| ZIKV/Malaysia 10 hpi_3 | IRF1 | 116 | 8780.599468 | 0.013211 | 1.359433058 | 0.443005 |
| ZIKV/Malaysia 24 hpi_3 | IRF1 | 445 | 7775.628155 | 0.05723 | 5.155637059 | 2.366151 |
| ZIKV/Malaysia 48 hpi_3 | IRF1 | 482 | 5457.964761 | 0.088311 | 7.266574043 | 2.861275 |
| ZIKV/Malaysia 4 hpi_1 | IFI44 | 90 | 18941.07792 | 0.004752 | 1.281025888 | 0.3573 |
| ZIKV/Malaysia 8 hpi_1 | IFI44 | 165 | 16004.07538 | 0.01031 | 2.893296008 | 1.532714 |
| ZIKV/Malaysia 10 hpi_1 | IFI44 | 324 | 20365.09781 | 0.01591 | 4.491201707 | 2.167102 |
| ZIKV/Malaysia 24 hpi_1 | IFI44 | 1394 | 16824.24388 | 0.082857 | 17.29228839 | 4.112057 |
| ZIKV/Malaysia 48 hpi_1 | IFI44 | 823 | 9016.561426 | 0.091276 | 20.31624738 | 4.344562 |

| | | | | | | |
|---|---|---|---|---|---|---|
| ZIKV/Malaysia 4 hpi_2 | IFI44 | 38 | 13310.81661 | 0.002855 | 0.76966012 | -0.37771 |
| ZIKV/Malaysia 8 hpi_2 | IFI44 | 65 | 15300.45305 | 0.004248 | 1.192198519 | 0.253624 |
| ZIKV/Malaysia 10 hpi_2 | IFI44 | 75 | 11873.49207 | 0.006317 | 1.783145769 | 0.834425 |
| ZIKV/Malaysia 24 hpi_2 | IFI44 | 354 | 7114.262677 | 0.049759 | 10.38481147 | 3.376403 |
| ZIKV/Malaysia 48 hpi_2 | IFI44 | 336 | 7202.033077 | 0.046653 | 10.38409777 | 3.376304 |
| ZIKV/Malaysia 4 hpi_3 | IFI44 | 29 | 8019.493292 | 0.003616 | 0.974924888 | -0.03664 |
| ZIKV/Malaysia 8 hpi_3 | IFI44 | 88 | 13577.51567 | 0.006481 | 1.818870886 | 0.863043 |
| ZIKV/Malaysia 10 hpi_3 | IFI44 | 107 | 8780.599468 | 0.012186 | 3.440041336 | 1.782426 |
| ZIKV/Malaysia 24 hpi_3 | IFI44 | 546 | 7775.628155 | 0.070219 | 14.65488484 | 3.87331 |
| ZIKV/Malaysia 48 hpi_3 | IFI44 | 484 | 5457.964761 | 0.088678 | 19.73782241 | 4.302891 |
| ZIKV/Malaysia 4 hpi_1 | IL1A | 29 | 18941.07792 | 0.001531 | 1.517458139 | 0.601657 |
| ZIKV/Malaysia 8 hpi_1 | IL1A | 19 | 16004.07538 | 0.001187 | 0.899153518 | -0.15336 |
| ZIKV/Malaysia 10 hpi_1 | IL1A | 16 | 20365.09781 | 0.000786 | 0.480801611 | -1.05649 |
| ZIKV/Malaysia 24 hpi_1 | IL1A | 66 | 16824.24388 | 0.003923 | 3.108293068 | 1.636123 |
| ZIKV/Malaysia 48 hpi_1 | IL1A | 148 | 9016.561426 | 0.016414 | 8.707056819 | 3.122185 |
| ZIKV/Malaysia 4 hpi_2 | IL1A | 13 | 13310.81661 | 0.000977 | 0.967970373 | -0.04697 |
| ZIKV/Malaysia 8 hpi_2 | IL1A | 15 | 15300.45305 | 0.00098 | 0.742502301 | -0.42953 |
| ZIKV/Malaysia 10 hpi_2 | IL1A | 18 | 11873.49207 | 0.001516 | 0.927740403 | -0.10821 |
| ZIKV/Malaysia 24 hpi_2 | IL1A | 45 | 7114.262677 | 0.006325 | 5.011828448 | 2.325337 |
| ZIKV/Malaysia 48 hpi_2 | IL1A | 116 | 7202.033077 | 0.016107 | 8.543847469 | 3.094886 |
| ZIKV/Malaysia 4 hpi_3 | IL1A | 10 | 8019.493292 | 0.001247 | 1.235880511 | 0.305539 |
| ZIKV/Malaysia 8 hpi_3 | IL1A | 15 | 13577.51567 | 0.001105 | 0.836723144 | -0.25718 |
| ZIKV/Malaysia 10 hpi_3 | IL1A | 11 | 8780.599468 | 0.001253 | 0.766656726 | -0.38335 |
| ZIKV/Malaysia 24 hpi_3 | IL1A | 21 | 7775.628155 | 0.002701 | 2.139919275 | 1.097556 |
| ZIKV/Malaysia 48 hpi_3 | IL1A | 95 | 5457.964761 | 0.017406 | 9.233013845 | 3.206802 |

| | | | | | | |
|---|---|---|---|---|---|---|
| ZIKV/Malaysia 4 hpi_1 | IFIT1 | 485 | 18941.07792 | 0.025606 | 1.201618381 | 0.264979 |
| ZIKV/Malaysia 8 hpi_1 | IFIT1 | 1865 | 16004.07538 | 0.116533 | 7.500884555 | 2.907061 |
| ZIKV/Malaysia 10 hpi_1 | IFIT1 | 4268 | 20365.09781 | 0.209574 | 11.30245787 | 3.498565 |
| ZIKV/Malaysia 24 hpi_1 | IFIT1 | 29505 | 16824.24388 | 1.753719 | 52.18735429 | 5.705628 |
| ZIKV/Malaysia 48 hpi_1 | IFIT1 | 11329 | 9016.561426 | 1.256466 | 51.92392916 | 5.698328 |
| ZIKV/Malaysia 4 hpi_2 | IFIT1 | 204 | 13310.81661 | 0.015326 | 0.719208783 | -0.47552 |
| ZIKV/Malaysia 8 hpi_2 | IFIT1 | 406 | 15300.45305 | 0.026535 | 1.707992567 | 0.772302 |
| ZIKV/Malaysia 10 hpi_2 | IFIT1 | 770 | 11873.49207 | 0.06485 | 3.497415619 | 1.806289 |
| ZIKV/Malaysia 24 hpi_2 | IFIT1 | 6358 | 7114.262677 | 0.893698 | 26.5947458 | 4.733069 |
| ZIKV/Malaysia 48 hpi_2 | IFIT1 | 6486 | 7202.033077 | 0.900579 | 37.21677616 | 5.217881 |
| ZIKV/Malaysia 4 hpi_3 | IFIT1 | 141 | 8019.493292 | 0.017582 | 0.825090714 | -0.27738 |
| ZIKV/Malaysia 8 hpi_3 | IFIT1 | 902 | 13577.51567 | 0.066433 | 4.276125652 | 2.096304 |
| ZIKV/Malaysia 10 hpi_3 | IFIT1 | 1181 | 8780.599468 | 0.134501 | 7.253718825 | 2.858721 |
| ZIKV/Malaysia 24 hpi_3 | IFIT1 | 11589 | 7775.628155 | 1.490426 | 44.35225399 | 5.470936 |
| ZIKV/Malaysia 48 hpi_3 | IFIT1 | 7094 | 5457.964761 | 1.299752 | 53.71274832 | 5.747193 |
| ZIKV/Malaysia 4 hpi_1 | IFIT2 | 180 | 18941.07792 | 0.009503 | 1.286956455 | 0.363963 |
| ZIKV/Malaysia 8 hpi_1 | IFIT2 | 380 | 16004.07538 | 0.023744 | 3.94660921 | 1.980614 |
| ZIKV/Malaysia 10 hpi_1 | IFIT2 | 659 | 20365.09781 | 0.032359 | 5.254110014 | 2.393446 |
| ZIKV/Malaysia 24 hpi_1 | IFIT2 | 10408 | 16824.24388 | 0.618631 | 58.01357101 | 5.858319 |
| ZIKV/Malaysia 48 hpi_1 | IFIT2 | 6061 | 9016.561426 | 0.672207 | 67.49577805 | 6.076725 |
| ZIKV/Malaysia 4 hpi_2 | IFIT2 | 90 | 13310.81661 | 0.006761 | 0.915659167 | -0.12712 |
| ZIKV/Malaysia 8 hpi_2 | IFIT2 | 130 | 15300.45305 | 0.008496 | 1.412245431 | 0.497991 |
| ZIKV/Malaysia 10 hpi_2 | IFIT2 | 155 | 11873.49207 | 0.013054 | 2.119597895 | 1.083791 |
| ZIKV/Malaysia 24 hpi_2 | IFIT2 | 2043 | 7114.262677 | 0.28717 | 26.92999923 | 4.751142 |
| ZIKV/Malaysia 48 hpi_2 | IFIT2 | 4143 | 7202.033077 | 0.575254 | 57.76078559 | 5.852018 |

| | | | | | | |
|---|---|---|---|---|---|---|
| ZIKV/Malaysia 4 hpi_3 | IFIT2 | 62 | 8019.493292 | 0.007731 | 1.046985819 | 0.066242 |
| ZIKV/Malaysia 8 hpi_3 | IFIT2 | 191 | 13577.51567 | 0.014067 | 2.338213541 | 1.225407 |
| ZIKV/Malaysia 10 hpi_3 | IFIT2 | 160 | 8780.599468 | 0.018222 | 2.958666834 | 1.564947 |
| ZIKV/Malaysia 24 hpi_3 | IFIT2 | 3442 | 7775.628155 | 0.442665 | 41.51196133 | 5.375455 |
| ZIKV/Malaysia 48 hpi_3 | IFIT2 | 3700 | 5457.964761 | 0.677908 | 68.06820002 | 6.088909 |
| ZIKV/Malaysia 4 hpi_1 | DHX58 | 7 | 18941.07792 | 0.00037 | 1.041433786 | 0.058571 |
| ZIKV/Malaysia 8 hpi_1 | DHX58 | 3 | 16004.07538 | 0.000187 | 0.412759498 | -1.27663 |
| ZIKV/Malaysia 10 hpi_1 | DHX58 | 15 | 20365.09781 | 0.000737 | 1.537151735 | 0.62026 |
| ZIKV/Malaysia 24 hpi_1 | DHX58 | 138 | 16824.24388 | 0.008202 | 20.36369141 | 4.347927 |
| ZIKV/Malaysia 48 hpi_1 | DHX58 | 99 | 9016.561426 | 0.01098 | 14.78727432 | 3.886284 |
| ZIKV/Malaysia 4 hpi_2 | DHX58 | 6 | 13310.81661 | 0.000451 | 1.270237308 | 0.345098 |
| ZIKV/Malaysia 8 hpi_2 | DHX58 | 5 | 15300.45305 | 0.000327 | 0.719568466 | -0.4748 |
| ZIKV/Malaysia 10 hpi_2 | DHX58 | 11 | 11873.49207 | 0.000926 | 1.933419967 | 0.951155 |
| ZIKV/Malaysia 24 hpi_2 | DHX58 | 35 | 7114.262677 | 0.00492 | 12.21380899 | 3.610441 |
| ZIKV/Malaysia 48 hpi_2 | DHX58 | 61 | 7202.033077 | 0.00847 | 11.40692547 | 3.511838 |
| ZIKV/Malaysia 4 hpi_3 | DHX58 | 2 | 8019.493292 | 0.000249 | 0.702783216 | -0.50885 |
| ZIKV/Malaysia 8 hpi_3 | DHX58 | 4 | 13577.51567 | 0.000295 | 0.648703271 | -0.62437 |
| ZIKV/Malaysia 10 hpi_3 | DHX58 | 6 | 8780.599468 | 0.000683 | 1.426064156 | 0.512039 |
| ZIKV/Malaysia 24 hpi_3 | DHX58 | 57 | 7775.628155 | 0.007331 | 18.19920211 | 4.185803 |
| ZIKV/Malaysia 48 hpi_3 | DHX58 | 67 | 5457.964761 | 0.012276 | 16.5324781 | 4.047231 |
| ZIKV/Malaysia 4 hpi_1 | MX2 | 3 | 18941.07792 | 0.000158 | 1.114227227 | 0.156043 |
| ZIKV/Malaysia 8 hpi_1 | MX2 | 11 | 16004.07538 | 0.000687 | 6.410369233 | 2.680407 |
| ZIKV/Malaysia 10 hpi_1 | MX2 | 26 | 20365.09781 | 0.001277 | 4.451940755 | 2.154434 |
| ZIKV/Malaysia 24 hpi_1 | MX2 | 277 | 16824.24388 | 0.016464 | 54.76538535 | 5.775192 |
| ZIKV/Malaysia 48 hpi_1 | MX2 | 50 | 9016.561426 | 0.005545 | 15.8767239 | 3.988841 |

| | | | | | | |
|---|---|---|---|---|---|---|
| ZIKV/Malaysia 4 hpi_2 | MX2 | 1 | 13310.81661 | 7.51E-05 | 0.52850914 | -0.92 |
| ZIKV/Malaysia 8 hpi_2 | MX2 | 2 | 15300.45305 | 0.000131 | 1.219120554 | 0.285841 |
| ZIKV/Malaysia 10 hpi_2 | MX2 | 4 | 11873.49207 | 0.000337 | 1.174746213 | 0.232349 |
| ZIKV/Malaysia 24 hpi_2 | MX2 | 46 | 7114.262677 | 0.006466 | 21.50749692 | 4.426768 |
| ZIKV/Malaysia 48 hpi_2 | MX2 | 8 | 7202.033077 | 0.001111 | 3.180289893 | 1.669158 |
| ZIKV/Malaysia 4 hpi_3 | MX2 | 0.375899675 | 8019.493292 | 4.69E-05 | 0.329748041 | -1.60056 |
| ZIKV/Malaysia 8 hpi_3 | MX2 | 4 | 13577.51567 | 0.000295 | 2.747645041 | 1.458196 |
| ZIKV/Malaysia 10 hpi_3 | MX2 | 11 | 8780.599468 | 0.001253 | 4.368486991 | 2.127134 |
| ZIKV/Malaysia 24 hpi_3 | MX2 | 73 | 7775.628155 | 0.009388 | 31.22836958 | 4.964785 |
| ZIKV/Malaysia 48 hpi_3 | MX2 | 38 | 5457.964761 | 0.006962 | 19.93355244 | 4.317127 |
| ZIKV/Malaysia 4 hpi_1 | IRF2 | 1065 | 18941.07792 | 0.056227 | 1.142917014 | 0.192721 |
| ZIKV/Malaysia 8 hpi_1 | IRF2 | 1045 | 16004.07538 | 0.065296 | 1.104120988 | 0.142898 |
| ZIKV/Malaysia 10 hpi_1 | IRF2 | 1367 | 20365.09781 | 0.067125 | 1.038094958 | 0.053938 |
| ZIKV/Malaysia 24 hpi_1 | IRF2 | 1654 | 16824.24388 | 0.098311 | 1.409678069 | 0.495366 |
| ZIKV/Malaysia 48 hpi_1 | IRF2 | 1147 | 9016.561426 | 0.12721 | 1.315980061 | 0.396138 |
| ZIKV/Malaysia 4 hpi_2 | IRF2 | 797 | 13310.81661 | 0.059876 | 1.217091985 | 0.283438 |
| ZIKV/Malaysia 8 hpi_2 | IRF2 | 914 | 15300.45305 | 0.059737 | 1.010119763 | 0.014526 |
| ZIKV/Malaysia 10 hpi_2 | IRF2 | 687 | 11873.49207 | 0.05786 | 0.89481517 | -0.16034 |
| ZIKV/Malaysia 24 hpi_2 | IRF2 | 587 | 7114.262677 | 0.08251 | 1.183118371 | 0.242594 |
| ZIKV/Malaysia 48 hpi_2 | IRF2 | 777 | 7202.033077 | 0.107886 | 1.116073366 | 0.158432 |
| ZIKV/Malaysia 4 hpi_3 | IRF2 | 474 | 8019.493292 | 0.059106 | 1.20143753 | 0.264762 |
| ZIKV/Malaysia 8 hpi_3 | IRF2 | 759 | 13577.51567 | 0.055901 | 0.945262494 | -0.08121 |
| ZIKV/Malaysia 10 hpi_3 | IRF2 | 581 | 8780.599468 | 0.066169 | 1.023309563 | 0.033243 |
| ZIKV/Malaysia 24 hpi_3 | IRF2 | 719 | 7775.628155 | 0.092468 | 1.325908027 | 0.406981 |
| ZIKV/Malaysia 48 hpi_3 | IRF2 | 640 | 5457.964761 | 0.11726 | 1.213042686 | 0.27863 |

| | | | | | | |
|---|---|---|---|---|---|---|
| ZIKV/Malaysia 4 hpi_1 | IFNL1 | 41 | 18941.07792 | 0.002165 | 1.079979163 | 0.111003 |
| ZIKV/Malaysia 8 hpi_1 | IFNL1 | 42 | 16004.07538 | 0.002624 | 1.516466074 | 0.600713 |
| ZIKV/Malaysia 10 hpi_1 | IFNL1 | 39 | 20365.09781 | 0.001915 | 1.049710491 | 0.069991 |
| ZIKV/Malaysia 24 hpi_1 | IFNL1 | 699 | 16824.24388 | 0.041547 | 22.08638161 | 4.465085 |
| ZIKV/Malaysia 48 hpi_1 | IFNL1 | 1277 | 9016.561426 | 0.141628 | 62.35387851 | 5.962407 |
| ZIKV/Malaysia 4 hpi_2 | IFNL1 | 18 | 13310.81661 | 0.001352 | 0.6746896 | -0.5677 |
| ZIKV/Malaysia 8 hpi_2 | IFNL1 | 35 | 15300.45305 | 0.002288 | 1.321836533 | 0.402544 |
| ZIKV/Malaysia 10 hpi_2 | IFNL1 | 32 | 11873.49207 | 0.002695 | 1.477280424 | 0.562944 |
| ZIKV/Malaysia 24 hpi_2 | IFNL1 | 242 | 7114.262677 | 0.034016 | 18.08291416 | 4.176555 |
| ZIKV/Malaysia 48 hpi_2 | IFNL1 | 845 | 7202.033077 | 0.117328 | 51.65532737 | 5.690845 |
| ZIKV/Malaysia 4 hpi_3 | IFNL1 | 15 | 8019.493292 | 0.00187 | 0.933212487 | -0.09972 |
| ZIKV/Malaysia 8 hpi_3 | IFNL1 | 27 | 13577.51567 | 0.001989 | 1.149099004 | 0.200503 |
| ZIKV/Malaysia 10 hpi_3 | IFNL1 | 25 | 8780.599468 | 0.002847 | 1.56065631 | 0.642153 |
| ZIKV/Malaysia 24 hpi_3 | IFNL1 | 294 | 7775.628155 | 0.03781 | 20.09994171 | 4.329119 |
| ZIKV/Malaysia 48 hpi_3 | IFNL1 | 748 | 5457.964761 | 0.137047 | 60.33709427 | 5.914973 |
| ZIKV/Malaysia 4 hpi_1 | EIF2AK2 | 5912 | 18941.07792 | 0.312126 | 1.047422583 | 0.066844 |
| ZIKV/Malaysia 8 hpi_1 | EIF2AK2 | 6067 | 16004.07538 | 0.379091 | 1.166049689 | 0.221629 |
| ZIKV/Malaysia 10 hpi_1 | EIF2AK2 | 8383 | 20365.09781 | 0.411636 | 1.18544354 | 0.245427 |
| ZIKV/Malaysia 24 hpi_1 | EIF2AK2 | 10120 | 16824.24388 | 0.601513 | 1.702666945 | 0.767796 |
| ZIKV/Malaysia 48 hpi_1 | EIF2AK2 | 4200 | 9016.561426 | 0.46581 | 1.365565645 | 0.449499 |
| ZIKV/Malaysia 4 hpi_2 | EIF2AK2 | 4046 | 13310.81661 | 0.303963 | 1.020031015 | 0.028613 |
| ZIKV/Malaysia 8 hpi_2 | EIF2AK2 | 5377 | 15300.45305 | 0.351428 | 1.080959436 | 0.112312 |
| ZIKV/Malaysia 10 hpi_2 | EIF2AK2 | 4325 | 11873.49207 | 0.364257 | 1.049000159 | 0.069015 |
| ZIKV/Malaysia 24 hpi_2 | EIF2AK2 | 3427 | 7114.262677 | 0.481708 | 1.363543369 | 0.447361 |
| ZIKV/Malaysia 48 hpi_2 | EIF2AK2 | 2594 | 7202.033077 | 0.360176 | 1.055891023 | 0.078461 |

| | | | | | | |
|---|---|---|---|---|---|---|
| ZIKV/Malaysia 4 hpi_3 | EIF2AK2 | 2416 | 8019.493292 | 0.301266 | 1.010979152 | 0.015753 |
| ZIKV/Malaysia 8 hpi_3 | EIF2AK2 | 4632 | 13577.51567 | 0.341152 | 1.049353678 | 0.069501 |
| ZIKV/Malaysia 10 hpi_3 | EIF2AK2 | 3266 | 8780.599468 | 0.371956 | 1.071173751 | 0.099193 |
| ZIKV/Malaysia 24 hpi_3 | EIF2AK2 | 4340 | 7775.628155 | 0.558154 | 1.579934176 | 0.659864 |
| ZIKV/Malaysia 48 hpi_3 | EIF2AK2 | 2385 | 5457.964761 | 0.436976 | 1.281037649 | 0.357313 |
| ZIKV/Malaysia 4 hpi_1 | GBP2 | 188 | 18941.07792 | 0.009926 | 1.060861939 | 0.085237 |
| ZIKV/Malaysia 8 hpi_1 | GBP2 | 182 | 16004.07538 | 0.011372 | 1.362131182 | 0.445866 |
| ZIKV/Malaysia 10 hpi_1 | GBP2 | 219 | 20365.09781 | 0.010754 | 1.129544709 | 0.175741 |
| ZIKV/Malaysia 24 hpi_1 | GBP2 | 403 | 16824.24388 | 0.023954 | 1.729772944 | 0.790583 |
| ZIKV/Malaysia 48 hpi_1 | GBP2 | 993 | 9016.561426 | 0.110131 | 4.368049121 | 2.126989 |
| ZIKV/Malaysia 4 hpi_2 | GBP2 | 127 | 13310.81661 | 0.009541 | 1.019775868 | 0.028252 |
| ZIKV/Malaysia 8 hpi_2 | GBP2 | 131 | 15300.45305 | 0.008562 | 1.025522375 | 0.036359 |
| ZIKV/Malaysia 10 hpi_2 | GBP2 | 134 | 11873.49207 | 0.011286 | 1.185419707 | 0.245398 |
| ZIKV/Malaysia 24 hpi_2 | GBP2 | 129 | 7114.262677 | 0.018133 | 1.309421365 | 0.388929 |
| ZIKV/Malaysia 48 hpi_2 | GBP2 | 559 | 7202.033077 | 0.077617 | 3.078476956 | 1.622217 |
| ZIKV/Malaysia 4 hpi_3 | GBP2 | 86 | 8019.493292 | 0.010724 | 1.146191629 | 0.196848 |
| ZIKV/Malaysia 8 hpi_3 | GBP2 | 125 | 13577.51567 | 0.009206 | 1.102726561 | 0.141075 |
| ZIKV/Malaysia 10 hpi_3 | GBP2 | 79 | 8780.599468 | 0.008997 | 0.945036832 | -0.08156 |
| ZIKV/Malaysia 24 hpi_3 | GBP2 | 172 | 7775.628155 | 0.02212 | 1.597395925 | 0.675722 |
| ZIKV/Malaysia 48 hpi_3 | GBP2 | 434 | 5457.964761 | 0.079517 | 3.153829514 | 1.657105 |
| ZIKV/Malaysia 4 hpi_1 | TNF | 16 | 18941.07792 | 0.000845 | 1.663366879 | 0.734106 |
| ZIKV/Malaysia 8 hpi_1 | TNF | 14 | 16004.07538 | 0.000875 | 0.998954986 | -0.00151 |
| ZIKV/Malaysia 10 hpi_1 | TNF | 19 | 20365.09781 | 0.000933 | 1.310429435 | 0.39004 |
| ZIKV/Malaysia 24 hpi_1 | TNF | 46 | 16824.24388 | 0.002734 | 2.766175362 | 1.467893 |
| ZIKV/Malaysia 48 hpi_1 | TNF | 34 | 9016.561426 | 0.003771 | 5.289060053 | 2.403011 |

| | | | | | | |
|---|---|---|---|---|---|---|
| ZIKV/Malaysia 4 hpi_2 | TNF | 7 | 13310.81661 | 0.000526 | 1.035538137 | 0.050381 |
| ZIKV/Malaysia 8 hpi_2 | TNF | 10 | 15300.45305 | 0.000654 | 0.746352825 | -0.42207 |
| ZIKV/Malaysia 10 hpi_2 | TNF | 7 | 11873.49207 | 0.00059 | 0.828068211 | -0.27218 |
| ZIKV/Malaysia 24 hpi_2 | TNF | 6 | 7114.262677 | 0.000843 | 0.853254891 | -0.22895 |
| ZIKV/Malaysia 48 hpi_2 | TNF | 27 | 7202.033077 | 0.003749 | 5.258346242 | 2.394609 |
| ZIKV/Malaysia 4 hpi_3 | TNF | 5 | 8019.493292 | 0.000623 | 1.227710113 | 0.29597 |
| ZIKV/Malaysia 8 hpi_3 | TNF | 13 | 13577.51567 | 0.000957 | 1.093380971 | 0.128796 |
| ZIKV/Malaysia 10 hpi_3 | TNF | 10 | 8780.599468 | 0.001139 | 1.599640429 | 0.677748 |
| ZIKV/Malaysia 24 hpi_3 | TNF | 12 | 7775.628155 | 0.001543 | 1.561360524 | 0.642804 |
| ZIKV/Malaysia 48 hpi_3 | TNF | 13 | 5457.964761 | 0.002382 | 3.340820576 | 1.740203 |
| ZIKV/Malaysia 4 hpi_1 | RSAD2 | 63 | 18941.07792 | 0.003326 | 0.987223388 | -0.01855 |
| ZIKV/Malaysia 8 hpi_1 | RSAD2 | 57 | 16004.07538 | 0.003562 | 1.086371943 | 0.119518 |
| ZIKV/Malaysia 10 hpi_1 | RSAD2 | 99 | 20365.09781 | 0.004861 | 1.455200477 | 0.541218 |
| ZIKV/Malaysia 24 hpi_1 | RSAD2 | 701 | 16824.24388 | 0.041666 | 12.19090303 | 3.607733 |
| ZIKV/Malaysia 48 hpi_1 | RSAD2 | 253 | 9016.561426 | 0.028059 | 6.990831356 | 2.805464 |
| ZIKV/Malaysia 4 hpi_2 | RSAD2 | 24 | 13310.81661 | 0.001803 | 0.535163048 | -0.90195 |
| ZIKV/Malaysia 8 hpi_2 | RSAD2 | 47 | 15300.45305 | 0.003072 | 0.936974649 | -0.09392 |
| ZIKV/Malaysia 10 hpi_2 | RSAD2 | 34 | 11873.49207 | 0.002864 | 0.857185043 | -0.22232 |
| ZIKV/Malaysia 24 hpi_2 | RSAD2 | 238 | 7114.262677 | 0.033454 | 9.788146807 | 3.291036 |
| ZIKV/Malaysia 48 hpi_2 | RSAD2 | 376 | 7202.033077 | 0.052207 | 13.00714505 | 3.701232 |
| ZIKV/Malaysia 4 hpi_3 | RSAD2 | 34 | 8019.493292 | 0.00424 | 1.2583793 | 0.331567 |
| ZIKV/Malaysia 8 hpi_3 | RSAD2 | 49 | 13577.51567 | 0.003609 | 1.100804106 | 0.138558 |
| ZIKV/Malaysia 10 hpi_3 | RSAD2 | 33 | 8780.599468 | 0.003758 | 1.125029491 | 0.169963 |
| ZIKV/Malaysia 24 hpi_3 | RSAD2 | 329 | 7775.628155 | 0.042312 | 12.37980569 | 3.629917 |
| ZIKV/Malaysia 48 hpi_3 | RSAD2 | 353 | 5457.964761 | 0.064676 | 16.1136241 | 4.010209 |

| | | | | | | |
|---|---|---|---|---|---|---|
| ZIKV/Malaysia 4 hpi_1 | DDX58 | 1505 | 18941.07792 | 0.079457 | 1.344943006 | 0.427545 |
| ZIKV/Malaysia 8 hpi_1 | DDX58 | 2022 | 16004.07538 | 0.126343 | 1.890362987 | 0.918663 |
| ZIKV/Malaysia 10 hpi_1 | DDX58 | 3418 | 20365.09781 | 0.167836 | 2.385039031 | 1.254013 |
| ZIKV/Malaysia 24 hpi_1 | DDX58 | 11137 | 16824.24388 | 0.661961 | 9.214439136 | 3.203896 |
| ZIKV/Malaysia 48 hpi_1 | DDX58 | 4762 | 9016.561426 | 0.528139 | 7.495181046 | 2.905963 |
| ZIKV/Malaysia 4 hpi_2 | DDX58 | 681 | 13310.81661 | 0.051161 | 0.865993204 | -0.20757 |
| ZIKV/Malaysia 8 hpi_2 | DDX58 | 987 | 15300.45305 | 0.064508 | 0.965178201 | -0.05113 |
| ZIKV/Malaysia 10 hpi_2 | DDX58 | 939 | 11873.49207 | 0.079084 | 1.123820781 | 0.168412 |
| ZIKV/Malaysia 24 hpi_2 | DDX58 | 2603 | 7114.262677 | 0.365885 | 5.093080176 | 2.348538 |
| ZIKV/Malaysia 48 hpi_2 | DDX58 | 2752 | 7202.033077 | 0.382114 | 5.422842615 | 2.439049 |
| ZIKV/Malaysia 4 hpi_3 | DDX58 | 505 | 8019.493292 | 0.062972 | 1.065900145 | 0.092072 |
| ZIKV/Malaysia 8 hpi_3 | DDX58 | 1175 | 13577.51567 | 0.08654 | 1.29482834 | 0.372761 |
| ZIKV/Malaysia 10 hpi_3 | DDX58 | 1075 | 8780.599468 | 0.122429 | 1.739779583 | 0.798905 |
| ZIKV/Malaysia 24 hpi_3 | DDX58 | 4072 | 7775.628155 | 0.523688 | 7.289681053 | 2.865856 |
| ZIKV/Malaysia 48 hpi_3 | DDX58 | 3063 | 5457.964761 | 0.561198 | 7.964342932 | 2.993555 |
| ZIKV/Malaysia 4 hpi_1 | TRIM25 | 4687 | 18941.07792 | 0.247452 | 1.063638289 | 0.089008 |
| ZIKV/Malaysia 8 hpi_1 | TRIM25 | 4411 | 16004.07538 | 0.275617 | 1.141745872 | 0.191242 |
| ZIKV/Malaysia 10 hpi_1 | TRIM25 | 5834 | 20365.09781 | 0.286471 | 1.17523992 | 0.232955 |
| ZIKV/Malaysia 24 hpi_1 | TRIM25 | 6375 | 16824.24388 | 0.378917 | 1.62037586 | 0.696328 |
| ZIKV/Malaysia 48 hpi_1 | TRIM25 | 2521 | 9016.561426 | 0.279597 | 1.445783769 | 0.531852 |
| ZIKV/Malaysia 4 hpi_2 | TRIM25 | 3093 | 13310.81661 | 0.232367 | 0.998800889 | -0.00173 |
| ZIKV/Malaysia 8 hpi_2 | TRIM25 | 3813 | 15300.45305 | 0.249208 | 1.032346513 | 0.045927 |
| ZIKV/Malaysia 10 hpi_2 | TRIM25 | 2980 | 11873.49207 | 0.250979 | 1.029637635 | 0.042137 |
| ZIKV/Malaysia 24 hpi_2 | TRIM25 | 2246 | 7114.262677 | 0.315704 | 1.350053522 | 0.433017 |
| ZIKV/Malaysia 48 hpi_2 | TRIM25 | 1570 | 7202.033077 | 0.217994 | 1.127238947 | 0.172793 |

| | | | | | | |
|---|---|---|---|---|---|---|
| ZIKV/Malaysia 4 hpi_3 | TRIM25 | 1857 | 8019.493292 | 0.231561 | 0.995333624 | -0.00675 |
| ZIKV/Malaysia 8 hpi_3 | TRIM25 | 3496 | 13577.51567 | 0.257485 | 1.06663073 | 0.093061 |
| ZIKV/Malaysia 10 hpi_3 | TRIM25 | 2337 | 8780.599468 | 0.266155 | 1.0918957 | 0.126835 |
| ZIKV/Malaysia 24 hpi_3 | TRIM25 | 2592 | 7775.628155 | 0.333349 | 1.425511234 | 0.511479 |
| ZIKV/Malaysia 48 hpi_3 | TRIM25 | 1379 | 5457.964761 | 0.252658 | 1.306486672 | 0.385692 |
| ZIKV/Malaysia 4 hpi_1 | CCL2 | 2871 | 18941.07792 | 0.151575 | 1.33376014 | 0.415499 |
| ZIKV/Malaysia 8 hpi_1 | CCL2 | 1951 | 16004.07538 | 0.121906 | 0.855356635 | -0.2254 |
| ZIKV/Malaysia 10 hpi_1 | CCL2 | 2503 | 20365.09781 | 0.122906 | 1.051850433 | 0.07293 |
| ZIKV/Malaysia 24 hpi_1 | CCL2 | 1119 | 16824.24388 | 0.066511 | 1.237328915 | 0.307229 |
| ZIKV/Malaysia 48 hpi_1 | CCL2 | 1041 | 9016.561426 | 0.115454 | 3.967039701 | 1.988063 |
| ZIKV/Malaysia 4 hpi_2 | CCL2 | 2551 | 13310.81661 | 0.191649 | 1.686378246 | 0.753928 |
| ZIKV/Malaysia 8 hpi_2 | CCL2 | 2347 | 15300.45305 | 0.153394 | 1.076290103 | 0.106067 |
| ZIKV/Malaysia 10 hpi_2 | CCL2 | 1634 | 11873.49207 | 0.137617 | 1.177750308 | 0.236034 |
| ZIKV/Malaysia 24 hpi_2 | CCL2 | 585 | 7114.262677 | 0.082229 | 1.529736398 | 0.613283 |
| ZIKV/Malaysia 48 hpi_2 | CCL2 | 1192 | 7202.033077 | 0.165509 | 5.686930316 | 2.50765 |
| ZIKV/Malaysia 4 hpi_3 | CCL2 | 1394 | 8019.493292 | 0.173826 | 1.529554929 | 0.613112 |
| ZIKV/Malaysia 8 hpi_3 | CCL2 | 2109 | 13577.51567 | 0.15533 | 1.089875311 | 0.124163 |
| ZIKV/Malaysia 10 hpi_3 | CCL2 | 1241 | 8780.599468 | 0.141334 | 1.209559551 | 0.274482 |
| ZIKV/Malaysia 24 hpi_3 | CCL2 | 712 | 7775.628155 | 0.091568 | 1.703472554 | 0.768479 |
| ZIKV/Malaysia 48 hpi_3 | CCL2 | 1151 | 5457.964761 | 0.210884 | 7.246050547 | 2.857195 |
| ZIKV/Malaysia 4 hpi_1 | CCL4 | 12 | 18941.07792 | 0.000634 | 0.886805953 | -0.17331 |
| ZIKV/Malaysia 8 hpi_1 | CCL4 | 10 | 16004.07538 | 0.000625 | 1.058712564 | 0.082311 |
| ZIKV/Malaysia 10 hpi_1 | CCL4 | 27 | 20365.09781 | 0.001326 | 1.76703474 | 0.82133 |
| ZIKV/Malaysia 24 hpi_1 | CCL4 | 35 | 16824.24388 | 0.00208 | 2.070657495 | 1.050089 |
| ZIKV/Malaysia 48 hpi_1 | CCL4 | 29 | 9016.561426 | 0.003216 | 3.346407768 | 1.742613 |

| | | | | | | |
|---|---|---|---|---|---|---|
| ZIKV/Malaysia 4 hpi_2 | CCL4 | 7 | 13310.81661 | 0.000526 | 0.73611452 | -0.442 |
| ZIKV/Malaysia 8 hpi_2 | CCL4 | 11 | 15300.45305 | 0.000719 | 1.218139567 | 0.284679 |
| ZIKV/Malaysia 10 hpi_2 | CCL4 | 5 | 11873.49207 | 0.000421 | 0.561253887 | -0.83327 |
| ZIKV/Malaysia 24 hpi_2 | CCL4 | 14 | 7114.262677 | 0.001968 | 1.95872704 | 0.969916 |
| ZIKV/Malaysia 48 hpi_2 | CCL4 | 38 | 7202.033077 | 0.005276 | 5.489721243 | 2.456733 |
| ZIKV/Malaysia 4 hpi_3 | CCL4 | 3 | 8019.493292 | 0.000374 | 0.523632231 | -0.93337 |
| ZIKV/Malaysia 8 hpi_3 | CCL4 | 8 | 13577.51567 | 0.000589 | 0.998339672 | -0.0024 |
| ZIKV/Malaysia 10 hpi_3 | CCL4 | 9 | 8780.599468 | 0.001025 | 1.366111561 | 0.450075 |
| ZIKV/Malaysia 24 hpi_3 | CCL4 | 11 | 7775.628155 | 0.001415 | 1.408098322 | 0.493748 |
| ZIKV/Malaysia 48 hpi_3 | CCL4 | 41 | 5457.964761 | 0.007512 | 7.815826981 | 2.966399 |
| ZIKV/Malaysia 4 hpi_1 | OAS1 | 2723 | 18941.07792 | 0.143762 | 1.0463606 | 0.06538 |
| ZIKV/Malaysia 8 hpi_1 | OAS1 | 3554 | 16004.07538 | 0.222068 | 1.214701287 | 0.280602 |
| ZIKV/Malaysia 10 hpi_1 | OAS1 | 4818 | 20365.09781 | 0.236581 | 1.322260677 | 0.403007 |
| ZIKV/Malaysia 24 hpi_1 | OAS1 | 10982 | 16824.24388 | 0.652749 | 4.097465938 | 2.034732 |
| ZIKV/Malaysia 48 hpi_1 | OAS1 | 6305 | 9016.561426 | 0.699269 | 3.662120395 | 1.872679 |
| ZIKV/Malaysia 4 hpi_2 | OAS1 | 1892 | 13310.81661 | 0.14214 | 1.034558039 | 0.049015 |
| ZIKV/Malaysia 8 hpi_2 | OAS1 | 2977 | 15300.45305 | 0.194569 | 1.064283185 | 0.089882 |
| ZIKV/Malaysia 10 hpi_2 | OAS1 | 2384 | 11873.49207 | 0.200783 | 1.12218529 | 0.166311 |
| ZIKV/Malaysia 24 hpi_2 | OAS1 | 2942 | 7114.262677 | 0.413535 | 2.595865818 | 1.376216 |
| ZIKV/Malaysia 48 hpi_2 | OAS1 | 3087 | 7202.033077 | 0.428629 | 2.244760391 | 1.166561 |
| ZIKV/Malaysia 4 hpi_3 | OAS1 | 1187 | 8019.493292 | 0.148014 | 1.077313787 | 0.107439 |
| ZIKV/Malaysia 8 hpi_3 | OAS1 | 2606 | 13577.51567 | 0.191935 | 1.049872972 | 0.070215 |
| ZIKV/Malaysia 10 hpi_3 | OAS1 | 1965 | 8780.599468 | 0.223789 | 1.25076343 | 0.322809 |
| ZIKV/Malaysia 24 hpi_3 | OAS1 | 4181 | 7775.628155 | 0.537706 | 3.375313774 | 1.755022 |
| ZIKV/Malaysia 48 hpi_3 | OAS1 | 3156 | 5457.964761 | 0.578238 | 3.028271017 | 1.598494 |

| | | | | | | |
|---|---|---|---|---|---|---|
| ZIKV/Malaysia 4 hpi_1 | ISG20 | 557 | 18941.07792 | 0.029407 | 1.117427523 | 0.160181 |
| ZIKV/Malaysia 8 hpi_1 | ISG20 | 382 | 16004.07538 | 0.023869 | 1.000238036 | 0.000343 |
| ZIKV/Malaysia 10 hpi_1 | ISG20 | 471 | 20365.09781 | 0.023128 | 0.961378407 | -0.05682 |
| ZIKV/Malaysia 24 hpi_1 | ISG20 | 2742 | 16824.24388 | 0.162979 | 4.254669165 | 2.089047 |
| ZIKV/Malaysia 48 hpi_1 | ISG20 | 2239 | 9016.561426 | 0.248321 | 4.870088065 | 2.283948 |
| ZIKV/Malaysia 4 hpi_2 | ISG20 | 331 | 13310.81661 | 0.024867 | 0.944913717 | -0.08175 |
| ZIKV/Malaysia 8 hpi_2 | ISG20 | 402 | 15300.45305 | 0.026274 | 1.101012763 | 0.138831 |
| ZIKV/Malaysia 10 hpi_2 | ISG20 | 273 | 11873.49207 | 0.022992 | 0.955749627 | -0.0653 |
| ZIKV/Malaysia 24 hpi_2 | ISG20 | 878 | 7114.262677 | 0.123414 | 3.221799576 | 1.687867 |
| ZIKV/Malaysia 48 hpi_2 | ISG20 | 1547 | 7202.033077 | 0.2148 | 4.21268386 | 2.07474 |
| ZIKV/Malaysia 4 hpi_3 | ISG20 | 270 | 8019.493292 | 0.033668 | 1.279339165 | 0.355399 |
| ZIKV/Malaysia 8 hpi_3 | ISG20 | 337 | 13577.51567 | 0.02482 | 1.040112173 | 0.056739 |
| ZIKV/Malaysia 10 hpi_3 | ISG20 | 244 | 8780.599468 | 0.027789 | 1.155116043 | 0.208038 |
| ZIKV/Malaysia 24 hpi_3 | ISG20 | 1235 | 7775.628155 | 0.15883 | 4.146344421 | 2.05184 |
| ZIKV/Malaysia 48 hpi_3 | ISG20 | 1430 | 5457.964761 | 0.262002 | 5.138412634 | 2.361323 |
| ZIKV/Malaysia 4 hpi_1 | IRF7 | 57 | 18941.07792 | 0.003009 | 1.114414453 | 0.156286 |
| ZIKV/Malaysia 8 hpi_1 | IRF7 | 75 | 16004.07538 | 0.004686 | 1.904651595 | 0.929527 |
| ZIKV/Malaysia 10 hpi_1 | IRF7 | 126 | 20365.09781 | 0.006187 | 2.280834573 | 1.189562 |
| ZIKV/Malaysia 24 hpi_1 | IRF7 | 497 | 16824.24388 | 0.029541 | 10.41701912 | 3.380871 |
| ZIKV/Malaysia 48 hpi_1 | IRF7 | 174 | 9016.561426 | 0.019298 | 4.564380994 | 2.190419 |
| ZIKV/Malaysia 4 hpi_2 | IRF7 | 34 | 13310.81661 | 0.002554 | 0.945912115 | -0.08022 |
| ZIKV/Malaysia 8 hpi_2 | IRF7 | 42 | 15300.45305 | 0.002745 | 1.11565488 | 0.157891 |
| ZIKV/Malaysia 10 hpi_2 | IRF7 | 57 | 11873.49207 | 0.004801 | 1.769726409 | 0.823526 |
| ZIKV/Malaysia 24 hpi_2 | IRF7 | 124 | 7114.262677 | 0.01743 | 6.146309374 | 2.61972 |
| ZIKV/Malaysia 48 hpi_2 | IRF7 | 94 | 7202.033077 | 0.013052 | 3.087068936 | 1.626238 |

| | | | | | | |
|---|---|---|---|---|---|---|
| ZIKV/Malaysia 4 hpi_3 | IRF7 | 23 | 8019.493292 | 0.002868 | 1.062080606 | 0.086893 |
| ZIKV/Malaysia 8 hpi_3 | IRF7 | 52 | 13577.51567 | 0.00383 | 1.556567292 | 0.638368 |
| ZIKV/Malaysia 10 hpi_3 | IRF7 | 47 | 8780.599468 | 0.005353 | 1.973256007 | 0.980578 |
| ZIKV/Malaysia 24 hpi_3 | IRF7 | 173 | 7775.628155 | 0.022249 | 7.845727994 | 2.971907 |
| ZIKV/Malaysia 48 hpi_3 | IRF7 | 112 | 5457.964761 | 0.02052 | 4.853565345 | 2.279045 |
| ZIKV/Malaysia 4 hpi_1 | ISG15 | 294 | 18941.07792 | 0.015522 | 1.028055454 | 0.039918 |
| ZIKV/Malaysia 8 hpi_1 | ISG15 | 568 | 16004.07538 | 0.035491 | 2.757796211 | 1.463516 |
| ZIKV/Malaysia 10 hpi_1 | ISG15 | 1071 | 20365.09781 | 0.05259 | 3.290140909 | 1.718149 |
| ZIKV/Malaysia 24 hpi_1 | ISG15 | 9482 | 16824.24388 | 0.563591 | 35.78796 | 5.161402 |
| ZIKV/Malaysia 48 hpi_1 | ISG15 | 6597 | 9016.561426 | 0.731654 | 58.03060075 | 5.858742 |
| ZIKV/Malaysia 4 hpi_2 | ISG15 | 119 | 13310.81661 | 0.00894 | 0.59212877 | -0.75602 |
| ZIKV/Malaysia 8 hpi_2 | ISG15 | 216 | 15300.45305 | 0.014117 | 1.09696781 | 0.133521 |
| ZIKV/Malaysia 10 hpi_2 | ISG15 | 232 | 11873.49207 | 0.019539 | 1.222421687 | 0.289742 |
| ZIKV/Malaysia 24 hpi_2 | ISG15 | 2121 | 7114.262677 | 0.298133 | 18.93142563 | 4.242711 |
| ZIKV/Malaysia 48 hpi_2 | ISG15 | 2697 | 7202.033077 | 0.374478 | 29.70143025 | 4.89246 |
| ZIKV/Malaysia 4 hpi_3 | ISG15 | 141 | 8019.493292 | 0.017582 | 1.164517678 | 0.219733 |
| ZIKV/Malaysia 8 hpi_3 | ISG15 | 320 | 13577.51567 | 0.023568 | 1.831361537 | 0.872917 |
| ZIKV/Malaysia 10 hpi_3 | ISG15 | 327 | 8780.599468 | 0.037241 | 2.329888369 | 1.220261 |
| ZIKV/Malaysia 24 hpi_3 | ISG15 | 3416 | 7775.628155 | 0.439321 | 27.89683449 | 4.80203 |
| ZIKV/Malaysia 48 hpi_3 | ISG15 | 3172 | 5457.964761 | 0.581169 | 46.095017 | 5.526539 |
| ZIKV/Malaysia 4 hpi_1 | IL6 | 616 | 18941.07792 | 0.032522 | 2.064938184 | 1.046099 |
| ZIKV/Malaysia 8 hpi_1 | IL6 | 125 | 16004.07538 | 0.007811 | 1.535727538 | 0.618922 |
| ZIKV/Malaysia 10 hpi_1 | IL6 | 102 | 20365.09781 | 0.005009 | 1.400805978 | 0.486257 |
| ZIKV/Malaysia 24 hpi_1 | IL6 | 554 | 16824.24388 | 0.032929 | 9.988799092 | 3.320311 |
| ZIKV/Malaysia 48 hpi_1 | IL6 | 3448 | 9016.561426 | 0.382407 | 69.10878697 | 6.110797 |

| | | | | | | |
|---|---|---|---|---|---|---|
| ZIKV/Malaysia 4 hpi_2 | IL6 | 90 | 13310.81661 | 0.006761 | 0.429307863 | -1.21992 |
| ZIKV/Malaysia 8 hpi_2 | IL6 | 40 | 15300.45305 | 0.002614 | 0.514032346 | -0.96007 |
| ZIKV/Malaysia 10 hpi_2 | IL6 | 45 | 11873.49207 | 0.00379 | 1.059981687 | 0.084039 |
| ZIKV/Malaysia 24 hpi_2 | IL6 | 108 | 7114.262677 | 0.015181 | 4.605034918 | 2.203212 |
| ZIKV/Malaysia 48 hpi_2 | IL6 | 793 | 7202.033077 | 0.110108 | 19.89871511 | 4.314603 |
| ZIKV/Malaysia 4 hpi_3 | IL6 | 74 | 8019.493292 | 0.009228 | 0.585889648 | -0.7713 |
| ZIKV/Malaysia 8 hpi_3 | IL6 | 62 | 13577.51567 | 0.004566 | 0.897854832 | -0.15545 |
| ZIKV/Malaysia 10 hpi_3 | IL6 | 25 | 8780.599468 | 0.002847 | 0.796306309 | -0.3286 |
| ZIKV/Malaysia 24 hpi_3 | IL6 | 156 | 7775.628155 | 0.020063 | 6.085947242 | 2.605482 |
| ZIKV/Malaysia 48 hpi_3 | IL6 | 805 | 5457.964761 | 0.147491 | 26.65459645 | 4.736312 |
| ZIKV/Malaysia 4 hpi_1 | IFNL2 | 16 | 18941.07792 | 0.000845 | 1.265570353 | 0.339788 |
| ZIKV/Malaysia 8 hpi_1 | IFNL2 | 53 | 16004.07538 | 0.003312 | 4.195656713 | 2.068897 |
| ZIKV/Malaysia 10 hpi_1 | IFNL2 | 76 | 20365.09781 | 0.003732 | 5.58033097 | 2.480351 |
| ZIKV/Malaysia 24 hpi_1 | IFNL2 | 4023 | 16824.24388 | 0.239119 | 226.7903513 | 7.825215 |
| ZIKV/Malaysia 48 hpi_1 | IFNL2 | 12737 | 9016.561426 | 1.412623 | 1063.834367 | 10.05506 |
| ZIKV/Malaysia 4 hpi_2 | IFNL2 | 14 | 13310.81661 | 0.001052 | 1.575775473 | 0.656062 |
| ZIKV/Malaysia 8 hpi_2 | IFNL2 | 33 | 15300.45305 | 0.002157 | 2.732526077 | 1.450235 |
| ZIKV/Malaysia 10 hpi_2 | IFNL2 | 34 | 11873.49207 | 0.002864 | 4.281868409 | 2.09824 |
| ZIKV/Malaysia 24 hpi_2 | IFNL2 | 1260 | 7114.262677 | 0.177109 | 167.9773575 | 7.392123 |
| ZIKV/Malaysia 48 hpi_2 | IFNL2 | 6436 | 7202.033077 | 0.893637 | 672.9901946 | 9.394442 |
| ZIKV/Malaysia 4 hpi_3 | IFNL2 | 8 | 8019.493292 | 0.000998 | 1.494562424 | 0.579723 |
| ZIKV/Malaysia 8 hpi_3 | IFNL2 | 44 | 13577.51567 | 0.003241 | 4.105698269 | 2.037628 |
| ZIKV/Malaysia 10 hpi_3 | IFNL2 | 34 | 8780.599468 | 0.003872 | 5.790120683 | 2.533593 |
| ZIKV/Malaysia 24 hpi_3 | IFNL2 | 1444 | 7775.628155 | 0.185708 | 176.1334354 | 7.460525 |
| ZIKV/Malaysia 48 hpi_3 | IFNL2 | 5394 | 5457.964761 | 0.98828 | 744.2657393 | 9.539674 |

| | | | | | | |
|---|---|---|---|---|---|---|
| ZIKV/Malaysia 4 hpi_1 | IFNA2 | 5 | 18941.07792 | 0.000264 | 0.479270524 | -1.06109 |
| ZIKV/Malaysia 8 hpi_1 | IFNA2 | 6 | 16004.07538 | 0.000375 | 0.543538695 | -0.87955 |
| ZIKV/Malaysia 10 hpi_1 | IFNA2 | 15 | 20365.09781 | 0.000737 | 1.067983713 | 0.09489 |
| ZIKV/Malaysia 24 hpi_1 | IFNA2 | 22 | 16824.24388 | 0.001308 | 2.054257875 | 1.038617 |
| ZIKV/Malaysia 48 hpi_1 | IFNA2 | 35 | 9016.561426 | 0.003882 | 4.095554674 | 2.034059 |
| ZIKV/Malaysia 4 hpi_2 | IFNA2 | 12 | 13310.81661 | 0.000902 | 1.63678619 | 0.710866 |
| ZIKV/Malaysia 8 hpi_2 | IFNA2 | 8 | 15300.45305 | 0.000523 | 0.758045897 | -0.39964 |
| ZIKV/Malaysia 10 hpi_2 | IFNA2 | 11 | 11873.49207 | 0.000926 | 1.343303325 | 0.425785 |
| ZIKV/Malaysia 24 hpi_2 | IFNA2 | 7 | 7114.262677 | 0.000984 | 1.545738338 | 0.628296 |
| ZIKV/Malaysia 48 hpi_2 | IFNA2 | 20 | 7202.033077 | 0.002777 | 2.929952053 | 1.550877 |
| ZIKV/Malaysia 4 hpi_3 | IFNA2 | 4 | 8019.493292 | 0.000499 | 0.905583433 | -0.14308 |
| ZIKV/Malaysia 8 hpi_3 | IFNA2 | 5 | 13577.51567 | 0.000368 | 0.533899478 | -0.90536 |
| ZIKV/Malaysia 10 hpi_3 | IFNA2 | 2 | 8780.599468 | 0.000228 | 0.330267394 | -1.59829 |
| ZIKV/Malaysia 24 hpi_3 | IFNA2 | 9 | 7775.628155 | 0.001157 | 1.818339029 | 0.862621 |
| ZIKV/Malaysia 48 hpi_3 | IFNA2 | 12 | 5457.964761 | 0.002199 | 2.319723104 | 1.213953 |
| ZIKV/Malaysia 4 hpi_1 | POS_C | 3170 | 18941.07792 | 0.167361 | 0.908085995 | -0.1391 |
| ZIKV/Malaysia 8 hpi_1 | POS_C | 3282 | 16004.07538 | 0.205073 | 0.855943033 | -0.22441 |
| ZIKV/Malaysia 10 hpi_1 | POS_C | 3447 | 20365.09781 | 0.16926 | 0.741505111 | -0.43147 |
| ZIKV/Malaysia 24 hpi_1 | POS_C | 3668 | 16824.24388 | 0.218019 | 0.822452852 | -0.282 |
| ZIKV/Malaysia 48 hpi_1 | POS_C | 3763 | 9016.561426 | 0.417343 | 1.501721768 | 0.586618 |
| ZIKV/Malaysia 4 hpi_2 | POS_C | 2789 | 13310.81661 | 0.209529 | 1.136884173 | 0.185085 |
| ZIKV/Malaysia 8 hpi_2 | POS_C | 3660 | 15300.45305 | 0.239209 | 0.99842091 | -0.00228 |
| ZIKV/Malaysia 10 hpi_2 | POS_C | 2816 | 11873.49207 | 0.237167 | 1.03899522 | 0.055189 |
| ZIKV/Malaysia 24 hpi_2 | POS_C | 2411 | 7114.262677 | 0.338897 | 1.278452372 | 0.354398 |
| ZIKV/Malaysia 48 hpi_2 | POS_C | 3011 | 7202.033077 | 0.418076 | 1.504360243 | 0.58915 |

| | | | | | | |
|---|---|---|---|---|---|---|
| ZIKV/Malaysia 4 hpi_3 | POS_C | 1984 | 8019.493292 | 0.247397 | 1.34235426 | 0.424765 |
| ZIKV/Malaysia 8 hpi_3 | POS_C | 2456 | 13577.51567 | 0.180887 | 0.754996473 | -0.40546 |
| ZIKV/Malaysia 10 hpi_3 | POS_C | 2335 | 8780.599468 | 0.265927 | 1.164989694 | 0.220317 |
| ZIKV/Malaysia 24 hpi_3 | POS_C | 2522 | 7775.628155 | 0.324347 | 1.223564415 | 0.29109 |
| ZIKV/Malaysia 48 hpi_3 | POS_C | 2161 | 5457.964761 | 0.395935 | 1.424689564 | 0.510648 |
| ZIKV/Malaysia 4 hpi_1 | POS_A | 40240 | 18941.07792 | 2.124483 | 0.959679746 | -0.05938 |
| ZIKV/Malaysia 8 hpi_1 | POS_A | 38959 | 16004.07538 | 2.434317 | 0.84406657 | -0.24457 |
| ZIKV/Malaysia 10 hpi_1 | POS_A | 45328 | 20365.09781 | 2.225769 | 0.801741201 | -0.31879 |
| ZIKV/Malaysia 24 hpi_1 | POS_A | 47102 | 16824.24388 | 2.79965 | 0.913066651 | -0.13121 |
| ZIKV/Malaysia 48 hpi_1 | POS_A | 44516 | 9016.561426 | 4.937137 | 1.533460885 | 0.616791 |
| ZIKV/Malaysia 4 hpi_2 | POS_A | 34902 | 13310.81661 | 2.622078 | 1.184455263 | 0.244224 |
| ZIKV/Malaysia 8 hpi_2 | POS_A | 44070 | 15300.45305 | 2.880307 | 0.998707352 | -0.00187 |
| ZIKV/Malaysia 10 hpi_2 | POS_A | 34895 | 11873.49207 | 2.9389 | 1.058617043 | 0.082181 |
| ZIKV/Malaysia 24 hpi_2 | POS_A | 28200 | 7114.262677 | 3.963868 | 1.292759981 | 0.370454 |
| ZIKV/Malaysia 48 hpi_2 | POS_A | 36339 | 7202.033077 | 5.045659 | 1.567167349 | 0.648159 |
| ZIKV/Malaysia 4 hpi_3 | POS_A | 24561 | 8019.493292 | 3.062662 | 1.383477704 | 0.468299 |
| ZIKV/Malaysia 8 hpi_3 | POS_A | 28896 | 13577.51567 | 2.128224 | 0.737932951 | -0.43844 |
| ZIKV/Malaysia 10 hpi_3 | POS_A | 28412 | 8780.599468 | 3.23577 | 1.16555235 | 0.221014 |
| ZIKV/Malaysia 24 hpi_3 | POS_A | 29581 | 7775.628155 | 3.804323 | 1.240726492 | 0.311185 |
| ZIKV/Malaysia 48 hpi_3 | POS_A | 25219 | 5457.964761 | 4.620587 | 1.435141255 | 0.521193 |
| ZIKV/Malaysia 4 hpi_1 | POS_F | 72 | 18941.07792 | 0.003801 | 1.020989763 | 0.029968 |
| ZIKV/Malaysia 8 hpi_1 | POS_F | 75 | 16004.07538 | 0.004686 | 0.904847041 | -0.14425 |
| ZIKV/Malaysia 10 hpi_1 | POS_F | 69 | 20365.09781 | 0.003388 | 0.693710139 | -0.5276 |
| ZIKV/Malaysia 24 hpi_1 | POS_F | 79 | 16824.24388 | 0.004696 | 0.90274584 | -0.14761 |
| ZIKV/Malaysia 48 hpi_1 | POS_F | 70 | 9016.561426 | 0.007763 | 1.298185339 | 0.376496 |

| | | | | | | |
|---|---|---|---|---|---|---|
| ZIKV/Malaysia 4 hpi_2 | POS_F | 50 | 13310.81661 | 0.003756 | 1.008925007 | 0.012819 |
| ZIKV/Malaysia 8 hpi_2 | POS_F | 67 | 15300.45305 | 0.004379 | 0.845502717 | -0.24212 |
| ZIKV/Malaysia 10 hpi_2 | POS_F | 65 | 11873.49207 | 0.005474 | 1.120857344 | 0.164603 |
| ZIKV/Malaysia 24 hpi_2 | POS_F | 30 | 7114.262677 | 0.004217 | 0.810709604 | -0.30274 |
| ZIKV/Malaysia 48 hpi_2 | POS_F | 52 | 7202.033077 | 0.00722 | 1.20733513 | 0.271826 |
| ZIKV/Malaysia 4 hpi_3 | POS_F | 34 | 8019.493292 | 0.00424 | 1.138742607 | 0.187442 |
| ZIKV/Malaysia 8 hpi_3 | POS_F | 49 | 13577.51567 | 0.003609 | 0.696819447 | -0.52114 |
| ZIKV/Malaysia 10 hpi_3 | POS_F | 47 | 8780.599468 | 0.005353 | 1.095945966 | 0.132177 |
| ZIKV/Malaysia 24 hpi_3 | POS_F | 65 | 7775.628155 | 0.008359 | 1.607133052 | 0.684489 |
| ZIKV/Malaysia 48 hpi_3 | POS_F | 42 | 5457.964761 | 0.007695 | 1.286761827 | 0.363745 |
| ZIKV/Malaysia 4 hpi_1 | POS_D | 806 | 18941.07792 | 0.042553 | 0.939162995 | -0.09055 |
| ZIKV/Malaysia 8 hpi_1 | POS_D | 820 | 16004.07538 | 0.051237 | 0.868161559 | -0.20396 |
| ZIKV/Malaysia 10 hpi_1 | POS_D | 834 | 20365.09781 | 0.040952 | 0.702010116 | -0.51044 |
| ZIKV/Malaysia 24 hpi_1 | POS_D | 966 | 16824.24388 | 0.057417 | 0.871727786 | -0.19805 |
| ZIKV/Malaysia 48 hpi_1 | POS_D | 946 | 9016.561426 | 0.104918 | 1.492848657 | 0.578068 |
| ZIKV/Malaysia 4 hpi_2 | POS_D | 678 | 13310.81661 | 0.050936 | 1.12417938 | 0.168872 |
| ZIKV/Malaysia 8 hpi_2 | POS_D | 885 | 15300.45305 | 0.057841 | 0.980068133 | -0.02905 |
| ZIKV/Malaysia 10 hpi_2 | POS_D | 704 | 11873.49207 | 0.059292 | 1.016384452 | 0.023446 |
| ZIKV/Malaysia 24 hpi_2 | POS_D | 581 | 7114.262677 | 0.081667 | 1.239896842 | 0.31022 |
| ZIKV/Malaysia 48 hpi_2 | POS_D | 691 | 7202.033077 | 0.095945 | 1.365175629 | 0.449087 |
| ZIKV/Malaysia 4 hpi_3 | POS_D | 531 | 8019.493292 | 0.066214 | 1.461363358 | 0.547315 |
| ZIKV/Malaysia 8 hpi_3 | POS_D | 561 | 13577.51567 | 0.041318 | 0.700099611 | -0.51437 |
| ZIKV/Malaysia 10 hpi_3 | POS_D | 553 | 8780.599468 | 0.06298 | 1.079604745 | 0.110503 |
| ZIKV/Malaysia 24 hpi_3 | POS_D | 632 | 7775.628155 | 0.08128 | 1.234016347 | 0.303362 |
| ZIKV/Malaysia 48 hpi_3 | POS_D | 527 | 5457.964761 | 0.096556 | 1.37386949 | 0.458245 |

| | | | | | | |
|---|---|---|---|---|---|---|
| ZIKV/Malaysia 4 hpi_1 | POS_B | 11583 | 18941.07792 | 0.611528 | 0.925598075 | -0.11154 |
| ZIKV/Malaysia 8 hpi_1 | POS_B | 11705 | 16004.07538 | 0.731376 | 0.85152906 | -0.23187 |
| ZIKV/Malaysia 10 hpi_1 | POS_B | 12937 | 20365.09781 | 0.635254 | 0.760456448 | -0.39506 |
| ZIKV/Malaysia 24 hpi_1 | POS_B | 13337 | 16824.24388 | 0.792725 | 0.83139449 | -0.26639 |
| ZIKV/Malaysia 48 hpi_1 | POS_B | 13877 | 9016.561426 | 1.539057 | 1.561784296 | 0.643195 |
| ZIKV/Malaysia 4 hpi_2 | POS_B | 10037 | 13310.81661 | 0.754048 | 1.141314412 | 0.190696 |
| ZIKV/Malaysia 8 hpi_2 | POS_B | 12849 | 15300.45305 | 0.839779 | 0.977740675 | -0.03248 |
| ZIKV/Malaysia 10 hpi_2 | POS_B | 10272 | 11873.49207 | 0.86512 | 1.03562807 | 0.050506 |
| ZIKV/Malaysia 24 hpi_2 | POS_B | 8562 | 7114.262677 | 1.203498 | 1.262204933 | 0.335946 |
| ZIKV/Malaysia 48 hpi_2 | POS_B | 10963 | 7202.033077 | 1.522209 | 1.544687782 | 0.627315 |
| ZIKV/Malaysia 4 hpi_3 | POS_B | 7432 | 8019.493292 | 0.926742 | 1.40270017 | 0.488207 |
| ZIKV/Malaysia 8 hpi_3 | POS_B | 8995 | 13577.51567 | 0.662492 | 0.771328714 | -0.37458 |
| ZIKV/Malaysia 10 hpi_3 | POS_B | 8476 | 8780.599468 | 0.96531 | 1.155564123 | 0.208597 |
| ZIKV/Malaysia 24 hpi_3 | POS_B | 9072 | 7775.628155 | 1.166722 | 1.223635601 | 0.291174 |
| ZIKV/Malaysia 48 hpi_3 | POS_B | 7761 | 5457.964761 | 1.421959 | 1.44295692 | 0.529028 |
| ZIKV/Malaysia 4 hpi_1 | POS_E | 104 | 18941.07792 | 0.005491 | 0.876069598 | -0.19088 |
| ZIKV/Malaysia 8 hpi_1 | POS_E | 122 | 16004.07538 | 0.007623 | 0.897164273 | -0.15656 |
| ZIKV/Malaysia 10 hpi_1 | POS_E | 143 | 20365.09781 | 0.007022 | 0.750271139 | -0.41452 |
| ZIKV/Malaysia 24 hpi_1 | POS_E | 152 | 16824.24388 | 0.009035 | 0.943746291 | -0.08353 |
| ZIKV/Malaysia 48 hpi_1 | POS_E | 142 | 9016.561426 | 0.015749 | 1.6985549 | 0.764308 |
| ZIKV/Malaysia 4 hpi_2 | POS_E | 98 | 13310.81661 | 0.007362 | 1.174711814 | 0.232307 |
| ZIKV/Malaysia 8 hpi_2 | POS_E | 132 | 15300.45305 | 0.008627 | 1.015342042 | 0.021966 |
| ZIKV/Malaysia 10 hpi_2 | POS_E | 120 | 11873.49207 | 0.010107 | 1.079870018 | 0.110858 |
| ZIKV/Malaysia 24 hpi_2 | POS_E | 93 | 7114.262677 | 0.013072 | 1.365526954 | 0.449458 |
| ZIKV/Malaysia 48 hpi_2 | POS_E | 103 | 7202.033077 | 0.014302 | 1.542461394 | 0.625234 |

| | | | | | | |
|---|---|---|---|---|---|---|
| ZIKV/Malaysia 4 hpi_3 | POS_E | 69 | 8019.493292 | 0.008604 | 1.372815338 | 0.457138 |
| ZIKV/Malaysia 8 hpi_3 | POS_E | 84 | 13577.51567 | 0.006187 | 0.72811789 | -0.45776 |
| ZIKV/Malaysia 10 hpi_3 | POS_E | 84 | 8780.599468 | 0.009567 | 1.022171629 | 0.031637 |
| ZIKV/Malaysia 24 hpi_3 | POS_E | 103 | 7775.628155 | 0.013247 | 1.383722383 | 0.468555 |
| ZIKV/Malaysia 48 hpi_3 | POS_E | 71 | 5457.964761 | 0.013009 | 1.403006914 | 0.488522 |
| ZIKV/Malaysia 4 hpi_1 | NEG_C | 10 | 18941.07792 | 0.000528 | 1.176875124 | 0.234961 |
| ZIKV/Malaysia 8 hpi_1 | NEG_C | 7 | 16004.07538 | 0.000437 | 0.730762808 | -0.45252 |
| ZIKV/Malaysia 10 hpi_1 | NEG_C | 10 | 20365.09781 | 0.000491 | 0.57630357 | -0.7951 |
| ZIKV/Malaysia 24 hpi_1 | NEG_C | 8 | 16824.24388 | 0.000476 | 0.977326908 | -0.03309 |
| ZIKV/Malaysia 48 hpi_1 | NEG_C | 8 | 9016.561426 | 0.000887 | 2.072948276 | 1.051684 |
| ZIKV/Malaysia 4 hpi_2 | NEG_C | 3 | 13310.81661 | 0.000225 | 0.502402311 | -0.99308 |
| ZIKV/Malaysia 8 hpi_2 | NEG_C | 3 | 15300.45305 | 0.000196 | 0.327586464 | -1.61005 |
| ZIKV/Malaysia 10 hpi_2 | NEG_C | 3 | 11873.49207 | 0.000253 | 0.296538167 | -1.75371 |
| ZIKV/Malaysia 24 hpi_2 | NEG_C | 8 | 7114.262677 | 0.001125 | 2.311242501 | 1.208669 |
| ZIKV/Malaysia 48 hpi_2 | NEG_C | 6 | 7202.033077 | 0.000833 | 1.94641554 | 0.96082 |
| ZIKV/Malaysia 4 hpi_3 | NEG_C | 2 | 8019.493292 | 0.000249 | 0.555927479 | -0.84703 |
| ZIKV/Malaysia 8 hpi_3 | NEG_C | 7 | 13577.51567 | 0.000516 | 0.861363989 | -0.21531 |
| ZIKV/Malaysia 10 hpi_3 | NEG_C | 9 | 8780.599468 | 0.001025 | 1.202973755 | 0.266605 |
| ZIKV/Malaysia 24 hpi_3 | NEG_C | 4 | 7775.628155 | 0.000514 | 1.057328484 | 0.080424 |
| ZIKV/Malaysia 48 hpi_3 | NEG_C | 5 | 5457.964761 | 0.000916 | 2.14031996 | 1.097826 |
| ZIKV/Malaysia 4 hpi_1 | NEG_D | 11 | 18941.07792 | 0.000581 | 1.56611607 | 0.647191 |
| ZIKV/Malaysia 8 hpi_1 | NEG_D | 11 | 16004.07538 | 0.000687 | 1.239545893 | 0.309812 |
| ZIKV/Malaysia 10 hpi_1 | NEG_D | 5 | 20365.09781 | 0.000246 | 0.724075817 | -0.46579 |
| ZIKV/Malaysia 24 hpi_1 | NEG_D | 9 | 16824.24388 | 0.000535 | 1.134505194 | 0.182063 |
| ZIKV/Malaysia 48 hpi_1 | NEG_D | 4 | 9016.561426 | 0.000444 | 0.653263653 | -0.61426 |

| | | | | | | |
|---|---|---|---|---|---|---|
| ZIKV/Malaysia 4 hpi_2 | NEG_D | 6 | 13310.81661 | 0.000451 | 1.215577078 | 0.281641 |
| ZIKV/Malaysia 8 hpi_2 | NEG_D | 8 | 15300.45305 | 0.000523 | 0.942944671 | -0.08475 |
| ZIKV/Malaysia 10 hpi_2 | NEG_D | 5 | 11873.49207 | 0.000421 | 1.241915584 | 0.312567 |
| ZIKV/Malaysia 24 hpi_2 | NEG_D | 7 | 7114.262677 | 0.000984 | 2.086736814 | 1.061249 |
| ZIKV/Malaysia 48 hpi_2 | NEG_D | 4 | 7202.033077 | 0.000555 | 0.817851264 | -0.29009 |
| ZIKV/Malaysia 4 hpi_3 | NEG_D | 0.022322957 | 8019.493292 | 2.78E-06 | 0.007506556 | -7.05763 |
| ZIKV/Malaysia 8 hpi_3 | NEG_D | 3 | 13577.51567 | 0.000221 | 0.398475346 | -1.32744 |
| ZIKV/Malaysia 10 hpi_3 | NEG_D | 2 | 8780.599468 | 0.000228 | 0.671747977 | -0.57401 |
| ZIKV/Malaysia 24 hpi_3 | NEG_D | 7 | 7775.628155 | 0.0009 | 1.909246885 | 0.933004 |
| ZIKV/Malaysia 48 hpi_3 | NEG_D | 5 | 5457.964761 | 0.000916 | 1.348989989 | 0.43188 |
| ZIKV/Malaysia 4 hpi_1 | NEG_E | 15 | 18941.07792 | 0.000792 | 0.622879119 | -0.68298 |
| ZIKV/Malaysia 8 hpi_1 | NEG_E | 15 | 16004.07538 | 0.000937 | 0.847353682 | -0.23896 |
| ZIKV/Malaysia 10 hpi_1 | NEG_E | 14 | 20365.09781 | 0.000687 | 0.551631937 | -0.85822 |
| ZIKV/Malaysia 24 hpi_1 | NEG_E | 10 | 16824.24388 | 0.000594 | 0.441040041 | -1.18102 |
| ZIKV/Malaysia 48 hpi_1 | NEG_E | 24 | 9016.561426 | 0.002662 | 2.201942011 | 1.138776 |
| ZIKV/Malaysia 4 hpi_2 | NEG_E | 8 | 13310.81661 | 0.000601 | 0.472718382 | -1.08095 |
| ZIKV/Malaysia 8 hpi_2 | NEG_E | 15 | 15300.45305 | 0.00098 | 0.886320958 | -0.1741 |
| ZIKV/Malaysia 10 hpi_2 | NEG_E | 18 | 11873.49207 | 0.001516 | 1.216471408 | 0.282702 |
| ZIKV/Malaysia 24 hpi_2 | NEG_E | 15 | 7114.262677 | 0.002108 | 1.56449773 | 0.6457 |
| ZIKV/Malaysia 48 hpi_2 | NEG_E | 15 | 7202.033077 | 0.002083 | 1.722946249 | 0.784878 |
| ZIKV/Malaysia 4 hpi_3 | NEG_E | 7 | 8019.493292 | 0.000873 | 0.686543904 | -0.54258 |
| ZIKV/Malaysia 8 hpi_3 | NEG_E | 8 | 13577.51567 | 0.000589 | 0.532688995 | -0.90863 |
| ZIKV/Malaysia 10 hpi_3 | NEG_E | 11 | 8780.599468 | 0.001253 | 1.005255331 | 0.007562 |
| ZIKV/Malaysia 24 hpi_3 | NEG_E | 12 | 7775.628155 | 0.001543 | 1.145141984 | 0.195526 |
| ZIKV/Malaysia 48 hpi_3 | NEG_E | 4 | 5457.964761 | 0.000733 | 0.606268279 | -0.72197 |

| | | | | | | |
|---|---|---|---|---|---|---|
| ZIKV/Malaysia 4 hpi_1 | NEG_A | 11 | 18941.07792 | 0.000581 | 0.968732734 | -0.04583 |
| ZIKV/Malaysia 8 hpi_1 | NEG_A | 11 | 16004.07538 | 0.000687 | 0.777572074 | -0.36295 |
| ZIKV/Malaysia 10 hpi_1 | NEG_A | 17 | 20365.09781 | 0.000835 | 1.073195472 | 0.101913 |
| ZIKV/Malaysia 24 hpi_1 | NEG_A | 12 | 16824.24388 | 0.000713 | 0.862057824 | -0.21414 |
| ZIKV/Malaysia 48 hpi_1 | NEG_A | 17 | 9016.561426 | 0.001885 | 1.820657967 | 0.86446 |
| ZIKV/Malaysia 4 hpi_2 | NEG_A | 8 | 13310.81661 | 0.000601 | 1.00253898 | 0.003658 |
| ZIKV/Malaysia 8 hpi_2 | NEG_A | 13 | 15300.45305 | 0.00085 | 0.961208538 | -0.05708 |
| ZIKV/Malaysia 10 hpi_2 | NEG_A | 13 | 11873.49207 | 0.001095 | 1.407606606 | 0.493244 |
| ZIKV/Malaysia 24 hpi_2 | NEG_A | 9 | 7114.262677 | 0.001265 | 1.528985335 | 0.612575 |
| ZIKV/Malaysia 48 hpi_2 | NEG_A | 12 | 7202.033077 | 0.001666 | 1.608964732 | 0.686133 |
| ZIKV/Malaysia 4 hpi_3 | NEG_A | 5 | 8019.493292 | 0.000623 | 1.040013691 | 0.056603 |
| ZIKV/Malaysia 8 hpi_3 | NEG_A | 12 | 13577.51567 | 0.000884 | 0.999860683 | -0.0002 |
| ZIKV/Malaysia 10 hpi_3 | NEG_A | 11 | 8780.599468 | 0.001253 | 1.610589742 | 0.687589 |
| ZIKV/Malaysia 24 hpi_3 | NEG_A | 6 | 7775.628155 | 0.000772 | 0.932623756 | -0.10063 |
| ZIKV/Malaysia 48 hpi_3 | NEG_A | 7 | 5457.964761 | 0.001283 | 1.238476308 | 0.308566 |
| ZIKV/Malaysia 4 hpi_1 | NEG_H | 2 | 18941.07792 | 0.000106 | 0.353675074 | -1.4995 |
| ZIKV/Malaysia 8 hpi_1 | NEG_H | 5 | 16004.07538 | 0.000312 | 3.038612655 | 1.603413 |
| ZIKV/Malaysia 10 hpi_1 | NEG_H | 7 | 20365.09781 | 0.000344 | 3.71029715 | 1.891535 |
| ZIKV/Malaysia 24 hpi_1 | NEG_H | 1 | 16824.24388 | 5.94E-05 | 0.220931927 | -2.17833 |
| ZIKV/Malaysia 48 hpi_1 | NEG_H | 3 | 9016.561426 | 0.000333 | 1.809946995 | 0.855947 |
| ZIKV/Malaysia 4 hpi_2 | NEG_H | 5 | 13310.81661 | 0.000376 | 1.258184854 | 0.331344 |
| ZIKV/Malaysia 8 hpi_2 | NEG_H | 2 | 15300.45305 | 0.000131 | 1.271339766 | 0.34635 |
| ZIKV/Malaysia 10 hpi_2 | NEG_H | 4 | 11873.49207 | 0.000337 | 3.636458854 | 1.862534 |
| ZIKV/Malaysia 24 hpi_2 | NEG_H | 3 | 7114.262677 | 0.000422 | 1.567420035 | 0.648392 |
| ZIKV/Malaysia 48 hpi_2 | NEG_H | 1 | 7202.033077 | 0.000139 | 0.755319046 | -0.40484 |

| | | | | | | |
|---|---|---|---|---|---|---|
| ZIKV/Malaysia 4 hpi_3 | NEG_H | 0.011300722 | 8019.493292 | 1.41E-06 | 0.004719961 | -7.72701 |
| ZIKV/Malaysia 8 hpi_3 | NEG_H | 4 | 13577.51567 | 0.000295 | 2.86533632 | 1.518704 |
| ZIKV/Malaysia 10 hpi_3 | NEG_H | 3 | 8780.599468 | 0.000342 | 3.688028264 | 1.88285 |
| ZIKV/Malaysia 24 hpi_3 | NEG_H | 2 | 7775.628155 | 0.000257 | 0.956067483 | -0.06482 |
| ZIKV/Malaysia 48 hpi_3 | NEG_H | 2 | 5457.964761 | 0.000366 | 1.993355762 | 0.995199 |
| ZIKV/Malaysia 4 hpi_1 | NEG_G | 11 | 18941.07792 | 0.000581 | 1.083677829 | 0.115936 |
| ZIKV/Malaysia 8 hpi_1 | NEG_G | 15 | 16004.07538 | 0.000937 | 3.151790555 | 1.656172 |
| ZIKV/Malaysia 10 hpi_1 | NEG_G | 9 | 20365.09781 | 0.000442 | 1.467770182 | 0.553626 |
| ZIKV/Malaysia 24 hpi_1 | NEG_G | 10 | 16824.24388 | 0.000594 | 1.264714325 | 0.338812 |
| ZIKV/Malaysia 48 hpi_1 | NEG_G | 7 | 9016.561426 | 0.000776 | 1.375337163 | 0.459785 |
| ZIKV/Malaysia 4 hpi_2 | NEG_G | 9 | 13310.81661 | 0.000676 | 1.261682279 | 0.335349 |
| ZIKV/Malaysia 8 hpi_2 | NEG_G | 8 | 15300.45305 | 0.000523 | 1.758257082 | 0.814146 |
| ZIKV/Malaysia 10 hpi_2 | NEG_G | 7 | 11873.49207 | 0.00059 | 1.958040296 | 0.96941 |
| ZIKV/Malaysia 24 hpi_2 | NEG_G | 2 | 7114.262677 | 0.000281 | 0.598174771 | -0.74136 |
| ZIKV/Malaysia 48 hpi_2 | NEG_G | 3 | 7202.033077 | 0.000417 | 0.7379352 | -0.43843 |
| ZIKV/Malaysia 4 hpi_3 | NEG_G | 9 | 8019.493292 | 0.001122 | 2.094149944 | 1.066365 |
| ZIKV/Malaysia 8 hpi_3 | NEG_G | 3 | 13577.51567 | 0.000221 | 0.743015068 | -0.42854 |
| ZIKV/Malaysia 10 hpi_3 | NEG_G | 4 | 8780.599468 | 0.000456 | 1.512996334 | 0.597408 |
| ZIKV/Malaysia 24 hpi_3 | NEG_G | 10 | 7775.628155 | 0.001286 | 2.736481455 | 1.452322 |
| ZIKV/Malaysia 48 hpi_3 | NEG_G | 5 | 5457.964761 | 0.000916 | 1.622898508 | 0.698573 |
| ZIKV/Malaysia 4 hpi_1 | NEG_F | 22 | 18941.07792 | 0.001161 | 1.067343296 | 0.094024 |
| ZIKV/Malaysia 8 hpi_1 | NEG_F | 26 | 16004.07538 | 0.001625 | 0.956396184 | -0.06432 |
| ZIKV/Malaysia 10 hpi_1 | NEG_F | 27 | 20365.09781 | 0.001326 | 0.795399212 | -0.33025 |
| ZIKV/Malaysia 24 hpi_1 | NEG_F | 25 | 16824.24388 | 0.001486 | 1.106136763 | 0.14553 |
| ZIKV/Malaysia 48 hpi_1 | NEG_F | 24 | 9016.561426 | 0.002662 | 1.433977551 | 0.520022 |

| | | | | | | |
|---|---|---|---|---|---|---|
| ZIKV/Malaysia 4 hpi_2 | NEG_F | 16 | 13310.81661 | 0.001202 | 1.104590793 | 0.143512 |
| ZIKV/Malaysia 8 hpi_2 | NEG_F | 24 | 15300.45305 | 0.001569 | 0.923425846 | -0.11493 |
| ZIKV/Malaysia 10 hpi_2 | NEG_F | 19 | 11873.49207 | 0.0016 | 0.960026071 | -0.05885 |
| ZIKV/Malaysia 24 hpi_2 | NEG_F | 17 | 7114.262677 | 0.00239 | 1.778784752 | 0.830892 |
| ZIKV/Malaysia 48 hpi_2 | NEG_F | 23 | 7202.033077 | 0.003194 | 1.720460797 | 0.782795 |
| ZIKV/Malaysia 4 hpi_3 | NEG_F | 14 | 8019.493292 | 0.001746 | 1.604232253 | 0.681883 |
| ZIKV/Malaysia 8 hpi_3 | NEG_F | 19 | 13577.51567 | 0.001399 | 0.823812473 | -0.27961 |
| ZIKV/Malaysia 10 hpi_3 | NEG_F | 15 | 8780.599468 | 0.001708 | 1.02488464 | 0.035462 |
| ZIKV/Malaysia 24 hpi_3 | NEG_F | 15 | 7775.628155 | 0.001929 | 1.436018875 | 0.522075 |
| ZIKV/Malaysia 48 hpi_3 | NEG_F | 12 | 5457.964761 | 0.002199 | 1.184465936 | 0.244237 |
| ZIKV/Malaysia 4 hpi_1 | NEG_B | 9 | 18941.07792 | 0.000475 | 0.890860371 | -0.16673 |
| ZIKV/Malaysia 8 hpi_1 | NEG_B | 9 | 16004.07538 | 0.000562 | 0.565504395 | -0.82239 |
| ZIKV/Malaysia 10 hpi_1 | NEG_B | 8 | 20365.09781 | 0.000393 | 0.514015015 | -0.96012 |
| ZIKV/Malaysia 24 hpi_1 | NEG_B | 10 | 16824.24388 | 0.000594 | 1.066879122 | 0.093397 |
| ZIKV/Malaysia 48 hpi_1 | NEG_B | 10 | 9016.561426 | 0.001109 | 1.06923606 | 0.09658 |
| ZIKV/Malaysia 4 hpi_2 | NEG_B | 9 | 13310.81661 | 0.000676 | 1.267679977 | 0.342191 |
| ZIKV/Malaysia 8 hpi_2 | NEG_B | 7 | 15300.45305 | 0.000458 | 0.460063536 | -1.12009 |
| ZIKV/Malaysia 10 hpi_2 | NEG_B | 7 | 11873.49207 | 0.00059 | 0.771421773 | -0.37441 |
| ZIKV/Malaysia 24 hpi_2 | NEG_B | 6 | 7114.262677 | 0.000843 | 1.513812635 | 0.598187 |
| ZIKV/Malaysia 48 hpi_2 | NEG_B | 11 | 7202.033077 | 0.001527 | 1.472489193 | 0.558257 |
| ZIKV/Malaysia 4 hpi_3 | NEG_B | 5 | 8019.493292 | 0.000623 | 1.168947206 | 0.22521 |
| ZIKV/Malaysia 8 hpi_3 | NEG_B | 12 | 13577.51567 | 0.000884 | 0.888761016 | -0.17013 |
| ZIKV/Malaysia 10 hpi_3 | NEG_B | 7 | 8780.599468 | 0.000797 | 1.04314863 | 0.060945 |
| ZIKV/Malaysia 24 hpi_3 | NEG_B | 10 | 7775.628155 | 0.001286 | 2.308422443 | 1.206907 |
| ZIKV/Malaysia 48 hpi_3 | NEG_B | 7 | 5457.964761 | 0.001283 | 1.236465079 | 0.306221 |

| | | | | | | |
|---|---|---|---|---|---|---|
| ZIKV/Malaysia 4 hpi_1 | ACTB | 147570 | 18941.07792 | 7.791003 | 0.908229628 | -0.13887 |
| ZIKV/Malaysia 8 hpi_1 | ACTB | 125621 | 16004.07538 | 7.849313 | 0.878491384 | -0.1869 |
| ZIKV/Malaysia 10 hpi_1 | ACTB | 160076 | 20365.09781 | 7.860311 | 0.896036499 | -0.15837 |
| ZIKV/Malaysia 24 hpi_1 | ACTB | 113206 | 16824.24388 | 6.728742 | 0.8468725 | -0.23978 |
| ZIKV/Malaysia 48 hpi_1 | ACTB | 53793 | 9016.561426 | 5.966022 | 0.77923197 | -0.35988 |
| ZIKV/Malaysia 4 hpi_2 | ACTB | 122149 | 13310.81661 | 9.176672 | 1.069762808 | 0.097291 |
| ZIKV/Malaysia 8 hpi_2 | ACTB | 134928 | 15300.45305 | 8.818562 | 0.986969292 | -0.01892 |
| ZIKV/Malaysia 10 hpi_2 | ACTB | 107560 | 11873.49207 | 9.058835 | 1.032662257 | 0.046368 |
| ZIKV/Malaysia 24 hpi_2 | ACTB | 52156 | 7114.262677 | 7.331188 | 0.922695751 | -0.11607 |
| ZIKV/Malaysia 48 hpi_2 | ACTB | 48483 | 7202.033077 | 6.731849 | 0.879257975 | -0.18564 |
| ZIKV/Malaysia 4 hpi_3 | ACTB | 73990 | 8019.493292 | 9.226269 | 1.075544485 | 0.105067 |
| ZIKV/Malaysia 8 hpi_3 | ACTB | 118762 | 13577.51567 | 8.746961 | 0.978955697 | -0.03068 |
| ZIKV/Malaysia 10 hpi_3 | ACTB | 82705 | 8780.599468 | 9.419061 | 1.073726264 | 0.102626 |
| ZIKV/Malaysia 24 hpi_3 | ACTB | 59179 | 7775.628155 | 7.610832 | 0.95789141 | -0.06207 |
| ZIKV/Malaysia 48 hpi_3 | ACTB | 37359 | 5457.964761 | 6.844859 | 0.894018402 | -0.16162 |
| ZIKV/Malaysia 4 hpi_1 | GAPDH | 249786 | 18941.07792 | 13.18753 | 1.087827439 | 0.12145 |
| ZIKV/Malaysia 8 hpi_1 | GAPDH | 213837 | 16004.07538 | 13.36141 | 1.093714219 | 0.129236 |
| ZIKV/Malaysia 10 hpi_1 | GAPDH | 265834 | 20365.09781 | 13.05341 | 1.024988255 | 0.035607 |
| ZIKV/Malaysia 24 hpi_1 | GAPDH | 260380 | 16824.24388 | 15.47648 | 1.090917126 | 0.125542 |
| ZIKV/Malaysia 48 hpi_1 | GAPDH | 183606 | 9016.561426 | 20.3632 | 1.373096201 | 0.457433 |
| ZIKV/Malaysia 4 hpi_2 | GAPDH | 154700 | 13310.81661 | 11.62213 | 0.95869888 | -0.06085 |
| ZIKV/Malaysia 8 hpi_2 | GAPDH | 184476 | 15300.45305 | 12.0569 | 0.986931877 | -0.01898 |
| ZIKV/Malaysia 10 hpi_2 | GAPDH | 142642 | 11873.49207 | 12.01348 | 0.94333037 | -0.08416 |
| ZIKV/Malaysia 24 hpi_2 | GAPDH | 109698 | 7114.262677 | 15.41945 | 1.086897289 | 0.120216 |
| ZIKV/Malaysia 48 hpi_2 | GAPDH | 128299 | 7202.033077 | 17.81428 | 1.201221791 | 0.264503 |

| | | | | | | |
|---|---|---|---|---|---|---|
| ZIKV/Malaysia 4 hpi_3 | GAPDH | 92929 | 8019.493292 | 11.58789 | 0.955874645 | -0.06511 |
| ZIKV/Malaysia 8 hpi_3 | GAPDH | 158970 | 13577.51567 | 11.70833 | 0.958399228 | -0.0613 |
| ZIKV/Malaysia 10 hpi_3 | GAPDH | 101745 | 8780.599468 | 11.58748 | 0.909879274 | -0.13625 |
| ZIKV/Malaysia 24 hpi_3 | GAPDH | 107193 | 7775.628155 | 13.78577 | 0.97174124 | -0.04136 |
| ZIKV/Malaysia 48 hpi_3 | GAPDH | 83800 | 5457.964761 | 15.35371 | 1.035305052 | 0.050056 |
| ZIKV/Malaysia 4 hpi_1 | HPRT1 | 14046 | 18941.07792 | 0.741563 | 0.996210307 | -0.00548 |
| ZIKV/Malaysia 8 hpi_1 | HPRT1 | 11494 | 16004.07538 | 0.718192 | 1.004983935 | 0.007172 |
| ZIKV/Malaysia 10 hpi_1 | HPRT1 | 14315 | 20365.09781 | 0.702918 | 0.977509712 | -0.03282 |
| ZIKV/Malaysia 24 hpi_1 | HPRT1 | 11635 | 16824.24388 | 0.691562 | 0.884313708 | -0.17737 |
| ZIKV/Malaysia 48 hpi_1 | HPRT1 | 5735 | 9016.561426 | 0.636052 | 0.829644093 | -0.26944 |
| ZIKV/Malaysia 4 hpi_2 | HPRT1 | 9627 | 13310.81661 | 0.723246 | 0.971604078 | -0.04156 |
| ZIKV/Malaysia 8 hpi_2 | HPRT1 | 11064 | 15300.45305 | 0.723116 | 1.011873894 | 0.01703 |
| ZIKV/Malaysia 10 hpi_2 | HPRT1 | 8603 | 11873.49207 | 0.724555 | 1.007598902 | 0.010921 |
| ZIKV/Malaysia 24 hpi_2 | HPRT1 | 5041 | 7114.262677 | 0.708577 | 0.906071199 | -0.1423 |
| ZIKV/Malaysia 48 hpi_2 | HPRT1 | 3858 | 7202.033077 | 0.535682 | 0.698725287 | -0.5172 |
| ZIKV/Malaysia 4 hpi_3 | HPRT1 | 5803 | 8019.493292 | 0.723612 | 0.972094977 | -0.04083 |
| ZIKV/Malaysia 8 hpi_3 | HPRT1 | 10068 | 13577.51567 | 0.74152 | 1.037627346 | 0.053288 |
| ZIKV/Malaysia 10 hpi_3 | HPRT1 | 6304 | 8780.599468 | 0.717946 | 0.998408493 | -0.0023 |
| ZIKV/Malaysia 24 hpi_3 | HPRT1 | 5541 | 7775.628155 | 0.712611 | 0.911230382 | -0.13411 |
| ZIKV/Malaysia 48 hpi_3 | HPRT1 | 3181 | 5457.964761 | 0.582818 | 0.760207746 | -0.39553 |
| ZIKV/Malaysia 4 hpi_1 | ABCF1 | 4193 | 18941.07792 | 0.221371 | 1.044779332 | 0.063198 |
| ZIKV/Malaysia 8 hpi_1 | ABCF1 | 3324 | 16004.07538 | 0.207697 | 1.029283009 | 0.04164 |
| ZIKV/Malaysia 10 hpi_1 | ABCF1 | 4143 | 20365.09781 | 0.203436 | 1.019857439 | 0.028367 |
| ZIKV/Malaysia 24 hpi_1 | ABCF1 | 2998 | 16824.24388 | 0.178195 | 0.995648174 | -0.00629 |
| ZIKV/Malaysia 48 hpi_1 | ABCF1 | 1388 | 9016.561426 | 0.153939 | 1.00529752 | 0.007623 |

| | | | | | | |
|---|---|---|---|---|---|---|
| ZIKV/Malaysia 4 hpi_2 | ABCF1 | 2882 | 13310.81661 | 0.216516 | 1.021865361 | 0.031205 |
| ZIKV/Malaysia 8 hpi_2 | ABCF1 | 3107 | 15300.45305 | 0.203066 | 1.006332131 | 0.009107 |
| ZIKV/Malaysia 10 hpi_2 | ABCF1 | 2328 | 11873.49207 | 0.196067 | 0.982914054 | -0.02486 |
| ZIKV/Malaysia 24 hpi_2 | ABCF1 | 1199 | 7114.262677 | 0.168535 | 0.941670825 | -0.08671 |
| ZIKV/Malaysia 48 hpi_2 | ABCF1 | 1177 | 7202.033077 | 0.163426 | 1.067253141 | 0.093902 |
| ZIKV/Malaysia 4 hpi_3 | ABCF1 | 1630 | 8019.493292 | 0.203255 | 0.959279309 | -0.05998 |
| ZIKV/Malaysia 8 hpi_3 | ABCF1 | 2768 | 13577.51567 | 0.203866 | 1.010299528 | 0.014783 |
| ZIKV/Malaysia 10 hpi_3 | ABCF1 | 1757 | 8780.599468 | 0.2001 | 1.003133259 | 0.004513 |
| ZIKV/Malaysia 24 hpi_3 | ABCF1 | 1330 | 7775.628155 | 0.171047 | 0.955709682 | -0.06536 |
| ZIKV/Malaysia 48 hpi_3 | ABCF1 | 904 | 5457.964761 | 0.16563 | 1.081642626 | 0.113224 |
| ZIKV/Malaysia 4 hpi_1 | SDHA | 1123 | 18941.07792 | 0.059289 | 0.966981333 | -0.04844 |
| ZIKV/Malaysia 8 hpi_1 | SDHA | 1023 | 16004.07538 | 0.063921 | 1.00140776 | 0.00203 |
| ZIKV/Malaysia 10 hpi_1 | SDHA | 1388 | 20365.09781 | 0.068156 | 1.086164488 | 0.119243 |
| ZIKV/Malaysia 24 hpi_1 | SDHA | 1311 | 16824.24388 | 0.077923 | 1.216561319 | 0.282809 |
| ZIKV/Malaysia 48 hpi_1 | SDHA | 758 | 9016.561426 | 0.084068 | 1.095578712 | 0.131693 |
| ZIKV/Malaysia 4 hpi_2 | SDHA | 797 | 13310.81661 | 0.059876 | 0.976554862 | -0.03423 |
| ZIKV/Malaysia 8 hpi_2 | SDHA | 980 | 15300.45305 | 0.06405 | 1.003431411 | 0.004942 |
| ZIKV/Malaysia 10 hpi_2 | SDHA | 768 | 11873.49207 | 0.064682 | 1.03080232 | 0.043768 |
| ZIKV/Malaysia 24 hpi_2 | SDHA | 527 | 7114.262677 | 0.074077 | 1.15650519 | 0.209772 |
| ZIKV/Malaysia 48 hpi_2 | SDHA | 686 | 7202.033077 | 0.095251 | 1.241321647 | 0.311877 |
| ZIKV/Malaysia 4 hpi_3 | SDHA | 510 | 8019.493292 | 0.063595 | 1.03720899 | 0.052707 |
| ZIKV/Malaysia 8 hpi_3 | SDHA | 877 | 13577.51567 | 0.064592 | 1.011917689 | 0.017092 |
| ZIKV/Malaysia 10 hpi_3 | SDHA | 560 | 8780.599468 | 0.063777 | 1.016380897 | 0.023441 |
| ZIKV/Malaysia 24 hpi_3 | SDHA | 608 | 7775.628155 | 0.078193 | 1.220773133 | 0.287795 |
| ZIKV/Malaysia 48 hpi_3 | SDHA | 538 | 5457.964761 | 0.098572 | 1.284596911 | 0.361316 |

| | | | | | | |
|---|---|---|---|---|---|---|
| ZIKV/Malaysia 4 hpi_1 | PGK1 | 52724 | 18941.07792 | 2.78358 | 1.06950449 | 0.096943 |
| ZIKV/Malaysia 8 hpi_1 | PGK1 | 48036 | 16004.07538 | 3.001485 | 1.12497088 | 0.169888 |
| ZIKV/Malaysia 10 hpi_1 | PGK1 | 58114 | 20365.09781 | 2.853608 | 0.993798028 | -0.00898 |
| ZIKV/Malaysia 24 hpi_1 | PGK1 | 75396 | 16824.24388 | 4.48139 | 1.257444861 | 0.330495 |
| ZIKV/Malaysia 48 hpi_1 | PGK1 | 49134 | 9016.561426 | 5.449306 | 1.008520638 | 0.012241 |
| ZIKV/Malaysia 4 hpi_2 | PGK1 | 33800 | 13310.81661 | 2.539288 | 0.975643043 | -0.03557 |
| ZIKV/Malaysia 8 hpi_2 | PGK1 | 42186 | 15300.45305 | 2.757173 | 1.033401507 | 0.047401 |
| ZIKV/Malaysia 10 hpi_2 | PGK1 | 32183 | 11873.49207 | 2.710492 | 0.943956368 | -0.08321 |
| ZIKV/Malaysia 24 hpi_2 | PGK1 | 31953 | 7114.262677 | 4.4914 | 1.260253588 | 0.333714 |
| ZIKV/Malaysia 48 hpi_2 | PGK1 | 34945 | 7202.033077 | 4.852102 | 0.897994232 | -0.15522 |
| ZIKV/Malaysia 4 hpi_3 | PGK1 | 20729 | 8019.493292 | 2.584827 | 0.993139773 | -0.00993 |
| ZIKV/Malaysia 8 hpi_3 | PGK1 | 34102 | 13577.51567 | 2.511652 | 0.941379139 | -0.08715 |
| ZIKV/Malaysia 10 hpi_3 | PGK1 | 22794 | 8780.599468 | 2.59595 | 0.904066213 | -0.1455 |
| ZIKV/Malaysia 24 hpi_3 | PGK1 | 27822 | 7775.628155 | 3.578103 | 1.003989249 | 0.005744 |
| ZIKV/Malaysia 48 hpi_3 | PGK1 | 24348 | 5457.964761 | 4.461004 | 0.825612348 | -0.27646 |

Table 5. Nanostring analysis of differentially expressed cytokines between ZIKV/Dakar and ZIKV/Malaysia infections.

| Time post-infection (hpi) | Gene | FC difference | BH adjusted p-value |
|---|---|---|---|
| 4 | IFNL2 | 2.679783 | 0.841364 |
| 4 | CCL2 | 2.033298 | 0.519167 |
| 4 | IFNB1 | 3.961337 | 0.841364 |
| 4 | IFNL1 | 3.716979 | 0.870238 |
| 4 | IFNL3 | 3.969843 | 0.841364 |
| 4 | IL6 | 3.777113 | 0.841364 |
| 4 | IL18 | 3.690076 | 0.841364 |
| 4 | IL1A | 2.061215 | 0.841364 |
| 4 | IL1B | 3.326466 | 0.841364 |
| 4 | CXCL10 | 2.134705 | 0.519167 |
| 4 | CCL4 | 3.014883 | 0.423 |
| 4 | IFNA2 | 2.810096 | 0.892045 |
| 4 | CCL3 | 2.951361 | 0.841364 |
| 4 | TNF | 2.321261 | 0.841364 |
| 4 | IFNA4 | 2.610225 | 0.892045 |
| 8 | IFNL2 | 3.878044 | 0.870238 |
| 8 | CCL2 | 3.071096 | 0.841364 |
| 8 | IFNB1 | 2.504508 | 0.913929 |
| 8 | IFNL1 | 3.50202 | 0.892045 |
| 8 | IFNL3 | 2.361284 | 0.870238 |

| | | | |
|---|---|---|---|
| 8 | IL6 | 3.619074 | 0.986 |
| 8 | IL18 | 3.859443 | 0.841364 |
| 8 | IL1A | 2.300716 | 0.841364 |
| 8 | IL1B | 2.713884 | 0.7625 |
| 8 | CXCL10 | 3.035764 | 0.841364 |
| 8 | CCL4 | 2.790826 | 0.841364 |
| 8 | IFNA2 | 2.396497 | 0.841364 |
| 8 | CCL3 | 2.247255 | 0.841364 |
| 8 | TNF | 3.447482 | 0.967808 |
| 8 | IFNA4 | 2.232235 | 0.841364 |
| 10 | IFNL2 | 2.658882 | 0.841364 |
| 10 | CCL2 | 3.000831 | 0.841364 |
| 10 | IFNB1 | 2.429254 | 0.870238 |
| 10 | IFNL1 | 3.957813 | 0.841364 |
| 10 | IFNL3 | 3.999524 | 0.841364 |
| 10 | IL6 | 2.820834 | 0.913929 |
| 10 | IL18 | 3.9551 | 0.841364 |
| 10 | IL1A | 3.700891 | 0.841364 |
| 10 | IL1B | 2.207247 | 0.910075 |
| 10 | CXCL10 | 2.027598 | 0.841364 |
| 10 | CCL4 | 3.97233 | 0.841364 |
| 10 | IFNA2 | 2.354593 | 0.841364 |
| 10 | CCL3 | 3.96457 | 0.841364 |
| 10 | TNF | 3.421393 | 0.870238 |
| 10 | IFNA4 | 3.777054 | 0.841364 |

| | | | |
|---|---|---|---|
| 24 | IFNL2 | 3.931857 | 0.841364 |
| 24 | CCL2 | 3.90913 | 0.930634 |
| 24 | IFNB1 | 3.787529 | 0.423 |
| 24 | IFNL1 | 3.752515 | 0.423 |
| 24 | IFNL3 | 3.192391 | 0.423 |
| 24 | IL6 | 3.899674 | 0.841364 |
| 24 | IL18 | 3.537904 | 0.841364 |
| 24 | IL1A | 3.44196 | 0.841364 |
| 24 | IL1B | 2.224174 | 0.519167 |
| 24 | CXCL10 | 2.087756 | 0.519167 |
| 24 | CCL4 | 3.398212 | 0.841364 |
| 24 | IFNA2 | 3.130533 | 0.841364 |
| 24 | CCL3 | 3.986307 | 0.841364 |
| 24 | TNF | 3.092207 | 0.841364 |
| 24 | IFNA4 | 3.072954 | 0.841364 |
| 48 | IFNL2 | 3.745907 | 0.841364 |
| 48 | CCL2 | 3.865489 | 0.841364 |
| 48 | IFNB1 | 2.98761 | 0.841364 |
| 48 | IFNL1 | 2.206411 | 0.913929 |
| 48 | IFNL3 | 3.51116 | 0.841364 |
| 48 | IL6 | 3.604787 | 0.967808 |
| 48 | IL18 | 2.443495 | 0.982095 |
| 48 | IL1A | 2.145732 | 0.60675 |
| 48 | IL1B | 3.634993 | 0.870238 |
| 48 | CXCL10 | 3.86747 | 0.870238 |

| | | | |
|---|---|---|---|
| 48 | CCL4 | 3.988182 | 0.854464 |
| 48 | IFNA2 | 3.814453 | 0.841364 |
| 48 | CCL3 | 3.998479 | 0.423 |
| 48 | TNF | 2.770507 | 0.841364 |
| 48 | IFNA4 | 3.640746 | 0.647727 |

Table 6. Nanostring analysis of differentially expressed IRF3-, NFκB-, and IFN-target genes between ZIKV/Dakar and ZIKV/Malaysia infections.

| Time post-infection (hpi) | Gene | FC difference | BH adjusted p-value |
|---|---|---|---|
| 4 | IFITM1 | 2.01106281 | 0.293617021 |
| 4 | MX1 | 2.000084 | 0.306804 |
| 4 | IFIT1 | 2.00188 | 0.386139 |
| 4 | ISG15 | 2.021342 | 0.3624 |
| 4 | OAS1 | 2.002351 | 0.238421 |
| 4 | DDX58 | 2.035201 | 0.242927 |
| 4 | IFIT2 | 2.012329 | 0.178364 |
| 4 | EIF2AK2 | 2.014883 | 0.225 |
| 4 | TRIM25 | 2.016654 | 0.233425 |
| 4 | ISG20 | 2.74895 | 0.464 |
| 4 | IFI44 | 2.028264 | 0.247143 |
| 4 | IFIH1 | 2.006296 | 0.206471 |
| 4 | IRF1 | 2.030356 | 0.120828 |
| 4 | IRF2 | 2.256617 | 0.058759 |
| 4 | GBP1 | 2.018434 | 0.10898 |
| 4 | RSAD2 | 2.29859 | 0.469811 |
| 4 | GBP2 | 2.047481 | 0.120828 |
| 4 | IRF7 | 2.007413 | 0.242927 |
| 4 | MX2 | 2.014332 | 0.293617 |
| 4 | TLR3 | 2.912075 | 0.096261 |

| | | | |
|---|---|---|---|
| 4 | DHX58 | 2.932421 | 0.120828 |
| 4 | IRF5 | 2.273662 | 0.097532 |
| 8 | IFITM1 | 2.21007 | 0.242927 |
| 8 | MX1 | 2.054082 | 0.242927 |
| 8 | IFIT1 | 3.379838 | 0.313939 |
| 8 | ISG15 | 2.214352 | 0.27236 |
| 8 | OAS1 | 2.269296 | 0.144787 |
| 8 | DDX58 | 3.65668 | 0.851379 |
| 8 | IFIT2 | 3.883991 | 0.652222 |
| 8 | EIF2AK2 | 2.715299 | 0.075907 |
| 8 | TRIM25 | 3.975019 | 0.042369 |
| 8 | ISG20 | 2.135655 | 0.210435 |
| 8 | IFI44 | 2.360735 | 0.154065 |
| 8 | IFIH1 | 2.442521 | 0.11256 |
| 8 | IRF1 | 3.121854 | 0.712364 |
| 8 | IRF2 | 3.157759 | 0.962017 |
| 8 | GBP1 | 3.693403 | 0.038716 |
| 8 | RSAD2 | 2.162647 | 0.238421 |
| 8 | GBP2 | 2.477231 | 0.092182 |
| 8 | IRF7 | 2.194754 | 0.293617 |
| 8 | MX2 | 2.853647 | 0.242927 |
| 8 | TLR3 | 2.260122 | 0.038716 |
| 8 | DHX58 | 2.271725 | 0.120828 |
| 8 | IRF5 | 2.098805 | 0.725405 |
| 10 | IFITM1 | 2.240227 | 0.263448 |

| | | | |
|---|---|---|---|
| 10 | MX1 | 2.250617 | 0.242927 |
| 10 | IFIT1 | 3.448372 | 0.30375 |
| 10 | ISG15 | 2.466854 | 0.263448 |
| 10 | OAS1 | 2.576354 | 0.120828 |
| 10 | DDX58 | 2.052298 | 0.89641 |
| 10 | IFIT2 | 2.177292 | 0.434118 |
| 10 | EIF2AK2 | 3.979555 | 0.04175 |
| 10 | TRIM25 | 3.097229 | 0.247143 |
| 10 | ISG20 | 2.419907 | 0.298105 |
| 10 | IFI44 | 3.339023 | 0.164762 |
| 10 | IFIH1 | 3.337363 | 0.144787 |
| 10 | IRF1 | 3.067654 | 0.937627 |
| 10 | IRF2 | 3.999848 | 0.824211 |
| 10 | GBP1 | 3.931045 | 0.068333 |
| 10 | RSAD2 | 3.990373 | 0.210857 |
| 10 | GBP2 | 3.109081 | 0.038716 |
| 10 | IRF7 | 2.159886 | 0.221408 |
| 10 | MX2 | 3.995032 | 0.791786 |
| 10 | TLR3 | 2.777579 | 0.041143 |
| 10 | DHX58 | 3.174429 | 0.263448 |
| 10 | IRF5 | 2.596835 | 0.281333 |
| 24 | IFITM1 | 3.217036 | 0.120828 |
| 24 | MX1 | 3.055033 | 0.042369 |
| 24 | IFIT1 | 3.450833 | 0.058759 |
| 24 | ISG15 | 3.718149 | 0.0729 |

| | | | |
|---|---|---|---|
| 24 | OAS1 | 3.96555 | 0.0375 |
| 24 | DDX58 | 3.855521 | 0.0632 |
| 24 | IFIT2 | 3.942042 | 0.293617 |
| 24 | EIF2AK2 | 3.149279 | 0.038716 |
| 24 | TRIM25 | 3.534853 | 0.0338 |
| 24 | ISG20 | 2.287891 | 0.268636 |
| 24 | IFI44 | 2.770119 | 0.067636 |
| 24 | IFIH1 | 3.864149 | 0.067636 |
| 24 | IRF1 | 2.57568 | 0.827478 |
| 24 | IRF2 | 3.521367 | 0.072649 |
| 24 | GBP1 | 3.700326 | 0.435728 |
| 24 | RSAD2 | 2.467175 | 0.176308 |
| 24 | GBP2 | 3.694239 | 0.657248 |
| 24 | IRF7 | 3.917089 | 0.04175 |
| 24 | MX2 | 3.278929 | 0.133831 |
| 24 | TLR3 | 2.327921 | 0.0729 |
| 24 | DHX58 | 3.394659 | 0.804956 |
| 24 | IRF5 | 2.914097 | 0.1035 |
| 48 | IFITM1 | 3.293274 | 0.0375 |
| 48 | MX1 | 2.041829 | 0.0729 |
| 48 | IFIT1 | 2.085328 | 0.075907 |
| 48 | ISG15 | 2.508281 | 0.04175 |
| 48 | OAS1 | 2.82872 | 0.038716 |
| 48 | DDX58 | 3.079213 | 0.0336 |
| 48 | IFIT2 | 3.65412 | 0.01662 |

| | | | |
|---|---|---|---|
| 48 | EIF2AK2 | 2.50024 | 0.038716 |
| 48 | TRIM25 | 3.307311 | 0.01662 |
| 48 | ISG20 | 2.525638 | 0.041143 |
| 48 | IFI44 | 2.582342 | 0.038716 |
| 48 | IFIH1 | 2.0615 | 0.0338 |
| 48 | IRF1 | 2.05017 | 0.235135 |
| 48 | IRF2 | 3.378219 | 0.0336 |
| 48 | GBP1 | 2.627788 | 0.038716 |
| 48 | RSAD2 | 3.207628 | 0.067636 |
| 48 | GBP2 | 3.962117 | 0.995 |
| 48 | IRF7 | 2.205937 | 0.058759 |
| 48 | MX2 | 2.037574 | 0.074927 |
| 48 | TLR3 | 2.095692 | 0.068333 |
| 48 | DHX58 | 3.064633 | 0.038716 |
| 48 | IRF5 | 2.464675 | 0.068333 |

**References**


1. Dick GWA, Kitchen SF, Haddow AJ. 1952. Zika Virus (I). Isolations and serological specificity. Trans R Soc Trop Med Hyg 46:509–520.
2. MacNamara FN. 1954. Zika virus : A report on three cases of human infection during an epidemic of jaundice in Nigeria. Trans R Soc Trop Med Hyg 48:139–145.
3. Haddow AD, Schuh AJ, Yasuda CY, Kasper MR, Heang V, Huy R, Guzman H, Tesh RB, Weaver SC. 2012. Genetic Characterization of Zika Virus Strains: Geographic Expansion of the Asian Lineage. PLoS Negl Trop Dis 6.
4. Marchette NJ, Garcia R, Rudnick A. 1969. Isolation of Zika Virus from Aedes Aegypti Mosquitoes in Malaysia *. Am J Trop Med Hyg 18:411–415.
5. Musso D, Gubler DJ. 2016. Zika Virus. Clin Microbiol Rev 29:487–524.
6. Wikan N, Smith DR. 2017. Zika virus from a Southeast Asian perspective. Asian Pac J Trop Med 10:1–5.
7. Rather IA, Lone JB, Bajpai VK, Paek WK, Lim J. 2017. Zika Virus: An Emerging Worldwide Threat. Front Microbiol 8.
8. Faye O, Freire CCM, Iamarino A, Faye O, Oliveira JVC de, Diallo M, Zanotto PMA, Sall AA. 2014. Molecular Evolution of Zika Virus during Its Emergence in the 20th Century. PLoS Negl Trop Dis 8:e2636.
9. Duffy MR, Chen T-H, Hancock WT, Powers AM, Kool JL, Lanciotti RS, Pretrick M, Marfel M, Holzbauer S, Dubray C, Guillaumot L, Griggs A, Bel M, Lambert AJ, Laven J, Kosoy O, Panella A, Biggerstaff BJ, Fischer M, Hayes EB. 2009. Zika Virus Outbreak on Yap Island, Federated States of Micronesia. N Engl J Med 360:2536–2543.
10. Campos GS, Bandeira AC, Sardi SI. 2015. Zika Virus Outbreak, Bahia, Brazil. Emerg Infect Dis 21.

11. Cao-Lormeau V-M, Roche C, Teissier A, Robin E, Berry A-L, Mallet H-P, Sall AA, Musso D. 2014. Zika Virus, French Polynesia, South Pacific, 2013. Emerg Infect Dis 20:1085–1086.
12. Wang L, Valderramos SG, Wu A, Ouyang S, Li C, Brasil P, Bonaldo M, Coates T, Nielsen-Saines K, Jiang T, Aliyari R, Cheng G. 2016. From Mosquitos to Humans: Genetic Evolution of Zika Virus. Cell Host Microbe 19:561–565.
13. Faria NR, Azevedo R do S da S, Kraemer MUG, Souza R, Cunha MS, Hill SC, Thézé J, Bonsall MB, Bowden TA, Rissanen I, Rocco IM, Nogueira JS, Maeda AY, Vasami FG da S, Macedo FL de L, Suzuki A, Rodrigues SG, Cruz ACR, Nunes BT, Medeiros DB de A, Rodrigues DSG, Queiroz ALN, da Silva EVP, Henriques DF, da Rosa EST, de Oliveira CS, Martins LC, Vasconcelos HB, Casseb LMN, Simith D de B, Messina JP, Abade L, Lourenço J, Alcantara LCJ, de Lima MM, Giovanetti M, Hay SI, de Oliveira RS, Lemos P da S, de Oliveira LF, de Lima CPS, da Silva SP, de Vasconcelos JM, Franco L, Cardoso JF, Vianez-Júnior JL da SG, Mir D, Bello G, Delatorre E, Khan K, Creatore M, Coelho GE, de Oliveira WK, Tesh R, Pybus OG, Nunes MRT, Vasconcelos PFC. 2016. Zika virus in the Americas: Early epidemiological and genetic findings. Science 352:345–349.
14. D'Ortenzio E, Matheron S, de Lamballerie X, Hubert B, Piorkowski G, Maquart M, Descamps D, Damond F, Yazdanpanah Y, Leparc-Goffart I. 2016. Evidence of Sexual Transmission of Zika Virus. N Engl J Med 374:2195–2198.
15. Musso D, Richard V, Teissier A, Stone M, Lanteri MC, Latoni G, Alsina J, Reik R, Busch MP. 2017. Detection of Zika virus RNA in semen of asymptomatic blood donors. Clin Microbiol Infect Off Publ Eur Soc Clin Microbiol Infect Dis 23:1001.e1-1001.e3.
16. Musso D, Roche C, Robin E, Nhan T, Teissier A, Cao-Lormeau V-M. 2015. Potential Sexual Transmission of Zika Virus. Emerg Infect Dis 21:359–361.
17. Musso D, Nhan T, Robin E, Roche C, Bierlaire D, Zisou K, Yan AS, Cao-Lormeau VM, Broult J. 2014. Potential for Zika virus transmission through blood transfusion

demonstrated during an outbreak in French Polynesia, November 2013 to February 2014. Eurosurveillance 19:20761.

18. Driggers RW, Ho C-Y, Korhonen EM, Kuivanen S, Jääskeläinen AJ, Smura T, Rosenberg A, Hill DA, DeBiasi RL, Vezina G, Timofeev J, Rodriguez FJ, Levanov L, Razak J, Iyengar P, Hennenfent A, Kennedy R, Lanciotti R, du Plessis A, Vapalahti O. 2016. Zika Virus Infection with Prolonged Maternal Viremia and Fetal Brain Abnormalities. N Engl J Med 374:2142–2151.
19. Motta IJF, Spencer BR, Cordeiro da Silva SG, Arruda MB, Dobbin JA, Gonzaga YBM, Arcuri IP, Tavares RCBS, Atta EH, Fernandes RFM, Costa DA, Ribeiro LJ, Limonte F, Higa LM, Voloch CM, Brindeiro RM, Tanuri A, Ferreira OC. 2016. Evidence for Transmission of Zika Virus by Platelet Transfusion. N Engl J Med 375:1101–1103.
20. Mitchell C. 2016. PAHO/WHO | WHO announces a Public Health Emergency of International Concern. Pan Am Health Organ World Health Organ. https://www3.paho.org/hq/index.php?option=com_content&view=article&id=11640:2016-who-statement-on-1st-meeting-ihr-2005-emergency-committee-on-zika-virus&Itemid=0&lang=en#gsc.tab=0. Retrieved 14 December 2022.
21. Foy BD, Kobylinski KC, Foy JLC, Blitvich BJ, Travassos da Rosa A, Haddow AD, Lanciotti RS, Tesh RB. 2011. Probable Non–Vector-borne Transmission of Zika Virus, Colorado, USA. Emerg Infect Dis 17:880–882.
22. Wongsurawat T, Athipanyasilp N, Jenjaroenpun P, Jun S-R, Kaewnapan B, Wassenaar TM, Leelahakorn N, Angkasekwinai N, Kantakamalakul W, Ussery DW, Sutthent R, Nookaew I, Horthongkham N. 2018. Case of Microcephaly after Congenital Infection with Asian Lineage Zika Virus, Thailand. Emerg Infect Dis 24:1758–1761.
23. Lan PT, Quang LC, Huong VTQ, Thuong NV, Hung PC, Huong TTLN, Thao HP, Thao NTT, Mounts AW, Nolen LD. 2017. Fetal Zika Virus Infection in Vietnam. PLoS Curr 9:ecurrents.outbreaks.1c8f631e0ef8cd7777d639eba48647fa.

24. World Health Organization. 2022. map-of-countries_with_zika_transmission_feb2022.pdf. https://cdn.who.int/media/docs/default-source/documents/emergencies/zika/map-of-countries_with_zika_transmission_feb2022.pdf?sfvrsn=802a352a_5. Retrieved 14 December 2022.
25. Philip C, Novick CG, Novick LF. 2019. Local Transmission of Zika Virus in Miami-Dade County: The Florida Department of Health Rises to the Challenge. J Public Health Manag Pract 25:277–287.
26. Brady OJ, Hay SI. 2019. The first local cases of Zika virus in Europe. The Lancet 394:1991–1992.
27. Durand GA, Piorkowski G, Thirion L, Ninove L, Giron S, Zandotti C, Denis J, Badaut C, Failloux A-B, Grard G, Leparc-Goffart I, de Lamballerie X. 2020. Vector-Borne Transmission of the Zika Virus Asian Genotype in Europe. 3. Viruses 12:296.
28. Hill SC, Vasconcelos J, Neto Z, Jandondo D, Zé-Zé L, Aguiar RS, Xavier J, Thézé J, Mirandela M, Cândido ALM, Vaz F, Sebastião C dos S, Wu C-H, Kraemer MUG, Melo A, Schamber-Reis BLF, Azevedo GS de, Tanuri A, Higa LM, Clemente C, Silva SP da, Candido D da S, Claro IM, Quibuco D, Domingos C, Pocongo B, Watts AG, Khan K, Alcantara LCJ, Sabino EC, Lackritz E, Pybus OG, Alves M-J, Afonso J, Faria NR. 2019. Emergence of the Asian lineage of Zika virus in Angola: an outbreak investigation. Lancet Infect Dis 19:1138–1147.
29. CDC. 2021. Reporting and Surveillance - Zika Virus. Cent Dis Control Prev. http://www.cdc.gov/zika/reporting/index.html. Retrieved 14 December 2022.
30. Rossati A. 2016. Global Warming and Its Health Impact. Int J Occup Environ Med 8:7–20.
31. Pielnaa P, Al-Saadawe M, Saro A, Dama MF, Zhou M, Huang Y, Huang J, Xia Z. 2020. Zika virus-spread, epidemiology, genome, transmission cycle, clinical manifestation, associated challenges, vaccine and antiviral drug development. Virology 543:34–42.

32. Lee JK, Shin OS. 2019. Advances in Zika Virus–Host Cell Interaction: Current Knowledge and Future Perspectives. Int J Mol Sci 20.

33. Oehler E, Watrin L, Larre P, Leparc-Goffart I, Lastère S, Valour F, Baudouin L, Mallet HP, Musso D, Ghawche F. 2014. Zika virus infection complicated by Guillain-Barré syndrome – case report, French Polynesia, December 2013. Eurosurveillance 19:20720.

34. Cao-Lormeau V-M, Blake A, Mons S, Lastère S, Roche C, Vanhomwegen J, Dub T, Baudouin L, Teissier A, Larre P, Vial A-L, Decam C, Choumet V, Halstead SK, Willison HJ, Musset L, Manuguerra J-C, Despres P, Fournier E, Mallet H-P, Musso D, Fontanet A, Neil J, Ghawché F. 2016. Guillain-Barré Syndrome outbreak associated with Zika virus infection in French Polynesia: a case-control study. The Lancet 387:1531–1539.

35. Weaver SC, Costa F, Garcia-Blanco MA, Ko AI, Ribeiro GS, Saade G, Shi P-Y, Vasilakis N. 2016. Zika Virus: History, Emergence, Biology, and Prospects for Control. Antiviral Res 130:69–80.

36. dos Santos T, Rodriguez A, Almiron M, Sanhueza A, Ramon P, de Oliveira WK, Coelho GE, Badaró R, Cortez J, Ospina M, Pimentel R, Masis R, Hernandez F, Lara B, Montoya R, Jubithana B, Melchor A, Alvarez A, Aldighieri S, Dye C, Espinal MA. 2016. Zika Virus and the Guillain–Barré Syndrome — Case Series from Seven Countries. N Engl J Med 375:1598–1601.

37. Sun LH. 2016. Zika causes a unique syndrome of devastating birth defects. Wash Post.

38. Sarno M, Sacramento GA, Khouri R, do Rosário MS, Costa F, Archanjo G, Santos LA, Nery N, Vasilakis N, Ko AI, de Almeida ARP. 2016. Zika Virus Infection and Stillbirths: A Case of Hydrops Fetalis, Hydranencephaly and Fetal Demise. PLoS Negl Trop Dis 10:e0004517.

39. Adams Waldorf KM, Nelson BR, Stencel-Baerenwald JE, Studholme C, Kapur RP, Armistead B, Walker CL, Merillat S, Vornhagen J, Tisoncik-Go J, Baldessari A, Coleman M, Dighe MK, Shaw DWW, Roby JA, Santana-Ufret V, Boldenow E, Li J, Gao X, Davis

MA, Swanstrom JA, Jensen K, Widman DG, Baric RS, Medwid JT, Hanley KA, Ogle J, Gough GM, Lee W, English C, Durning WM, Thiel J, Gatenby C, Dewey EC, Fairgrieve MR, Hodge RD, Grant RF, Kuller L, Dobyns WB, Hevner RF, Gale M, Rajagopal L. 2018. Congenital Zika Virus Infection as a Silent Pathology With Loss of Neurogenic Output in the Fetal Brain. Nat Med 24:368–374.

40. Adams Waldorf KM, Stencel-Baerenwald JE, Kapur RP, Studholme C, Boldenow E, Vornhagen J, Baldessari A, Dighe MK, Thiel J, Merillat S, Armistead B, Tisoncik-Go J, Davis MA, Dewey EC, Fairgrieve MR, Gatenby C, Richards T, Garden GA, Fernandez E, Diamond MS, Juul SE, Grant RF, Kuller L, Shaw DWW, Ogle J, Gough GM, Lee W, English C, Hevner RF, Dobyns WB, Gale M, Rajagopal L. 2016. Fetal brain lesions after subcutaneous inoculation of Zika virus in a pregnant nonhuman primate. Nat Med 22:1256–1259.

41. Dudley DM, Van Rompay KK, Coffey LL, Ardeshir A, Keesler RI, Bliss-Moreau E, Grigsby PL, Steinbach RJ, Hirsch AJ, MacAllister RP, Pecoraro HL, Colgin LM, Hodge T, Streblow DN, Tardif S, Patterson JL, Tamhankar M, Seferovic M, Aagaard KM, Martín CS-S, Chiu CY, Panganiban AT, Veazey RS, Wang X, Maness NJ, Gilbert MH, Bohm RP, Adams Waldorf KM, Gale M, Rajagopal L, Hotchkiss CE, Mohr EL, Capuano SV, Simmons HA, Mejia A, Friedrich TC, Golos TG, O'Connor DH. 2018. Miscarriage and stillbirth following maternal Zika virus infection in nonhuman primates. Nat Med 24:1104–1107.

42. Miner JJ, Diamond MS. 2017. Zika Virus Pathogenesis and Tissue Tropism. Cell Host Microbe 21:134–142.

43. Bhatnagar J, Rabeneck DB, Martines RB, Reagan-Steiner S, Ermias Y, Estetter LBC, Suzuki T, Ritter J, Keating MK, Hale G, Gary J, Muehlenbachs A, Lambert A, Lanciotti R, Oduyebo T, Meaney-Delman D, Bolaños F, Saad EAP, Shieh W-J, Zaki SR. 2017. Zika

Virus RNA Replication and Persistence in Brain and Placental Tissue. Emerg Infect Dis 23:405–414.

44. Tang H, Hammack C, Ogden SC, Wen Z, Qian X, Li Y, Yao B, Shin J, Zhang F, Lee EM, Christian KM, Didier RA, Jin P, Song H, Ming G. 2016. Zika Virus Infects Human Cortical Neural Progenitors and Attenuates Their Growth. Cell Stem Cell 18:587–590.

45. Dang J, Tiwari SK, Lichinchi G, Qin Y, Patil VS, Eroshkin AM, Rana TM. 2016. Zika Virus Depletes Neural Progenitors in Human Cerebral Organoids through Activation of the Innate Immune Receptor TLR3. Cell Stem Cell 19:258–265.

46. Ferraris P, Cochet M, Hamel R, Gladwyn-Ng I, Alfano C, Diop F, Garcia D, Talignani L, Montero-Menei CN, Nougairède A, Yssel H, Nguyen L, Coulpier M, Missé D. 2019. Zika virus differentially infects human neural progenitor cells according to their state of differentiation and dysregulates neurogenesis through the Notch pathway. Emerg Microbes Infect 8:1003–1016.

47. Gazeta RE, Bertozzi APAP, Dezena R de C de AB, Silva ACB, Fajardo TCG, Catalan DT, Rizzo M de FV, Moron AF, Soriano-Arandes A, Clemente NS, Quintella T, Ventura DF, Damico FM, França V de CR de M, Almeida JPG de, Zara AL de SA, Pires LC, Jundiaí CZV, Passos SD. 2021. Three-Year Clinical Follow-Up of Children Intrauterine Exposed to Zika Virus. Viruses 13:523.

48. Mulkey SB, Arroyave-Wessel M, Peyton C, Bulas DI, Fourzali Y, Jiang J, Russo S, McCarter R, Msall ME, du Plessis AJ, DeBiasi RL, Cure C. 2020. Neurodevelopmental Abnormalities in Children With In Utero Zika Virus Exposure Without Congenital Zika Syndrome. JAMA Pediatr 174:269–276.

49. Bertolli J, Attell JE, Rose C, Moore CA, Melo F, Staples JE, Kotzky K, Krishna N, Satterfield-Nash A, Pereira IO, Pessoa A, Smith DC, Santelli ACF e S, Boyle CA, Peacock G. 2020. Functional Outcomes among a Cohort of Children in Northeastern

Brazil Meeting Criteria for Follow-Up of Congenital Zika Virus Infection. Am J Trop Med Hyg 102:955–963.

50. Barrows NJ, Campos RK, Liao K-C, Prasanth KR, Soto-Acosta R, Yeh S-C, Schott-Lerner G, Pompon J, Sessions OM, Bradrick SS, Garcia-Blanco MA. 2018. Biochemistry and Molecular Biology of Flaviviruses. Chem Rev 118:4448–4482.

51. Kaufmann B, Rossmann MG. 2011. Molecular mechanisms involved in the early steps of flavivirus cell entry. Microbes Infect Inst Pasteur 13:1–9.

52. Tabata T, Petitt M, Puerta-Guardo H, Michlmayr D, Wang C, Fang-Hoover J, Harris E, Pereira L. 2016. Zika Virus Targets Different Primary Human Placental Cells, Suggesting Two Routes for Vertical Transmission. Cell Host Microbe 20:155–166.

53. Meertens L, Labeau A, Dejarnac O, Cipriani S, Sinigaglia L, Bonnet-Madin L, Le Charpentier T, Hafirassou ML, Zamborlini A, Cao-Lormeau V-M, Coulpier M, Missé D, Jouvenet N, Tabibiazar R, Gressens P, Schwartz O, Amara A. 2017. Axl Mediates ZIKA Virus Entry in Human Glial Cells and Modulates Innate Immune Responses. Cell Rep 18:324–333.

54. Hamel R, Dejarnac O, Wichit S, Ekchariyawat P, Neyret A, Luplertlop N, Perera-Lecoin M, Surasombatpattana P, Talignani L, Thomas F, Cao-Lormeau V-M, Choumet V, Briant L, Desprès P, Amara A, Yssel H, Missé D. 2015. Biology of Zika Virus Infection in Human Skin Cells. J Virol 89:8880–8896.

55. Wells MF, Salick MR, Wiskow O, Ho DJ, Worringer KA, Ihry RJ, Kommineni S, Bilican B, Klim JR, Hill EJ, Kane LT, Ye C, Kaykas A, Eggan K. 2016. Genetic Ablation of AXL Does Not Protect Human Neural Progenitor Cells and Cerebral Organoids from Zika Virus Infection. Cell Stem Cell 19:703–708.

56. Carro SD, Cherry S. 2020. Beyond the Surface: Endocytosis of Mosquito-Borne Flaviviruses. Viruses 13.

57. Mazeaud C, Freppel W, Chatel-Chaix L. 2018. The Multiples Fates of the Flavivirus RNA Genome During Pathogenesis. Front Genet 9:595.

58. Brand C, Bisaillon M, Geiss BJ. 2017. Organization of the Flavivirus RNA replicase complex. WIREs RNA 8:e1437.

59. Mukhopadhyay S, Kuhn RJ, Rossmann MG. 2005. A structural perspective of the flavivirus life cycle. Nat Rev Microbiol 3:13–22.

60. Kim J-A, Seong R-K, Son SW, Shin OS. 2019. Insights into ZIKV-Mediated Innate Immune Responses in Human Dermal Fibroblasts and Epidermal Keratinocytes. J Invest Dermatol 139:391–399.

61. Foo S-S, Chen W, Chan Y, Bowman JW, Chang L-C, Choi Y, Yoo JS, Ge J, Cheng G, Bonnin A, Nielsen-Saines K, Brasil P, Jung JU. 2017. Asian Zika virus strains target CD14+ blood monocytes and induce M2-skewed immunosuppression during pregnancy. Nat Microbiol 2:1558–1570.

62. Michlmayr D, Andrade P, Gonzalez K, Balmaseda A, Harris E. 2017. CD14+CD16+ monocytes are the main target of Zika virus infection in peripheral blood mononuclear cells in a paediatric study in Nicaragua. Nat Microbiol 2:1462–1470.

63. Coldbeck-Shackley RC, Eyre NS, Beard MR. 2020. The Molecular Interactions of ZIKV and DENV with the Type-I IFN Response. 3. Vaccines 8:530.

64. Beaver JT, Lelutiu N, Habib R, Skountzou I. 2018. Evolution of Two Major Zika Virus Lineages: Implications for Pathology, Immune Response, and Vaccine Development. Front Immunol 9.

65. Göertz GP, Abbo SR, Fros JJ, Pijlman GP. 2018. Functional RNA during Zika virus infection. Virus Res 254:41–53.

66. Roby JA, Pijlman GP, Wilusz J, Khromykh AA. 2014. Noncoding Subgenomic Flavivirus RNA: Multiple Functions in West Nile Virus Pathogenesis and Modulation of Host Responses. Viruses 6:404–427.

67. Ruggieri A, Helm M, Chatel-Chaix L. 2021. An epigenetic ‘extreme makeover’: the methylation of flaviviral RNA (and beyond). RNA Biol 1–13.

68. Dong H, Ray D, Ren S, Zhang B, Puig-Basagoiti F, Takagi Y, Ho CK, Li H, Shi P-Y. 2007. Distinct RNA elements confer specificity to flavivirus RNA cap methylation events. J Virol 81:4412–4421.

69. Ray D, Shah A, Tilgner M, Guo Y, Zhao Y, Dong H, Deas TS, Zhou Y, Li H, Shi P-Y. 2006. West Nile Virus 5′-Cap Structure Is Formed by Sequential Guanine N-7 and Ribose 2′-O Methylations by Nonstructural Protein 5. J Virol 80:8362–8370.

70. Daffis S, Szretter KJ, Schriewer J, Li J, Youn S, Errett J, Lin T-Y, Schneller S, Zust R, Dong H, Thiel V, Sen GC, Fensterl V, Klimstra WB, Pierson TC, Buller RM, Gale Jr M, Shi P-Y, Diamond MS. 2010. 2′-O methylation of the viral mRNA cap evades host restriction by IFIT family members. 7322. Nature 468:452–456.

71. Hyde JL, Diamond MS. 2015. Innate immune restriction and antagonism of viral RNA lacking 2′-O methylation. Virology 479–480:66–74.

72. Szretter KJ, Daniels BP, Cho H, Gainey MD, Yokoyama WM, Jr MG, Virgin HW, Klein RS, Sen GC, Diamond MS. 2012. 2′-O Methylation of the Viral mRNA Cap by West Nile Virus Evades Ifit1-Dependent and -Independent Mechanisms of Host Restriction In Vivo. PLOS Pathog 8:e1002698.

73. Kimura T, Katoh H, Kayama H, Saiga H, Okuyama M, Okamoto T, Umemoto E, Matsuura Y, Yamamoto M, Takeda K. 2013. Ifit1 Inhibits Japanese Encephalitis Virus Replication through Binding to 5′ Capped 2′-O Unmethylated RNA. J Virol 87:9997–10003.

74. Filomatori CV, Lodeiro MF, Alvarez DE, Samsa MM, Pietrasanta L, Gamarnik AV. 2006. A 5′ RNA element promotes dengue virus RNA synthesis on a circular genome. Genes Dev 20:2238–2249.

75. Liu Z-Y, Li X-F, Jiang T, Deng Y-Q, Ye Q, Zhao H, Yu J-Y, Qin C-F. 2016. Viral RNA switch mediates the dynamic control of flavivirus replicase recruitment by genome cyclization. eLife 5:e17636.

76. Fajardo T, Sanford TJ, Mears HV, Jasper A, Storrie S, Mansur DS, Sweeney TR. 2020. The flavivirus polymerase NS5 regulates translation of viral genomic RNA. Nucleic Acids Res 48:5081–5093.

77. Khromykh AA, Meka H, Guyatt KJ, Westaway EG. 2001. Essential role of cyclization sequences in flavivirus RNA replication. J Virol 75:6719–6728.

78. Alvarez DE, Lodeiro MF, Ludueña SJ, Pietrasanta LI, Gamarnik AV. 2005. Long-Range RNA-RNA Interactions Circularize the Dengue Virus Genome. J Virol 79:6631–6643.

79. Khromykh AA, Kondratieva N, Sgro J-Y, Palmenberg A, Westaway EG. 2003. Significance in Replication of the Terminal Nucleotides of the Flavivirus Genome. J Virol 77:10623–10629.

80. Cleaves GR, Ryan TE, Walter Schlesinger R. 1981. Identification and characterization of type 2 dengue virus replicative intermediate and replicative form RNAs. Virology 111:73–83.

81. Kim Y-G, Yoo J-S, Kim J-H, Kim C-M, Oh J-W. 2007. Biochemical characterization of a recombinant Japanese encephalitis virus RNA-dependent RNA polymerase. BMC Mol Biol 8:59.

82. Clarke BD, Roby JA, Slonchak A, Khromykh AA. 2015. Functional non-coding RNAs derived from the flavivirus 3′ untranslated region. Virus Res 206:53–61.

83. Akiyama BM, Laurence HM, Massey AR, Costantino DA, Xie X, Yang Y, Shi P-Y, Nix JC, Beckham JD, Kieft JS. 2016. Zika virus produces noncoding RNAs using a multi-pseudoknot structure that confounds a cellular exonuclease. Science 354:1148–1152.

84. Slonchak A, Wang X, Aguado J, Sng JDJ, Chaggar H, Freney ME, Yan K, Torres FJ, Amarilla AA, Balea R, Setoh YX, Peng N, Watterson D, Wolvetang E, Suhrbier A,

Khromykh AA. 2022. Zika virus noncoding RNA cooperates with the viral protein NS5 to inhibit STAT1 phosphorylation and facilitate viral pathogenesis. Sci Adv 8:eadd8095.

85. Pierson TC, Diamond MS. 2020. The continued threat of emerging flaviviruses. Nat Microbiol https://doi.org/10.1038/s41564-020-0714-0.

86. Pierson TC, Graham BS. 2016. Zika virus: immunity and vaccine development. Cell 167:625–631.

87. Zhang Y, Corver J, Chipman PR, Zhang W, Pletnev SV, Sedlak D, Baker TS, Strauss JH, Kuhn RJ, Rossmann MG. 2003. Structures of immature flavivirus particles. EMBO J 22:2604–2613.

88. Sirohi D, Chen Z, Sun L, Klose T, Pierson TC, Rossmann MG, Kuhn RJ. 2016. The 3.8 Å resolution cryo-EM structure of Zika virus. Science 352:467–470.

89. Kuhn RJ, Zhang W, Rossmann MG, Pletnev SV, Corver J, Lenches E, Jones CT, Mukhopadhyay S, Chipman PR, Strauss EG, Baker TS, Strauss JH. 2002. Structure of dengue virus: implications for flavivirus organization, maturation, and fusion. Cell 108:717–725.

90. Tan TY, Fibriansah G, Kostyuchenko VA, Ng T-S, Lim X-X, Zhang S, Lim X-N, Wang J, Shi J, Morais MC, Corti D, Lok S-M. 2020. Capsid protein structure in Zika virus reveals the flavivirus assembly process. Nat Commun 11.

91. Rana J, Slon Campos JL, Leccese G, Francolini M, Bestagno M, Poggianella M, Burrone OR. 2018. Role of Capsid Anchor in the Morphogenesis of Zika Virus. J Virol 92:e01174-18.

92. Oliveira ERA, Mohana-Borges R, de Alencastro RB, Horta BAC. 2017. The flavivirus capsid protein: Structure, function and perspectives towards drug design. Virus Res 227:115–123.

93. Slomnicki LP, Chung D-H, Parker A, Hermann T, Boyd NL, Hetman M. 2017. Ribosomal stress and Tp53-mediated neuronal apoptosis in response to capsid protein of the Zika virus. Sci Rep 7:16652.

94. Fontaine KA, Leon KE, Khalid MM, Tomar S, Jimenez-Morales D, Dunlap M, Kaye JA, Shah PS, Finkbeiner S, Krogan NJ, Ott M. 2018. The Cellular NMD Pathway Restricts Zika Virus Infection and Is Targeted by the Viral Capsid Protein. mBio 9:e02126-18.

95. Jaffrey S, Wilkinson MF. 2018. Nonsense-mediated RNA decay in the brain: Emerging modulator of neural development and disease. Nat Rev Neurosci 19:715–728.

96. Zeng J, Dong S, Luo Z, Xie X, Fu B, Li P, Liu C, Yang X, Chen Y, Wang X, Liu Z, Wu J, Yan Y, Wang F, Chen J-F, Zhang J, Long G, Goldman SA, Li S, Zhao Z, Liang Q. 2020. The Zika Virus Capsid Disrupts Corticogenesis by Suppressing Dicer Activity and miRNA Biogenesis. Cell Stem Cell 27:618-632.e9.

97. Jinek M, Doudna JA. 2009. A three-dimensional view of the molecular machinery of RNA interference. Nature 457:405–412.

98. Rajman M, Schratt G. 2017. MicroRNAs in neural development: from master regulators to fine-tuners. Dev Camb Engl 144:2310–2322.

99. Yoshii K, Igarashi M, Ichii O, Yokozawa K, Ito K, Kariwa H, Takashima I. 2012. A conserved region in the prM protein is a critical determinant in the assembly of flavivirus particles. J Gen Virol 93:27–38.

100. Zhang Q, Hunke C, Yau YH, Seow V, Lee S, Tanner LB, Guan XL, Wenk MR, Fibriansah G, Chew PL, Kukkaro P, Biuković G, Shi P-Y, Shochat SG, Grüber G, Lok S-M. 2012. The Stem Region of Premembrane Protein Plays an Important Role in the Virus Surface Protein Rearrangement during Dengue Maturation*. J Biol Chem 287:40525–40534.

101. Nambala P, Yu W-Y, Lo Y-C, Lin CW, Su W-C. 2020. Ubiquitination of Zika Virus Precursor Membrane Protein Promotes the Release of Viral Proteins. Virus Res 198065.

102. Yuan L, Huang X-Y, Liu Z-Y, Zhang F, Zhu X-L, Yu J-Y, Ji X, Xu Y-P, Li G, Li C, Wang H-J, Deng Y-Q, Wu M, Cheng M-L, Ye Q, Xie D-Y, Li X-F, Wang X, Shi W, Hu B, Shi P-Y, Xu Z, Qin C-F. 2017. A single mutation in the prM protein of Zika virus contributes to fetal microcephaly. Science 358:933–936.

103. Nakayama E, Kato F, Tajima S, Ogawa S, Yan K, Takahashi K, Sato Y, Suzuki T, Kawai Y, Inagaki T, Taniguchi S, Le TT, Tang B, Prow NA, Uda A, Maeki T, Lim C-K, Khromykh AA, Suhrbier A, Saijo M. 2021. Neuroinvasiveness of the MR766 strain of Zika virus in IFNAR-/- mice maps to prM residues conserved amongst African genotype viruses. PLOS Pathog 17:e1009788.

104. Chávez JH, Silva JR, Amarilla AA, Moraes Figueiredo LT. 2010. Domain III peptides from flavivirus envelope protein are useful antigens for serologic diagnosis and targets for immunization. Biologicals 38:613–618.

105. Ngono AE, Shresta S. 2018. Immune Response to Dengue and Zika. Annu Rev Immunol 36:279–308.

106. Beasley DWC, Whiteman MC, Zhang S, Huang CY-H, Schneider BS, Smith DR, Gromowski GD, Higgs S, Kinney RM, Barrett ADT. 2005. Envelope Protein Glycosylation Status Influences Mouse Neuroinvasion Phenotype of Genetic Lineage 1 West Nile Virus Strains. J Virol 79:8339–8347.

107. Miller JL, deWet BJM, Martinez-Pomares L, Radcliffe CM, Dwek RA, Rudd PM, Gordon S. 2008. The Mannose Receptor Mediates Dengue Virus Infection of Macrophages. PLOS Pathog 4:e17.

108. Pokidysheva E, Zhang Y, Battisti AJ, Bator-Kelly CM, Chipman PR, Xiao C, Gregorio GG, Hendrickson WA, Kuhn RJ, Rossmann MG. 2006. Cryo-EM Reconstruction of Dengue Virus in Complex with the Carbohydrate Recognition Domain of DC-SIGN. Cell 124:485–493.

109. Carbaugh DL, Baric RS, Lazear HM. 2019. Envelope Protein Glycosylation Mediates Zika Virus Pathogenesis. J Virol 93:e00113-19.

110. Fontes-Garfias CR, Shan C, Luo H, Muruato AE, Medeiros DBA, Mays E, Xie X, Zou J, Roundy CM, Wakamiya M, Rossi SL, Wang T, Weaver SC, Shi P-Y. 2017. Functional analysis of glycosylation of Zika virus envelope protein. Cell Rep 21:1180–1190.

111. Gong D, Zhang T-H, Zhao D, Du Y, Chapa TJ, Shi Y, Wang L, Contreras D, Zeng G, Shi P-Y, Wu T-T, Arumugaswami V, Sun R. 2018. High-Throughput Fitness Profiling of Zika Virus E Protein Reveals Different Roles for Glycosylation during Infection of Mammalian and Mosquito Cells. iScience 1:97–111.

112. Annamalai AS, Pattnaik A, Sahoo BR, Muthukrishnan E, Natarajan SK, Steffen D, Vu HLX, Delhon G, Osorio FA, Petro TM, Xiang S-H, Pattnaik AK. 2017. Zika Virus Encoding Nonglycosylated Envelope Protein Is Attenuated and Defective in Neuroinvasion. J Virol 91:e01348-17.

113. Mossenta M, Marchese S, Poggianella M, Slon Campos JL, Burrone OR. 2017. Role of N-glycosylation on Zika virus E protein secretion, viral assembly and infectivity. Biochem Biophys Res Commun 492:579–586.

114. Guo Y, Bao L, Xu Y, Li F, Lv Q, Fan F, Qin C. 2021. The Ablation of Envelope Protein Glycosylation Enhances the Neurovirulence of ZIKV and Cell Apoptosis in Newborn Mice. J Immunol Res 2021:5317662.

115. Wichit S, Gumpangseth N, Hamel R, Yainoy S, Arikit S, Punsawad C, Missé D. 2021. Chikungunya and Zika Viruses: Co-Circulation and the Interplay between Viral Proteins and Host Factors. Pathog Basel Switz 10.

116. Rajah MM, Monel B, Schwartz O. 2020. The entanglement between flaviviruses and ER-shaping proteins. PLOS Pathog 16:e1008389.

117. Neufeldt CJ, Joyce MA, Van Buuren N, Levin A, Kirkegaard K, Gale Jr. M, Tyrrell DLJ, Wozniak RW. 2016. The Hepatitis C Virus-Induced Membranous Web and Associated

Nuclear Transport Machinery Limit Access of Pattern Recognition Receptors to Viral Replication Sites. PLoS Pathog 12:e1005428.

118. Ci Y, Liu Z-Y, Zhang N-N, Niu Y, Yang Y, Xu C, Yang W, Qin C-F, Shi L. 2019. Zika NS1–induced ER remodeling is essential for viral replication. J Cell Biol 219:e201903062.
119. Youn S, Ambrose RL, Mackenzie JM, Diamond MS. 2013. Non-structural protein-1 is required for West Nile virus replication complex formation and viral RNA synthesis. Virol J 10:339.
120. Lindenbach BD, Rice CM. 1999. Genetic interaction of flavivirus nonstructural proteins NS1 and NS4A as a determinant of replicase function. J Virol 73:4611–4621.
121. Hilgenfeld R. 2016. Zika virus NS1, a pathogenicity factor with many faces. EMBO J 35:2631–2633.
122. Brown WC, Akey DL, Konwerski JR, Tarrasch JT, Skiniotis G, Kuhn RJ, Smith JL. 2016. Extended surface for membrane association in Zika virus NS1 structure. 9. Nat Struct Mol Biol 23:865–867.
123. Xu X, Song H, Qi J, Liu Y, Wang H, Su C, Shi Y, Gao GF. 2016. Contribution of intertwined loop to membrane association revealed by Zika virus full-length NS1 structure. EMBO J 35:2170–2178.
124. Akey DL, Brown WC, Dutta S, Konwerski J, Jose J, Jurkiw TJ, DelProposto J, Ogata CM, Skiniotis G, Kuhn RJ, Smith JL. 2014. Flavivirus NS1 structures reveal surfaces for associations with membranes and the immune system. Science 343:881–885.
125. Noisakran S, Dechtawewat T, Avirutnan P, Kinoshita T, Siripanyaphinyo U, Puttikhunt C, Kasinrerk W, Malasit P, Sittisombut N. 2008. Association of dengue virus NS1 protein with lipid rafts. J Gen Virol 89:2492–2500.
126. Płaszczyca A, Scaturro P, Neufeldt CJ, Cortese M, Cerikan B, Ferla S, Brancale A, Pichlmair A, Bartenschlager R. 2019. A novel interaction between dengue virus nonstructural protein 1 and the NS4A-2K-4B precursor is required for viral RNA

replication but not for formation of the membranous replication organelle. PLOS Pathog 15:e1007736.

127. Youn S, Li T, McCune BT, Edeling MA, Fremont DH, Cristea IM, Diamond MS. 2012. Evidence for a Genetic and Physical Interaction between Nonstructural Proteins NS1 and NS4B That Modulates Replication of West Nile Virus. J Virol 86:7360–7371.
128. Westaway EG, Mackenzie JM, Kenney MT, Jones MK, Khromykh AA. 1997. Ultrastructure of Kunjin virus-infected cells: colocalization of NS1 and NS3 with double-stranded RNA, and of NS2B with NS3, in virus-induced membrane structures. J Virol 71:6650–6661.
129. Scaturro P, Cortese M, Chatel-Chaix L, Fischl W, Bartenschlager R. 2015. Dengue Virus Non-structural Protein 1 Modulates Infectious Particle Production via Interaction with the Structural Proteins. PLOS Pathog 11:e1005277.
130. Jacobs MG, Robinson PJ, Bletchly C, Mackenzie JM, Young PR. 2000. Dengue virus nonstructural protein 1 is expressed in a glycosyl-phosphatidylinositol-linked form that is capable of signal transduction. FASEB J 14:1603–1610.
131. Flamand M, Megret F, Mathieu M, Lepault J, Rey FA, Deubel V. 1999. Dengue virus type 1 nonstructural glycoprotein NS1 is secreted from mammalian cells as a soluble hexamer in a glycosylation-dependent fashion. J Virol 73:6104–6110.
132. Gutsche I, Coulibaly F, Voss JE, Salmon J, d'Alayer J, Ermonval M, Larquet E, Charneau P, Krey T, Mégret F, Guittet E, Rey FA, Flamand M. 2011. Secreted dengue virus nonstructural protein NS1 is an atypical barrel-shaped high-density lipoprotein. Proc Natl Acad Sci U S A 108:8003–8008.
133. Young PR, Hilditch PA, Bletchly C, Halloran W. 2000. An antigen capture enzyme-linked immunosorbent assay reveals high levels of the dengue virus protein NS1 in the sera of infected patients. J Clin Microbiol 38:1053–1057.

134. Liu Y, Liu J, Du S, Shan C, Nie K, Zhang R, Li X-F, Zhang R, Wang T, Qin C-F, Wang P, Shi P-Y, Cheng G. 2017. Evolutionary enhancement of Zika virus infectivity in Aedes aegypti mosquitoes. Nature 545:482–486.

135. Wessel AW, Dowd KA, Biering SB, Zhang P, Edeling MA, Nelson CA, Funk KE, DeMaso CR, Klein RS, Smith JL, Cao TM, Kuhn RJ, Fremont DH, Harris E, Pierson TC, Diamond MS. 2021. Levels of Circulating NS1 Impact West Nile Virus Spread to the Brain. J Virol 95:e00844-21.

136. Puerta-Guardo H, Tabata T, Petitt M, Dimitrova M, Glasner DR, Pereira L, Harris E. 2020. Zika Virus Nonstructural Protein 1 Disrupts Glycosaminoglycans and Causes Permeability in Developing Human Placentas. J Infect Dis 221:313–324.

137. Wang C, Puerta-Guardo H, Biering SB, Glasner DR, Tran EB, Patana M, Gomberg TA, Malvar C, Lo NTN, Espinosa DA, Harris E. 2019. Endocytosis of flavivirus NS1 is required for NS1-mediated endothelial hyperpermeability and is abolished by a single N-glycosylation site mutation. PLoS Pathog 15:e1007938.

138. Puerta-Guardo H, Dr G, Da E, Sb B, M P, K R, C W, Pr B, E H. 2019. Flavivirus NS1 Triggers Tissue-Specific Vascular Endothelial Dysfunction Reflecting Disease Tropism. Cell Rep 26.

139. Zhang X, Xie X, Zou J, Xia H, Shan C, Chen X, Shi P-Y. 2019. Genetic and biochemical characterizations of Zika virus NS2A protein. Emerg Microbes Infect 8:585–602.

140. Xie X, Gayen S, Kang C, Yuan Z, Shi P-Y. 2013. Membrane Topology and Function of Dengue Virus NS2A Protein. J Virol 87:4609–4622.

141. Mackenzie JM, Khromykh AA, Jones MK, Westaway EG. 1998. Subcellular localization and some biochemical properties of the flavivirus Kunjin nonstructural proteins NS2A and NS4A. Virology 245:203–215.

142. Xie X, Zou J, Puttikhunt C, Yuan Z, Shi P-Y. 2014. Two Distinct Sets of NS2A Molecules Are Responsible for Dengue Virus RNA Synthesis and Virion Assembly. J Virol 89:1298–1313.

143. Wu R-H, Tsai M-H, Chao D-Y, Yueh A. 2015. Scanning mutagenesis studies reveal a potential intramolecular interaction within the C-terminal half of dengue virus NS2A involved in viral RNA replication and virus assembly and secretion. J Virol 89:4281–4295.

144. Kümmerer BM, Rice CM. 2002. Mutations in the yellow fever virus nonstructural protein NS2A selectively block production of infectious particles. J Virol 76:4773–4784.

145. Leung JY, Pijlman GP, Kondratieva N, Hyde J, Mackenzie JM, Khromykh AA. 2008. Role of Nonstructural Protein NS2A in Flavivirus Assembly. J Virol 82:4731–4741.

146. Liu WJ, Chen HB, Khromykh AA. 2003. Molecular and functional analyses of Kunjin virus infectious cDNA clones demonstrate the essential roles for NS2A in virus assembly and for a nonconservative residue in NS3 in RNA replication. J Virol 77:7804–7813.

147. Voßmann S, Wieseler J, Kerber R, Kümmerer BM. 2015. A basic cluster in the N terminus of yellow fever virus NS2A contributes to infectious particle production. J Virol 89:4951–4965.

148. Xie X, Zou J, Zhang X, Zhou Y, Routh AL, Kang C, Popov VL, Chen X, Wang Q-Y, Dong H, Shi P-Y. 2019. Dengue NS2A Protein Orchestrates Virus Assembly. Cell Host Microbe 26:606-622.e8.

149. Zhang X, Xie X, Xia H, Zou J, Huang L, Popov VL, Chen X, Shi P-Y. 2019. Zika Virus NS2A-Mediated Virion Assembly. mBio 10:e02375-19.

150. Shrivastava G, García-Cordero J, León-Juárez M, Oza G, Tapia-Ramírez J, Villegas-Sepulveda N, Cedillo-Barrón L. 2017. NS2A comprises a putative viroporin of Dengue virus 2. Virulence 8:1450–1456.

151. Chang Y-S, Liao C-L, Tsao C-H, Chen M-C, Liu C-I, Chen L-K, Lin Y-L. 1999. Membrane Permeabilization by Small Hydrophobic Nonstructural Proteins of Japanese Encephalitis Virus. J Virol 73:6257–6264.

152. Melian EB, Edmonds JH, Nagasaki TK, Hinzman E, Floden N, Khromykh AAY 2013. 2013. West Nile virus NS2A protein facilitates virus-induced apoptosis independently of interferon response. J Gen Virol 94:308–313.

153. Clum S, Ebner KE, Padmanabhan R. 1997. Cotranslational Membrane Insertion of the Serine Proteinase Precursor NS2B-NS3(Pro) of Dengue Virus Type 2 Is Required for Efficient in Vitro Processing and Is Mediated through the Hydrophobic Regions of NS2B*. J Biol Chem 272:30715–30723.

154. Li Y, Li Q, Wong YL, Liew LSY, Kang C. 2015. Membrane topology of NS2B of dengue virus revealed by NMR spectroscopy. Biochim Biophys Acta BBA - Biomembr 1848:2244–2252.

155. Bera AK, Kuhn RJ, Smith JL. 2007. Functional Characterization of cis and trans Activity of the Flavivirus NS2B-NS3 Protease*. J Biol Chem 282:12883–12892.

156. Chambers TJ, Grakoui A, Rice CM. 1991. Processing of the yellow fever virus nonstructural polyprotein: a catalytically active NS3 proteinase domain and NS2B are required for cleavages at dibasic sites. J Virol 65:6042–6050.

157. Chappell KJ, Stoermer MJ, Fairlie DP, Young PR. 2008. Mutagenesis of the West Nile virus NS2B cofactor domain reveals two regions essential for protease activity. J Gen Virol 89:1010–1014.

158. Falgout B, Pethel M, Zhang YM, Lai CJ. 1991. Both nonstructural proteins NS2B and NS3 are required for the proteolytic processing of dengue virus nonstructural proteins. J Virol 65:2467–2475.

159. Xing H, Xu S, Jia F, Yang Y, Xu C, Qin C, Shi L. 2020. Zika NS2B is a crucial factor recruiting NS3 to the ER and activating its protease activity. Virus Res 275:197793.

160. Yusof R, Clum S, Wetzel M, Murthy HM, Padmanabhan R. 2000. Purified NS2B/NS3 serine protease of dengue virus type 2 exhibits cofactor NS2B dependence for cleavage of substrates with dibasic amino acids in vitro. J Biol Chem 275:9963–9969.

161. Lei J, Hansen G, Nitsche C, Klein CD, Zhang L, Hilgenfeld R. 2016. Crystal structure of Zika virus NS2B-NS3 protease in complex with a boronate inhibitor. Science 353:503–505.

162. Erbel P, Schiering N, D'Arcy A, Renatus M, Kroemer M, Lim SP, Yin Z, Keller TH, Vasudevan SG, Hommel U. 2006. Structural basis for the activation of flaviviral NS3 proteases from dengue and West Nile virus. Nat Struct Mol Biol 13:372–373.

163. Chambers TJ, Nestorowicz A, Amberg SM, Rice CM. 1993. Mutagenesis of the yellow fever virus NS2B protein: effects on proteolytic processing, NS2B-NS3 complex formation, and viral replication. J Virol 67:6797–6807.

164. Falgout B, Miller RH, Lai CJ. 1993. Deletion analysis of dengue virus type 4 nonstructural protein NS2B: identification of a domain required for NS2B-NS3 protease activity. J Virol 67:2034–2042.

165. Li X-D, Deng C-L, Ye H-Q, Zhang H-L, Zhang Q-Y, Chen D-D, Zhang P-T, Shi P-Y, Yuan Z-M, Zhang B. 2016. Transmembrane Domains of NS2B Contribute to both Viral RNA Replication and Particle Formation in Japanese Encephalitis Virus. J Virol 90:5735–5749.

166. León-Juárez M, Martínez-Castillo M, Shrivastava G, García-Cordero J, Villegas-Sepulveda N, Mondragón-Castelán M, Mondragón-Flores R, Cedillo-Barrón L. 2016. Recombinant Dengue virus protein NS2B alters membrane permeability in different membrane models. Virol J 13:1.

167. Li H, Clum S, You S, Ebner KE, Padmanabhan R. 1999. The serine protease and RNA-stimulated nucleoside triphosphatase and RNA helicase functional domains of dengue virus type 2 NS3 converge within a region of 20 amino acids. J Virol 73:3108–3116.

168. Wengler G, Czaya G, Farber PM, Hegemann JH. 1991. In vitro synthesis of West Nile virus proteins indicates that the amino-terminal segment of the NS3 protein contains the active centre of the protease which cleaves the viral polyprotein after multiple basic amino acids. J Gen Virol 72:851–858.

169. Chambers TJ, Weir RC, Grakoui A, McCourt DW, Bazan JF, Fletterick RJ, Rice CM. 1990. Evidence that the N-terminal domain of nonstructural protein NS3 from yellow fever virus is a serine protease responsible for site-specific cleavages in the viral polyprotein. Proc Natl Acad Sci U S A 87:8898–8902.

170. Cui T, Sugrue RJ, Xu Q, Lee AK, Chan YC, Fu J. 1998. Recombinant dengue virus type 1 NS3 protein exhibits specific viral RNA binding and NTPase activity regulated by the NS5 protein. Virology 246:409–417.

171. Mastrangelo E, Milani M, Bollati M, Selisko B, Peyrane F, Pandini V, Sorrentino G, Canard B, Konarev PV, Svergun DI, de Lamballerie X, Coutard B, Khromykh AA, Bolognesi M. 2007. Crystal structure and activity of Kunjin virus NS3 helicase; protease and helicase domain assembly in the full length NS3 protein. J Mol Biol 372:444–455.

172. Wang C-C, Huang Z-S, Chiang P-L, Chen C-T, Wu H-N. 2009. Analysis of the nucleoside triphosphatase, RNA triphosphatase, and unwinding activities of the helicase domain of dengue virus NS3 protein. FEBS Lett 583:691–696.

173. Gebhard LG, Kaufman SB, Gamarnik AV. 2012. Novel ATP-Independent RNA Annealing Activity of the Dengue Virus NS3 Helicase. PLOS ONE 7:e36244.

174. Warrener P, Tamura JK, Collett MS. 1993. RNA-stimulated NTPase activity associated with yellow fever virus NS3 protein expressed in bacteria. J Virol 67:989–996.

175. Xu S, Ci Y, Wang L, Yang Y, Zhang L, Xu C, Qin C, Shi L. 2019. Zika virus NS3 is a canonical RNA helicase stimulated by NS5 RNA polymerase. Nucleic Acids Res 47:8693–8707.

176. Utama A, Shimizu H, Morikawa S, Hasebe F, Morita K, Igarashi A, Hatsu M, Takamizawa K, Miyamura T. 2000. Identification and characterization of the RNA helicase activity of Japanese encephalitis virus NS3 protein. FEBS Lett 465:74–78.

177. Yon C, Teramoto T, Mueller N, Phelan J, Ganesh VK, Murthy KHM, Padmanabhan R. 2005. Modulation of the Nucleoside Triphosphatase/RNA Helicase and 5′-RNA Triphosphatase Activities of Dengue Virus Type 2 Nonstructural Protein 3 (NS3) by Interaction with NS5, the RNA-dependent RNA Polymerase *. J Biol Chem 280:27412–27419.

178. Chen CJ, Kuo MD, Chien LJ, Hsu SL, Wang YM, Lin JH. 1997. RNA-protein interactions: involvement of NS3, NS5, and 3' noncoding regions of Japanese encephalitis virus genomic RNA. J Virol 71:3466–3473.

179. Miller S, Kastner S, Krijnse-Locker J, Bühler S, Bartenschlager R. 2007. The Non-structural Protein 4A of Dengue Virus Is an Integral Membrane Protein Inducing Membrane Alterations in a 2K-regulated Manner *. J Biol Chem 282:8873–8882.

180. Lin C, Amberg SM, Chambers TJ, Rice CM. 1993. Cleavage at a novel site in the NS4A region by the yellow fever virus NS2B-3 proteinase is a prerequisite for processing at the downstream 4A/4B signalase site. J Virol 67:2327–2335.

181. Roosendaal J, Westaway EG, Khromykh A, Mackenzie JM. 2006. Regulated cleavages at the West Nile virus NS4A-2K-NS4B junctions play a major role in rearranging cytoplasmic membranes and Golgi trafficking of the NS4A protein. J Virol 80:4623–4632.

182. Kaufusi PH, Kelley JF, Yanagihara R, Nerurkar VR. 2014. Induction of endoplasmic reticulum-derived replication-competent membrane structures by West Nile virus non-structural protein 4B. PloS One 9:e84040.

183. Teo CSH, Chu JJH. 2014. Cellular Vimentin Regulates Construction of Dengue Virus Replication Complexes through Interaction with NS4A Protein. J Virol 88:1897–1913.

184. Lee CM, Xie X, Zou J, Li S-H, Lee MYQ, Dong H, Qin C-F, Kang C, Shi P-Y. 2015. Determinants of Dengue Virus NS4A Protein Oligomerization. J Virol 89:6171–6183.

185. Stern O, Hung Y-F, Valdau O, Yaffe Y, Harris E, Hoffmann S, Willbold D, Sklan EH. 2013. An N-Terminal Amphipathic Helix in Dengue Virus Nonstructural Protein 4A Mediates Oligomerization and Is Essential for Replication. J Virol 87:4080–4085.

186. Shiryaev SA, Chernov AV, Aleshin AE, Shiryaeva TN, Strongin AY. 2009. NS4A regulates the ATPase activity of the NS3 helicase: a novel cofactor role of the non-structural protein NS4A from West Nile virus. J Gen Virol 90:2081–2085.

187. McLean JE, Wudzinska A, Datan E, Quaglino D, Zakeri Z. 2011. Flavivirus NS4A-induced Autophagy Protects Cells against Death and Enhances Virus Replication *. J Biol Chem 286:22147–22159.

188. Liang Q, Luo Z, Zeng J, Chen W, Foo S-S, Lee S-A, Ge J, Wang S, Goldman SA, Zlokovic BV, Zhao Z, Jung JU. 2016. Zika Virus NS4A and NS4B Proteins Deregulate Akt-mTOR Signaling in Human Fetal Neural Stem Cells to Inhibit Neurogenesis and Induce Autophagy. Cell Stem Cell 19:663–671.

189. Shah PS, Link N, Jang GM, Sharp PP, Zhu T, Swaney DL, Johnson JR, Von Dollen J, Ramage HR, Satkamp L, Newton B, Aguirre S, Hüttenhain R, Petit MJ, Baum T, Everitt A, Laufman O, Tassetto M, Shales M, Stevenson E, Iglesias GN, Shokat L, Tripathi S, Balasubramaniam V, Webb LG, Willsey AJ, Garcia-Sastre A, Pollard KS, Cherry S, Gamarnik AV, Marazzi I, Taunton J, Fernandez-Sesma A, Bellen HJ, Andino R, Krogan NJ. 2018. Comparative flavivirus-host protein interaction mapping reveals mechanisms of dengue and Zika virus pathogenesis. Cell 175:1931-1945.e18.

190. Miller S, Sparacio S, Bartenschlager R. 2006. Subcellular Localization and Membrane Topology of the Dengue Virus Type 2 Non-structural Protein 4B *. J Biol Chem 281:8854–8863.

191. Zou J, Lee LT, Wang QY, Xie X, Lu S, Yau YH, Yuan Z, Geifman Shochat S, Kang C, Lescar J, Shi P-Y. 2015. Mapping the Interactions between the NS4B and NS3 Proteins of Dengue Virus. J Virol 89:3471–3483.

192. Umareddy I, Chao A, Sampath A, Gu F, Vasudevan SG. 2006. Dengue virus NS4B interacts with NS3 and dissociates it from single-stranded RNA. J Gen Virol 87:2605–2614.

193. Zou J, Xie X, Wang Q-Y, Dong H, Lee MY, Kang C, Yuan Z, Shi P-Y. 2015. Characterization of Dengue Virus NS4A and NS4B Protein Interaction. J Virol 89:3455–3470.

194. Chatel-Chaix L, Fischl W, Scaturro P, Cortese M, Kallis S, Bartenschlager M, Fischer B, Bartenschlager R. 2015. A Combined Genetic-Proteomic Approach Identifies Residues within Dengue Virus NS4B Critical for Interaction with NS3 and Viral Replication. J Virol 89:7170–7186.

195. Grant D, Tan GK, Qing M, Ng JKW, Yip A, Zou G, Xie X, Yuan Z, Schreiber MJ, Schul W, Shi P-Y, Alonso S. 2011. A Single Amino Acid in Nonstructural Protein NS4B Confers Virulence to Dengue Virus in AG129 Mice through Enhancement of Viral RNA Synthesis. J Virol 85:7775–7787.

196. Gorman MJ, Caine EA, Zaitsev K, Begley MC, Weger-Lucarelli J, Uccellini MB, Tripathi S, Morrison J, Yount BL, Dinnon KH, Rückert C, Young MC, Zhu Z, Robertson SJ, McNally KL, Ye J, Cao B, Mysorekar IU, Ebel GD, Baric RS, Best SM, Artyomov MN, Garcia-Sastre A, Diamond MS. 2018. An Immunocompetent Mouse Model of Zika Virus Infection. Cell Host Microbe 23:672-685.e6.

197. Hanley KA, Manlucu LR, Gilmore LE, Blaney JE, Hanson CT, Murphy BR, Whitehead SS. 2003. A trade-off in replication in mosquito versus mammalian systems conferred by a point mutation in the NS4B protein of dengue virus type 4. Virology 312:222–232.

198. Ji W, Luo G. 2020. Zika virus NS5 nuclear accumulation is protective of protein degradation and is required for viral RNA replication. Virology 541:124–135.
199. Conde JN, Schutt W, Mladinich M, Sohn S-Y, Hearing P, Mackow ER. 2020. NS5 Sumoylation Directs Nuclear Responses that Permit Zika Virus to Persistently Infect Human Brain Microvascular Endothelial Cells. J Virol JVI.01086-20, jvi;JVI.01086-20v1.
200. Zhao Y, Soh TS, Zheng J, Chan KWK, Phoo WW, Lee CC, Tay MYF, Swaminathan K, Cornvik TC, Lim SP, Shi P-Y, Lescar J, Vasudevan SG, Luo D. 2015. A Crystal Structure of the Dengue Virus NS5 Protein Reveals a Novel Inter-domain Interface Essential for Protein Flexibility and Virus Replication. PLoS Pathog 11:e1004682.
201. Guyatt KJ, Westaway EG, Khromykh AA. 2001. Expression and purification of enzymatically active recombinant RNA-dependent RNA polymerase (NS5) of the flavivirus Kunjin. J Virol Methods 92:37–44.
202. Tan B-H, Fu J, Sugrue RJ, Yap E-H, Chan Y-C, Tan YH. 1996. Recombinant Dengue Type 1 Virus NS5 Protein Expressed inEscherichia coliExhibits RNA-Dependent RNA Polymerase Activity. Virology 216:317–325.
203. Issur M, Geiss BJ, Bougie I, Picard-Jean F, Despins S, Mayette J, Hobdey SE, Bisaillon M. 2009. The flavivirus NS5 protein is a true RNA guanylyltransferase that catalyzes a two-step reaction to form the RNA cap structure. RNA 15:2340–2350.
204. Egloff M-P, Benarroch D, Selisko B, Romette J-L, Canard B. 2002. An RNA cap (nucleoside-2′-O-)-methyltransferase in the flavivirus RNA polymerase NS5: crystal structure and functional characterization. EMBO J 21:2757–2768.
205. Coloma J, Jain R, Rajashankar KR, García-Sastre A, Aggarwal AK. 2016. Structures of NS5 Methyltransferase from Zika Virus. Cell Rep 16:3097–3102.
206. Geiss BJ, Thompson AA, Andrews AJ, Sons RL, Gari HH, Keenan SM, Peersen OB. 2009. Analysis of Flavivirus NS5 Methyltransferase Cap Binding. J Mol Biol 385:1643–1654.

207. Zhao B, Yi G, Du F, Chuang Y-C, Vaughan RC, Sankaran B, Kao CC, Li P. 2017. Structure and function of the Zika virus full-length NS5 protein. Nat Commun 8:14762.

208. Zhou Y, Ray D, Zhao Y, Dong H, Ren S, Li Z, Guo Y, Bernard KA, Shi P-Y, Li H. 2007. Structure and Function of Flavivirus NS5 Methyltransferase. J Virol 81:3891–3903.

209. Egloff M-P, Decroly E, Malet H, Selisko B, Benarroch D, Ferron F, Canard B. 2007. Structural and Functional Analysis of Methylation and 5′-RNA Sequence Requirements of Short Capped RNAs by the Methyltransferase Domain of Dengue Virus NS5. J Mol Biol 372:723–736.

210. Gullberg RC, Jordan Steel J, Moon SL, Soltani E, Geiss BJ. 2015. Oxidative stress influences positive strand RNA virus genome synthesis and capping. Virology 475:219–229.

211. Godoy AS, Lima GMA, Oliveira KIZ, Torres NU, Maluf FV, Guido RVC, Oliva G. 2017. Crystal structure of Zika virus NS5 RNA-dependent RNA polymerase. Nat Commun 8:14764.

212. Albentosa-González L, Jimenez de Oya N, Arias A, Clemente-Casares P, Martin-Acebes MÁ, Saiz JC, Sabariegos R, Mas A. 2021. Akt Kinase Intervenes in Flavivirus Replication by Interacting with Viral Protein NS5. Viruses 13.

213. Lu G, Gong P. 2013. Crystal Structure of the Full-Length Japanese Encephalitis Virus NS5 Reveals a Conserved Methyltransferase-Polymerase Interface. PLoS Pathog 9:e1003549.

214. Klema VJ, Ye M, Hindupur A, Teramoto T, Gottipati K, Padmanabhan R, Choi KH. 2016. Dengue Virus Nonstructural Protein 5 (NS5) Assembles into a Dimer with a Unique Methyltransferase and Polymerase Interface. PLoS Pathog 12:e1005451.

215. Potisopon S, Priet S, Collet A, Decroly E, Canard B, Selisko B. 2014. The methyltransferase domain of dengue virus protein NS5 ensures efficient RNA synthesis initiation and elongation by the polymerase domain. Nucleic Acids Res 42:11642–11656.

216. Rusanov T, Kent T, Saeed M, Hoang TM, Thomas C, Rice CM, Pomerantz RT. 2018. Identification of a Small Interface between the Methyltransferase and RNA Polymerase of NS5 that is Essential for Zika Virus Replication. Sci Rep 8:17384.

217. Ferrero DS, Ruiz-Arroyo VM, Soler N, Usón I, Guarné A, Verdaguer N. 2019. Supramolecular arrangement of the full-length Zika virus NS5. PLoS Pathog 15:e1007656.

218. Brooks AJ, Johansson M, John AV, Xu Y, Jans DA, Vasudevan SG. 2002. The Interdomain Region of Dengue NS5 Protein That Binds to the Viral Helicase NS3 Contains Independently Functional Importin β1 and Importin α/β-Recognized Nuclear Localization Signals *. J Biol Chem 277:36399–36407.

219. Johansson M, Brooks AJ, Jans DA, Vasudevan SG. 2001. A small region of the dengue virus-encoded RNA-dependent RNA polymerase, NS5, confers interaction with both the nuclear transport receptor importin-β and the viral helicase, NS3. J Gen Virol 82:735–745.

220. López-Denman AJ, Tuipulotu DE, Ross JB, Trenerry AM, White PA, Mackenzie JM. 2021. Nuclear localisation of West Nile virus NS5 protein modulates host gene expression. Virology 559:131–144.

221. Maio FAD, Risso G, Iglesias NG, Shah P, Pozzi B, Gebhard LG, Mammi P, Mancini E, Yanovsky MJ, Andino R, Krogan N, Srebrow A, Gamarnik AV. 2016. The Dengue Virus NS5 Protein Intrudes in the Cellular Spliceosome and Modulates Splicing. PLOS Pathog 12:e1005841.

222. Saade M, Ferrero DS, Blanco-Ameijeiras J, Gonzalez-Gobartt E, Flores-Mendez M, Ruiz-Arroyo VM, Martínez-Sáez E, Ramón Y Cajal S, Akizu N, Verdaguer N, Martí E. 2020. Multimerization of Zika Virus-NS5 Causes Ciliopathy and Forces Premature Neurogenesis. Cell Stem Cell 27:920-936.e8.

223. Li P, Jiang H, Peng H, Zeng W, Zhong Y, He M, Xie L, Chen J, Guo D, Wu J, Li C-M. 2021. Non-Structural Protein 5 of Zika Virus Interacts with p53 in Human Neural

Progenitor Cells and Induces p53-Mediated Apoptosis. Virol Sin https://doi.org/10.1007/s12250-021-00422-7.

224. Aubry F, Jacobs S, Darmuzey M, Lequime S, Delang L, Fontaine A, Jupatanakul N, Miot EF, Dabo S, Manet C, Montagutelli X, Baidaliuk A, Gámbaro F, Simon-Lorière E, Gilsoul M, Romero-Vivas CM, Cao-Lormeau V-M, Jarman RG, Diagne CT, Faye O, Faye O, Sall AA, Neyts J, Nguyen L, Kaptein SJF, Lambrechts L. 2021. Recent African strains of Zika virus display higher transmissibility and fetal pathogenicity than Asian strains. Nat Commun 12:916.

225. Fernandes RS, O'Connor O, Bersot MIL, Girault D, Dokunengo MR, Pocquet N, Dupont-Rouzeyrol M, Lourenço-de-Oliveira R. 2020. Vector Competence of Aedes aegypti, Aedes albopictus and Culex quinquefasciatus from Brazil and New Caledonia for Three Zika Virus Lineages. Pathog Basel Switz 9:575.

226. Ou TP, Auerswald H, In S, Peng B, Pang S, Boyer S, Choeung R, Dupont-Rouzeyrol M, Dussart P, Duong V. 2021. Replication Variance of African and Asian Lineage Zika Virus Strains in Different Cell Lines, Mosquitoes and Mice. 6. Microorganisms 9:1250.

227. Smith DR, Sprague TR, Hollidge BS, Valdez SM, Padilla SL, Bellanca SA, Golden JW, Coyne SR, Kulesh DA, Miller LJ, Haddow AD, Koehler JW, Gromowski GD, Jarman RG, Alera MTP, Yoon I-K, Buathong R, Lowen RG, Kane CD, Minogue TD, Bavari S, Tesh RB, Weaver SC, Linthicum KJ, Pitt ML, Nasar F. 2018. African and Asian Zika Virus Isolates Display Phenotypic Differences Both In Vitro and In Vivo. Am J Trop Med Hyg 98:432–444.

228. Weger-Lucarelli J, Rückert C, Chotiwan N, Nguyen C, Luna SMG, Fauver JR, Foy BD, Perera R, Black WC, Kading RC, Ebel GD. 2016. Vector Competence of American Mosquitoes for Three Strains of Zika Virus. PLoS Negl Trop Dis 10:e0005101.

229. Calvez E, O'Connor O, Pol M, Rousset D, Faye O, Richard V, Tarantola A, Dupont-Rouzeyrol M. 2018. Differential transmission of Asian and African Zika virus lineages by Aedes aegypti from New Caledonia. Emerg Microbes Infect 7:159.

230. Willard KA, Demakovsky L, Tesla B, Goodfellow FT, Stice SL, Murdock CC, Brindley MA. 2017. Zika Virus Exhibits Lineage-Specific Phenotypes in Cell Culture, in Aedes aegypti Mosquitoes, and in an Embryo Model. Viruses 9.

231. Bowen JR, Quicke KM, Maddur MS, O'Neal JT, McDonald CE, Fedorova NB, Puri V, Shabman RS, Pulendran B, Suthar MS. 2017. Zika Virus Antagonizes Type I Interferon Responses during Infection of Human Dendritic Cells. PLoS Pathog 13.

232. Anfasa F, Siegers JY, van der Kroeg M, Mumtaz N, Stalin Raj V, de Vrij FMS, Widagdo W, Gabriel G, Salinas S, Simonin Y, Reusken C, Kushner SA, Koopmans MPG, Haagmans B, Martina BEE, van Riel D. 2017. Phenotypic Differences between Asian and African Lineage Zika Viruses in Human Neural Progenitor Cells. mSphere 2.

233. Shao Q, Herrlinger S, Zhu Y-N, Yang M, Goodfellow F, Stice SL, Qi X-P, Brindley MA, Chen J-F. 2017. The African Zika virus MR-766 is more virulent and causes more severe brain damage than current Asian lineage and dengue virus. Dev Camb Engl 144:4114–4124.

234. Hamel R, Ferraris P, Wichit S, Diop F, Talignani L, Pompon J, Garcia D, Liégeois F, Sall AA, Yssel H, Missé D. 2017. African and Asian Zika virus strains differentially induce early antiviral responses in primary human astrocytes. Infect Genet Evol J Mol Epidemiol Evol Genet Infect Dis 49:134–137.

235. Simonin Y, Loustalot F, Desmetz C, Foulongne V, Constant O, Fournier-Wirth C, Leon F, Molès J-P, Goubaud A, Lemaitre J-M, Maquart M, Leparc-Goffart I, Briant L, Nagot N, Van de Perre P, Salinas S. 2016. Zika Virus Strains Potentially Display Different Infectious Profiles in Human Neural Cells. EBioMedicine 12:161–169.

236. Goodfellow FT, Willard KA, Wu X, Scoville S, Stice SL, Brindley MA. 2018. Strain-Dependent Consequences of Zika Virus Infection and Differential Impact on Neural Development. Viruses 10:550.

237. Li G, Bos S, Tsetsarkin KA, Pletnev AG, Després P, Gadea G, Zhao RY. 2019. The Roles of prM-E Proteins in Historical and Epidemic Zika Virus-mediated Infection and Neurocytotoxicity. Viruses 11.

238. Hernández-Sarmiento LJ, Valdés-López JF, Urcuqui-Inchima S. 2023. American-Asian- and African lineages of Zika virus induce differential pro-inflammatory and Interleukin 27-dependent antiviral responses in human monocytes. Virus Res 325:199040.

239. Udenze D, Trus I, Berube N, Gerdts V, Karniychuk U. 2019. The African strain of Zika virus causes more severe in utero infection than Asian strain in a porcine fetal transmission model. Emerg Microbes Infect 8:1098–1107.

240. Barnard TR, Rajah MM, Sagan SM. 2018. Contemporary Zika Virus Isolates Induce More dsRNA and Produce More Negative-Strand Intermediate in Human Astrocytoma Cells. Viruses 10:728.

241. Setoh YX, Peng NY, Nakayama E, Amarilla AA, Prow NA, Suhrbier A, Khromykh AA. 2018. Fetal Brain Infection Is Not a Unique Characteristic of Brazilian Zika Viruses. Viruses 10:541.

242. Esser-Nobis K, Aarreberg LD, Roby JA, Fairgrieve MR, Green R, Gale M. 2019. Comparative Analysis of African and Asian Lineage-Derived Zika Virus Strains Reveals Differences in Activation of and Sensitivity to Antiviral Innate Immunity. J Virol 93:e00640-19.

243. Bos S, Viranaicken W, Frumence E, Li G, Després P, Zhao RY, Gadea G. 2019. The Envelope Residues E152/156/158 of Zika Virus Influence the Early Stages of Virus Infection in Human Cells. Cells 8:1444.

244. Bos S, Viranaicken W, Turpin J, El-Kalamouni C, Roche M, Krejbich-Trotot P, Desprès P, Gadea G. 2018. The structural proteins of epidemic and historical strains of Zika virus differ in their ability to initiate viral infection in human host cells. Virology 516:265–273.

245. Liu J, Liu Y, Shan C, Nunes BTD, Yun R, Haller SL, Rafael GH, Azar SR, Andersen CR, Plante K, Vasilakis N, Shi P-Y, Weaver SC. 2021. Role of mutational reversions and fitness restoration in Zika virus spread to the Americas. 1. Nat Commun 12:595.

246. Yu X, Shan C, Zhu Y, Ma E, Wang J, Wang P, Shi P-Y, Cheng G. 2021. A mutation-mediated evolutionary adaptation of Zika virus in mosquito and mammalian host. Proc Natl Acad Sci 118:e2113015118.

247. Collette NM, Lao VHI, Weilhammer DR, Zingg B, Cohen SD, Hwang M, Coffey LL, Grady SL, Zemla AT, Borucki MK. 2020. Single Amino Acid Mutations Affect Zika Virus Replication In Vitro and Virulence In Vivo. Viruses 12.

248. Sheridan MA, Balaraman V, Schust DJ, Ezashi T, Roberts RM, Franz AWE. 2018. African and Asian strains of Zika virus differ in their ability to infect and lyse primitive human placental trophoblast. PLoS ONE 13.

249. Devhare P, Meyer K, Steele R, Ray RB, Ray R. 2017. Zika virus infection dysregulates human neural stem cell growth and inhibits differentiation into neuroprogenitor cells. Cell Death Dis 8:e3106.

250. Rosenfeld AB, Doobin DJ, Warren AL, Racaniello VR, Vallee RB. 2017. Replication of early and recent Zika virus isolates throughout mouse brain development. Proc Natl Acad Sci U S A 114:12273–12278.

251. Lee JK, Kim J-A, Oh S-J, Lee E-W, Shin OS. 2020. Zika Virus Induces Tumor Necrosis Factor-Related Apoptosis Inducing Ligand (TRAIL)-Mediated Apoptosis in Human Neural Progenitor Cells. Cells 9.

252. Gabriel E, Ramani A, Karow U, Gottardo M, Natarajan K, Gooi LM, Goranci-Buzhala G, Krut O, Peters F, Nikolic M, Kuivanen S, Korhonen E, Smura T, Vapalahti O, Papantonis

A, Schmidt-Chanasit J, Riparbelli M, Callaini G, Krönke M, Utermöhlen O, Gopalakrishnan J. 2017. Recent Zika Virus Isolates Induce Premature Differentiation of Neural Progenitors in Human Brain Organoids. Cell Stem Cell 20:397-406.e5.

253. Lazear HM, Govero J, Smith AM, Platt DJ, Fernandez E, Miner JJ, Diamond MS. 2016. A Mouse Model of Zika Virus Pathogenesis. Cell Host Microbe 19:720–730.

254. Jaeger AS, Murrieta RA, Goren LR, Crooks CM, Moriarty RV, Weiler AM, Rybarczyk S, Semler MR, Huffman C, Mejia A, Simmons HA, Fritsch M, Osorio JE, Eickhoff JC, O'Connor SL, Ebel GD, Friedrich TC, Aliota MT. 2019. Zika viruses of African and Asian lineages cause fetal harm in a mouse model of vertical transmission. PLoS Negl Trop Dis 13:e0007343.

255. Shan C, Xia H, Haller SL, Azar SR, Liu Y, Liu J, Muruato AE, Chen R, Rossi SL, Wakamiya M, Vasilakis N, Pei R, Fontes-Garfias CR, Singh SK, Xie X, Weaver SC, Shi P-Y. 2020. A Zika virus envelope mutation preceding the 2015 epidemic enhances virulence and fitness for transmission. Proc Natl Acad Sci 117:20190–20197.

256. Nunes BTD, Fontes-Garfias CR, Shan C, Muruato AE, Nunes JGC, Burbano RMR, Vasconcelos PFC, Shi P-Y, Medeiros DBA. 2020. Zika structural genes determine the virulence of African and Asian lineages. Emerg Microbes Infect 9:1023–1033.

257. Tripathi S, Balasubramaniam VRMT, Brown JA, Mena I, Grant A, Bardina SV, Maringer K, Schwarz MC, Maestre AM, Sourisseau M, Albrecht RA, Krammer F, Evans MJ, Fernandez-Sesma A, Lim JK, García-Sastre A. 2017. A novel Zika virus mouse model reveals strain specific differences in virus pathogenesis and host inflammatory immune responses. PLOS Pathog 13:e1006258.

258. Bohm EK, Vangorder-Braid JT, Jaeger AS, Moriarty RV, Baczenas JJ, Bennett NC, O'Connor SL, Fritsch MK, Fuhler NA, Noguchi KK, Aliota MT. 2021. Zika Virus Infection of Pregnant Ifnar1-/- Mice Triggers Strain-Specific Differences in Fetal Outcomes. J Virol 95:e0081821.

259. Zhang F, Wang H-J, Wang Q, Liu Z-Y, Yuan L, Huang X-Y, Li G, Ye Q, Yang H, Shi L, Deng Y-Q, Qin C-F, Xu Z. 2017. American Strain of Zika Virus Causes More Severe Microcephaly Than an Old Asian Strain in Neonatal Mice. EBioMedicine 25:95–105.

260. Dowall SD, Graham VA, Rayner E, Hunter L, Atkinson B, Pearson G, Dennis M, Hewson R. 2017. Lineage-dependent differences in the disease progression of Zika virus infection in type-I interferon receptor knockout (A129) mice. PLoS Negl Trop Dis 11.

261. Andersen MD, Alstrup AKO, Duvald CS, Mikkelsen EFR, Vendelbo MH, Ovesen PG, Pedersen M, Andersen MD, Alstrup AKO, Duvald CS, Mikkelsen EFR, Vendelbo MH, Ovesen PG, Pedersen M. 2018. Animal Models of Fetal Medicine and ObstetricsExperimental Animal Models of Human Diseases - An Effective Therapeutic Strategy. IntechOpen. https://www.intechopen.com/state.item.id. Retrieved 16 December 2022.

262. Crooks CM, Weiler AM, Rybarczyk SL, Bliss MI, Jaeger AS, Murphy ME, Simmons HA, Mejia A, Fritsch MK, Hayes JM, Eickhoff JC, Mitzey AM, Razo E, Braun KM, Brown EA, Yamamoto K, Shepherd PM, Possell A, Weaver K, Antony KM, Morgan TK, Newman CM, Dudley DM, Schultz-Darken N, Peterson E, Katzelnick LC, Balmaseda A, Harris E, O'Connor DH, Mohr EL, Golos TG, Friedrich TC, Aliota MT. 2021. Previous exposure to dengue virus is associated with increased Zika virus burden at the maternal-fetal interface in rhesus macaques. PLoS Negl Trop Dis 15:e0009641.

263. Loo Y-M, Gale M. 2011. Immune signaling by RIG-I-like receptors. Immunity 34:680–692.

264. Dutta S, Das N, Mukherjee P. 2020. Picking up a Fight: Fine Tuning Mitochondrial Innate Immune Defenses Against RNA Viruses. Front Microbiol 11:1990.

265. Onomoto K, Onoguchi K, Yoneyama M. 2021. Regulation of RIG-I-like receptor-mediated signaling: interaction between host and viral factors. 3. Cell Mol Immunol 18:539–555.

266. Chow KT, Gale M, Loo Y-M. 2018. RIG-I and Other RNA Sensors in Antiviral Immunity. Annu Rev Immunol 36:667–694.

267. Honda K, Yanai H, Takaoka A, Taniguchi T. 2005. Regulation of the type I IFN induction: a current view. Int Immunol 17:1367–1378.

268. Chazal M, Beauclair G, Gracias S, Najburg V, Simon-Lorière E, Tangy F, Komarova AV, Jouvenet N. 2018. RIG-I Recognizes the 5’ Region of Dengue and Zika Virus Genomes. Cell Rep 24:320–328.

269. Schilling M, Bridgeman A, Gray N, Hertzog J, Hublitz P, Kohl A, Rehwinkel J. 2020. RIG-I Plays a Dominant Role in the Induction of Transcriptional Changes in Zika Virus-Infected Cells, which Protect from Virus-Induced Cell Death. 6. Cells 9:1476.

270. Plociennikowska A, Frankish J, Moraes T, Prete DD, Kahnt F, Acuna C, Slezak M, Binder M, Bartenschlager R. 2021. TLR3 activation by Zika virus stimulates inflammatory cytokine production which dampens the antiviral response induced by RIG-I-like receptors. J Virol https://doi.org/10.1128/JVI.01050-20.

271. Yoneyama M, Kikuchi M, Matsumoto K, Imaizumi T, Miyagishi M, Taira K, Foy E, Loo Y-M, Gale M Jr, Akira S, Yonehara S, Kato A, Fujita T. 2005. Shared and Unique Functions of the DExD/H-Box Helicases RIG-I, MDA5, and LGP2 in Antiviral Innate Immunity1. J Immunol 175:2851–2858.

272. Errett JS, Suthar MS, McMillan A, Diamond MS, Gale M. 2013. The Essential, Nonredundant Roles of RIG-I and MDA5 in Detecting and Controlling West Nile Virus Infection. J Virol 87:11416–11425.

273. Khan S, Lew I, Wu F, Fritts L, Fontaine KA, Tomar S, Trapecar M, Shehata HM, Ott M, Miller CJ, Sanjabi S. 2019. Low expression of RNA sensors impacts Zika virus infection in the lower female reproductive tract. Nat Commun 10.

274. Suthar MS, Ma DY, Thomas S, Lund JM, Zhang N, Daffis S, Rudensky AY, Bevan MJ, Clark EA, Kaja M-K, Diamond MS, Jr MG. 2010. IPS-1 Is Essential for the Control of West Nile Virus Infection and Immunity. PLOS Pathog 6:e1000757.

275. Esser-Nobis K, Hatfield LD, Gale M. 2020. Spatiotemporal dynamics of innate immune signaling via RIG-I–like receptors. Proc Natl Acad Sci https://doi.org/10.1073/pnas.1921861117.

276. Cui S, Eisenächer K, Kirchhofer A, Brzózka K, Lammens A, Lammens K, Fujita T, Conzelmann K-K, Krug A, Hopfner K-P. 2008. The C-Terminal Regulatory Domain Is the RNA 5′-Triphosphate Sensor of RIG-I. Mol Cell 29:169–179.

277. Hornung V, Ellegast J, Kim S, Brzózka K, Jung A, Kato H, Poeck H, Akira S, Conzelmann K-K, Schlee M, Endres S, Hartmann G. 2006. 5’-Triphosphate RNA Is the Ligand for RIG-I. Science 314:994–997.

278. Marq J-B, Kolakofsky D, Garcin D. 2010. Unpaired 5′ ppp-Nucleotides, as Found in Arenavirus Double-stranded RNA Panhandles, Are Not Recognized by RIG-I. J Biol Chem 285:18208–18216.

279. Schlee M, Roth A, Hornung V, Hagmann CA, Wimmenauer V, Barchet W, Coch C, Janke M, Mihailovic A, Wardle G, Juranek S, Kato H, Kawai T, Poeck H, Fitzgerald KA, Takeuchi O, Akira S, Tuschl T, Latz E, Ludwig J, Hartmann G. 2009. Recognition of 5’ triphosphate by RIG-I helicase requires short blunt double-stranded RNA as contained in panhandle of negative-strand virus. Immunity 31:25–34.

280. Schmidt A, Schwerd T, Hamm W, Hellmuth JC, Cui S, Wenzel M, Hoffmann FS, Michallet M-C, Besch R, Hopfner K-P, Endres S, Rothenfusser S. 2009. 5′-triphosphate RNA requires base-paired structures to activate antiviral signaling via RIG-I. Proc Natl Acad Sci 106:12067–12072.

281. Takahasi K, Yoneyama M, Nishihori T, Hirai R, Kumeta H, Narita R, Gale M, Inagaki F, Fujita T. 2008. Nonself RNA-Sensing Mechanism of RIG-I Helicase and Activation of Antiviral Immune Responses. Mol Cell 29:428–440.

282. Hertzog J, Dias Junior AG, Rigby RE, Donald CL, Mayer A, Sezgin E, Song C, Jin B, Hublitz P, Eggeling C, Kohl A, Rehwinkel J. 2018. Infection with a Brazilian isolate of Zika

virus generates RIG-I stimulatory RNA and the viral NS5 protein blocks type I IFN induction and signaling. Eur J Immunol 48:1120–1136.

283. Pichlmair A, Schulz O, Tan CP, Näslund TI, Liljeström P, Weber F, Reis e Sousa C. 2006. RIG-I-Mediated Antiviral Responses to Single-Stranded RNA Bearing 5'-Phosphates. Science 314:997–1001.

284. Saito T, Hirai R, Loo Y-M, Owen D, Johnson CL, Sinha SC, Akira S, Fujita T, Gale M. 2007. Regulation of innate antiviral defenses through a shared repressor domain in RIG-I and LGP2. Proc Natl Acad Sci 104:582–587.

285. Saito T, Owen DM, Jiang F, Marcotrigiano J, Gale M. 2008. Innate immunity induced by composition-dependent RIG-I recognition of Hepatitis C virus RNA. Nature 454:523–527.

286. Schnell G, Loo Y-M, Marcotrigiano J, Jr MG. 2012. Uridine Composition of the Poly-U/UC Tract of HCV RNA Defines Non-Self Recognition by RIG-I. PLOS Pathog 8:e1002839.

287. Kowalinski E, Lunardi T, McCarthy AA, Louber J, Brunel J, Grigorov B, Gerlier D, Cusack S. 2011. Structural Basis for the Activation of Innate Immune Pattern-Recognition Receptor RIG-I by Viral RNA. Cell 147:423–435.

288. Gack MU, Shin YC, Joo C-H, Urano T, Liang C, Sun L, Takeuchi O, Akira S, Chen Z, Inoue S, Jung JU. 2007. TRIM25 RING-finger E3 ubiquitin ligase is essential for RIG-I-mediated antiviral activity. 7138. Nature 446:916–920.

289. Peisley A, Wu B, Xu H, Chen ZJ, Hur S. 2014. Structural basis for ubiquitin-mediated antiviral signal activation by RIG-I. Nature 509:110–114.

290. Matsumiya T, Stafforini DM. 2010. Function and Regulation of Retinoic Acid-Inducible Gene-I. Crit Rev Immunol 30:489–513.

291. Kell AM, Gale M. 2015. RIG-I in RNA virus recognition. Virology 479–480:110–121.

292. Ramos HJ, Gale M. 2011. RIG-I like receptors and their signaling crosstalk in the regulation of antiviral immunity. Curr Opin Virol 1:167–176.

293. Rehwinkel J, Gack MU. 2020. RIG-I-like receptors: their regulation and roles in RNA sensing. 9. Nat Rev Immunol 20:537–551.

294. Liu HM, Loo Y-M, Horner SM, Zornetzer GA, Katze MG, Gale M. 2012. The mitochondrial targeting chaperone 14-3-3ε regulates a RIG-I translocon that mediates membrane-association and innate antiviral immunity. Cell Host Microbe 11:528–537.

295. Kawai T, Takahashi K, Sato S, Coban C, Kumar H, Kato H, Ishii KJ, Takeuchi O, Akira S. 2005. IPS-1, an adaptor triggering RIG-I- and Mda5-mediated type I interferon induction. 10. Nat Immunol 6:981–988.

296. Seth RB, Sun L, Ea C-K, Chen ZJ. 2005. Identification and Characterization of MAVS, a Mitochondrial Antiviral Signaling Protein that Activates NF-κB and IRF3. Cell 122:669–682.

297. Yoneyama M, Kikuchi M, Natsukawa T, Shinobu N, Imaizumi T, Miyagishi M, Taira K, Akira S, Fujita T. 2004. The RNA helicase RIG-I has an essential function in double-stranded RNA-induced innate antiviral responses. 7. Nat Immunol 5:730–737.

298. Xu L-G, Wang Y-Y, Han K-J, Li L-Y, Zhai Z, Shu H-B. 2005. VISA Is an Adapter Protein Required for Virus-Triggered IFN-β Signaling. Mol Cell 19:727–740.

299. Zevini A, Olagnier D, Hiscott J. 2017. Crosstalk between Cytoplasmic RIG-I and STING Sensing Pathways. Trends Immunol 38:194–205.

300. Sharma S, tenOever BR, Grandvaux N, Zhou G-P, Lin R, Hiscott J. 2003. Triggering the Interferon Antiviral Response Through an IKK-Related Pathway. Science 300:1148–1151.

301. Sato M, Hata N, Asagiri M, Nakaya T, Taniguchi T, Tanaka N. 1998. Positive feedback regulation of type I IFN genes by the IFN-inducible transcription factor IRF-7. FEBS Lett 441:106–110.

302. Chattopadhyay S, Marques JT, Yamashita M, Peters KL, Smith K, Desai A, Williams BRG, Sen GC. 2010. Viral apoptosis is induced by IRF-3-mediated activation of Bax. EMBO J 29:1762–1773.

303. Quicke KM, Kim KY, Horvath CM, Suthar MS. 2019. RNA Helicase LGP2 Negatively Regulates RIG-I Signaling by Preventing TRIM25-Mediated Caspase Activation and Recruitment Domain Ubiquitination. J Interferon Cytokine Res 39:669–683.

304. Fitzgerald KA, Kagan JC. 2020. Toll-like Receptors and the Control of Immunity. Cell 180:1044–1066.

305. Daffis S, Samuel MA, Suthar MS, Gale M, Diamond MS. 2008. Toll-Like Receptor 3 Has a Protective Role against West Nile Virus Infection. J Virol 82:10349–10358.

306. Nazmi A, Mukherjee S, Kundu K, Dutta K, Mahadevan A, Shankar SK, Basu A. 2014. TLR7 is a key regulator of innate immunity against Japanese encephalitis virus infection. Neurobiol Dis 69:235–247.

307. Ojha CR, Rodriguez M, Karuppan MKM, Lapierre J, Kashanchi F, El-Hage N. 2019. Toll-like receptor 3 regulates Zika virus infection and associated host inflammatory response in primary human astrocytes. PloS One 14:e0208543.

308. Murakami Y, Fukui R, Motoi Y, Kanno A, Shibata T, Tanimura N, Saitoh S, Miyake K. 2014. Roles of the Cleaved N-Terminal TLR3 Fragment and Cell Surface TLR3 in Double-Stranded RNA Sensing. J Immunol 193:5208–5217.

309. Pohar J, Pirher N, Benčina M, Manček-Keber M, Jerala R. 2013. The Role of UNC93B1 Protein in Surface Localization of TLR3 Receptor and in Cell Priming to Nucleic Acid Agonists *. J Biol Chem 288:442–454.

310. Leonard JN, Ghirlando R, Askins J, Bell JK, Margulies DH, Davies DR, Segal DM. 2008. The TLR3 signaling complex forms by cooperative receptor dimerization. Proc Natl Acad Sci 105:258–263.

311. Alexopoulou L, Holt AC, Medzhitov R, Flavell RA. 2001. Recognition of double-stranded RNA and activation of NF-κB by Toll-like receptor 3. 6857. Nature 413:732–738.

312. Fukuda K, Watanabe T, Tokisue T, Tsujita T, Nishikawa S, Hasegawa T, Seya T, Matsumoto M. 2008. Modulation of Double-stranded RNA Recognition by the N-terminal Histidine-rich Region of the Human Toll-like Receptor 3 *. J Biol Chem 283:22787–22794.
313. Liu L, Botos I, Wang Y, Leonard JN, Shiloach J, Segal DM, Davies DR. 2008. Structural Basis of Toll-Like Receptor 3 Signaling with Double-Stranded RNA. Science 320:379–381.
314. Tatematsu M, Nishikawa F, Seya T, Matsumoto M. 2013. Toll-like receptor 3 recognizes incomplete stem structures in single-stranded viral RNA. 1. Nat Commun 4:1833.
315. Bouteiller O de, Merck E, Hasan UA, Hubac S, Benguigui B, Trinchieri G, Bates EEM, Caux C. 2005. Recognition of Double-stranded RNA by Human Toll-like Receptor 3 and Downstream Receptor Signaling Requires Multimerization and an Acidic pH *. J Biol Chem 280:38133–38145.
316. Fitzgerald KA, Rowe DC, Barnes BJ, Caffrey DR, Visintin A, Latz E, Monks B, Pitha PM, Golenbock DT. 2003. LPS-TLR4 Signaling to IRF-3/7 and NF-κB Involves the Toll Adapters TRAM and TRIF. J Exp Med 198:1043–1055.
317. Yamamoto M, Sato S, Hemmi H, Hoshino K, Kaisho T, Sanjo H, Takeuchi O, Sugiyama M, Okabe M, Takeda K, Akira S. 2003. Role of Adaptor TRIF in the MyD88-Independent Toll-Like Receptor Signaling Pathway. Science 301:640–643.
318. Sommereyns C, Paul S, Staeheli P, Michiels T. 2008. IFN-Lambda (IFN-λ) Is Expressed in a Tissue-Dependent Fashion and Primarily Acts on Epithelial Cells In Vivo. PLOS Pathog 4:e1000017.
319. Crosse KM, Monson EA, Beard MR, Helbig KJ. 2018. Interferon-Stimulated Genes as Enhancers of Antiviral Innate Immune Signaling. J Innate Immun 10:85–93.
320. Nan Y, Wu C, Zhang Y-J. 2017. Interplay between Janus Kinase/Signal Transducer and Activator of Transcription Signaling Activated by Type I Interferons and Viral Antagonism. Front Immunol 8.

321. Schneider WM, Chevillotte MD, Rice CM. 2014. Interferon-Stimulated Genes: A Complex Web of Host Defenses. Annu Rev Immunol 32:513–545.

322. Lamken P, Lata S, Gavutis M, Piehler J. 2004. Ligand-induced Assembling of the Type I Interferon Receptor on Supported Lipid Bilayers. J Mol Biol 341:303–318.

323. Bolen CR, Ding S, Robek MD, Kleinstein SH. 2014. Dynamic expression profiling of type I and type III interferon-stimulated hepatocytes reveals a stable hierarchy of gene expression. Hepatology 59:1262–1272.

324. Constantinescu SN, Croze E, Wang C, Murti A, Basu L, Mullersman JE, Pfeffer LM. 1994. Role of interferon alpha/beta receptor chain 1 in the structure and transmembrane signaling of the interferon alpha/beta receptor complex. Proc Natl Acad Sci 91:9602–9606.

325. Yan H, Krishnan K, Lim JT, Contillo LG, Krolewski JJ. 1996. Molecular characterization of an alpha interferon receptor 1 subunit (IFNaR1) domain required for TYK2 binding and signal transduction. Mol Cell Biol 16:2074–2082.

326. Greenlund AC, Morales MO, Viviano BL, Yan H, Krolewski J, Schreiber RD. 1995. Stat recruitment by tyrosine-phosphorylated cytokine receptors: An ordered reversible affinity-driven process. Immunity 2:677–687.

327. Heim MH, Kerr Ian M, Stark GR, Darnell JE. 1995. Contribution of STAT SH2 Groups to Specific Interferon Signaling by the Jak-STAT pathway. Science 267:1347–1349.

328. Ivashkiv LB, Donlin LT. 2014. Regulation of type I interferon responses. Nat Rev Immunol 14:36–49.

329. Schindler C, Shuai K, Prezioso VR, Darnell JE. 1992. Interferon-Dependent Tyrosine Phosphorylation of a Latent Cytoplasmic Transcription Factor. Science 257:809–813.

330. Veals SA, Schindler C, Leonard D, Fu XY, Aebersold R, Darnell JE, Levy DE. 1992. Subunit of an alpha-interferon-responsive transcription factor is related to interferon regulatory factor and Myb families of DNA-binding proteins. Mol Cell Biol 12:3315–3324.

331. Levy DE, Kessler DS, Pine R, Reich N, Darnell JE. 1988. Interferon-induced nuclear factors that bind a shared promoter element correlate with positive and negative transcriptional control. Genes Dev 2:383–393.

332. Schoggins JW, Wilson SJ, Panis M, Murphy MY, Jones CT, Bieniasz P, Rice CM. 2011. A diverse range of gene products are effectors of the type I interferon antiviral response. Nature 472:481–485.

333. Hayashida E, Ling ZL, Ashhurst TM, Viengkhou B, Jung SR, Songkhunawej P, West PK, King NJC, Hofer MJ. 2019. Zika virus encephalitis in immunocompetent mice is dominated by innate immune cells and does not require T or B cells. J Neuroinflammation 16:177.

334. Aliota MT, Caine EA, Walker EC, Larkin KE, Camacho E, Osorio JE. 2016. Characterization of Lethal Zika Virus Infection in AG129 Mice. PLoS Negl Trop Dis 10:e0004682.

335. Ding J, Aldo P, Roberts CM, Stabach P, Liu H, You Y, Qiu X, Jeong J, Maxwell A, Lindenbach B, Braddock D, Liao A, Mor G. 2021. Placenta-derived interferon-stimulated gene 20 controls ZIKA virus infection. EMBO Rep https://doi.org/10.15252/embr.202152450.

336. Ren K, Sun H, Chen L, Chen N, Yu L. 2021. Myxovirus resistance protein A activates type I IFN signaling pathway to inhibit zika virus replication. Virus Res 198534.

337. Wang Y, Huo Z, Lin Q, Lin Y, Chen C, Huang Y, Huang C, Zhang J, He J, Liu C, Zhang P. 2021. Positive Feedback Loop of Long Noncoding RNA OASL-IT1 and Innate Immune Response Restricts the Replication of Zika Virus in Epithelial A549 Cells. J Innate Immun 1–15.

338. Vanwalscappel B, Gadea G, Desprès P. 2019. A Viperin Mutant Bearing the K358R Substitution Lost its Anti-ZIKA Virus Activity. Int J Mol Sci 20.

339. Wu Y, Yang X, Yao Z, Dong X, Zhang D, Hu Y, Zhang S, Lin J, Chen J, An S, Ye H, Zhang S, Qiu Z, He Z, Huang M, Wei G, Zhu X. 2020. C19orf66 interrupts Zika virus replication by inducing lysosomal degradation of viral NS3. PLoS Negl Trop Dis 14:e0008083.

340. Hoek KHV der, Eyre NS, Shue B, Khantisitthiporn O, Glab-Ampi K, Carr JM, Gartner MJ, Jolly LA, Thomas PQ, Adikusuma F, Jankovic-Karasoulos T, Roberts CT, Helbig KJ, Beard MR. 2017. Viperin is an important host restriction factor in control of Zika virus infection. Sci Rep 7:4475.

341. Panayiotou C, Lindqvist R, Kurhade C, Vonderstein K, Pasto J, Edlund K, Upadhyay AS, Överby AK. 2018. Viperin Restricts Zika Virus and Tick-Borne Encephalitis Virus Replication by Targeting NS3 for Proteasomal Degradation. J Virol 92.

342. Savidis G, Perreira JM, Portmann JM, Meraner P, Guo Z, Green S, Brass AL. 2016. The IFITMs Inhibit Zika Virus Replication. Cell Rep 15:2323–2330.

343. Zu S, Li C, Li L, Deng Y-Q, Chen X, Luo D, Ye Q, Huang Y-J, Li X-F, Zhang R-R, Sun N, Zhang X, Aliyari SR, Nielsen-Saines K, Jung JU, Yang H, Qin C-F, Cheng G. 2022. TRIM22 suppresses Zika virus replication by targeting NS1 and NS3 for proteasomal degradation. Cell Biosci 12:139.

344. Strange DP, Jiyarom B, Sadri-Ardekani H, Cazares LH, Kenny TA, Ward MD, Verma S. 2021. Paracrine IFN Response Limits ZIKV Infection in Human Sertoli Cells. Front Microbiol 12:667146.

345. Hanrath AT, Hatton CF, Gothe F, Browne C, Vowles J, Leary P, Cockell SJ, Cowley SA, James WS, Hambleton S, Duncan CJA. 2022. Type I interferon receptor (IFNAR2) deficiency reveals Zika virus cytopathicity in human macrophages and microglia. Front Immunol 13.

346. David M, Chen HE, Goelz S, Larner AC, Neel BG. 1995. Differential regulation of the alpha/beta interferon-stimulated Jak/Stat pathway by the SH2 domain-containing tyrosine phosphatase SHPTP1. Mol Cell Biol 15:7050–7058.

347. Endo TA, Masuhara M, Yokouchi M, Suzuki R, Sakamoto H, Mitsui K, Matsumoto A, Tanimura S, Ohtsubo M, Misawa H, Miyazaki T, Leonor N, Taniguchi T, Fujita T, Kanakura Y, Komiya S, Yoshimura A. 1997. A new protein containing an SH2 domain that inhibits JAK kinases. 6636. Nature 387:921–924.

348. Babon JJ, Kershaw NJ, Murphy JM, Varghese LN, Laktyushin A, Young SN, Lucet IS, Norton RS, Nicola NA. 2012. Suppression of Cytokine Signaling by SOCS3: Characterization of the Mode of Inhibition and the Basis of Its Specificity. Immunity 36:239–250.

349. Kershaw NJ, Murphy JM, Liau NPD, Varghese LN, Laktyushin A, Whitlock EL, Lucet IS, Nicola NA, Babon JJ. 2013. SOCS3 binds specific receptor–JAK complexes to control cytokine signaling by direct kinase inhibition. 4. Nat Struct Mol Biol 20:469–476.

350. Liao J, Fu Y, Shuai K. 2000. Distinct roles of the NH2- and COOH-terminal domains of the protein inhibitor of activated signal transducer and activator of transcription (STAT) 1 (PIAS1) in cytokine-induced PIAS1–Stat1 interaction. Proc Natl Acad Sci 97:5267–5272.

351. Malakhova OA, Kim II K, Luo J-K, Zou W, Kumar KS, Fuchs SY, Shuai K, Zhang D-E. 2006. UBP43 is a novel regulator of interferon signaling independent of its ISG15 isopeptidase activity. EMBO J 25:2358–2367.

352. Myers MP, Andersen JN, Cheng A, Tremblay ML, Horvath CM, Parisien J-P, Salmeen A, Barford D, Tonks NK. 2001. TYK2 and JAK2 Are Substrates of Protein-tyrosine Phosphatase 1B *. J Biol Chem 276:47771–47774.

353. Sarasin-Filipowicz M, Wang X, Yan M, Duong FHT, Poli V, Hilton DJ, Zhang D-E, Heim MH. 2009. Alpha Interferon Induces Long-Lasting Refractoriness of JAK-STAT Signaling in the Mouse Liver through Induction of USP18/UBP43. Mol Cell Biol 29:4841–4851.

354. Song MM, Shuai K. 1998. The Suppressor of Cytokine Signaling (SOCS) 1 and SOCS3 but Not SOCS2 Proteins Inhibit Interferon-mediated Antiviral and Antiproliferative Activities *. J Biol Chem 273:35056–35062.

355. ten Hoeve J, de Jesus Ibarra-Sanchez M, Fu Y, Zhu W, Tremblay M, David M, Shuai K. 2002. Identification of a Nuclear Stat1 Protein Tyrosine Phosphatase. Mol Cell Biol 22:5662–5668.

356. You M, Yu D-H, Feng G-S. 1999. Shp-2 Tyrosine Phosphatase Functions as a Negative Regulator of the Interferon-Stimulated Jak/STAT Pathway. Mol Cell Biol 19:2416–2424.

357. Wang T, Town T, Alexopoulou L, Anderson JF, Fikrig E, Flavell RA. 2004. Toll-like receptor 3 mediates West Nile virus entry into the brain causing lethal encephalitis. 12. Nat Med 10:1366–1373.

358. Lima MC, de Mendonça LR, Rezende AM, Carrera RM, Aníbal-Silva CE, Demers M, D'Aiuto L, Wood J, Chowdari KV, Griffiths M, Lucena-Araujo AR, Barral-Netto M, Azevedo EAN, Alves RW, Farias PCS, Marques ETA, Castanha PMS, Donald CL, Kohl A, Nimgaonkar VL, Franca RFO. 2019. The Transcriptional and Protein Profile From Human Infected Neuroprogenitor Cells Is Strongly Correlated to Zika Virus Microcephaly Cytokines Phenotype Evidencing a Persistent Inflammation in the CNS. Front Immunol 10.

359. Yockey LJ, Jurado KA, Arora N, Millet A, Rakib T, Milano KM, Hastings AK, Fikrig E, Kong Y, Horvath TL, Weatherbee S, Kliman HJ, Coyne CB, Iwasaki A. 2018. Type I interferons instigate fetal demise after Zika virus infection. Sci Immunol 3.

360. Luo H, Li G, Wang B, Tian B, Gao J, Zou J, Shi S, Zhu S, Peng B-H, Adam A, Martinez A, Hein K, Winkelmann ER, Mahmoud Y, Zhou X, Shan C, Rossi S, Weaver S, Barrett ADT, Sun S-C, Zhang W, Shi P-Y, Wu P, Wang T. 2020. Peli1 signaling blockade attenuates congenital zika syndrome. PLoS Pathog 16.

361. Dowall SD, Graham VA, Hewson R. 2020. Lineage-dependent differences of Zika virus infection in a susceptible mouse model are associated with different profiles of cytokines, chemokines, growth factors and acute phase proteins. Cytokine 125:154864.

362. de Alwis R, Zellweger RM, Chua E, Wang L-F, Chawla T, Sessions OM, Marlier D, Connolly JE, von Messling V, Anderson DE. 2021. Systemic inflammation, innate immunity and pathogenesis after Zika virus infection in cynomolgus macaques are modulated by strain-specificity within the Asian lineage. Emerg Microbes Infect 10:1457–1470.

363. Gobillot TA, Humes D, Sharma A, Kikawa C, Overbaugh J. 2020. The Robust Restriction of Zika Virus by Type-I Interferon in A549 Cells Varies by Viral Lineage and Is Not Determined by IFITM3. 5. Viruses 12:503.

364. Best SM. 2017. The Many Faces of the Flavivirus NS5 Protein in Antagonism of Type I Interferon Signaling. J Virol 91.

365. Chen S, Wu Z, Wang M, Cheng A. 2017. Innate Immune Evasion Mediated by Flaviviridae Non-Structural Proteins. Viruses 9.

366. Estévez-Herrera J, Pérez-Yanes S, Cabrera-Rodríguez R, Márquez-Arce D, Trujillo-González R, Machado J-D, Madrid R, Valenzuela-Fernández A. 2021. Zika Virus Pathogenesis: A Battle for Immune Evasion. Vaccines 9.

367. Serman TM, Gack MU. 2019. Evasion of Innate and Intrinsic Antiviral Pathways by the Zika Virus. Viruses 11:970.

368. Airo AM, Felix-Lopez A, Mancinelli V, Evseev D, Lopez-Orozco J, Shire K, Paszkowski P, Frappier L, Magor KE, Hobman TC. 2022. Flavivirus Capsid Proteins Inhibit the Interferon Response. 5. Viruses 14:968.

369. Ma J, Ketkar H, Geng T, Lo E, Wang L, Xi J, Sun Q, Zhu Z, Cui Y, Yang L, Wang P. 2018. Zika Virus Non-structural Protein 4A Blocks the RLR-MAVS Signaling. Front Microbiol 9:1350.

370. Li A, Wang W, Wang Y, Chen K, Xiao F, Hu D, Hui L, Liu W, Feng Y, Li G, Tan Q, Liu Y, Wu K, Wu J. 2020. NS5 Conservative Site Is Required for Zika Virus to Restrict the RIG-I Signaling. Front Immunol 11:51.

371. Riedl W, Acharya D, Lee J-H, Liu G, Serman T, Chiang C, Chan YK, Diamond MS, Gack MU. 2019. Zika Virus NS3 Mimics a Cellular 14-3-3-Binding Motif to Antagonize RIG-I- and MDA5-Mediated Innate Immunity. Cell Host Microbe 26:493-503.e6.

372. Hu Y, Dong X, He Z, Wu Y, Zhang S, Lin J, Yang Y, Chen J, An S, Yin Y, Shen Z, Zeng G, Tian H, Cai J, Yang Y, Guan H, Wu J, Li M, Zhu X. 2019. Zika virus antagonizes interferon response in patients and disrupts RIG-I–MAVS interaction through its CARD-TM domains. Cell Biosci 9:46.

373. Li W, Li N, Dai S, Hou G, Guo K, Chen X, Yi C, Liu W, Deng F, Wu Y, Cao X. 2019. Zika virus circumvents host innate immunity by targeting the adaptor proteins MAVS and MITA. FASEB J 33:9929–9944.

374. Ngan NTT, Kim S-J, Lee JY, Myoung J. 2019. Zika Virus Proteins NS2A and NS4A Are Major Antagonists that Reduce IFN-β Promoter Activity Induced by the MDA5/RIG-I Signaling Pathway. J Microbiol Biotechnol 29:1665–1674.

375. Lin S, Yang S, He J, Guest JD, Ma Z, Yang L, Pierce BG, Tang Q, Zhang Y-J. 2019. Zika virus NS5 protein antagonizes type I interferon production via blocking TBK1 activation. Virology 527:180–187.

376. Wu Y, Liu Q, Zhou J, Xie W, Chen C, Wang Z, Yang H, Cui J. 2017. Zika virus evades interferon-mediated antiviral response through the co-operation of multiple nonstructural proteins in vitro. Cell Discov 3:17006.

377. Xia H, Luo H, Shan C, Muruato AE, Nunes BTD, Medeiros DBA, Zou J, Xie X, Giraldo MI, Vasconcelos PFC, Weaver SC, Wang T, Rajsbaum R, Shi P-Y. 2018. An evolutionary NS1 mutation enhances Zika virus evasion of host interferon induction. Nat Commun 9:1–13.

378. Lundberg R, Melén K, Westenius V, Jiang M, Österlund P, Khan H, Vapalahti O, Julkunen I, Kakkola L. 2019. Zika Virus Non-Structural Protein NS5 Inhibits the RIG-I Pathway and Interferon Lambda 1 Promoter Activation by Targeting IKK Epsilon. Viruses 11.

379. Kodani A, Knopp KA, Lullo ED, Retallack H, Kriegstein AR, DeRisi JL, Reiter JF. 2022. Zika virus alters centrosome organization to suppress the innate immune response. EMBO Rep 23:e52211.

380. Zhao Z, Tao M, Han W, Fan Z, Imran M, Cao S, Ye J. 2019. Nuclear localization of Zika virus NS5 contributes to suppression of type I interferon production and response. J Gen Virol https://doi.org/10.1099/jgv.0.001376.

381. Kumar A, Hou S, Airo AM, Limonta D, Mancinelli V, Branton W, Power C, Hobman TC. 2016. Zika virus inhibits type-I interferon production and downstream signaling. EMBO Rep 17:1766–1775.

382. Lang J, Cheng Y, Rolfe A, Hammack C, Vera D, Kyle K, Wang J, Meissner TB, Ren Y, Cowan C, Tang H. 2018. An hPSC-Derived Tissue-Resident Macrophage Model Reveals Differential Responses of Macrophages to ZIKV and DENV Infection. Stem Cell Rep 11:348–362.

383. Bos S, Poirier-Beaudouin B, Seffer V, Manich M, Mardi C, Desprès P, Gadea G, Gougeon M-L. 2020. Zika Virus Inhibits IFN-α Response by Human Plasmacytoid Dendritic Cells and Induces NS1-Dependent Triggering of CD303 (BDCA-2) Signaling. Front Immunol 11:582061.

384. Laurent-Rolle M, Boer EF, Lubick KJ, Wolfinbarger JB, Carmody AB, Rockx B, Liu W, Ashour J, Shupert WL, Holbrook MR, Barrett AD, Mason PW, Bloom ME, García-Sastre A, Khromykh AA, Best SM. 2010. The NS5 Protein of the Virulent West Nile Virus NY99 Strain Is a Potent Antagonist of Type I Interferon-Mediated JAK-STAT Signaling. J Virol 84:3503–3515.

385. Lin R-J, Chang B-L, Yu H-P, Liao C-L, Lin Y-L. 2006. Blocking of interferon-induced Jak-Stat signaling by Japanese encephalitis virus NS5 through a protein tyrosine phosphatase-mediated mechanism. J Virol 80:5908–5918.

386. Grant A, Ponia SS, Tripathi S, Balasubramaniam V, Miorin L, Sourisseau M, Schwarz MC, Sánchez-Seco MP, Evans MJ, Best SM, García-Sastre A. 2016. Zika virus targets human STAT2 to inhibit type I interferon signaling. Cell Host Microbe 19:882–890.

387. Roby JA, Esser-Nobis K, Dewey-Verstelle EC, Fairgrieve MR, Schwerk J, Lu AY, Soveg FW, Hemann EA, Hatfield LD, Keller BC, Shapiro A, Forero A, Stencel-Baerenwald JE, Savan R, Gale M. 2020. Flavivirus Nonstructural Protein NS5 Dysregulates HSP90 to Broadly Inhibit JAK/STAT Signaling. 4. Cells 9:899.

388. Thurmond S, Wang B, Song J, Hai R. 2018. Suppression of Type I Interferon Signaling by Flavivirus NS5. Viruses 10.

389. Fanunza E, Carletti F, Quartu M, Grandi N, Ermellino L, Milia J, Corona A, Capobianchi MR, Ippolito G, Tramontano E. 2021. Zika virus NS2A inhibits interferon signaling by degradation of STAT1 and STAT2. Virulence 12:1580–1596.

390. Fanunza E, Grandi N, Quartu M, Carletti F, Ermellino L, Milia J, Corona A, Capobianchi MR, Ippolito G, Tramontano E. 2021. INMI1 Zika Virus NS4B Antagonizes the Interferon Signaling by Suppressing STAT1 Phosphorylation. Viruses 13:2448.

391. Chen J, Yang Y, Yang Y, Zou P, Chen J, He Y, Shui S, Cui Y, Bai R, Liang Y, Hu Y, Jiang B, Lu L, Zhang X, Liu J, Xu J. 2018. AXL promotes Zika virus infection in astrocytes by antagonizing type I interferon signalling. Nat Microbiol 3:302–309.

392. Grabherr MG, Haas BJ, Yassour M, Levin JZ, Thompson DA, Amit I, Adiconis X, Fan L, Raychowdhury R, Zeng Q, Chen Z, Mauceli E, Hacohen N, Gnirke A, Rhind N, di Palma F, Birren BW, Nusbaum C, Lindblad-Toh K, Friedman N, Regev A. 2011. Full-length transcriptome assembly from RNA-Seq data without a reference genome. 7. Nat Biotechnol 29:644–652.

393. Waterhouse AM, Procter JB, Martin DMA, Clamp M, Barton GJ. 2009. Jalview Version 2--a multiple sequence alignment editor and analysis workbench. Bioinforma Oxf Engl 25:1189–1191.

394. Schindelin J, Arganda-Carreras I, Frise E, Kaynig V, Longair M, Pietzsch T, Preibisch S, Rueden C, Saalfeld S, Schmid B, Tinevez J-Y, White DJ, Hartenstein V, Eliceiri K, Tomancak P, Cardona A. 2012. Fiji: an open-source platform for biological-image analysis. 7. Nat Methods 9:676–682.

395. Davis MA, Voss K, Turnbull JB, Gustin AT, Knoll M, Muruato A, Hsiang T-Y, Dinnon III KH, Leist SR, Nickel K, Baric RS, Ladiges W, Akilesh S, Smith KD, Gale M. 2023. A C57BL/6 Mouse Model of SARS-CoV-2 Infection Recapitulates Age- and Sex-Based Differences in Human COVID-19 Disease and Recovery. 1. Vaccines 11:47.

396. Wikan N, Smith DR. 2016. Zika virus: history of a newly emerging arbovirus. Lancet Infect Dis 16:e119–e126.

397. Shan C, Xia H, Haller SL, Azar SR, Liu Y, Liu J, Muruato AE, Chen R, Rossi SL, Wakamiya M, Vasilakis N, Pei R, Fontes-Garfias CR, Singh SK, Xie X, Weaver SC, Shi P-Y. 2020. A Zika virus envelope mutation preceding the 2015 epidemic enhances virulence and fitness for transmission. Proc Natl Acad Sci 117:20190–20197.

398. Plociennikowska A, Frankish J, Moraes T, Del Prete D, Kahnt F, Acuna C, Slezak M, Binder M, Bartenschlager R. 2021. TLR3 Activation by Zika Virus Stimulates Inflammatory Cytokine Production Which Dampens the Antiviral Response Induced by RIG-I-Like Receptors. J Virol 95:e01050-20.

399. Simonin Y, Riel D van, Perre PV de, Rockx B, Salinas S. 2017. Differential virulence between Asian and African lineages of Zika virus. PLoS Negl Trop Dis 11:e0005821.

400. Yun S-I, Song B-H, Frank JC, Julander JG, Polejaeva IA, Davies CJ, White KL, Lee Y-M. 2016. Complete Genome Sequences of Three Historically Important, Spatiotemporally

Distinct, and Genetically Divergent Strains of Zika Virus: MR-766, P6-740, and PRVABC-59. Genome Announc 4.

401. Hiscott J. 2007. Triggering the Innate Antiviral Response through IRF-3 Activation. J Biol Chem 282:15325–15329.

402. Goytain A, Ng T. 2020. NanoString nCounter Technology: High-Throughput RNA Validation, p. 125–139. *In* Li, H, Elfman, J (eds.), Chimeric RNA: Methods and Protocols. Springer US, New York, NY.

403. Keller BC, Fredericksen BL, Samuel MA, Mock RE, Mason PW, Diamond MS, Gale M. 2006. Resistance to Alpha/Beta Interferon Is a Determinant of West Nile Virus Replication Fitness and Virulence. J Virol 80:9424–9434.

404. Liang J-J, Liao C-L, Liao J-T, Lee Y-L, Lin Y-L. 2009. A Japanese encephalitis virus vaccine candidate strain is attenuated by decreasing its interferon antagonistic ability. Vaccine 27:2746–2754.

405. Wang B, Thurmond S, Zhou K, Sánchez-Aparicio MT, Fang J, Lu J, Gao L, Ren W, Cui Y, Veit EC, Hong H, Evans MJ, O'Leary SE, García-Sastre A, Zhou ZH, Hai R, Song J. 2020. Structural basis for STAT2 suppression by flavivirus NS5. Nat Struct Mol Biol 1–11.

406. Ramos da Silva S, Cheng F, Huang I-C, Jung JU, Gao S-J. 2019. Efficiencies and kinetics of infection in different cell types/lines by African and Asian strains of Zika virus. J Med Virol 91:179–189.

407. Thorne LG, Bouhaddou M, Reuschl A-K, Zuliani-Alvarez L, Polacco B, Pelin A, Batra J, Whelan MVX, Hosmillo M, Fossati A, Ragazzini R, Jungreis I, Ummadi M, Rojc A, Turner J, Bischof ML, Obernier K, Braberg H, Soucheray M, Richards A, Chen K-H, Harjai B, Memon D, Hiatt J, Rosales R, McGovern BL, Jahun A, Fabius JM, White K, Goodfellow IG, Takeuchi Y, Bonfanti P, Shokat K, Jura N, Verba K, Noursadeghi M, Beltrao P, Kellis M, Swaney DL, García-Sastre A, Jolly C, Towers GJ, Krogan NJ. 2022. Evolution of enhanced innate immune evasion by SARS-CoV-2. Nature 602:487–495.

408. Ireland DDC, Manangeeswaran M, Lewkowicz AP, Engel K, Clark SM, Laniyan A, Sykes J, Lee H-N, McWilliams IL, Kelley-Baker L, Tonelli LH, Verthelyi D. 2020. Long-term persistence of infectious Zika virus: Inflammation and behavioral sequela in mice. PLoS Pathog 16:e1008689.